



University of Naples “Federico II”

Faculty of Science MM.FF.NN

Department of Chemistry

**TESI DI DOTTORATO IN SCIENZE CHIMICHE**

**“Preparation and characterization of heterogeneous  
catalysts obtained by Grafting”**

Candidata: Dott. **MARIANGELA COZZOLINO**

Tutore: Ch.mo Prof. **ELIO SANTACESARIA**

Relatore: Ch.mo Prof. **AUGUSTO DE RENZI**

Coordinatore: Ch.mo Prof. **ROSA LANZETTA**

**DOTTORATO DI RICERCA  
IN SCIENZE CHIMICHE (SETTORE CHIM/03)  
(XIX CICLO)**

*Novembre 2006*



*Al Prof. Elio Santacesaria*  
con stima e affetto

*Alla piccola Alessandra*  
con amore





*Ho trovato quello che il mio cuore desiderava di  
trovare, l'ho afferrato e non lo lascerò andare*  
Cantico dei Cantici, III,4



***Acknowledgements***

Felicissima di aver raggiunto questo ulteriore traguardo che ha rappresentato per me un momento importante di crescita, non solo da un punto di vista scientifico e culturale, ma anche umano - desidero ringraziare quanti hanno reso possibile tutto ciò.

Al Prof. Elio Santacesaria, desidero esprimere la mia viva riconoscenza per aver fortemente creduto in questo mio *iter* formativo.

Un *grazie* speciale va a Martino Di Serio e Riccardo Tesser per aver vivamente collaborato a questo progetto di ricerca.

GRAZIE a tutti i ragazzi del lab.: Stefano, Nicola, Francesco, Anita, Donato, Adele, Michela, Elena, Ida, Pasquale, Raffaele, Giovanni, Peppe, Eleonora, Grazia, Gaetano, Mimmo, Antonio. Grazie per i bei momenti trascorsi assieme, che rimarranno nel mio cuore.

Grazie all'amico Italo Giudicianni (direttore CIMCIF), il "re" dell' NMR, per le simpatiche e lunghe chiacchierate fatte assieme alla "corte delle risonanze magnetiche".

Un ringraziamento particolare va all'amico Vicente (Prof. Vicente Cortes Corberan - Istituto di Catalisi e Petrolchimica, Madrid), per avermi onorato della sua presenza come membro della commissione di Dottorato.

Desidero, inoltre, ringraziare il Prof. Eric M. Gagneaux (Université catholique de Louvain, Belgium) per la straordinaria accoglienza mostratami nel suo laboratorio di ricerca (Ottobre-Dicembre 2005) e per le interessanti discussioni scientifiche. Ringrazio, poi, il Prof. B. Delmon, per le lunghe chiacchierate in italiano, il Prof. Patricio Ruiz e tutti gli amici di Louvain-la-Neuve: Françoise, Andrea, Pierre, Moez, Monder, Michel, Cecilia, Caroline.

Un pensiero speciale va a tutte le persone conosciute ai vari convegni nazionali ed internazionali, in particolare all'amica spagnola Izaskun.

Un immenso “grazie” di cuore ai miei, che hanno sempre fortemente incoraggiato le mie passioni, alle mie sorelle, Ester ed Enza, pronte a sostenermi in ogni momento, e alla piccola Dadà, che mi regala sempre momenti di assoluta spensieratezza.

*Un profondo, immenso ringraziamento lo devo infine a tutti quei bambini, poco fortunati, che ho incontrato per due anni, la domenica mattina, presso il Policlinico II di Napoli. Il loro sorriso e la loro speranza, nonostante il dolore e la sofferenza, mi hanno insegnato ad amare la vita così tanto.*

TABLE OF CONTENTS

GENERAL INTRODUCTION.....19

1. Context of the thesis.....19

1.1 Catalysis background.....19

1.1.1 How does a catalyst work? .....21

1.2 Nanotechnology and catalysis.....24

1.3 Nano-structured metal oxides for redox applications.....27

1.4 Recent trends in the preparation of metal oxide catalysts.....30

1.4.1 Grafting of metal alkoxides on the surface of oxide.....38

1.4.1.1 Introduction, nomenclature and historical note of metal alkoxides.....38

1.4.1.2 Synthesis of Metal alkoxides.....40

1.4.1.3 Physical and chemical properties of metal alkoxides.....42

1.4.1.4 Metal alkoxides as precursors for the preparation of supported metal oxides by *Grafting*.....44

2. Strategy and content of the thesis.....51

3. References.....64

**PART A - TiO<sub>2</sub>/SiO<sub>2</sub> catalysts: Preparation, Characterization and Reactivity properties.....69**

**I - INTRODUCTION.....71**

Abstract.....71

1.1 TiO<sub>2</sub>/SiO<sub>2</sub> oxides: an example of advanced supports and catalytic nanomaterials.....72

1.2 Preparation of supported titania/silica materials.....78

1.3 Factors determining the maximum surface titanium coverage of silica.....87

1.4 Surface structures of molecularly dispersed supported TiO<sub>2</sub>/SiO<sub>2</sub> catalysts.....92

1.5 Catalytic performances of supported molecularly dispersed TiO<sub>2</sub>/SiO<sub>2</sub> oxides.....96

1.6 Conclusions.....100

1.7 References.....101

**EXPERIMENTAL SECTION.....107**

**II - Highly dispersed TiO<sub>2</sub>/SiO<sub>2</sub> catalysts for *Biodiesel production*.....109**

Abstract.....109

2.1 Catalysts preparation.....110

2.1.1 Investigation of the effect of the solvent on the *grafting* yield.....114

2.2 Techniques used for the catalyst characterization.....115

|  |     |
|--|-----|
| 2.3 Transesterification reaction of triglycerides with methanol:<br>materials and methods.....   | 120 |
| 2.4 Results and discussion.....  | 121 |
| 2.4.1 Evaluation of the surface monolayer coverage of silica by<br>titanium tetra-isopropoxide (Ti(O-Pr) <sup>i</sup> ) <sub>4</sub> .....                             | 121 |
| 2.4.2 Characterization results.....  | 125 |
| 2.4.2.1 Nitrogen adsorption (BET) measurements.....  | 125 |
| 2.4.2.2 XRD analyses.....  | 126 |
| 2.4.2.3 TEM/EDX analyses.....  | 128 |
| 2.4.2.4 UV-Vis Diffuse Reflectance Spectroscopy.....   | 132 |
| 2.4.2.5 Raman analysis of surface Ti species.....  | 134 |
| 2.4.2.6 Determination of the surface dispersion and structure<br>by XPS analyses.....  | 137 |
| 2.4.2.7 Acidic properties of supported TiO <sub>2</sub> /SiO <sub>2</sub><br>catalysts.....  | 143 |
| 2.4.2.7.1 Determination of the surface acidity by NH <sub>3</sub> -<br>TPD measurements.....   | 143 |
| 2.4.2.7.2 Determination of the strenght of surface acidic<br>sites by NH <sub>3</sub> -chemisorption.....  | 144 |
| 2.4.2.7.3 Study of the surface acidity of TiO <sub>2</sub> /SiO <sub>2</sub><br>catalysts by means of FT-IR measurements of CO and<br>NH <sub>3</sub> adsorption ..... | 148 |
| 2.4.2.7.3.1 Hydroxyls spectra of samples outgassed at<br>723 K.....  | 148 |
| 2.4.2.7.3.2 Adsorption of CO at nominal 77 K on<br>TiO <sub>2</sub> /SiO <sub>2</sub> catalysts.....   | 151 |

2.4.2.7.3.3 Adsorption of NH<sub>3</sub> at room temperature  
on TiO<sub>2</sub>/SiO<sub>2</sub> systems.....162

2.4.3 Catalytic performances of TiO<sub>2</sub>/SiO<sub>2</sub> in the transesterification  
of refined/edible oils with methanol.....168

2.4.3.1 Literature information on biodiesel  
production.....168

2.4.3.2 Catalytic screening of TiO<sub>2</sub>/SiO<sub>2</sub> catalysts.....170

2.4.3.3 Comparison of the catalytic performances of  
TiO<sub>2</sub>/SiO<sub>2</sub> catalysts with other heterogeneous catalytic  
systems.....174

2.4.3.4 Investigation of the stability of TiO<sub>2</sub>/SiO<sub>2</sub>  
catalysts.....176

2.4.3.4.1 Effect of the presence of water and temperature  
reaction.....179

2.5 Conclusions.....182

2.6 References.....183

**III - Design of the best catalyst (TiO<sub>2</sub>/SiO<sub>2</sub>) for the epoxidation  
reaction of cyclooctene.....187**

Abstract.....187

3.1 Catalysts preparation.....188

3.2 Techniques used in catalyst characterization.....192

3.3 Catalytic tests in the epoxidation of reaction.....193

3.4 Results and discussion.....194

3.4.1 Catalyst preparation.....194

3.4.2 Catalyst characterization.....194

3.4.2.1 Nitrogen adsorption (BET) measurements.....194



|   |     |
|---|-----|
| 3.4.2.2 X-ray diffraction analysis.....   | 195 |
| 3.4.2.3 Morphological analyses by TEM and EDX.....  | 198 |
| 3.4.2.4 FTIR spectroscopic analysis.....  | 199 |
| 3.4.2.4.1 Analysis of 3200-2700 cm <sup>-1</sup> spectral range..   | 199 |
| 3.4.2.4.2 Analysis of spectral range 4000-3500 cm <sup>-1</sup> ..  | 201 |
| 3.4.2.4.3 Determination of TiO <sub>2</sub> dispersion by DRIFT<br>analysis in the spectral range 1400-700 cm <sup>-1</sup> ..... | 203 |
| 3.4.2.5 Diffuse reflectance UV-Vis spectroscopy<br>analysis.....  | 207 |
| 3.4.2.6 Temperature programmed desorption (TPD)<br>analyses.....  | 210 |
| 3.4.3 Catalytic performances in the epoxidation reaction of<br>TiO <sub>2</sub> /SiO <sub>2</sub> catalysts.....                  | 211 |
| 3.5 Conclusions.....  | 215 |
| 3.6 References.....   | 216 |

**PART B - Supported vanadium oxide based catalysts for  
the ODH reactions.....219**

|  |            |
|--|------------|
| <b>IV - INTRODUCTION.....</b>  | <b>221</b> |
| Abstract.....  | 221        |
| 4.1 Introduction.....  | 221        |
| 4.2 Preparation methods of supported vanadium oxide catalysts....                    | 225        |
| 4.3 Characterization methods for supported vanadium oxides.....                      | 230        |
| 4.4 Factors influencing the dispersion of the surface vanadium oxide<br>species..... | 236        |

|   |                |
|---|----------------|
| 4.4.1 The support effect.....   | 236            |
| 4.4.2 The effect of vanadium oxide loading.....   | 239            |
| 4.5 Structural properties of highly dispersed supported vanadium oxide species.....   | 242            |
| 4.6 Reactivity/Selectivity properties of vanadium oxide catalysts in the Oxidative Dehydrogenation (ODH) reactions.....                                   | 246            |
| 4.7 Conclusions.....  | 249            |
| 4.8 References.....   | 250            |
| <br><b>EXPERIMENTAL SECTION.....</b>  | <br><b>255</b> |
| <br><b>V - ODH of n-butane to butenes by supported vanadium based catalysts.....</b>  | <br><b>257</b> |
| Abstract.....   | 257            |
| 5.1 Introduction to the ODH of n-butane to butenes.....   | 258            |
| 5.2 Experimental.....   | 264            |
| 5.2.1 Supports preparation.....   | 264            |
| 5.2.2 Catalysts preparation by impregnation.....  | 265            |
| 5.2.3 Catalysts preparation by grafting.....  | 267            |
| 5.2.4 Techniques used in catalysts characterisation.....  | 271            |
| 5.2.5 Catalytic tests.....  | 273            |
| 5.3 RESULTS AND DISCUSSION.....   | 274            |
| System V/SiO <sub>2</sub> : Chemical adsorption isotherm of vanadyl tri-alkoxide on silica.....   | 274            |
| System V/TiO <sub>2</sub> /SiO <sub>2</sub> : chemical adsorption isotherm of vanadyl tri-isopropoxide on TiO <sub>2</sub> /SiO <sub>2</sub> support..... | 278            |

Catalysts and supports characterization.....284

*X rays diffraction analyses*.....284

*Diffuse Reflectance UV Spectroscopy (DR-UV) analysis*.....286

*DRIFT analysis*.....290

*Raman spectroscopy*.....291

*XPS analysis on V/SiO<sub>2</sub> and V/ TiO<sub>2</sub>/SiO<sub>2</sub> catalysts*.....293

Kinetic runs in the Oxidative Dehydrogenation (ODH) of butane.....298

5.4 Conclusions.....307

5.5 References.....309

**VI - Catalytic screening of the ODH of methanol to formaldehyde by supported vanadium based catalysts.....315**

Abstract.....315

6.1 Introduction.....316

6.2 Supports and catalyst preparation.....321

6.3 Techniques used in catalyst characterization.....321

6.4 Methods, Techniques and Operating conditions used in the catalytic runs.....324

6.5 Results and discussion.....328

    6.5.1 Catalysts and supports characterization.....328

        6.5.1.1 Chemical composition and surface area/porosity determinations.....328

        6.5.1.2 Dispersion and structure analysis by XPS.....328

        6.5.1.3 Nature of the surface species by Raman spectroscopy.....331

|   |     |
|---|-----|
| 6.5.1.4 Analysis of the acidity of the catalysts by NH <sub>3</sub> -TPD.....     | 333 |
| 6.5.2 Catalytic performances obtained in the ODH of methanol to formaldehyde..... | 335 |
| 6.5.2.1 Comparison with a typical industrial catalyst.....                        | 342 |
| 6.6 Conclusion.....   | 347 |
| 6.7 References.....   | 348 |

|   |            |
|---|------------|
| <b>PART C - Kinetic study of the ODH of alcohols to aldehydes on V/TiO<sub>2</sub>/SiO<sub>2</sub> catalysts.....</b> | <b>351</b> |
|---|------------|

|   |            |
|---|------------|
| <b>VII - Kinetics of the oxidative dehydrogenation (ODH) of methanol to formaldehyde on nano-structured V/TiO<sub>2</sub>/SiO<sub>2</sub> based catalyst.....</b> | <b>353</b> |
| Abstract.....   | 353        |
| 7.1 Introduction.....   | 355        |
| 7.2 Catalyst and support preparation .....  | 360        |
| 7.3 Methods, Techniques and Operating conditions used in the catalytic runs.....  | 362        |
| 7.4 Results and discussion.....   | 367        |
| 7.4.1 Experimental approach.....  | 367        |
| 7.4.1.1 Effect of feed composition.....   | 370        |
| 7.4.1.2 Effect of presence of water in the feed.....  | 371        |
| 7.4.2 Theoretical approach.....   | 372        |
| 7.5 Conclusions.....  | 385        |

7.6 References.....386

List of symbols.....388

**VIII - Kinetics of the oxidative dehydrogenation (ODH) of ethanol to acetaldehyde on V<sub>2</sub>O<sub>5</sub>/TiO<sub>2</sub>/SiO<sub>2</sub> catalyst.....389**

Abstract.....389

8.1 Introduction.....390

8.2 Catalyst and support preparation.....394

8.3 Catalyst and Support Characterization Techniques.....397

8.4 Methods, Techniques and Operating Conditions used in the catalytic runs.....398

8.5 Results and Discussion.....399

*Catalyst and Support Characterization.....399*

*Catalyst Results.....402*

*Reaction Kinetics and Mechanism.....409*

8.6 Conclusions.....423

8.7 References.....424

List of symbols.....427

**Notes - Methanol vs Ethanol oxidative dehydrogenation (ODH) on V/TiO<sub>2</sub>/SiO<sub>2</sub> catalysts.....429**

General comments.....429

**GENERAL CONCLUSIONS.....431**

***Curriculum Vitae.....439***



# GENERAL INTRODUCTION

## 1. Context of the thesis

### 1.1 Catalysis background

Catalysis is the technology which allows to increase the activity, selectivity, speed and stability of a chemical reaction aided by a substance – the so-called catalyst – which is, to a first approximation, not consumed during the reaction [1].

Catalysis as phenomenon is becoming reasonably well understood on a conceptual level. Recognized as a phenomenon and utilized around 1816 by Davy in the mine safety lamp, and defined around 1835 by Berzelius, catalysis obtained an extensive empirical basis by the systematic experiments of Mittasch in the early 20<sup>th</sup> century. Studies of catalytic mechanisms became feasible when Langmuir-Hinshelwood kinetics became available in the mid 1920s. Since then, for many decades fundamental catalysis became more or less synonymous with kinetic analysis. The advent of spectroscopy, starting with infrared spectroscopy in the late 1950s, followed by a

range of other techniques for catalyst characterization and investigation of surface species, opened the opportunity to relate catalytic properties with composition and structure of materials. Surface science enabled to resolve surface structures and adsorbed species with atomic precision by the end of the 20<sup>th</sup> century.

Currently, catalysis has developed into a scientific discipline with a firm conceptual basis. The great importance of catalysis can be comprised by considering the strong impact having on the society. Without catalysts, various chemical reactions of great importance would proceed so slowly that they could not even be detected, although the reaction conditions (temperature and pressure) are thermodynamically favourable for the occurrence of the reactions [2–6]. Suitable catalysts provide a solution to this problem. They make it possible for the reactions to proceed at rates high enough to permit their commercial exploitation on a large scale, with resulting economic benefits for everyone. Thus, the catalysts can be defined as the “workhorses” of the chemical industry: more than 80 % of all modern chemicals come into in contact with at least one catalyst during the manufacture [7]. By summarizing, catalysts are indispensable in:

- Production of transportation fuels in one of the approximately 440 oil refineries all over the world.
- Production of bulk and fine chemicals in all the branches of the chemical industry.
- Prevention of pollution by avoiding formation of waste (unwanted by-products).



- Abatement of pollution in end-pipe solutions (automotive and industrial exhaust).

Other applications regard many processes occurring in living things, where enzymes are the catalysts. Moreover, they are important in the processing of foods and the production of medicines, in the manufacture of synthetic fibers and plastics, and in the production of many different chemicals with all kinds of uses [8-13].

### **1.1.1 How does a catalyst work?**

A catalyst accelerates a chemical reaction. It does so forming bonds with the reacting molecules, and by allowing these to react to a product, which detaches from the catalyst, and leaves it unaltered such that is available for the next reaction. In fact, it is possible to describe the catalytic reaction as a cycle event in which the catalyst participates and it is recovered in its original form at the end of the cycle.

A classical example of a catalytic reaction is depicted in Fig.1 where two molecules A and B react to give a product P.

As can be seen from Fig. 1, the cycle starts with the bonding of the molecules A and B to the catalyst. A and B then react within the complex to give a product P, which is also bound to the catalyst. In the final step, P separates from the catalyst, thus leaving the reaction cycle in its original state.

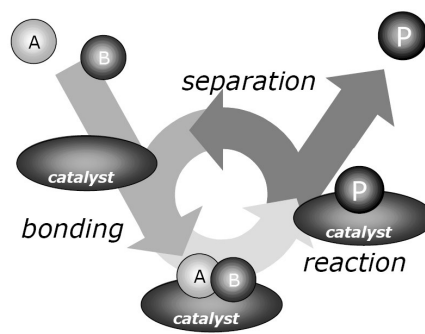


**Fig . 1:** Representation of a typical catalytic cycle event. [1]

In order to see how the catalyst accelerates a chemical reaction, it is fundamental to consider the potential energy diagram in Fig. 2, which compares the non-catalytic reaction and the catalytic reaction. This diagram illustrates several important points, some of them are reported below:

- The catalyst offers an alternative path for the reaction, which is obviously more complex, but energetically much more favourable.
- The activation energy of the catalytic reaction is significantly smaller than that of the un-catalyzed reaction.
- The catalyst accelerates both the forward and the reverse reaction to the same extent. In other words, if a catalyst accelerates the formation of the product P from A and B, it will do the same for the decomposition of P into A and B.

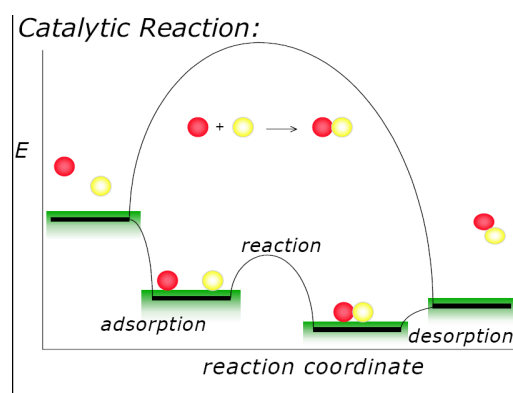


**Fig . 2:** Potential energy diagram of a heterogeneous catalytic reaction, with gaseous reactants and products and a solid catalyst [1]

Catalysts come in a multitude of forms, varying from atoms and molecules to large structures such as zeolites or enzymes.

In addition, they may be employed in various surroundings: in liquids, gases or at the surface of solids. There are two kinds of catalysts, heterogeneous and homogeneous, according to the phases involved in the processes [14].

- Heterogeneous catalysts are sometimes called surface catalysts because they position the reactant molecules on their surface. Oxide catalysts belong to this class.
- Homogeneous catalysts are catalysts that are present uniformly intermixed in the same phase with the reactant molecules. Together with metal coordination complexes, enzymes and biochemical catalysts in general are remarkably active examples of this group of catalysts.

## 1.2 Nanotechnology and catalysis

In recent years, there has been a huge increase in the interest in nanotechnology, a term that was virtually unheard of a decade ago [15].

A nanometer (nm) is one thousand millionth of a meter. A single human hair is about 80,000 nm wide, a red blood cell is approximately 7,000 nm wide, a DNA molecule 2 to 2.5 nm, and a water molecule almost 0.3 nm. It is worth that on a nanoscale, i.e. from around 100 nm to 1 nm size, immediately above that of atoms or molecular bonds, the properties of materials can be very different from those found on a larger scale.

The study of phenomena involved in the operation and manipulation of materials at atomic, molecular and macromolecular scales is “nano-science”, [16,17], while “nanotechnologies” are those technologies involved in the design, characterization, production and application of structures, devices and systems by controlling shape and size on a nanometer scale.

Today’s nanotechnology exploits the interaction of three technological trends:

- New and improved control of the size and manipulation of nanoscale building blocks.
- New and improved characterization of materials on a nanoscale (e.g., spatial resolution, chemical sensitivity).
- New and improved understanding of the relationships between nanostructure and its properties and how these can be engineered.

In many ways, nanotechnology has been part of catalysis technology, which, when coupled with macroscale reaction engineering technology, sets up the chemical process industry as we know to date. For example, petroleum and chemical processing companies are using nano-structured catalysts to remove pollutants, creating a €30 billion industry in 1999 with a foreseen potential of €100 billion per year by 2015. Thus, they represent the oldest commercial application of nanotechnology and it is foreseen as one of its main application lines in the future.

The nano-size has a spectacular aspect on the properties of the catalysts: the different rate of variation of area and volume means a much better use of the surface areas, and thus by decreasing particle size the catalytic activity may be promoted to a very high level, still unreachable. The greatest advantage foreseen from using nano-size catalysts will be the possibility to exploit the structure sensitivity by using a better tailored structure, leading to specificity and to a much increased selectivity. Definitively, this is the most promising potential area for development; by better tailoring the properties of the catalysts, highly structure sensitive reactions might be controlled. Furthermore, proximity relationships between different oxide nano-phases coexisting in composite catalysts can be better exploited, with process advantages when dealing with complex reactions.

It is well known that the catalytic properties of nano-particles of a given metal or metallic compound differ markedly from those of larger, bulk-like particles of the same material. Examples include the selective oxidation of propylene to propylene oxide, the oxidation of CO by gold nano-particles, the selective reduction of NO by iron

oxide nano-particles and the photocatalytic elimination of volatile organic compounds with titanium nano-particles.

Other examples report that nano-particles supported on polymers have been found to catalyze hydrogenation and carbon-carbon coupling reactions and, moreover, that metal clusters retaining their reactivity for extended periods of time and over a range of substrates.

Most of recent advances are a result of interdisciplinary developments involving nanotechnology. Major challenge for exploring nano-particles in heterogeneous catalysis are the control of the size, shape, surface and inter-particle contact. This is because with a better understanding of the connection between catalyst structure and catalytic chemistry, it will be possible to tailor catalytic properties to the precise needs of a particular process.

Of particular importance today is the possibility of characterizing, even at the nano level, a catalyst while it is working at the catalytic reaction in real or non-real conditions of temperature and fluid composition, and even checking the catalytic efficiency at the same time; this is the so-called *operando* type of study [7]. It is worth remarking that only two high resolution electron microscopes capable of studying materials under reactive atmosphere (above 1 torr) that exist in the world at this time have been installed, for the purpose of advanced catalytic nano-particle characterization, by leading chemical companies. These new characterization methods offer unprecedented opportunities to detail the electronic and physical properties of nano-structured catalysts and to “see” these catalysts functions in a realistic environment [7]. These studies allow to predict, for example, that by preparing nanometer-size islands of one oxide (such as  $\text{TiO}_2$ , to which

catalytic metal clusters are relatively strongly bound), surrounded completely by domains of a second oxide (such as  $\text{SiO}_2$ , to which the clusters bind much more weakly), it should be possible to deeply reduce catalyst aggregation into larger clusters, because an activation barrier exists for diffusion of the metal from one  $\text{TiO}_2$  island to another across the  $\text{SiO}_2$  surroundings, and thus to protect them against deactivation due to sintering.

Clearly, complete mastery of the connections between catalysis and nanostructure will be an extremely demanding challenge.

### **1.3 Nano-structured metal oxides for redox applications**

Metal oxide (MO) type materials are the main class of heterogeneous catalysts which play a key role in the production of petrochemicals, intermediates and fine chemicals and energy applications, as well as environmental protection [1]. MO catalysts are multifunctional materials. Some of them have a sophisticated intrinsic complexity, particularly when designed with a precise structure at the nanoscale to attain optimum performance. A step-forward in the design of such multifunctional nanostructured materials is necessary to address these complex problems. Additionally, in the case of oxides more than in the case of other catalysts, the reactor (the process) design have to adapted to each catalytic system and vice versa. This implies that innovations in all processes using such metal oxide catalysts need a tremendous contribution from chemical engineering and new reactor concepts (e.g., structured micro-reactors).

Furthermore, a better understanding of their catalytic features, as well as techniques to control them by a careful structure design on the nanometer scale level, are still needed. This nanostructure is also a key issue in the development of sustainable chemical processes, environmental protection and safety enhancement. As underlined before, nanotechnology opens new ways to get a better design and performance of these catalysts.

Among other application of oxide catalysts, their impact on environmental protection deserves a special mention. These catalysts are a key component to enable a sustainable chemistry and to improve environmental protection. Therefore, an intensified effort has to be made for a better understanding of the properties of these materials, the control of their reactivity and their design as multifunctional nanostructured materials.

Several environmental benefits will result from this, such as:

- Due to the multifunctional character of oxide-type catalytic materials, it will be possible to perform complex reaction in one step, thus implementing the principle of “green and sustainable chemistry” through process simplification, energy efficiency, and reduction of wastes, solvents and risks.
- The expected possible improvement of selectivity in the metal-oxide catalysts currently used for the seven large-scale petrochemical oxidation processes would generate an annual saving in feedstock materials of approximately €1,500 million worldwide, in addition to the benefits in



terms of saving resources and energy and improving process eco-compatibility.

- The use of oxide catalysts in a better utilization of fuels, either through advanced catalytic combustion (e.g., in gas turbine applications) or by integration in high temperature fuel cells, will allow to reduce fossil fuels consumption and the resulting amount of greenhouse gas CO<sub>2</sub>.

In the field of MO catalysts, several levels can be distinguished [15]:

- Oxide catalysts in general.
- NSO; Nano-structured Oxides for any type of application (both catalysis and other application).
- NSOC; Nano-structured Oxides for Catalysis applications specifically.
- NSOCRA; Nano-structured Oxides for Catalysis Redox Applications.

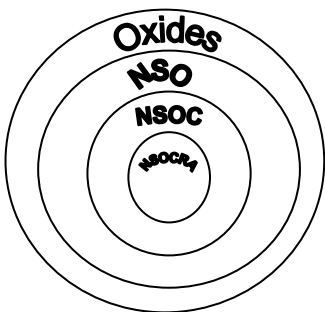


**Fig. 3:** Different levels can be distinguished in the field of MO catalysts.

In any case, the main application lines for the future of nanostructured catalytic oxides are listed in Table 1.

**Table 1:** Nano-structured Oxides (*NSO*) application lines

|   |  |
|---|--|
| <ul style="list-style-type: none"><li>• Direct production of H<sub>2</sub> from solar energy (photocatalysis)</li><li>• Catalytic reforming of light hydrocarbons</li><li>• Catalytic partial oxidation</li><li>• Water gas shift reaction</li><li>• Bioethanol production</li><li>• Catalytic reforming of biofuels</li><li>• Catalytic combustions of light hydrocarbons</li><li>• Catalytic filters</li><li>• VOC oxidation</li><li>• NO<sub>x</sub> abatement</li><li>• SO<sub>2</sub> abatement</li><li>• Fuel processing in fuel cells</li><li>• Fuel cell electrodes catalysis</li></ul> | <ul style="list-style-type: none"><li>• Batteries</li><li>• Selective oxidation processes</li><li>• Selective hydrogenation processes</li><li>• Methane to bulk chemicals</li><li>• Salt free processes</li><li>• Detection systems and devices</li><li>• Photocatalytic oxidation applications</li><li>• Electrochromic mirrors</li><li>• Gas sensors</li><li>• Production and conversion of synthesis gas</li><li>• Pigments with multifunctional catalytic properties</li></ul> |
|---|--|

**1.4 Recent trends in the preparation of metal oxide catalysts**

It is well known that the structure of the metal oxide catalysts is very complex. The active phase consists of nm-scale metal clusters, or metal sulphide and metal oxide phases deposited into the 10-100 nm pores of nm-scale support bodies. For optimum activity of the final catalysts, control on all these different length scales is required. In contrast to this complexity, straightforward techniques are being used in the industrial preparation of supported catalysts [18].

Recent trends in catalysts preparation have been presented at the 9<sup>th</sup> *International Symposium on the Scientific Bases for the Preparation of Heterogeneous Catalysts* (held in Louvain-la-Neuve on Sept. 10–14, 2006). Nowadays the range of materials used as catalysts is as wide as ever, and the techniques used to prepare them vary as much as their nature. However, some general tendencies can be identified and summarized as follows.

First, microporous and mesoporous oxides remain useful and highly selective catalysts, hence the techniques developed for their synthesis are continuously refined. Research in this area focuses mainly on preparing composite materials with tailored properties, and understanding/directing the effect of the templating agents. Post-synthetic modifications, such as surface grafting and functionalization, play an important role in defining the final physicochemical characteristics of the porous solids. Recently, P.A. Jacobs [19] developed a simple and direct synthesis procedure for composite material consisting of ZSM-5 nanocrystals embedded in a mesoporous silica matrix. This way resulted very interesting and useful to prepare composite materials which can combine the properties of both zeolites and mesoporous materials. The samples were characterized and their catalytic activity evaluated using decane hydroconversion. The adopted synthesis procedure can be summarized as follows:

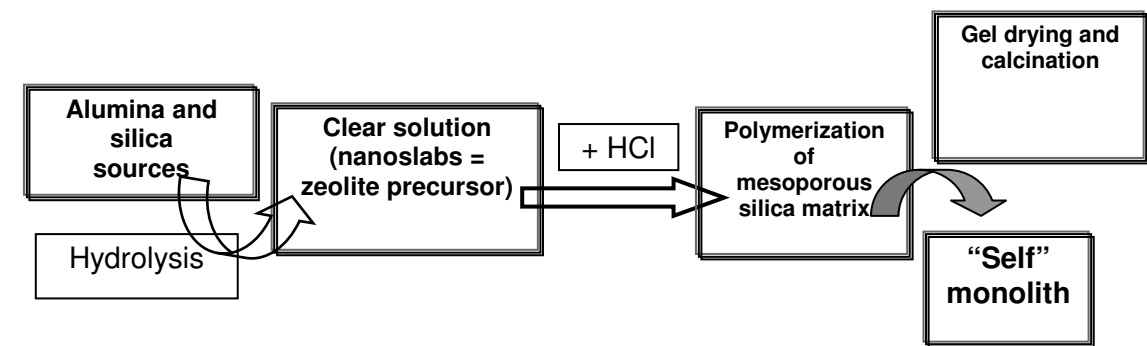
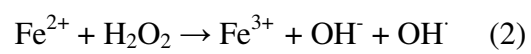
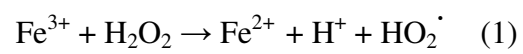


**Fig. 4:** Nanocrystals zeolite/mesoporous matrix composite (G. van Tendeloo, J.A. Martens, P.A. Jacobs, KULeuven, Belgium).

This generic synthesis method can possibly be applied to other zeolite precursor solutions and the matrix properties modified by controlling the pH shock and the drying conditions according to the classical concepts known in the art of sol-gel synthesis.

Another very interesting example is given by the preparation of heterogeneous catalysts by using Fenton's chemistry [20]. This technology, based on the generation of  $\text{OH}^\bullet$  radicals from  $\text{H}_2\text{O}_2$  in presence of Fe cations, has been applied for the treatment of wastewater to remove organic pollutants.

**Fenton-chemistry:** Hydrogen peroxide in presence of traces of transition metals (especially  $\text{Fe}^{\text{II/III}}$ ) produces  $\text{OH}^\bullet$



A recent work of I. Melian-Cabrera et al. [21] showed that this technology can be efficiently employed for three concepts:

- Decomplexation of metal-organic salts in solution ion-exchange: in this way metal-organic salts can be used for ion-exchange, since the ligands are removed by oxidation with  $\text{OH}^\bullet$  radicals. There are two major benefits: (i) the metal cations are liberated in a controlled way by titration, which controls their hydrolysis to inactive oxides and (ii) the oxidation leads to  $\text{CO}_2$  and  $\text{H}_2\text{O}$  as the only by-products.

- Combined detemplation & Fe(III) ion-exchange of zeolite: it combines several steps of the preparation of metal-exchanged zeolites in a single process. Application for Co(II) and Cu(II) can also be applied by modifying the original protocol.

- Detemplation of micro- and meso-porous materials can be done when the Fe-concentration is minimized to ppm levels.

These three examples demonstrate that the preparation of heterogeneous catalysts can benefit from radical chemistry.

Secondly, an important parameter that can now be controlled is particle size, with a general trend towards keeping it in the nanometer range, this being true for the grains of bulk oxides or the metallic/oxide particles of supported catalysts.

In line with this trend, the preparation of ultra fine particles in a reversed micelle system has received considerable attention because of its possibility to obtain mono-dispersed particles in nm size [22,23]. Recently, S. Naito et al. [24] described the synthesis of tailored-made hollow silica nano-spheres containing ultrafine particles of Rh, Ir or Rh/Ir bimetals in their cavities by using a crystal template method in a reversed micelle (RM) system. They investigated the adsorption behaviour of H<sub>2</sub> over these metal oxide nano-composites catalysts and found that an anomalously large amount of hydrogen was occluded inside the hollow space, which resulted in a unique catalytic behaviour for hydrogen exchange and hydrogenation of ethane over these catalysts.

Other aspects of the oxide or support morphology that may be controlled through the preparation method are the porosity, grain shape or crystal phase. Going one step further, investigations aim at

preparing nano-structured or hybrid materials, with not only a control on the size but also on the chemical nature of each building block. Support functionalization is sometimes the starting point of such a synthetic strategy, but sol-gel and colloidal chemistry are also widely used. In parallel, the development of macroscopic structures such as monolith, foams, layered materials or films is also important, with crucial questions related to scaling up [25].

Thirdly, much effort aims today at rational syntheses or preparation methods that are controlled at each step. These developments are usually linked to the application of *in situ* characterization techniques, which allow the monitoring of the catalyst at each stage of its genesis. In this context, the use of model systems, atomically-defined, is another useful tool.

Recently, spatially resolved spectroscopic techniques were developed to monitor the nature and the distribution of metal oxide precursors inside supported catalysts bodies, during their preparation. J.A. Bergwerff et al. [26] studied, for example, the influence of preparation on the catalytic activity of Co/Al<sub>2</sub>O<sub>3</sub> Fischer-Tropsch and Mo/Al<sub>2</sub>O<sub>3</sub> HDS catalysts by using the combination of Raman, UV-Vis and Magnetic resonance Imaging (MRI) techniques. They showed how a multi-technique approach can be applied to monitor the nature and macro-distribution of all components in the impregnation solution, throughout the preparation procedure of these materials. Due to the high Raman cross-section of Mo-O vibrations, Raman microscopy is ideally suited to study the speciation of Mo-complexes inside the catalyst bodies [27]. The d-d transitions of Co<sup>2+</sup>-complexes that can be observed by UV-Vis micro spectroscopy yield detailed

information on the nature and distribution of the Co-precursor in the extrudates [26]. The application of MRI in these studies provides additional advantage that characterization can be carried out in a non-invasive manner. The experimental procedure used for the spatially resolved Raman and UV-Vis spectroscopy measurements and a non-invasive MRI experiment are depicted in **Fig. 5**.



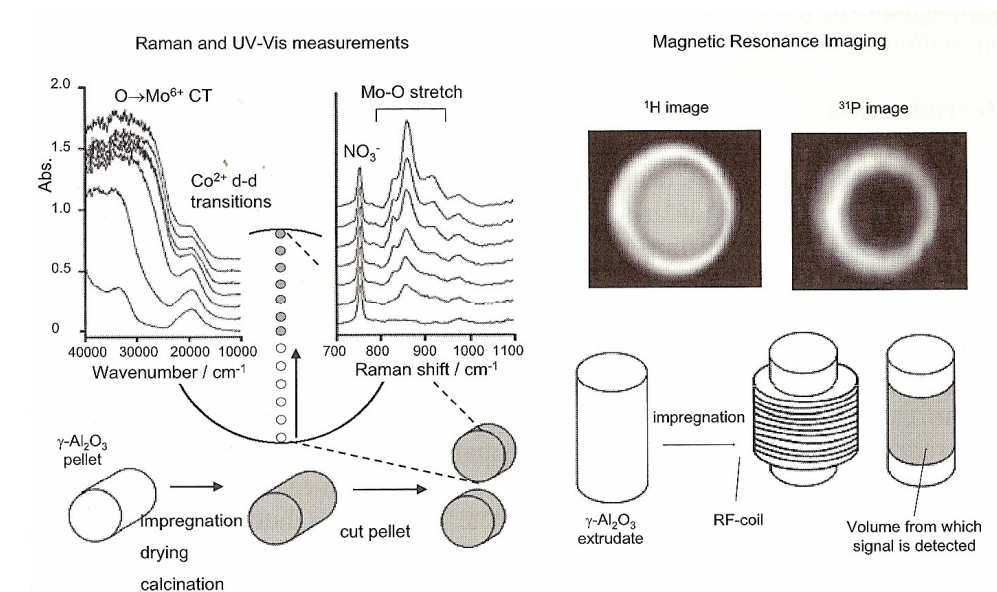


**Fig. 5:** Lay out of a spatially resolved Raman and UV-Vis spectroscopy experiment on bisected pellet (left) and a non-invasive MRI experiment (right)

Finally, recent ideas, such as bio-mimetic strategies or the concepts of self-assembly, are also applied to catalysts preparation. The introduction of polymers (or dendrimers) as supports, within a composite, or as sacrificial matrixes, is also an emerging field. Relatively recent techniques, such as the use of microwaves, magnetron sputtering, supercritical fluids, inductive plasma torch, flame spray pyrolysis, CVD, *etc.* are developed as well for solid materials synthesis [25].

### **1.4.1 Grafting of metal alkoxides on the surface of oxides**

#### **1.4.1.1 Introduction, nomenclature and historical note of metal alkoxides**

The binary metal alkoxides have the general formula  $M(OR)_x$  and can be considered to be derivatives of alcohols (ROH) in which the hydroxylic hydrogen has been replaced by a metal (M). Another way of defining the alkoxides is to consider them derivatives of metal hydroxides,  $M(OH)_x$  [28]. Metal alkoxides involve  $M^{\delta+}-O^{\delta-}-C$  bonds which are polarized in the direction shown due to the highly electronegative character of oxygen. The degree of polarization in an alkoxide molecule depends upon the electronegativity of the central (M) and the nature of these compounds varies from essentially covalent volatile monomers as in cases of electronegative elements like silicon, germanium, phosphorous and sulphur to more electrocovalent polymer solids in the cases of electropositive elements such as the alkali and the alkaline earth metals as well as the

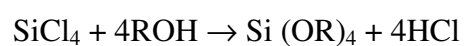
lanthanons. For derivatives of the same elements, the covalent character of the M–O bond increases with greater + I inductive effect of the alkyl group. The polarity of the M–O bond may also be partially offset in cases of electrophilic metals which undergo covalency expansion by intermolecular coordination through the oxygen atoms of the alkoxy groups. This type of molecular association appears to be sensitive to steric factors such as the ramification of the alkyl group.

There has been some confusion in the literature regarding the nomenclature of these alkoxy derivatives which have been termed as alkyl or aryl orthoesters (such as orthoborates, orthosilicates, orthoaluminates) and alternatively, as metal alkoxides (such as sodium, magnesium, aluminium or titanium alkoxides, etc.).

Although it would be arbitrary to draw any dividing line, the alkoxy derivatives of elements with electronegativity of 2.0 or less appear to have been generally termed as alkoxides whilst the others are termed orthoesters.

Further in keeping with the nomenclature generally adopted for metal alkoxides by most of the authors, the common names like methoxides, ethoxides, propoxides, (*n*- and *iso*-) and etc, have been retained as such. It is only in the cases of higher alkoxides that the nomenclature is derived strictly from IUPAC conventions.

The first reported synthesis of an alkoxide was by Ebelman [29] who in 1846 prepared silicon tetra-*iso*-amyloxide by a reaction between silicon tetrachloride and *iso*amyl alcohol:



Other historical notes can be found in [30].

#### 1.4.1.2 Synthesis of Metal alkoxides

The method required for the synthesis of alkoxy derivatives of an element generally depend on its electronegativity. Highly electropositive elements with valences up to three (like the alkali metals, alkaline earth metals and lanthanons), react directly with alcohols with the liberation of hydrogen and formation of metal alkoxides. In the case of comparatively less active metals, like beryllium and aluminium, a catalyst is generally required for successful synthesis of alkoxides.

Another general method of synthesis applicable to electronegative elements (like boron, silicon and phosphorous) is the reaction of their covalent halides with the appropriate alcohol. This method employing the anhydrous chloride as starting material does not appear to effect complete replacement of halide when the central metal atom is comparatively less electronegative.

Another method of general applicability in the case of electronegative elements is the esterification of their oxyacids or oxides (acid anhydrides) with alcohols, removing the water produced in the reaction continuously.

In the Table 2, we listed the main preparation routes adopted for the synthesis of metal alkoxides.

**Table 2:** Synthesis methods of Metal Alkoxides

|  |
|--|
| ➤ Reaction of Metals with Alcohols                     |
| ➤ Reaction of Metal halides with Alcohols              |
| ➤ Reaction of Metal hydroxide and Oxides with Alcohols |
| ➤ Transesterification reactions                        |
| ➤ Reactions of Metal Dialkylamides with Alcohols       |
| ➤ Miscellaneous Methods                                |
| ➤ Alcohol interchange                                  |

About the last method listed in Table 2 and named “Alcohol interchange”, it may be appropriate report more literature information.

It is worth that alkoxy derivates of the element tend to react with all the hydroxyl compounds resulting in the replacement of their alkoxy groups. For example, the reactions of alkoxides with alcohols, generally termed as alcoholysis or alcohol interchange reactions, can be represented by the following general equation:



These alcoholysis reactions have been widely put to synthetic uses for alkoxy derivates of various elements like zinc, aluminium, silicon, zirconium, titanium, vanadium and etc. The facility of alcoholysis reactions appears to depend upon a number of factors which can be summarized as follows:

a) *Interchangeability of different alkoxy groups*

In general, the facility for interchange of alkoxy groups increases from tertiary to secondary to primary groups.

b) *Fractionation in the presence of an inert solvent*

In order to complete an alcoholysis reaction, an excess of the higher boiling solvent reactant alcohol would be required. This can be sometimes avoided by use of a solvent which is higher boiling than even the reactant as well as the product alcohols. When the original alkoxide is ethoxides or isopropoxide, the use of an inert apolar solvent offers added advantage by virtue of the formation of a minimum azeotrope with ethanol or isopropanol which facilitates the removal of the alcohol by fractional distillation.

c) *Solubility factor*

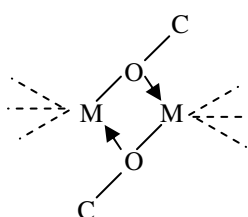
The solubility factor has been found to be quite useful for the synthesis of insoluble alkoxides. For example, when titanium ethoxides or isopropoxide is treated with methanol, an instantaneous reaction occurs with the separation of insoluble methoxides. Thus, the fractionation process is not necessary in such cases where insoluble derivatives are obtained.

#### **1.4.1.3 Physical and chemical properties of metal alkoxides**

The alkoxy derivatives of metals have at least one M–O–C system. Due to the strongly electronegative character of oxygen (electronegativity value, 3.5 on the Pauling scale), alkoxides of metallic elements exhibit strongly polar character. Thus metal-

oxygen bonds in these derivatives could be expected to have around 65% ionic character for metals with electronegativity values of 1.5-1.3 (e.g. aluminium, titanium, vanadium) to about 80% ionic character for more electropositive metals with electronegativity values of the order of 1.2-0.9 (e.g. alkali metals, alkaline earths and lanthanons). However, most of these alkoxides show a fair degree of volatility and solubility in common organic solvents; properties which can be considered as characteristics of covalent compounds.

The two factors, which have been postulated for explaining the attenuation in the polarity of the metal-oxygen bond, are the inductive effect (electron release) of the alkoxy or aryl groups at the oxygen atom (this increases with the branching of the alkyl chain) and the formation of oligomers through dative bonds of the type



The latter tendency is expected to decrease with the ramification on the alkyl group due to the steric factors [28].

#### **1.4.1.4 Metal alkoxides as precursors for the preparation of supported metal oxides by *Grafting***

In recent years, the commercial availability of the metal alkoxides has strongly encouraged the use of these interesting compounds for producing new ceramic materials and thin coating films by using the sol-gel and chemical vapor deposition (CVD) techniques [31]. Alkoxides are also largely used for the preparation of catalysts and/or catalytic supports, normally obtained by precipitation and/or coprecipitation as consequence of hydrolysis [32]. Some papers have recently been published dealing with the preparation of catalysts by anchoring metal alkoxides on the surface of oxides rich of hydroxyls. In particular, different works have been devoted to the preparation of vanadium based catalysts by grafting vanadyl alkoxides on the most common supports, such as  $\text{SiO}_2$ ,  $\text{TiO}_2$ ,  $\text{ZrO}_2$ ,  $\text{Al}_2\text{O}_3$ , with the aim of improving the redox properties and the dispersion of the catalysts prepared [33-37]. Other works have considered the possibility of modifying the acid-base properties of the most common supports by anchoring different metal alkoxides. It is a common practice, for example, to use this technique to immobilize alkaline metals on alumina [35]. More recently, silicated-alumina catalysts, that are active and selective in the skeletal isomerization of 1-butene to isobutene, have been prepared by grafting silicon alkoxide on  $\gamma$ -alumina [38] and on silica [39] as well as the effect of grafting aluminium alkoxides on silica [40] have been studied by Santacesaria et al.

Some papers have also been published on the preparation of titania-based catalysts by grafting titanium alkoxide on silica or alumina supports [36, 41-44]. It was found that this synthesis leads to



a TiO<sub>2</sub>-coated material with a very high dispersion which is useful both as catalytic support and catalyst material. Other works dealt with grafting alkoxides with the aim of modifying acidity of a surface [45].

The preparation of the supported metal oxide based catalysts by **Grafting** is generally based on a specific reaction between the hydroxyl groups (–OH) present onto the surface of the oxide used as support and a highly reactive precursor, such as TiCl<sub>4</sub> or Ti-alkoxide (Ti(O-Pr<sup>i</sup>)<sub>4</sub>), according to the following scheme:



It is well known that it is difficult to prepare well-dispersed supported metal oxide catalysts, especially on the silica surface. However, the hydroxyls generally act as the adsorptive/reactive sites, allowing the anchoring of metals.

The great attention devoted to the grafting technique is namely due to its flexibility. It is possible, in fact, to modify in a tailored way the surface properties of an oxide. Depending on the alkoxide concentration in solution, it is possible to obtain different coverage degrees and modify, consequently, the surface features.

For what concerns the acidity, hydroxyl-rich surfaces can be modified by grafting alkoxides:

- with low coverage degree to obtain, after steaming of the surface and calcination, a high dispersion of the

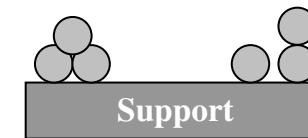
corresponding oxide or isolated acid sites of particular strength;

- with a monolayer, by completely altering the nature of the original surface as to the density of the hydroxyls and the kind of acidity;
- with multilayers, by repeating the treatments of steaming and calcination after each grafting operation, to obtain a solid with a chemically different surface but retaining the original mechanical and structural properties;

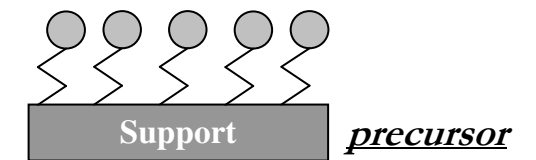
It is also possible, before grafting, to opportunely modify the available alkoxide to make it volatile, when we want to perform a gas-solid phase operation, or soluble in aprotic solvents, if we want a liquid-solid phase reaction, or, at last, it is possible to introduce by reaction another compound in the alkoxide molecule to obtain bifunctionality or superacidity.

So, the main goal of this technique is to direct even more the interaction between metallic precursors and supports. A clear picture of the attaching molecular precursor to specific sites of a support via covalent links is depicted in **Fig. 6**.

Without



With



activation

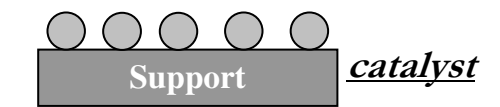
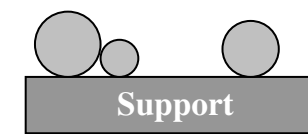
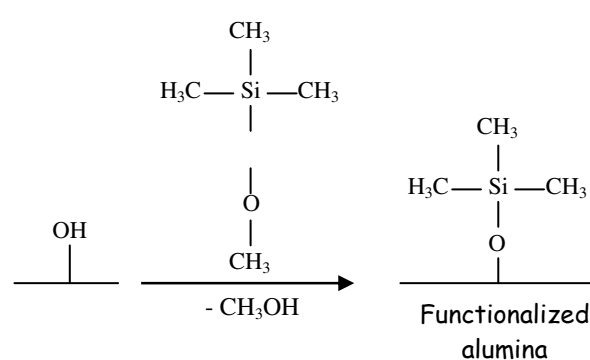


**Fig. 6:** Attachment by *Grafting* of molecular precursors to specific sites of a support via covalent links.

Recently, B. Fremon et al. [47] (IFP-LYON) approached to this preparation technique to improve the preparation of hydrotreating catalysts. They developed a new approach for controlling precursors-alumina interactions through surface functionalization. At this purpose, trimethylmethoxysilane (TMSiOMe) was chosen to functionalize  $\gamma$ -alumina surface. By *grafting* TMSiOMe on the hydroxyls of alumina and thus fine tuning support properties, they tried to modify the interaction between the active phase precursors and alumina during impregnation and drying. In this study, precursors of the active phase have been introduced by equilibrium adsorption alumina as well as of functionalized alumina with  $\text{Co}_2\text{Mo}_{10}(\text{Co})$  based impregnation solutions in order to maximize CoMoS phase formation.

Characterization and catalytic performances in toluene hydrogenation of catalysts prepared on both functionalization and bare supports were also carried out.



**Equation 1:** *Grafting* of TMSiOMe on alumina through reaction with hydroxyl groups.

At last, it is possible to modify the alkoxide (a) by reacting with a stoichiometric amount of water to obtain a partial condensation of the alkoxide molecules before grafting or (b) by preparing, always before grafting, a two metals heterometallic alkoxide.

A similar process of hydrolysis followed by condensation can be also made by using a mixture of two different alkoxides. In this way, not only a precursor of the active site is available but also the most favourable environment for the catalytic action.

Impressive examples of this type of synthesis approach have been reported in literature by Don Tilley et al. [46]. The authors focused on the synthesis of molecular single-source precursors ( $\text{OV}[\text{OSi}(\text{O}^t\text{Bu})_3]_3$ ) to vanadia-silica catalysts, as shown in the **Fig. 7**:

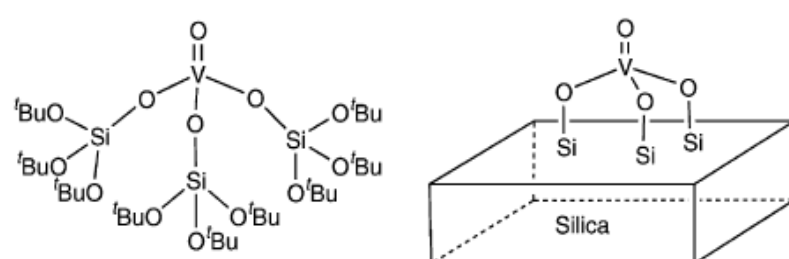
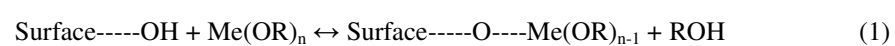


**Fig. 7:** Proposed geometries of isolated vanadium species on a silica surface

In most of cases, the grafting reaction is performed by contacting a given amount of support with an alkoxide solution, generally kept under inert gaseous atmosphere, at room temperature or at boiling solvent temperature, according to the observed reactivity. Apolar solvents are generally preferred giving place to higher grafting yields, provided that the alkoxide are soluble in those solvents. Often the

parent alcohol is used as solvent, but in this case it must be considered that the following equilibrium occurs:



In this condition, the reaction is much less favoured in the presence of an excess of the alcohol. However, this could be an advantage when a high dispersion of the catalyst is required.

The concentration of the alkoxide in the contacting solutions must be decided on the basis of the amount of the element that we want to anchor on the support, but taking into account the yields obtainable, depending on the equilibrium (1) and/or the reactivities of the involved reacting species. By assuming a conventional stoichiometry of 1 alkoxide molecule for 1 hydroxyl on the surface, we can roughly estimate the amount of the alkoxide that is enough for obtaining a monolayer coating. After a grafting experiment, it is possible to determine the yield of the reaction by measuring the amount of residual alkoxide in the solution. After grafting, the solid obtained is normally washed with the used solvent and then submitted to a steam treatment, at 150-190 °C, for eliminating, by hydrolysis, the residual alkoxide groups from the surface. The solid is then calcined at about 500°C. In order to obtain a multilayer coating, the described procedure of grafting, washing, steaming and calcination can be repeated several more times.

It is important to point out that the stoichiometry of the reaction between an alkoxide molecule and the hydroxyl groups, present on the surface of the support, can be responsible for the change of the

hydroxyls density giving place to respectively: an increase of the density for 1 to 1 stoichiometry, a contraction for a 3 hydroxyls to 1 alkoxide stoichiometry, while 2 to 1 stoichiometry gives invariance. Moreover, the overall stoichiometry can change with the concentration of the alkoxide solutions and this brings, in practice, to an average behaviour falling between 1:1 and 2:1.

Another possibility of modifying the grafting precursor is the reaction in a suitable solvent with an acid, for example sulphuric acid, having a strong electron-withdrawing effect on the metal. In this way, it is possible to obtain sulphated complexes of the type  $\text{Me(OR)}_{n-2}\text{SO}_4$  that can be grafted giving place to very strong acid catalysts. It is possible, at last, to favour the condensation of the alkoxides molecules, before grafting, by reacting them with stoichiometry amounts of water, in the presence of traces of HCl for promoting the condensation reaction by partial hydrolysis. The condensation reaction can be made by using only one type of alkoxide or, alternatively, by mixing two different alkoxides that can react with each other, giving place to a bimetallic alkoxide. However, other procedures can be followed for obtaining hetero-metallic alkoxides [48] to be grafted. The preparation of hetero-metallic alkoxides opens new perspective in the field of the preparation of catalysts by grafting technique.

## **2. Strategy and content of the thesis**

Heterogeneous catalysts are highly complex solids in which specific chemical functionalities are organized in such a way that

they are accessible to the reactants, ideally in an optimized fashion. The complexity refers to chemical, structural and textural levels, which all have a deep impact on the performances. Because of this multi-level complexity, the preparation methods have been continuously adapted and improved, essentially on the basis of experimental structure-activity relationships deduced from characterizations of the fresh and used catalysts. In recent years, the increasing availability of sophisticated *in-situ* and *operando* spectroscopic techniques has allowed to obtain pictures that can be considered “movies” of real catalysts at work. However, it is common opinion now that these dynamic aspects can ultimately be mastered only if more attention is paid to the characteristics of the catalytic materials, in a “back to basics” approach focused on defined precursors and innovative preparation methods.

This feeling is at the origin of the huge interest and the numerous efforts directed, during these three years of my PhD, for fine tuning the preparation of supported metal oxide materials, that are the main class of heterogeneous catalysts which play a key role in the production of petrochemicals, intermediates and fine chemicals and energy applications, as well as in environmental protection.

It is clear that the field of supported metal oxide catalysts is huge. So, I focused the PhD work on the preparation, characterization and catalytic performances of supported titanium and vanadium based catalysts.

The work described in this thesis was done at the **Naples Industrial Chemistry Laboratory (NICL)**, directed by Prof. Elio



Santacesaria) – Department of Chemistry - University of Naples “Federico II”.

The aim of this thesis has been to provide understanding of the relationships between the surface chemical properties of the catalysts and their catalytic performances, by investigating mainly the effect of preparation method, nature of the support and metal loading on the catalytic behaviour.

More precisely, I focused the research work on the study of vanadia based catalysts supported on the surface of different oxides, such as:  $\text{SiO}_2$ ,  $\text{TiO}_2$  and  $\text{TiO}_2/\text{SiO}_2$ . In all the cases, the experimental work has been performed on three different levels: preparation, characterization and catalytic performances of the supported vanadium based catalysts in the Oxidative Dehydrogenation (ODH) reactions of both alkanes to alkenes and alcohols to aldehydes. In particular, I studied the catalytic performances of the mentioned catalytic systems in the following reactions: ODHs of n-butane to butenes, methanol to formaldehydes and ethanol to acetaldehyde. In the latter cases, the thesis aimed to reach a complete understanding of the reaction mechanism.

Great attention was also devoted to the silica-supported titania catalysts, which represent an interesting example of advanced supports and catalytic nanomaterials applied in a wide range of reactions.

Due to the differences in these subjects, I organized this thesis in three different parts: part A, part B and part C. Each part aims to achieve a specific objective.

Part A aims to investigate the preparation, characterization and reactivity properties of  $\text{TiO}_2/\text{SiO}_2$  catalysts. Part B is completely

dedicated to the study of the catalytic performances of supported vanadia catalysts in the ODHs of both n-butane to butenes and methanol to formaldehyde. Finally, in Part C the kinetic study of vanadium based catalysts in the ODHs of both methanol to formaldehyde and ethanol to acetaldehyde is analysed in detail.

In the first part of the thesis, a general introduction of the subject is given in Chapter I, which reports a systematic investigation of the most recent results reported in literature about the preparation, characterization and catalytic performances of silica-supported titania ( $\text{TiO}_2/\text{SiO}_2$ ) catalysts. This effort has been made to provide a clear picture of the state of the art about the supported  $\text{TiO}_2/\text{SiO}_2$  catalysts in order to clarify the structure-property relationships. Special emphasis is attributed to the influence of the variables involved in the preparation routes on both the surface molecular dispersion and the reactivity properties of the supported titanium sites onto the silica surface. Combined results of different preparation/characterization techniques demonstrated that several factors are critical in controlling the dispersion capacity or the maximum surface coverage of titanium oxide species on silica: the concentration of surface hydroxyls and the specific surface area of silica, the pretreatment temperature and the maximum surface coverage of the precursors molecules.

The experimental section of the part A is then split in Chapter II and Chapter III.

Chapter II reports the investigation of the catalytic activity of a series of  $\text{TiO}_2/\text{SiO}_2$  catalysts in the transesterification of refined oils with methanol (*biodiesel production*). The catalysts were prepared by *grafting*

different amounts of  $\text{Ti}(\text{O}-\text{Pr}^i)_4$ , dissolved in an opportune anhydrous solvent, onto surface hydroxyls of silica. This approach resulted very useful to study the chemical adsorption of Ti-alkoxide onto silica surface. The maximum surface monolayer coverage of silica (Grace S432, specific surface area =  $282 \text{ m}^2/\text{g}$ , specific pore volume =  $1.02 \text{ cm}^3/\text{g}$ , hydroxyl groups =  $0.92 \text{ mmol/g}$ ) by  $\text{Ti}(\text{O}-\text{Pr}^i)_4$  precursors was found to be  $\sim 2.2 \text{ Ti atoms/nm}^2$  by adopting a one-step grafting procedure. The influence of the nature of the solvent, used for dispersing the mentioned alkoxide, and of Ti-loading on the final surface catalyst dispersion was also investigated. Thus, several characterization techniques, such as BET measurements,  $\text{NH}_3$ -TPD, RAMAN and XPS spectroscopies, were used. Moreover, an in-dept study of the grafted acidic titanium sites was carried out by both  $\text{NH}_3$ -TPD analyses and FT-IR spectroscopy of adsorbed CO and  $\text{NH}_3$ . In particular, the latter one enable us to establish interesting correlations between the electrophilic nature of supported  $\text{Ti}^{4+}$  sites, e.g. the acid strength of titanium cations, and their catalytic performances in the transesterification reaction of refined oil with methanol. Finally, the catalytic tests of the prepared  $\text{TiO}_2/\text{SiO}_2$  catalysts in biodiesel production showed that isolated  $\text{Ti}^{4+}$  cations have an appropriate Lewis acid strength to catalyze efficiently the transesterification of refined oil with methanol. Pure  $\text{TiO}_2$  resulted no active in the same reaction.

Chapter III presents the results of the investigation aiming at i) evaluating the influence of a different preparation procedure adopted on the surface structure and reactivity properties of the grafted

titanium sites and ii) evaluating their catalytic behaviour in the epoxidation reaction of cyclooctene with cumene hydroperoxide. We selected this reaction because it is very sensitive to the surface structure of the supported titanium species and, thus, very suitable to achieve the specific objective. As already reported in Chapter II, also in this case the deposition of increasing quantities of  $\text{TiO}_2$  onto silica surface was carried out by chemisorption of titanium alkoxide precursor  $(\text{Ti-OPr}^i)_4$ , dissolved in anhydrous toluene, onto surface hydroxyl groups of the support, followed by hydrolysis with steam water and calcination. The experimental evidences achieved suggested that grafting titanium alkoxide on the silica surface in toluene occurs easily and quantitatively for low coverage degree, giving place to highly dispersed titanium forming a monolayer. This aspect was confirmed by both XRD and TEM analyses, which showed a homogeneous surface dispersion until to the monolayer coverage. The attempt to obtain multilayer coatings of silica by repeating more times the grafting operation brings to the formation of amorphous agglomerates characterized by a lower surface  $\text{TiO}_2$  dispersion, as indicated by DRIFT analyses from a semi-quantitative point of view. However, BET results showed that the specific surface area does not change significantly with titanium loading, confirming in this way the possibility to prepare by grafting high-surface supported titania catalysts. All these observations appeared to be in agreement with the catalytic performances of  $\text{TiO}_2/\text{SiO}_2$  catalysts in the epoxidation reaction. The trend of the catalytic data showed that both the activity and the selectivity are influenced by the coordination environment of the surface titanium. At last, once again, the surface area and the

concentration of the hydroxyl groups of the SiO<sub>2</sub> resulted to be crucial to achieve good dispersion of the active sites and good catalytic performances in the epoxidation reaction.

As stated before, part B of the thesis deals with the study of the catalytic performances of supported vanadia based catalysts in the oxidative dehydrogenation reactions of n-butane to butenes and methanol to formaldehyde.

In particular, the second part of the work begins with Chapter IV that introduces the supported vanadium oxide based catalysts as very complex inorganic materials that play an important role in heterogeneous catalysis in both the gas and the liquid phase. This review/chapter reports an in-dept investigation about the current knowledge available in literature about this type of catalysts. Great attention is addressed to the several aspects ranging from the preparation methods, characterization techniques of molecular structures of vanadium oxides on the surface of different inorganic oxides/supports to the catalytic performances in the ODH reactions. The understanding of the fundamental relationships between the molecular structure of the different supported vanadium oxide species and their catalytic behaviour in reactions of interest in industrial field, such as the oxidative dehydrogenation (ODH) reactions of both alkanes to alkenes and alcohol to aldehydes, represented the main goal of this chapter. From the literature survey, it appears evident that the support characteristics (i.e., structure and chemical composition) have a tremendous impact on the properties of the supported vanadium

oxide catalysts. This support–effect results in the formation of specific, often not-well defined, molecular structures of metal oxides with, for example, special redox properties. A better insight into the formation and local structure of these molecular structures can be only obtained by paying more attention not only to the characterization techniques, preferably under *in situ* conditions, but also to new preparation methods for efficiently obtaining and stabilizing such materials.

Chapter V of the experimental section of part B focused on the study of the oxidative dehydrogenation reaction (ODH) of n-butane to butenes on supported vanadium based catalysts. For this purpose, many different vanadium based catalysts have been prepared and tested in the target reaction, with the aim to investigate the influence of several factors, such as: vanadium loading, type of support and synthesis procedure. The catalysts were prepared both by impregnation and grafting for a useful comparison. In particular, the grafting procedure was studied by contacting solutions of increasing concentrations of vanadyl tri-isopropoxide, dissolved in dioxane, with two different supports: SiO<sub>2</sub> and TiO<sub>2</sub>/SiO<sub>2</sub>. Grafting adsorption behaviour was studied using the isotherms obtained in the two cases. On silica we obtained an isotherm with two different recognisable plateaux. On the contrary, in the adsorption on TiO<sub>2</sub>/SiO<sub>2</sub> the system followed the Langmuir adsorption law with a saturation value at about 7% of adsorbed V<sub>2</sub>O<sub>5</sub>. By greatly increasing the vanadyl concentration multi-layer adsorption seems to occur. In this latter case, catalysts obtained after calcination resulted less dispersed. All these catalysts

were characterised by using many different techniques (XRD, DRUV, DRIFT, RAMAN and XPS) and tested in the ODH of butane. The results obtained showed the beneficial effect in the use of  $\text{TiO}_2/\text{SiO}_2$  support, prepared by grafting titanium alkoxide on silica, for preparing vanadium catalysts. We observed that, in this support, silica increases the ionicity of the Ti-O bonds. This favours the successive grafting of vanadyl tri-isopropoxide with a more defined structure, giving place after calcination to a relatively uniform class of catalytic sites that are, very probably, responsible for the higher selectivities observed. In fact, of the three different sites reported in the literature for vanadia catalysts, i.e., vanadium not isolated with tetrahedral coordination,  $\text{V}^{5+}$  species in square-pyramidal coordination and  $\text{V}^{5+}$  in distorted octahedral coordination, only one has been found largely prevalent in the catalysts prepared by grafting, corresponding to square-pyramidal coordination. These sites resulted to be the most selective ones. In particular, catalysts preparation by grafting allowed to increase the density of these sites, while, preparation by impregnation gave place to a broad site distribution and lower selectivity as a consequence. The dramatic effect of the type of support on the catalysts performances was further confirmed. In particular, the aggregation of vanadium oxide directly grafted on silica was demonstrated by both the low activities shown by these catalysts and by the presence of sites of different types on the surface. The best catalyst resulted the one prepared by grafting and containing 4.78 % wt  $\text{V}_2\text{O}_5$  on TSM support. This catalyst retains the high dispersion, characteristic of the sub-monolayer systems, giving place to the best catalytic performances in terms of both activity and selectivity. By

increasing further the vanadium loading, the activity increases but the selectivity strongly decreases for the appearance of other different active sites.

Chapter VI reports the results of the investigation of the catalytic screening of the oxidative dehydrogenation (ODH) of methanol to formaldehyde on supported vanadium based catalysts. The catalytic evolution of methanol is informative of the surface structure and behaviour of the catalyst and, in fact, it has been widely used in the literature as a test reaction. A wide range of by-products (e.g. dimethyl ether, dimethoxymethane, methyl formate, carbon oxides, hydrocarbons) can be obtained depending on both the redox properties and the acidity of the catalyst which, in turn, depend on the interaction between the active phase and the support. Thus, motivated to better understand the relationships between the surface properties and the catalytic performances of vanadia catalysts in the ODH of methanol, but first of all, motivated to develop a detailed kinetic analysis of the reaction, we decided to perform our work in two stages:

- 1) catalytic screening of the reaction by using different vanadia based catalysts prepared by *grafting*.
- 2) a kinetic study, which has been carried out on a nanostructured-vanadium catalyst, selected in the previous screening (details are given in Chapter VII).

The influence of the preparation method on the surface structure, acidic properties and catalytic activity was demonstrated by examining also the corresponding conventionally impregnated



catalysts. The catalysts were characterized by chemical analysis, BET, TPD, RAMAN and XPS spectroscopies and tested in the ODH of methanol to formaldehyde.

The results obtained showed that several factors influence the activity of vanadium based catalysts. They can be classified in two groups:

- a) Vanadium loading, preparation procedure and nature of the support, for what concerns the catalysts.
- b) Reaction temperature and feed composition, for what concerns the reaction operative conditions. For example, we noted that a small amount of water (2%), fed together with the other reactants, enhances both the activity and formaldehyde selectivity.

Thus, it is very important to tune both the catalysts properties and the operative conditions to obtain good catalytic results, specially in terms of formaldehyde selectivity. On the contrary, the selectivity to formaldehyde seems to be mainly influenced by the level of the methanol conversion achieved. Indeed, this study pointed out that the *grafting* method is very useful to prepare well-dispersed catalysts, an indispensable condition to design active and selective catalysts for the ODH reaction of methanol. In fact, the catalyst prepared according to the suggested procedure gave the best results when compared with the impregnated catalyst, characterized by the same amount of active species. A positive trend of selectivity with conversion was observed for all the catalysts of the  $V_{\text{graf}}/\text{TSM}$  series and attributed to the reaction sequence: methanol  $\rightarrow$  dimethoxymethane  $\rightarrow$  formaldehyde.

Finally, part C of the thesis reports the results about the kinetic study of the ODH of methanol to formaldehyde (Chapter VII) and ethanol to formaldehyde (Chapter VIII) on a nano-structured  $V_2O_5/TiO_2/SiO_2$  catalyst.

The investigation reported in Chapter VII allows to draw a complete picture of the catalytic mechanism of the Oxidative Dehydrogenation of methanol to formaldehyde by supported vanadium based catalysts. A detailed kinetic analysis of the reaction was carried out on a nano-structured supported vanadium oxide catalyst, selected in a preliminary catalytic screening. An exhaustive set of experimental runs was conducted in an isothermal packed bed tubular reactor by investigating several operative conditions, such as: temperature, contact time, methanol/oxygen feed molar ratio and water feed concentration. In this way, a detailed kinetic model was developed to interpret the collected integral data of a tubular packed-bed reactor. The adopted reaction rate expressions was of the Mars van Krevelen – Langmuir Hinshelwood type and a good agreement was found between the model theoretical prediction and the experimental data. The kinetic model was formulated on the basis of a reaction mechanism that led us to a rake-type reaction scheme in which all the observed products away from adsorbed species of methanol, formaldehyde and formic acid. The agreement between the model and the experimental data can be considered satisfactory and the latter ones could be used, in perspective, to simulate pilot-plant data with a sufficient reliability.

A similar approach was adopted to study from a kinetic point view the ODH of ethanol to acetaldehyde, whose results are given in Chapter VIII. The investigation showed that, also in this case, catalysts prepared by grafting vanadyl tri-isopropoxide on the surface of silica coated with  $\text{TiO}_2$  are very active and selective. This type of catalyst ( $\text{V}_2\text{O}_5/\text{TiO}_2/\text{SiO}_2$ ) gives rise to high conversion of ethanol to acetaldehyde at very low temperature (130-180 °C), which represents a useful perspective in view of industrial applications. The high dispersion of the catalyst strongly improves the selectivity and the activity is a linear function of supported vanadium amount. Acetaldehyde is relatively stable on this catalyst and this is the reason for the high selectivities observed. The acid and basic properties of the catalyst have a minimal influence on the catalyst performance in this reaction, and therefore, only the redox properties are responsible for the reaction. The mechanism of the reaction does not involve surface lattice oxygen, because, at the temperature used, the oxygen exchange reaction is too slow. We have suggested two different possible mechanisms that, when simplified, correspond in the kinetic analysis to a classical Mars and van Krevelen kinetic law. The kinetic parameters for all of the occurring reactions were evaluated and the activation energy found for the main reaction to acetaldehyde is in agreement with the values reported in the literature on the same type of catalyst.

At last, discussion about similarities and differences found for methanol and ethanol oxidative dehydrogenation conclude the part C.

The most important conclusions of the PhD work are summarized in the last section of the thesis.

### 3. References

- [1] I. Chorkendoff, J.W. Niemantsverdriet, “*Concepts of Modern Catalysis and Kinetics*”, **2003**, WILEY-VCH GmbH & Co.
- [2] M. Bowker, *The Basis and Application of Heterogeneous Catalysis* (1998), Oxford University Press, Oxford.
- [3] J.M. Thomas and W.J. Thomas, *Principles and Practice of Heterogeneous Catalysis* (1997), VCH, Weinheim.
- [4] G. Ertl, H. Knözinger and J. Weitkampp (Eds.), *Handbook of Heterogeneous Catalysis* (1997), VCH, Weinheim.
- [5] G.A. Somorjai, *Introduction to Surface Chemistry and Catalysis* (1994), Wiley, New York.
- [6] J.A. Moulijn, P.N.W.M. van Leeuwen, R.A. van Santen (Eds.), *Catalysis: an Integrated Approach to Homogeneous, Heterogeneous and Industrial Catalysis* (1993), Elsevier, Amsterdam.
- [7] B.M. Weckhuysen, *Nature*, **2006**, 439, 548.
- [8] B.C. gates, *Catalytic Chemistry* (1992), Wiley, new York.
- [9] I.M. Campbell, *Catalysis at Surface* (1998), Chapman & hall, London.
- [10] M. Boudart and G. Djega-Mariadassou, *Kinetic of Heterogeneous Catalytic reactions* (1984), Princeton University press, Princeton.
- [11] J.R. Anderson and M. Boudart, *Catalysis, Science and Technology*, Springer, Berlin, several volumes from 1981.
- [12] B.C. gates, J.R. Katzer and G.C.A. Shuit, *Chemistry of catalytic Processes* (1979), McGraw Hill, New York.
- [13] R.A. van Santen and J.W. Niemantsverdriet, *Chemical Kinetics and Catalysis* (1995), plenum, New York.

- [14] D. Sanfilippo, *The Catalytic Process from Laboratory to the Industrial Plant*, 3<sup>rd</sup> Seminar of Catalysis, Rimini, June 19-24, 1999.
- [15] The CONCORDE NSCOCRA White Paper – A technology Roadmap on Nanostructured Oxide Catalysts for Redox Applications, SOCINTEC, Group AZERTIA.
- [16] Recent advances in nanotechnologies research, Paper Applied Catalysis Elsevier (2001).
- [17] Nanoscale Science, Engineering and Technology Research Directions, U.S. Department of Energy – Basic Energy Sciences, Nanosciences/Nanotechnology Group (2000).
- [18] J. Hagen (Eds.), *Industrial catalysis: A Practical Approach*. Wiley-VCH: Weinheim, 1999.
- [19] P.A. Jacobs et al., *Studies in Surface Science and Catalysis*, **2006**, 162, 259.
- [20] H.J.H. Fenton, J. Chem. Soc., **1894**, 65, 899.
- [21] I. Melian-Cabrera et al, *Studies in Surface Science and Catalysis*, **2006**, 162, 37.
- [22] T. Myiao et al., Chemistry Letters, **1999**, 1125.
- [23] A. J. Zarur, Nature, **2000**, 403, 65.
- [24] S. naito et al., *Studies in Surface Science and Catalysis*, **2006**, 162, 63.
- [25] S. Hermans, P.Ruiz, M. Dellivers, E.M. Gaigneaux, *Book of Abstracts*, 4<sup>th</sup> EFCATS School on Catalysis, Tsars Village (St. Petersburg), Russia.
- [26] J.A. Bergwerff, *Studies in Surface Science and Catalysis*, **2006**, 162, 175.
- [27] J.A. Bergwerff et al., *J.Am. Chem. Soc.*, **2004**, 126, 14548.

- [28] J.M. Connolly and G.M. Dyson, *J. Chem. Soc.*, 828 (1973).
- [29] A. Lamy, *Ann. Chim.*, **1864**, 3, 373.
- [30] W.A. Kahlbaum, K. Roth and P. Seidler, *Z. Anorg. Alleg. Chem.*, 1902, 29, 223.
- [31] L.L. Hench and J.K. West, *Chem. Rev.*, **1990**, 90, 33.
- [32] S. Klein, S. Thorimbert and W.F. Mayer, *J. Catal.*, **1996**, 163, 476.
- [33] J. Kijenski, A. Baiker, M. Glinski, P. Dollenmeier, A. Wokaun, *J. Catal.*, 1986, 101, 1.
- [34] M. Schraml-Marth, A. Wokaun, A. Baiker, *J. Catal.*, **1990**, 124, 86.
- [35] U. Scharf, M. Schraml-Marth, A. Wokaun, A. Baiker, *J. Chem. Soc. Faraday Trans.*, **1991**, 87, 3299.
- [36] A. Fernandez, J. Leyrer, A.R. Gonzalez-Elipé, G. Munuera, H. Knoezinger, *J. Catal.*, **1988**, 112, 489.
- [37] S. Srinivasan, A.K. Datye, M.H. Smith, C.H.F. Peden, *J. Catal.*, **1994**, 145, 565.
- [38] P. Iengo et al., *Applied Catalysis A: General* **1998**, 170, 225.
- [39] P. Iengo et al. / *Applied Catalysis A: General*, **1999**, 178 97.
- [40] P. Iengo, M. Di Serio, A. Sorrentino, V. Solinas, E. Santacesaria, *Appl. Catal. A*, **1998**, 167, 85.
- [41] M.G. Reichmann, A.T. Bell, *Appl. Catal.*, **1987**, 32, 315.
- [42] A. Munoz, G. MunÄera, in: G. Poncelet, P.A. Jacobs, P. Grange, B. Delmon (Eds.), *Preparation of Catalysts V*, Stud. Surf. Sci. Catal., **1991**, 63, 627.
- [43] P. Wauthoz, M. Ruwet, T. Macheij, P. Grange, *Appl. Catal.*, **1991**, 69, 149.

- [44] D.F. Ollis, E. Pelizetti, N. Serpone, *Environ. Sci. Technol.*, **1991**, 25, 1523.
- [45] R. Castillo, B. Koch, P. Ruiz, B. Delmon, *J. Catal.*, **1996**, 161, 524.
- [46] T.D. Tilley et al., *Journal of Molecular Catalysis A: Chemical*, 2002, 182–183, 17.
- [47] B. Fremon et al., *Studies in Surface Science and Catalysis*, **2006**, 162, 291.
- [48] K.C. Caulton, L.G. Hubert-Pfalzgraf, *Chem. Rev.*, **1990**, 90, 969.





# **PART A**

**TiO<sub>2</sub>/SiO<sub>2</sub> catalysts:**

**Preparation, Characterization  
and Reactivity properties**



# I

## INTRODUCTION

### **Abstract**

This chapter reports a systematic investigation of the literature about recent results on preparation, characterization and catalytic performances of silica-supported titania ( $\text{TiO}_2/\text{SiO}_2$ ) catalysts. This effort is made to provide a clear picture of the state of the art about the supported  $\text{TiO}_2/\text{SiO}_2$  catalysts to clarify the structure-property relationships. Special emphasis is attributed to the influence of the variables involved in the preparation routes on both the surface molecular dispersion and the reactivity properties of the supported titanium sites onto the silica surface.

Combined results of different preparation/characterization techniques demonstrated that several factors are critical in controlling the dispersion capacity or the maximum surface coverage of titanium oxide species on silica: the concentration of surface hydroxyls and the

specific surface area of silica, the pretreatment temperature and the maximum surface coverage of the precursors molecules.

### **1.1 TiO<sub>2</sub>/SiO<sub>2</sub> oxides: an example of advanced supports and catalytic nanomaterials**

Heterogenisation of catalytic homogeneous systems for selective oxidation reactions in liquid phase is still currently considered a priority research field.

The heterogeneous systems display clear advantage compared to their homogeneous counterparts such as ease of recovery and recycling of active species and consequently being more attractive from an environmental point of view.

Furthermore, heterogeneous catalytic systems have the potential to be used in gas phase processes (i.e., without solvent), which may result in appreciably lower operating cost [1].

In this context, serious efforts have been addressed towards the preparation of heterogeneous Ti(IV) catalysts for oxidation reactions and numerous strategies have been described in the literature for the immobilization of redox-active species within an in-organic matrix, in order to minimize the leaching phenomena [1].

*Titania-silica*, including both mixed and supported oxides, represents a novel class of materials that have attracted much attention in recent years.

These solids have extensively been used as efficient catalysts and supports for a wide variety of reactions, as summarized in Table 1.1,

such as: selective oxidations [2] and epoxidations of olefins with alkyl hydro-peroxide [3], isomerization [4], dehydration [5], esterification and transesterification reactions [6-8].

Table 1.1: Summary of various reactions for titania-silica as catalysts and supports

| Catalysts   | Preparation method           | Reaction temperature (K) | Reactions  | Reference     |
|---|------------------------------|--------------------------|--|---------------|
| TiO <sub>2</sub> -SiO <sub>2</sub>                                | Sol-gel                      | RT                       | Photodecomposition of chlorinated phenols                                      | [1,2]         |
| TiO <sub>2</sub> -SiO <sub>2</sub>                                | Sol-gel/CVD                  | RT                       | Photoreduction of CO <sub>2</sub>  | [3,4]         |
| TiO <sub>2</sub> -SiO <sub>2</sub>                                | Sol-gel                      | RT                       | Photodecomposition of rhodamine-6G and phenol                                  | [5,6]         |
| TiO <sub>2</sub> -SiO <sub>2</sub>                                | Sol-gel                      | 380                      | Complete photocatalytic oxidation of C <sub>2</sub> H <sub>4</sub>             | [7]           |
| TiO <sub>2</sub> /SiO <sub>2</sub>                                | Impregnation                 | RT                       | Photooxidation of propane  | [8]           |
| TiO <sub>2</sub> /SiO <sub>2</sub>                                | Precipitation                | 673                      | Catalytic decomposition of 1,2-dichloroethane                                  | [9]           |
| TiO <sub>2</sub> -SiO <sub>2</sub>                                | –                            | 823                      | Catalytic decomposition of Freon 12  | [10]          |
| TiO <sub>2</sub> /SiO <sub>2</sub>                                | Precipitation                | 523–673                  | Catalytic decomposition of chloroform  | [11]          |
| TiO <sub>2</sub> -SiO <sub>2</sub>                                | Sol-gel/coprecipitation      | 423–523                  | Isomerization of 1-butene  | [12–18]       |
| TiO <sub>2</sub> -SiO <sub>2</sub>                                | Sol-gel                      | 523                      | Isomerization of methylcyclohexane to propanal                                 | [18]          |
| TiO <sub>2</sub> -SiO <sub>2</sub>                                | Sol-gel/coprecipitation      | –                        | Methanol dehydration   | [19]          |
| TiO <sub>2</sub> -SiO <sub>2</sub>                                | Coprecipitation              | 493                      | Ethene hydration   | [15]          |
| TiO <sub>2</sub> -SiO <sub>2</sub>                                | Coprecipitation              | 723                      | Phenol amination   | [15]          |
| TiO <sub>2</sub> -SiO <sub>2</sub>                                | Coprecipitation              | 673                      | Cumene desalkylation   | [20]          |
| TiO <sub>2</sub> -SiO <sub>2</sub>                                | Sol-gel                      | –                        | Decane hydrocracking   | [21]          |
| TiO <sub>2</sub> -SiO <sub>2</sub>                                | Sol-gel/impregnation         | –                        | Propanol dehydration   | [12,20,36,37] |
| TiO <sub>2</sub> -SiO <sub>2</sub>                                | Coprecipitation              | 303                      | Solvolysis of <i>cis</i> -2,3-epoxybutane                                      | [22]          |
| TiO <sub>2</sub> -SiO <sub>2</sub>                                | Sol-gel                      | 493                      | Aminoxidation of cyclohexanone   | [23]          |
| TiO <sub>2</sub> -SiO <sub>2</sub>                                | Sol-gel                      | 333                      | Epoxidation of $\alpha$ -isophorene by TBHP                                    | [24,25]       |
| TiO <sub>2</sub> -SiO <sub>2</sub>                                | Sol-gel/coprecipitation      | 323–363                  | Epoxidation of olefins by TBHP/NBH <sub>4</sub> PH <sub>2</sub> O <sub>2</sub> | [21,22,26–31] |
| TiO <sub>2</sub> /SiO <sub>2</sub>                                | Impregnation                 | 363–383                  | Epoxidation of olefins by TBHP/EBHP  | [31–33]       |
| TiO <sub>2</sub> -SiO <sub>2</sub>                                | Sol-gel                      | 353                      | Selective oxidation of cyclohexane by TBHP                                     | [34]          |
| TiO <sub>2</sub> -SiO <sub>2</sub>                                | Sol-gel                      | 353                      | Hydroxylation of phenol by H <sub>2</sub> O <sub>2</sub>                       | [35]          |
| TiO <sub>2</sub> -SiO <sub>2</sub>                                | Sol-gel                      | 353                      | Oxidation of benzene and toluene by H <sub>2</sub> O <sub>2</sub>              | [35]          |
| TiO <sub>2</sub> /SiO <sub>2</sub>                                | Impregnation                 | 503                      | Methanol oxidation   | [36,38]       |
| Rh/TiO <sub>2</sub> -SiO <sub>2</sub>                             | Sol-gel                      | 303                      | Benzene hydrogenation  | [39]          |
| Ni/TiO <sub>2</sub> -SiO <sub>2</sub>                             | Coprecipitation              | 548                      | CO hydrogenation   | [14]          |
| CrO <sub>3</sub> /TiO <sub>2</sub> -SiO <sub>2</sub>              | Coprecipitation/impregnation | 373–383                  | Ethylene polymerization  | [40,41]       |
| V <sub>2</sub> O <sub>5</sub> /TiO <sub>2</sub> -SiO <sub>2</sub> | Sol-gel/impregnation         | 370–570                  | SCR of NO with NH <sub>3</sub>   | [42–44]       |
| V <sub>2</sub> O <sub>5</sub> /TiO <sub>2</sub> -SiO <sub>2</sub> | Coprecipitation              | 353                      | Synthesis of isobutyraldehyde from ethanol+methanol                            | [45]          |
| V <sub>2</sub> O <sub>5</sub> /TiO <sub>2</sub> /SiO <sub>2</sub> | Precipitation                | 423–823                  | NO reduction with CO   | [46]          |
| V <sub>2</sub> O <sub>5</sub> /TiO <sub>2</sub> /SiO <sub>2</sub> | Precipitation                | 600–700                  | Selective oxidation of toluene   | [47]          |
| V <sub>2</sub> O <sub>5</sub> /TiO <sub>2</sub> /SiO <sub>2</sub> | Precipitation                | 533–673                  | Selective oxidation of <i>o</i> -xylene  | [48]          |

In the last decades, a large volume of literature has been generated on titanium-substituted zeolites in the framework, including TS-1 [9], Ti- $\beta$  [10], Ti-incorporated ordered mesoporous silica [11,12] and amorphous xerogels.

Great attention has been devoted to the study of their catalytic performances in epoxidation reactions of the olefinic substrates with hydrogen peroxide and alkyl hydroperoxides [2,3].

However, despite good activity with alkyl hydroperoxides, the catalytic performances of most the solids mentioned above with hydrogen peroxide appeared far from that of TS-1, whose catalytic performance resulted superior to titania-silica mixed catalysts, but limited sterically to relatively small reactants that are capable of penetrating into the narrow channels where most active sites are located.

To overcome this drawback, new catalytic systems, based on zeolitic or amorphous materials (Ti-MCM-41 [13], Ti-MCM-48 [14], Ti-HMS [15] and Ti-MSU [16]), were developed.

However, the catalytic activity of these modified hydrothermal mesoporous materials was quite small as compared to that shown by TS-1 and Ti- $\beta$ -zeolites. So, alternative approaches were developed for the covalent attachment of Ti species onto the internal mesoporous silica surface.

In the last years, the utility and applications of supported metal oxides on silica substrates have attracted growing interest towards the production of catalysts characterized by the presence of high

percentage of the metal oxide in a dispersed state (two-dimensional surface metal oxide overlayers) [17-20].

An interesting example is given by supported titania on silica catalysts ( $\text{TiO}_2/\text{SiO}_2$ ), which have been considered as advanced support materials as substitutes for pure  $\text{TiO}_2$ . The higher mechanical strength, thermal stability and specific surface area of the supported titania oxides, respect to  $\text{TiO}_2$ , have attracted much attention and driven the interest towards the use of these materials not only as catalytic supports, but also as catalysts through the generation of new catalytic active sites [3-8]. Titanium oxide modified silica takes advantage of the properties of  $\text{TiO}_2$  (an n-type semiconductor and an active catalytic support) and  $\text{SiO}_2$  (large surface area, high thermal stability and good mechanical strength).

In general, the applications of titania/silica materials as catalysts and supports fall into three categories based on their unique physico-chemical properties [21]: (i) photocatalysis that is associated with the support effect and the quantum-size of the particles; (ii) acid and/or oxidation catalysis that are related to the generation of new acid sites due to the interaction of  $\text{SiO}_2$  with  $\text{TiO}_2$ ; and (iii) excellent catalytic support materials that possess enhanced thermal and mechanical stability due to  $\text{SiO}_2$  while preserving the catalytic performance of  $\text{TiO}_2$ .

In the past years, great attention has been addressed to the structural properties of titania-silica materials, generally prepared by sol-gel and coprecipitation methods, trying to understand the



relationships between the physico-chemical properties and their reactivity in a wide range of applied reactions.

A recent review, proposed by X. Gao and I.E. Wachs [21], focused on the investigation and development of amorphous titania-silica mixed oxides as catalysts, attributing special emphasis on the structural characterization and establishment of the relationships between the structural characteristics and the reactivity properties. A comparison with the structural properties of the supported titania/silica oxides has also been reported.

However, despite the large number of papers devoted to the amorphous mixed  $\text{TiO}_2$ - $\text{SiO}_2$  oxides, only few attention has been paid to investigate the molecular structure of the supported Ti-sites onto silica surface and its influence on their catalytic behaviour.

In the present chapter, recent results about the preparation, characterization and catalytic studies of silica-supported titania ( $\text{TiO}_2/\text{SiO}_2$ ) catalysts have been reviewed on the basis of combined results of different preparation/characterization techniques and research-investigations.

In this way, an effort was made in order to provide a clear picture of the state of the art about the supported  $\text{TiO}_2/\text{SiO}_2$  catalysts to clarify the structure-property relationships.

Special emphasis will be attributed to the influence of the variables involved in the preparation routes on both the surface molecular dispersion and reactivity properties of the supported titanium sites onto silica surface.

## 1.2 Preparation of supported titania/silica materials

In contrast to the mixed oxides, generally indicated as  $\text{TiO}_2\text{-SiO}_2$ , the supported titania/silica materials ( $\text{TiO}_2/\text{SiO}_2$ ) present the peculiarity that the specific interaction between  $\text{TiO}_2$  and the silica substrate is limited to the surface.

It is well known from the literature that the silica surface is quite inert with respect to the other oxide supports and, consequently, it is quite difficult to reach monolayer dispersion of titanium oxide species on silica, because many factors seem to determine the dispersion capacity of the silica surface.

The structure of the surface of silica is characterized by either siloxane groups with the oxygen on the surface ( $\equiv\text{Si-O-Si}\equiv$ ) or one of three types of hydroxyls: isolated hydroxyls, ( $\equiv\text{SiOH}$ ), H-bonded hydroxyls ( $\equiv\text{SiO-H}\cdots\text{OH-Si}\equiv$ ) and geminal hydroxyls ( $=\text{Si}(\text{OH})_2$ ) [22].

Of all the chemical surface modification reactions on silica, the surface hydroxyls generally act as the adsorptive/reactive sites because of their hydrophilic character. The highest concentration of hydroxyls on the silica surface is preferred in order to prepare high surface coverage of molecularly dispersed  $\text{TiO}_2/\text{SiO}_2$  catalysts and it is best realized at low temperatures. Thus, the preparation of highly dispersed metal oxides on silica by impregnation, liquid-phase grafting or chemical vapour deposition methods often involve a highly reactive precursor, such as  $\text{TiCl}_4$  or Ti-alkoxides, to react with the surface hydroxyls on silica [23-25]. The titration of the surface

hydroxyls with the Ti-precursors is either mono-functional (one Ti-alkoxide molecule per one OH group; see Fig. 1.1) or bi-functional (one Ti-alkoxide molecule titrating two OH groups; see Fig 1.2) depending on the pre-treatment temperature, the reaction temperature, and the size and reactivity of the precursor [23, 26-27].

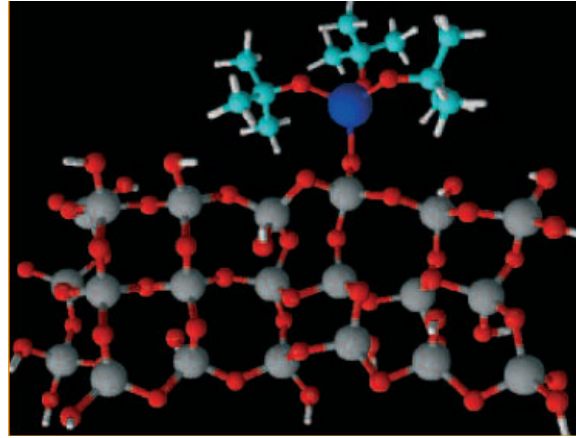


**Fig. 1.1:** Reaction of a Ti-alkoxide molecule with one hydroxyl of silica (grey: silicon; red: oxygen; white: hydrogen; sky-blu: carbon; blu: titanium)

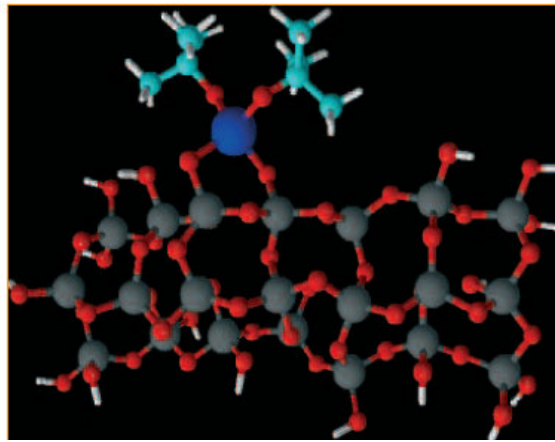


**Fig. 1.2:** Reaction of a Ti-alkoxide molecule with two hydroxyls of silica (grey: silicon; red: oxygen; white: hydrogen; sky-blu: carbon; blu: titanium)

Two types of Ti species, highly dispersed surface  $\text{TiO}_x$  species and  $\text{TiO}_2$  crystallites, may be present on the silica surface, depending on chemical compositions, namely  $\text{TiO}_2$  loading, and preparation conditions [19, 23, 27-29].

First attempts to prepare  $\text{TiO}_2/\text{SiO}_2$  oxides were carried out by using the “incipient wetness impregnation” of a silica substrate from a solution of Ti-precursors. According to this procedure, the support is contacted with a solution of appropriate concentration, corresponding in quantity to the total known pore volume of the support, or slightly less.

Unlike the “wet impregnation”, according to which the support is dipped into an excess amount of solution, the incipient wetness impregnation allows a quite precise control of the concentration of the active titanium oxide on the support, even if it suffers from the tendency of many metal-based species to agglomerate on the surface of the support during dehydration.

Reichmann and Bell [30] in a work of 1987 studied the factors influencing the phase structure of supported titania and concluded that the final structure depends on stable intermediates formed during the impregnation of silica.

Fernandez *et al.* [31] observed that highly dispersed  $\text{TiO}_2$  phases supported onto silica can be prepared by reacting titanium (IV) alkoxides,  $\text{Ti(OR)}_4$ , with the silica surface and calcination in air.

Munoz and Munuera [32] found that the incipient impregnation of  $\text{SiO}_2$  with an *n*-hexane solution of  $\text{Ti(OR)}_4$  leads to  $\text{TiO}_2$ -coated material with an extremely high dispersion.

Wauthoz et al. [33] showed that the impregnation of silica with titanium (IV) normal propoxide,  $\text{Ti(OC}_3\text{H}_7)_4$ , results in the formation of  $\text{TiO}_2$  agglomerates and a poor titania dispersion.

More recently, Gao et al. [23] proposed a two-steps impregnation procedure of 2-propanol solution of titanium isopropoxide to prepare highly dispersed  $\text{TiO}_2/\text{SiO}_2$  samples with loadings higher than 8 % by weight of  $\text{TiO}_2$ . According to this procedure, the maximum surface coverage of  $\text{Ti(O-Pr}^i)_4$  precursor was found to be  $\sim 4$  Ti atoms/ $\text{nm}^2$ .

Later, several papers were published dealing with the preparation of catalysts by anchoring metal alkoxides on the surface of oxides rich of hydroxyls, with the aim of improving the redox properties and the dispersion of the catalysts prepared [34-37]. This very promising strategy for the production of well-defined and highly active sites on the surface of an oxide support involves grafting of an organometallic species, followed by activation of the resulting “site” via further chemical reactions [38-40].

Castillo et al. [19] studied the deposition of titanium over silica using three methods: (a) precipitation with  $\text{TiCl}_4$  and ammonium hydroxide in aqueous solution, (b) grafting with Ti (IV) isopropoxide in isopropyl alcohol, and (c) grafting with a solution of  $\text{TiCl}_4$  in *n*-hexane. They found that the method of preparation influences deeply the morphology and dispersion of the coated oxide. Unlike the

impregnation which permits to deposit  $\text{TiO}_2$  at the external parts of the silica particles, the grafting method provides the best external superficial dispersion of titania, preventing the formation of crystallites. In addition, a strong interaction metal-support with the formation of  $\text{Ti-O-Si}$  bonds occurs. Anchored titania should form a monolayer on silica and a crystalline phase of rutile or anatase can be observed only for a 15-20 % by weight of  $\text{TiO}_2$  loading charge, depending on the silica surface [19].

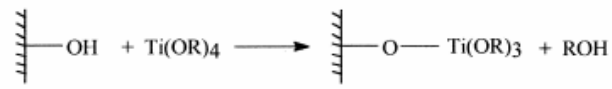
According to Wauthoz [33], the dispersion of titania strongly depends on the length of alkyl chain of the alkoxide used for grafting [33], while other authors suggested that the presence of H-bonded hydroxyls on the surface is responsible for an efficient grafting.

Iengo et al. [41] performed an in-depth study on the preparation and characterization of the properties of catalysts obtained by grafting different amounts of titanium alkoxide dissolved in anhydrous toluene on silica (Aldrich,  $S_{\text{BET}}=450 \text{ m}^2/\text{g}$ ), followed by steaming and calcination in air at  $T=500 \text{ }^\circ\text{C}$ , until to reach the monolayer coverage. This was made with the aim to investigate the factors controlling the maximum surface coverage of titanium oxide on silica.

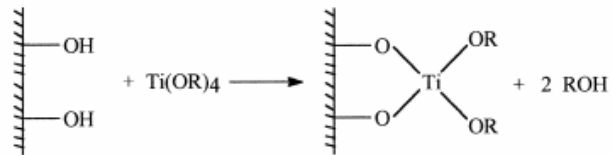
They also investigated the possibility to obtain multilayers of  $\text{TiO}_2$  on  $\text{SiO}_2$  by repeating more times the grafting operation of titanium tetra-isopropoxide, followed by steaming and calcination. This is possible because after the calcination step, some of  $\text{Si-OH}$  groups become reexposed and can further react with more  $\text{Ti}(\text{O-Pr})_4$  precursor molecules. Thus, a higher loading of  $\sim 26\% \text{ wt TiO}_2/\text{SiO}_2$ ,

which correspond to  $\sim 6$  Ti atoms/nm<sup>2</sup>, is reached by employing three grafting steps.

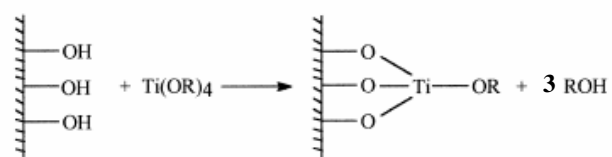
According to Iengo and co-workers [41], the grafting reaction between the  $\text{Ti}(\text{O}-\text{Pr})_4$  precursor molecules and the hydroxyls on the silica surface may occur following different possible stoichiometries, as showed in the following schemes (1-3).



Scheme 1.



Scheme 2.



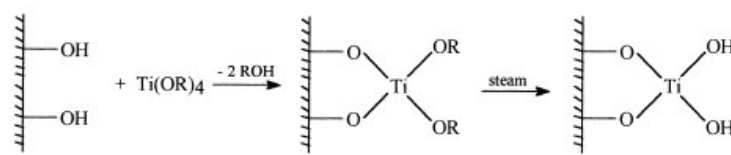
Scheme 3.

The experimental evidences achieved [41] suggested that grafting titanium alkoxide on the silica surface occurs easily and quantitatively at low coverage degree, giving place to highly dispersed titanium species forming a monolayer coverage, as indicated by XRD and TEM analyses [41,42].

On the contrary, the deposition onto SiO<sub>2</sub> surface of larger amounts of TiO<sub>2</sub> than the monolayer coating of silica by employing more grafting steps brings to the formation of amorphous agglomerates characterized by a lower surface TiO<sub>2</sub> dispersion, as indicated by DRIFT analyses from a semi-quantitative point of view [42].

However, textural analyses carried out by BET method showed, for all the prepared TiO<sub>2</sub>/SiO<sub>2</sub> catalysts ranging from sub-monolayer to tri-layer TiO<sub>2</sub> coatings, that the specific surface area does not change significantly with titanium loading, confirming in this way the possibility to prepare by grafting high-surface supported titania catalysts.

In particular, TGA measurements revealed that the hydroxyl densities of all the catalysts prepared by grafting remain roughly constant by increasing the amount of grafted titania. This fact suggested the prevalence of the stoichiometry for the grafting reaction (see Scheme 4) in agreement with the suggestions of Srinivasan et al. [28].



Scheme 4.

In general, the findings of the literature suggest that it is important to develop methods which permit to achieve the controlled chemical



modification of surfaces via the introduction of well-defined active sites, provided that for multicomponent catalysts optimum performance should result from maximization of surface area, homogeneity and active site distribution.

By synthesizing a variety of multicomponent oxide materials with tailored properties, Don Tilley et al. [43,44] employed a molecular building-block approach referred to as the *thermolytic molecular precursor* (TMP) method. This molecular precursor approach employs metal complexes containing oxygen-rich ligands, such as those with the general formulas  $L_nM[OSi(O^tBu)_3]_m$  and  $L_nM[O_2P(O^tBu)_2]_m$ , where  $L_n$  = alkoxide, amide, alkyl, etc.

Potential advantages of this approach derive from the molecular-level control over the structure of the catalytic site, the generation of site-isolated catalysts, and the ease with which the grafting reactions can be monitored to provide information about the nature of the grafted moiety.

According to the TMP method, first, the precursor is bonded to the surface of the oxide support (e.g., silica) via protonolysis reactions. In the case of an alkoxy (siloxo) species of the type  $M[OSi(O^tBu)_3]_n$ , this surface-attachment chemistry may occur with loss of  $HO^tBu$  or  $HOSi(O^tBu)_3$ , to result in bonding to the surface through  $M-O-(\text{surface})$  or  $Si-O-(\text{surface})$  linkages, respectively. Calcination should then lead to introduction of  $MO_x \cdot nSiO_2$  or  $MO_x \cdot (n-1)SiO_2$  species onto the oxide surface, in a manner similar to that observed for bulk transformations.

Thus, the new site may be “partially supported” by the few equivalents of silica that are derived from the molecular precursor. This latter effect is expected to aid in the introduction and stabilization of single metal atom sites.

The method described above was first investigated for the introduction of titanium sites onto silica. Don Tilley et al. [43] focused the attention on use of the precursor  $\text{Ti}[\text{OSi}(\text{O}^t\text{Bu})_3]_4$ , which is known to be an efficient source of dispersed  $\text{TiO}_2\cdot 4\text{SiO}_2$  materials [45]. Then, the synthesis of other single-site catalysts prepared from oxygen-rich titanium precursors was investigated.

For the molecular precursors, the Ti:Si ratio was varied to probe the influence of siloxy ligands on the grafting chemistry and the catalytic behaviour of the resulting catalysts. These comparisons showed that fewer siloxide ligands typically result in greater titanium loadings. This is attributed to the steric properties of the  $-\text{OSi}(\text{O}^t\text{Bu})_3$  ligand, which can retard the protonolysis reaction in the more sterically encumbered cases (i.e.,  $\text{Ti}[\text{OSi}(\text{O}^t\text{Bu})_3]_4$ ).

On the other hand, the siloxy ligands provide an enhancement of the catalytic activity and selectivity [43]. Thus, the optimum precursor was found to be the tris(siloxide)  $(i\text{PrO})\text{Ti}[\text{OSi}(\text{O}^t\text{Bu})_3]_3$  [46]. The support materials investigated in these cases were aerosil and the high surface-area, mesoporous silicas MCM-41 [47] and SBA-15 [48-50]. The best results in terms of catalyst performance were observed for the tris(siloxide) as precursor and a mesoporous silica as support.

Thus, it has been found that this approach leads to nanostructures which do not resemble the molecular species from which they are derived. However, these structures have catalytic properties that are distinctly better than similar structures obtained by conventional, aqueous methods. These results were generally attributed to a more highly dispersed material that is initially generated by the thermolytic molecular precursor (TMP) method.

Thus, from the scrutiny of literature, it appears well evident that the dispersion capacity is closely related to the surface properties of the silica support, mainly to the concentration of the hydroxyl groups and the specific surface area of the starting support, and the preparation conditions (e.g., the pretreatment temperature, the grafting reaction/impregnation time, the reactivity and molecular size of the precursor).

### **1.3 Factors determining the maximum surface titanium coverage of silica**

The dispersion of surface titanium oxide species on the  $\text{SiO}_2$  support may be influenced by several factors regarding both the nature of the support (silica) and the preparation method employed [23].

It is generally accepted in literature that the highest concentration of hydroxyls on the silica surface is preferred in order to prepare highly molecular dispersed  $\text{TiO}_2/\text{SiO}_2$  catalysts.

In most of cases, a pretreatment temperature of 120 °C was used to remove the physi-sorbed water as well as to preserve the highest

amount of hydroxyls on the silica surface. Thermogravimetry (TG) is generally used as a simple and inexpensive physical method to determine the total amount of OH groups of silica samples [51].

The reaction time is also an important experimental parameter in determining the overall conversion of surface hydroxyls reacting with the reactive precursors. Prolonged reaction times significantly enhanced the efficiency of the reaction of surface hydroxyls, especially for less reactive H-bonded hydroxyls [52,53]. The grafting reaction between the hydroxyls and Ti-alkoxide is usually performed under N<sub>2</sub> flow to prevent the hydrolysis of the alkoxide introduced in the reaction medium but also to ensure complete reaction between the reagent and the surface hydroxyls as well as removing most of the solvent.

Another critical factor, that is rarely addressed in literature, regarding the preparation of highly molecular dispersed TiO<sub>2</sub>/SiO<sub>2</sub> catalysts, is the maximum surface coverage of the precursor molecules. By studying the reaction of a variety of reactive hydrogen-sequestering reagents with the silica surface, Morrow and Mcfarlan [29] found that the inaccessible hydroxyls and the number of H-bonded hydroxyls, that do not react, increase with the apparent size of the reactant molecule precursor. In addition, the porosity, size, and morphology of the silica pores may influence the maximum surface coverage of a precursor. Very small pores may be inaccessible to large precursor molecules. Therefore, the maximum surface coverage of the precursor molecules is associated with the steric hindrance effect [22].

They found that the maximum surface coverage of titanium tetra-isopropoxide precursor in one-step impregnation was found to be  $\sim 2.5$  Ti atoms/nm<sup>2</sup>, which is similar to the maximum trimethylsilyl (TMS) surface coverage of 2.2-2.7 groups/nm<sup>2</sup>.

However, after calcination, some of Si-OH groups become re-exposed and can further react with more Ti(O-Pr<sup>i</sup>)<sub>4</sub> precursor molecules. Thus, a higher loading of 12 % TiO<sub>2</sub>/SiO<sub>2</sub> (actual amount of 14.75 wt %), which corresponds to  $\sim 4$  Ti atoms/nm<sup>2</sup>, is reached by employing two impregnation steps.

As well as the concentration of hydroxyls, the reaction time and other variables involved in the synthesis route of the catalysts, also the solvent used has a great importance as it may contribute to determine the surface structure of the catalytic component. From scrutiny of literature, it is evident that no systematic studies have been made on the influence of the solvent employed in the preparation of titanium-supported amorphous silica catalysts in the chemical environment of titanium.

Capel-Sanchez et al. [54] have recently addressed the attention to the role played by the solvent in the chemical environment of titanium, trying to understand the relationships with its performance in the epoxidation of primary alkenes with hydrogen peroxide. The samples were prepared by dispersing titanium isopropoxide (0.75 g) in an organic solvent (cyclohexanol, 1-phenylethanol, 1-hexanol, 2-(2-ethoxyethoxy)ethanol, diglyme, and acetophenone) and then mixing the solution with the silica substrate. These solvents were selected in

order to obtain quite different affinities between the Ti-isopropoxide precursor and the solvent, and therefore to determine hydrolysis rates of this precursor with the hydroxyl groups of the silica also different. One large difference observed was the amount of titanium incorporated to the silica substrate. The chemical analyses shown in Fig. 1.3 revealed that the highest Ti loading was achieved using acetophenone and toluene solvents, but lower with alcohols.

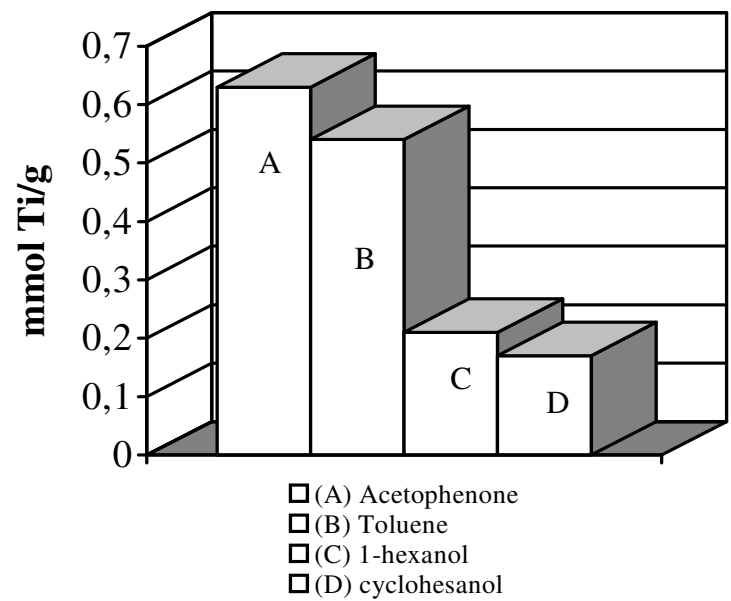


**Fig. 1.3:** Influence of the solvent on the amount of titanium supported onto silica surface

One tempting explanation of this behaviour is the different chelating capacities of the polar groups of the solvent molecule with titanium isopropoxide precursor in solution. The strongest interaction of alcohols with the Ti precursor in solution has a protective effect on

this precursor, hindering its hydrolysis on the hydroxyls groups of the silica. This effect was more pronounced with cyclohexanol, which interacts strongly with titanium isopropoxide. The opposite occurred with the acetophenone and toluene solvents.

The influence of the solvent on the amount of the supported titanium was also analysed by Santacesaria et al. in several papers [8, 41, 42, 55]. They investigated the preparation of  $\text{TiO}_2/\text{SiO}_2$  catalysts by contacting titanium tetra-isopropoxide in different solvents, such as isopropanol, dioxane and toluene, followed by the *grafting* step onto  $\text{SiO}_2$ . Finally, they found that the amount of the titanium supported onto silica surface decreases with the hydrophilic character of the solvent, while an almost quantitative *grafting* yield is obtained by dispersing the titanium precursor in toluene before the *grafting* reaction.

In other words, in the current preparation, due to the sterical hindrance effect, the maximum surface coverage of the  $\text{Ti}(\text{O-Pr})_4$  precursor in a one-step grafting was found to be  $\sim 2.2$  Ti atoms/ $\text{nm}^2$ , which is similar to the maximum trimethylsilyl (TMS) surface coverage of 2.2-2.7 groups/ $\text{nm}^2$  [23]. This value is in a close agreement with the findings of Gao et al. [23], giving 8.10 % wt  $\text{TiO}_2$  for the  $\text{TiO}_2$  monolayer on silica. Moreover, as the hydroxyls density on the silica surface is 0.92  $\text{mmol}_{\text{OH}}/\text{g}_{\text{SiO}_2}$  [55], by comparing this value with the number of titanium atoms anchored on the surface, a stoichiometry of about 1 hydroxyl per Ti atom can be deduced. Another important observation is the strong affinity of titanium

alkoxide with the silica surface, showed by the steep rise in the initial part of the adsorption isotherm (see **Fig 2.1** Chapter II). Saturation of the adsorbed alkoxide monolayer is reached at a relatively low alkoxide equilibrium concentration (0.01 mmol<sub>Ti</sub>/ml).

The results [55] confirm that the reactivity of the surface hydroxyl groups and the specific surface area of the silica determine the maximum surface coverage of an organometallic precursor for one-step grafting.

#### **1.4 Surface structures of molecularly dispersed supported TiO<sub>2</sub>/SiO<sub>2</sub> catalysts**

Investigation of surface structures of the molecularly dispersed TiO<sub>2</sub>/SiO<sub>2</sub> oxides is of fundamental importance not only to understand the coordination geometry of the Ti cations but also to correlate it with the corresponding catalytic performances.

Despite the large number of papers devoted to investigate the surface structure of the mixed TiO<sub>2</sub>-SiO<sub>2</sub> catalysts, only few attention has been addressed to characterize the surface of supported titania/silica oxides.

However, in the last years, the number of research articles devoted to the characterization of supported metal oxides has been growth in literature, mainly due to the combined use of in-situ Raman, UV-vis-NIR DRS and XANES spectroscopies, which resulted very informative to understand the surface structure of molecularly dispersed supported TiO<sub>2</sub>/SiO<sub>2</sub> oxides under various conditions.



The structure of the Ti cations in supported  $\text{TiO}_2/\text{SiO}_2$  oxides has extensively been investigated by means of X-ray diffraction analysis [8,19,31,42,56]. In most of cases, it was revealed that the titanium phase was not observed by XRD below 8% by weight of  $\text{TiO}_2$  for  $\text{TiO}_2/\text{SiO}_2$  prepared by impregnation and below 15% by weight of  $\text{TiO}_2$  for the grafted ones. Weak XRD peaks of anatase were detected at higher loadings. However, the absence of lines from the crystalline phase in XRD patterns related to the samples at low Ti loading does not necessary rule out the presence of small particles on the surface of the investigated samples. In general, XRD analyses reported in literature confirmed, from a qualitative point of view, the higher titanium dispersion that can be obtained by using the alkoxide *grafting* method than the impregnation. At this purpose, several studies have been reported by several authors [8,19,41,42,55].

A recent work [42] showed that charging on  $\text{SiO}_2$  increasing quantities of  $\text{TiO}_2$ , by repeating more times the grafting operation of titanium alkoxide onto high-surface silica, does not reduce the high surface titania dispersion observed for the sub-monolayer  $\text{TiO}_2/\text{SiO}_2$  catalysts. This was attributed by the authors to the high stability of Si–O–Ti bonds as consequence of the molecular dispersion of Ti species grafted on silica.

The possibility to prepare high-dispersed  $\text{TiO}_2/\text{SiO}_2$  multilayers by titanium alkoxide grafting on the silica substrate was also investigated by TEM micrographs, which showed the absence of well-defined crystalline  $\text{TiO}_2$ -phase on the surface of the support [42].

The formation of Ti–O–Si bridging bonds as consequence of the deposition of Ti species on the SiO<sub>2</sub> surface has thoroughly been investigated by using combined in-situ Raman, UV-vis-NIR DRS and XANES spectroscopies. It was found that the surface structure of TiO<sub>x</sub> species on silica is a strong function of environmental conditions as well as the TiO<sub>2</sub> loading.

In the dehydrated state, for a low loading of TiO<sub>2</sub> (1 %wt), the surface Ti atoms are predominantly located at isolated TiO<sub>4</sub> sites (the LMCT band ~47 600 cm<sup>-1</sup>); while at a medium loading of 5 %wt TiO<sub>2</sub>, the silica surface may possess a higher amount of TiO<sub>4</sub> dimer or one-dimensional polymerized TiO<sub>4</sub> species; for higher Ti loadings (~17%wt TiO<sub>2</sub>), two-dimensional, polymerized TiO<sub>5</sub> units are predominantly present on the silica surface [21,23].

Upon hydration, some of the Ti–O–Si bridging bonds on these molecularly dispersed TiO<sub>2</sub>/SiO<sub>2</sub> samples are hydrolyzed by H<sub>2</sub>O molecules, which results in an increase in the average coordination number of the Ti cations by about 1, as indicated by XANES. Hydration also decreases the edge energies of the LMTC transitions of the higher loading samples of 5% and 17% TiO<sub>2</sub>/SiO<sub>2</sub>, suggesting an increase in the total number of Ti–O–Ti bonds.

Pronounced structural changes upon hydration were also provided by Raman analyses [21,23]. A Raman band appears at 940-960 cm<sup>-1</sup>, which is most likely due to the Ti perturbed Si–OH. This is due to the adsorption of water that breaks the Ti–O–Si bridging bonds, resulting

in the formation of Ti–OH hydroxyls as well as the Ti perturbed Si–OH.

Experimental evidences about the formation of the Ti–O–Si bridging bonds as consequence of the interaction between TiO<sub>2</sub> and SiO<sub>2</sub> come also from XPS surface analyses [8]. The BEs of O1s of prepared supports displayed an asymmetry towards BE values. The main component at  $532.7 \pm 0.2$  eV is in agreement with the O (1s) BE for SiO<sub>2</sub>. A second one, appearing at lower BE, is at  $530.0 \pm 0.3$  eV higher than O(1s) in TiO<sub>2</sub>. This peak, whose position is intermediate between those in SiO<sub>2</sub> (533.0 eV corresponding to oxygen in Si–O–Si bonds) and TiO<sub>2</sub> (529.6 eV corresponding to oxygen in Ti–O–Ti bonds), can reasonably be assigned to oxygen in the Si–O–Ti bridging bonds [23]. From the results reported, it can be seen that the blue shift of both O1s and Ti 2p<sub>3/2</sub> BE values of the TiO<sub>2</sub>/SiO<sub>2</sub> catalysts with respect to pure TiO<sub>2</sub> could be associated with the formation of Ti–O–Si bonds, which results in an increase in the effective positive charge on Ti and a decrease in the effective negative charge on O since the Si atoms are more electronegative less polarisable than the Ti atoms [21, 23].

IR spectroscopy also provides interesting information about the formation of Ti–O–Si bonds in a simple way. The IR band observed at 910–960 cm<sup>–1</sup> is widely accepted as the characteristic vibration due to the formation of Ti–O–Si bonds [57–65], whose position depends on the chemical composition of the sample as well as the instrument calibration. The intensity of this IR band, compared to that due to Si–

O–Si at ca.  $1210\text{ cm}^{-1}$ , has been used as reference to evaluate the surface titanium dispersion. In fact, the dispersion of Ti in the  $\text{SiO}_2$  substrate has been associated with the ratio of IR vibration due to Ti–O–Si bond at  $930\text{--}960\text{ cm}^{-1}$  to that due to Si–O–Si at ca.  $1210\text{ cm}^{-1}$  [21,23,42]. However, with respect to XPS and Raman, IR spectroscopy is not sensitive to the formation of  $\text{TiO}_2$  crystallites.

Moisture has a pronounced effect on the surface structure of highly dispersed titanium oxide species on silica. Hydration can break the Ti–O–Si bridging bonds, which result in the formation of Ti–OH as well as Si–OH that may be perturbed by the nearby Ti cation. The Raman band at  $940\text{--}960\text{ cm}^{-1}$  is most likely due to the Ti perturbed Si–OH. Hydration also shifts the LMCT band to lower wavenumbers, indicating an increase in the average coordination number of Ti cations. XANES analysis demonstrates that the coordination of Ti atoms on the dehydrated 1%  $\text{TiO}_2/\text{SiO}_2$  sample predominantly changes from 4 to 5 upon hydration and that the coordination of the Ti atoms on the 12%  $\text{TiO}_2/\text{SiO}_2$  sample predominantly changes from 5 to 6 upon hydration. Thus, hydration appears to increase the average coordination number of the surface Ti cations by 1.

### **1.5 Catalytic performances of supported molecularly dispersed $\text{TiO}_2/\text{SiO}_2$ oxides**

It is well known from the literature that the catalytic performances of titanium oxide appear to be completely modified by the interaction

with the silica support, which is associated to the changes in the molecular structure and coordination environment.

It is widely recognized in literature that, with respect to pure  $\text{TiO}_2$ , the surface of the molecularly dispersed  $\text{TiO}_2/\text{SiO}_2$  oxides is mainly characterized by the presence of redox sites as well as a low amount of acidic sites.

The peculiar catalytic performance of the highly dispersed  $\text{TiO}_2/\text{SiO}_2$  catalysts in comparison with  $\text{TiO}_2$  crystallites was early demonstrated by Sheldon for liquid-phase olefins epoxidation reactions with hydrogen peroxide and alkyl hydroperoxide [67,68].

The pure  $\text{TiO}_2$  phase is not active for the epoxidation reaction, while the highly dispersed  $\text{TiO}_2/\text{SiO}_2$  catalysts exhibit high reactivity and high selectivity to epoxide [68]. The formation of  $\text{Ti-O-Si}$  bonds is crucial as demonstrated by the much lower activities showed by  $\text{TiO}_2$  supported on the other oxides and the physical mixtures of  $\text{TiO}_2$  and  $\text{SiO}_2$  [68]. Sheldon suggested that the active sites are the isolated monomeric titanyl  $(\text{SiO})_2\text{Ti=O}$  bonds on the silica surface. However, no experimental evidence has been found for this type of species.

A recent work of Thomas and co-workers [50] investigated the catalytic performances of supported  $\text{TiO}_2/\text{SiO}_2$  oxides, prepared by grafting Ti (IV) on the internal surface of MCM-41 by reaction of  $((\text{Cp}_2)\text{TiCl}_2)$  and subsequent calcination. These materials showed a higher activity in the epoxidation of olefins in the presence of *tert*-butylhydroperoxide (TBHP) than hydrothermally synthesized Ti-MCM-41 materials [49]. XANES/XAFS studies demonstrated that all

Ti atoms are isolated and located on the wall of MCM-41 mesopores. This characterization study suggested that the surface active Ti centers on  $\text{TiO}_2/\text{SiO}_2$  supported oxides for epoxidation reactions might also be isolated  $\text{TiO}_4$  units instead of  $(\text{SiO})_2\text{Ti}=\text{O}$  species.

An in-dept discussion about the strong impact of the structural characteristics on catalytic properties of the molecularly dispersed  $\text{TiO}_2/\text{SiO}_2$  in methanol oxidation, widely used as “probe-reaction” to evaluate the nature of Ti-sites, has been reported by Gao and co-workers [23]. With respect to pure  $\text{TiO}_2$  crystallites, they found that the molecularly dispersed  $\text{TiO}_2/\text{SiO}_2$  catalysts are much more active for methanol oxidation and are highly selective to the redox products. In addition, the catalytic tests performed revealed that the catalytic activity of these catalysts are a strong function of  $\text{TiO}_2$  loading, which is associated with changes in the coordination geometry and the degree of polymerization of the surface Ti atoms. Although high selectivity towards the redox products (> 92%), the specific catalytic activity (TOF) of the different surface Ti species decreases in the order: isolated  $\text{TiO}_4$  species > polymerized  $\text{TiO}_4$  species > polymerized  $\text{TiO}_5$  species. This trend indicates that the isolation of Ti-sites, associated with the prevalence on the surface of silica of Ti–O–Si bridging bonds per Ti atom is particularly favourable for methanol oxidation, in terms of both activity and selectivity.

Moreover, the production of redox products (formaldehyde and methyl-formate) instead of dehydration product (dimethyl ether)

suggested an increased oxidizing potential and a decreased acidity of the Ti cations when dispersed onto SiO<sub>2</sub> surface.

Alcohol dehydration is known to be catalyzed by both Lewis and Brönsted acidic sites and is considered as a measure of the total acidity. The pure TiO<sub>2</sub> phase, possessing only Lewis acidic sites, catalyzes methanol dehydration to dimethyl ether. Therefore, the surface titanium oxide species on silica support possess a lower acidity relative to the pure TiO<sub>2</sub> phase since the reaction products are exclusively redox products.

The fact that the surface Ti cations on silica act as redox sites rather than acid sites also suggests an increased oxidizing potential of the Ti cations. The increased oxidizing potential of the Ti(IV) cations, due to the formation of Ti–O–Si bridging bonds, is experimentally detected by the increased BE values of Ti 2p<sub>3/2</sub> and O1s and the higher LMCT transitions of the Ti atoms in the molecularly dispersed TiO<sub>2</sub>/SiO<sub>2</sub> catalysts.

With respect to pure TiO<sub>2</sub>-phase which possesses only strong Lewis acidic sites, the highly dispersed TiO<sub>2</sub>/SiO<sub>2</sub> catalysts show lower acidity in terms of both density and strength.

A recent investigation of the surface acidity of TiO<sub>2</sub>/SiO<sub>2</sub> supported oxides by means of FT-IR spectroscopy of adsorbed probe molecules, CO and NH<sub>3</sub>, has been reported by Bonelli and co-workers [70]. This study strongly suggested that the interaction between titania and silica in silica-supported titania catalysts gives place to supported Ti<sup>4+</sup> sites, characterized by a weaker Lewis acidity than on pure TiO<sub>2</sub>.

In addition, the FTIR results achieved allowed to establish interesting correlations between the electrophilic nature of supported  $\text{Ti}^{4+}$  sites, e.g. the acid strength of titanium cations, and their catalytic performances in the transesterification reaction of vegetable oils with methanol (biodiesel production) [8].

However, further investigation, in association with other oxidation reactions such as epoxidation reactions, may be necessary to provide additional fundamental insights into the relationship between the structural characteristics and the reactivity property of this type of the catalyst.

## 1.6 Conclusions

Several factors are shown to be critical in controlling the dispersion capacity or the maximum surface coverage of surface titanium oxide species on silica: the concentration of surface hydroxyls on silica, the specific surface area of silica, the pretreatment temperature, and the maximum surface coverage of the precursors molecules.

Experimental monolayer dispersion of titanium oxide on silica is reached at  $\sim 2.2 \text{ Ti atoms/nm}^2$  by employing a one step grafting procedure, as resulted from the chemical adsorption study of increasing quantities of titanium tetra-isopropoxide onto silica surface.

Site isolation and the maximum number of Ti–O–Si bridging bonds per Ti atom for isolated  $\text{TiO}_4$  sites are responsible for the highest specific catalytic activity (TOF) of the 1%  $\text{TiO}_2/\text{SiO}_2$  sample. Polymerization of the surface Ti species decreases the relative fraction



of Ti–O–Si bonds and, therefore, significantly decreases the activity of the Ti active sites.

### 1.7 References

- [1] R. A. Sheldon, I.W.C.E. Arends, H.E.B. Lempers, *Catal. Today*, **1998**, *41*, 387.
- [2] S. Klein, J.A. Martens, R. Parton, K. Vercruysse, P. Jacobs, W.F. Maier, *Catal. Lett.*, **1996**, *38* 209.
- [3] R. Hutter, T. Mallat, A. Baiker, *J. Catal.*, **1995**, *153*, 177.
- [4] Z. Liu, J. Tabora, R.J. Davis, *J. Catal.*, **1994**, *149*, 117.
- [5] P.K. Doolin, S. Alerasool, J.F. Hoffman, *Catal. Lett.*, **1994**, *25*, 209.
- [6] S. Wang, X. Ma, H. Guo, J. Gong, X. Yang, G. Xu, *J. Mol. Catal. A : Chemical*, **2004**, *214*, 273.
- [7] W. Kim and J.S. Lee, *Journal of Catalysis*, **1999**, *185*, 307.
- [8] M. Cozzolino, R. Tesser, M. Di Serio, M. Ledda, G. Minutillo, E. Santacesaria, *Studies in Surface Science and Catalysis, E. Gaigneaux et al. (Editors)*, **2006**, *162*, 299.
- [9] M. Taramasso, C. Perego, B. Notari, US Patent 4410501, **1983**.
- [10] M.A. Camblor, A. Corma, A. Martinez, J. Perez-Pariente, *J. Chem. Soc., Chem. Commun.*, **1992**, 589.
- [11] C.T. Kresge, M.E. Leonowicz, W.J. Roth, J.C. Vartuli, J.S. Beck, *Nature*, **1992**, *359*, 710.
- [12] D. Zhao, J. Feng, Q. Huo, N. Melosh, G.H. Fredrickson, B.F. Chmelka, G.D. Stucky, *Science*, **1998**, *279*, 548.

- [13] A. Corma, M.T. Navarro, J. Perez-Pariente, *J. Chem. Soc., Chem. Commun.*, **1994**, 147.
- [14] M. Morey, A. Davison, G. Stucky, *Micropor. Mater.*, **1996**, 6, 99.
- [15] P.T. Tanev, M. Chibwe, T.J. Pinnavia, *Nature*, **1994**, 368, 321.
- [16] S.A. Bagshaw, E. Pouzet, T.J. Pinnavia, *Science*, **1995**, 296, 1242
- [17] R.D. Roark, S.D. Kohler, J.G. Ekerdt, I. Wachs, *Catal. Lett.* **1992**, 16, 77.
- [18] R.D. Roark, S.D. Kohler, J.G. Ekerdt, *Catal. Lett.* **1992**, 16, 71.
- [19] R. Castillo, B. Koch, P. Ruiz, B. Delmon, *J. Catal.* **1996**, 161, 524.
- [20] G. C. Bond, S. F. Tahir, *Appl. Catal.* **1991**, 71, 1.
- [21] X. Gao, I.E. Wachs, *Catalysis Today*, **1999**, 51, 233.
- [22] E.F. Vansant, P.V.D. Voort, K.C. Vranken, *Stud. Sci. Surf. Catal.*, **1995**, 93.
- [23] X. Gao, S.R. Bare, J.L.G. Fierro, M.A. Banares, I.E. Wachs, *J. Phys. Chem. B*, **1998**, 102, 5653.
- [24] I. Grohmann, W. Pilz, G. Walther, H. Kosslick, V.A. Tuan, *Surf. Interface Anal.*, **1994**, 22, 403.
- [25] D. Trong, L. Le Noe, L. Bonneviot, *Chem. Commun.*, **1996**, 299.
- [26] R. Mariscal, J.M. Palacios, M. Galan-Fereres, J.L.G. Fierro, *Appl. Catal. A General*, **1994**, 116, 205.
- [27] S. Haukka, E. Lakomaa, A. Root, *J. Phys. Chem.*, **1993**, 97, 5085.
- [28] S. Srinivasan, A.K. Datye, M.H. Smith, C.H.F. Peden, *J. Catal.*, **1994**, 145, 565.
- [29] B.A. Morrow, A.J. Mcfarlan, *J. Noncryst. Solids*, **1990**, 120, 61.

- [30] M.G. Reichmann, A.T. Bell, *Appl. Catal.*, **1987**, 32, 315.
- [31] A. Fernandez, J. Leyer, A. Gonzalez, G. Münera, H. Knözinger, *J. Catal.*, **1998**, 112, 489.
- [32] A. Muñoz, G. Munuera, *Stud. Sci. Surf. Catal.*, **1991**, 63, 627.
- [33] P. Wauthoz, M. Ruwet, T. Machej, P. Grange, *Appl. Catal.*, **1991**, 69, 149.
- [34] J. Kijenski, A. Baiker, M. Glinski, P. Dollenmeier, A. Wokaun, *J. Catal.*, **1986**, 101, 1.
- [35] A. Baiker, P. Dollenmaier, M. Glinski, A. Reller, *Appl. Catal.*, **1987**, 35, 351.
- [36] M. Schraml-Marth, A. Wokaun, A. Baiker, *J. Catal.*, **1990**, 124, 86.
- [37] U. Scharf, M. Schraml-Marth, A. Wokaun, A. Baiker, *J. Chem. Soc., Faraday Trans.*, **1991**, 87(19), 3299.
- [38] K.W. Terry, C.G. Lugmair, T.D. Tilley, *J. Am. Chem. Soc.*, **1997**, 119, 9745.
- [39] R. Rulkens, T.D. Tilley, *J. Am. Chem. Soc.*, **1998**, 120, 9959.
- [40] C.G. Lugmair, T.D. Tilley, *Inorg. Chem.*, **1998**, 37, 764.
- [41] P. Iengo, G. Aprile, M. Di Serio, D. Gazzoli, E. Santacesaria, *Applied Catalysis A: General*, **1999**, 178, 97.
- [42] M. Cozzolino, R. Tesser, M. Di Serio, E. Santacesaria, 2<sup>nd</sup> Concorde meeting proceedings, **2006**, submitted to *Applied Catalysis A: General*.
- [43] T. Don Tilley, *Journal of Molecular Catalysis A: Chemical*, **2002**, 182–183, 17.

- [44] Kyle L. Fuldala and T. Don Tilley, *Journal of Catalysis*, **2003**, 216, 265.
- [45] M.P. Coles, C.G. Lugmair, K.W. Terry, T.D. Tilley, *Chem. Mater.*, **2000**, 12, 122.
- [46] T. Gunji, T. Kasahara, Y. Abe, J. Sol–Gel Sci. Technol. 13 (1998) 975.
- [47] J.S. Beck, J.C. Vartuli, W.J. Roth, M.E. Leonowicz, C.T. Kresge, K.T. Schmitt, C.T.W. Chu, D.H. Olson, E.W. Sheppard, S.B. McCullen, J.B. Higgins, J.L. Schlenker, *J. Am. Chem. Soc.*, **1992**, 114, 10834.
- [48] D. Zhao, J. Feng, Q. Huo, N. Melosh, G.H. Fredrickson, B.F. Chmelka, G.D. Stucky, *Science*, **1998**, 279, 548.
- [49] G. Calleja, R. van Grieken, R. García, J.A. Melero, J. Iglesias, *Journal of Molecular Catalysis A: Chemical*, **2002**, 182–183, 215.
- [50] T. Maschmeyer, F. Rey, G. Sankar, J.M. Thomas, *Nature*, **1995**, 378, 159.
- [51] S. Ek, A. Root, M. Peussa, L. Niinistö, *Thermochimica acta*, **2001**, 379, 201.
- [52] P. Van Der Voort, I. Gillis-D’Hamers, K. C. Vrancken, E. F. Vansant, *J. Chem. Soc., Faraday Trans.* **1991**, 87, 3899.
- [53] P. Van Der Voort, I. Gillis-D’Hamers, E. F. Vansant, *J. Chem. Soc., Faraday Trans.* **1990**, 86, 3751.
- [54] M.C. Capel-Sanchez, J.M. Campos-Martin, J.L.G. Fierro, *Journal of Catalysis*, **2003**, 217, 195.

- [55] E. Santacesaria, M. Cozzolino, M. Di Serio, A.M. Venezia, R. Tesser, *Applied Catalysis A: General*, **2004**, 270, 177.
- [56] S. Srinivasan, A.K. Datye, M.H. Smith, I.E. wachs, G. Deo, J.M. Jengh, A.M. Turek, C.H.F. Peden, *Journal of Catalysis*, **1991**, 131, 260.
- [57] S. Klein, S. Thorimbert, W.F. Maier, *J. Catal.*, **1996**, 163, 476.
- [58] A. Keshavaraja, V. Ramaswamy, H.S. Soni, A.V. Ramaswamy, P. Ratnasamy, *J. Catal.*, **1995**, 157, 501.
- [59] M. Schraml-Marth, K.L. Walther, A. Wokaun, B.E. Handy, A.J. Baiker, *J. Noncryst. Solids*, **1992**, 143, 93.
- [60] D.C.M. Dutoit, M. Schneider, A. Baiker, *J. Catal.*, **1995**, 153, 165.
- [61] Z. Liu, R.J. Davis, *J. Phys. Chem.* **1994**, 98, 1253.
- [62] M. Aizawa, Y. Nosaka, N. Fujii, *J. Noncryst. Solids*, **1991**, 128, 77.
- [63] A. Chmel, G.M. Eranosyan, A.A. Kharshak, *J. Noncryst. Solids*, **1992**, 146, 213.
- [64] I.M.M. Salvado, J.M.F. Navarro, *J. Noncryst. Solids*, **1992**, 147, 256.
- [65] C.C. Perry, X. Li, D.N. Waters, *Spectrochim. Acta*, **1991**, 47, 1487.
- [66] S. Pei, D.S. Yang, *Catal. Lett.*, **1933**, 21, 333.
- [67] R.A. Sheldon, J. A. Van Doorn, *J. Catal.*, **1973**, 31, 427.
- [68] R.A. Sheldon, *J. Mol. Catal.* **1980**, 7, 107.

- [69] R. Hutter, T. Mallat, A. Baiker, J. Chem. Soc. Faraday Trans., **1995**, *91*, 1261.
- [70] B. Bonelli, M. Cozzolino, R. Tesser, M. Di Serio, M. Piumetti, E. Garrone, E. Santacesaria, **2006**, submitted to Journal of Catalysis.

**PART A**  
**EXPERIMENTAL**  
**SECTION**





# II

## EXPERIMENTAL SECTION

### Highly dispersed $\text{TiO}_2/\text{SiO}_2$ catalysts for *Biodiesel production*

#### Abstract

In the present chapter, an investigation of the catalytic behavior of several  $\text{TiO}_2/\text{SiO}_2$  catalysts in the transesterification of refined oils with methanol (*biodiesel production*) has been reported. Preparation by *grafting*  $\text{Ti}(\text{O}-\text{Pr}^i)_4$  on silica of a series of supported  $\text{TiO}_2/\text{SiO}_2$  oxides has been carried out by evaluating the influence of the nature of the solvent, used for dispersing the mentioned alkoxide, and of Ti-loading on the final surface catalyst dispersion.

The maximum surface monolayer coverage of silica (Grace S432, specific surface area=  $282 \text{ m}^2/\text{g}$ , specific pore volume =  $1.02 \text{ cm}^3/\text{g}$ , hydroxyl groups =  $0.92 \text{ mmol/g}$ ) by  $\text{Ti}(\text{O}-\text{Pr}^i)_4$  precursors was found to be  $\sim 2.2 \text{ Ti atoms/nm}^2$  by adopting a one-steps grafting procedure.

The analysis of the surface properties by using several characterization techniques, such as BET measurements,  $\text{NH}_3$ -TPD, RAMAN and XPS spectroscopies, was also carried out.

The combined characterization techniques revealed the consumption of surface Si–OH groups and the formation of Ti–O–Si bridging bonds by charging increasing amounts of titanium alkoxide on the silica surface. As consequence of that, the generation of new acidic catalytic sites was observed. An in-dept study of the surface acidic titanium sites was carried out by both  $\text{NH}_3$ -TPD analyses and FT-IR spectroscopy of adsorbed CO.

The catalytic results obtained in the transesterification of refined oils with methanol (*biodiesel production*) showed that the activity of the systems investigated depends strongly on the surface structure of Ti-sites grafted on  $\text{SiO}_2$ , which determines the acid surface properties of the final solid.

## 2.1 Catalysts preparation

A commercial silica (Grace S432, specific surface area=  $282 \text{ m}^2/\text{g}$ , pore volume =  $1.02 \text{ cm}^3/\text{g}$ , hydroxyl groups =  $0.92 \text{ mmol/g}$ ) was used as base support. A commercial  $\text{TiO}_2$  support (anatase, Aldrich, specific surface area =  $80 \text{ m}^2/\text{g}$ ) was also used for some comparisons.

A series of  $\text{TiO}_2/\text{SiO}_2$  catalysts, characterized by increasing quantities of supported  $\text{TiO}_2$ , were prepared by the *grafting* reaction between titanium tetra-isopropoxide ( $\text{Ti}(\text{O-Pr}^i)_4$ , Aldrich, 99.999% purity) and the hydroxyls groups present on the surface of  $\text{SiO}_2$ .

According to this preparation method, the support was prepared by contacting the silica, calcined at  $500^\circ\text{C}$  for 8h, with a solution of titanium tetra-isopropoxide dissolved in dioxane, at room temperature. Different concentrations were used in order to evaluate the adsorption

behaviour of titanium alkoxide on the surface of the support used. The solids obtained were then filtered, washed with dioxane solvent, dried at  $120^\circ\text{C}$  overnight, heated at  $200^\circ\text{C}$  for 2h and then calcined at  $500^\circ\text{C}$  for 2 hours (in this way burning off the residual alkoxide groups). The amount of adsorbed titanium was determined by the colorimetric analysis suggested by Ettre [1]. The operative conditions adopted and the adsorption results are reported in Table 2.1. The catalysts are labelled XTS-D/, where X corresponds to the % by weight of  $\text{TiO}_2$ , T to  $\text{TiO}_2$ , S to  $\text{SiO}_2$ , D to Dioxane.

| <b>Table 2.1</b> - Operative conditions used for the preparation of TiO <sub>2</sub> /SiO <sub>2</sub> catalysts. The precursor (Ti(O-Pr <sup>i</sup> ) <sub>4</sub> ) was dissolved in 50 cm <sup>3</sup> of dioxane. |  |                             |   |   |                             |  |   |  |
|--|--|-----------------------------|---|---|-----------------------------|--|---|--|
| Catalysts  | Alkoxide<br>(Ti(O-Pr <sup>i</sup> ) <sub>4</sub> )<br>initial<br>amount<br>(g) | Amount<br>of support<br>(g) | Metal<br>residual<br>amount<br>(mmol <sub>Ti</sub> /cm <sup>3</sup> ) | Anchored<br>metal<br>(mmol <sub>Ti</sub> /g <sub>SiO2</sub> ) | Titanium<br>adsorbed<br>(%) | Supported<br>Titanium<br>oxide<br>(% wt TiO <sub>2</sub> ) | S <sub>BET</sub><br>(m <sup>2</sup> /g) | Pore<br>Volume<br>(cm <sup>3</sup> /g) |
| SiO <sub>2</sub>   | -  | -                           | -   | -   | -                           | -  | 282                                     | 1.02                                   |
| <b>0.92TS-D</b>  | 0.106  | 3.2                         | 0.0002  | 0.114   | 96.8                        | 0.92   | 285                                     | 1.15                                   |
| <b>1.80TS-D</b>  | 0.211  | 3.1                         | 0.0008  | 0.226   | 94.2                        | 1.80   | 283                                     | 1.14                                   |
| <b>3.09TS-D</b>  | 0.377  | 3.2                         | 0.0019  | 0.386   | 93.4                        | 3.09   | 285                                     | 0.80                                   |
| <b>5.74TS-D</b>  | 0.633  | 3.0                         | 0.0014  | 0.718   | 96.9                        | 5.74   | 278                                     | 0.85                                   |
| <b>7.07TS-D</b>  | 0.832  | 3.0                         | 0.0057  | 0.885   | 90.4                        | 7.07   | -                                       | -                                      |
| <b>7.62TS-D</b>  | 1.038  | 3.3                         | 0.0104  | 0.953   | 86.1                        | 7.62   | 282                                     | 1.0                                    |
| <b>7.73TS-D</b>  | 1.094  | 3.2                         | 0.0141  | 0.967   | 80.4                        | 7.73   | 280                                     | 1.1                                    |

Each catalyst reported in Table 2.1 was prepared by employing 1 step of grafting.

However, after calcination, some of Si-OH groups become re-exposed and can further react with more  $(\text{Ti}(\text{O-Pr}^i)_4)$  precursor molecules. Thus, a higher loading of  $\text{TiO}_2$  and, consequently, a better coverage of the silica surface can be reached by employing two and more grafting steps.

So, we used an excess of the grafting reagent compared to the monolayer and we repeated the grafting procedure two and three times for preparing  $\text{TiO}_2/\text{SiO}_2$  catalysts with higher  $\text{TiO}_2$  loading. More precisely, an amount of alkoxide corresponding to about 1.5 times the hydroxyls density on silica was used in each grafting step. The solid obtained after the first step of the grafting reaction was filtered, washed with toluene and oven-dried at 120 °C for 12 h. The solid was then submitted to a flux of steam for 2 h, at 150 °C, in order to eliminate the residual alkoxide groups by hydrolysis. Finally, the obtained solid was calcined at 500 °C for 2 h.

The operative conditions adopted and the related adsorption results are gathered in Table 2.2.

**Table 2.2** - Operative conditions used for the preparation of TiO<sub>2</sub>/SiO<sub>2</sub> catalysts by sequential grafting steps.

| Acronym for   |   |  |                           |  |  |
|---|---|--|---------------------------|--|--|
| TiO <sub>2</sub> /SiO <sub>2</sub><br>after<br>sequential<br>grafting steps | TiO <sub>2</sub><br>anchored<br>(mmol <sub>Ti</sub> /g) | TiO <sub>2</sub><br>anchored<br>(% wt) | Titanium<br>adsorbed<br>% | Specific<br>surface<br>area<br>(m <sup>2</sup> /g) | Pore<br>volume<br>(cm <sup>3</sup> /g) |
| 7.07TS-D<br>1 <sup>st</sup> step  | 0.88  | 7.07                                   | 90.4                      | -  | -                                      |
| 11TS-D<br>2 <sup>st</sup> step  | 1.38  | 11.0                                   | 78.3                      | 279  | 0.9                                    |
| 20TS-D<br>3 <sup>st</sup> step  | 2.50  | 20                                     | 60.5                      | 274  | 0.8                                    |

**2.1.1 Investigation of the effect of the solvent on the grafting yield**

In order to investigate the effect of the solvent on the grafting reaction yield, i.e. the maximum amount of titanium alkoxide that it is possible to charge on SiO<sub>2</sub>, some samples were prepared also by dispersing the same amount of Ti-alkoxide in two different solvents: isopropanol (parent alcohol) and toluene.

The method adopted for the preparation of the catalyst by using isopropanol as solvent was similar to that one described above. A different procedure was used for the catalysts prepared in toluene. In this case, the reaction was performed in a jacketed glass-reactor of 200 cm<sup>3</sup> for 6h, under stirring, at boiling temperature of toluene (388 K). The solid was filtered off, washed with toluene, dried at 393 K

overnight, hydrolyzed with steam and, finally, calcined at 773 K for 2 h. In all the mentioned cases, the amount of adsorbed titanium was determined by the colorimetric analysis suggested by Snell and Ettre [1], by evaluating the quantity of titanium remaining in solution after the grafting reaction. The operative conditions and the adsorption results are listed in Table 2.3. The catalysts are labelled XTS-Tol/I, where X corresponds to the % by weight of TiO<sub>2</sub>, T to TiO<sub>2</sub>, S to SiO<sub>2</sub>, Tol to Toluene and I to Isopropanol.

**Table 2.3** - Operative conditions used for the preparation of TiO<sub>2</sub>/SiO<sub>2</sub> catalysts.

| Acronym    | Alkoxide<br>(Ti(O-Pr <sup>i</sup> ) <sub>4</sub> )<br>initial<br>amount<br>(g) | Amount<br>of<br>support<br>(g) | Steps<br>of<br>Grafting | Anchored<br>metal<br>(mmol <sub>Ti</sub> /g <sub>SiO<sub>2</sub></sub> ) |
|------------|--|--------------------------------|-------------------------|--|
| 7TS-Tol    | 1.04   | 4.00                           | 1                       | 0.88   |
| 7.30TS-I   | 1.18   | 3.00                           | 1                       | 0.91   |
| 17.8TS-Tol | 9.26   | 23.70                          | 3                       | 2.23   |

**2.2 Techniques used for the catalyst characterization**

Different techniques were used for catalysts characterization, such as: BET, X-ray diffraction (XRD), TEM/EDX, Diffuse reflectance UV-Vis (DRUV), Laser-Raman (LRS) and X-ray photoelectronic (XPS) spectroscopies, Temperature Programmed Desorption of ammonia (NH<sub>3</sub>-TPD), NH<sub>3</sub>-chemisorption analysis and FT-IR measurements of CO and NH<sub>3</sub> adsorption.

Textural analyses were carried out by using a Thermoquest Sorptomatic 1990 Instrument (Fisons Instrument) and by determining the nitrogen adsorption/desorption isotherms at 77K. The samples were thermally pretreated under vacuum overnight up to 473K (heating rate=1K/min). Specific surface area ( $S_{\text{BET}}$ ) and pore size distributions were determined by using the BET and Dollimore-Heal methods [2,3].

XRD analyses were carried out by using a Philips diffractometer. The scans were collected in the range  $5\text{-}60^\circ$  ( $2\theta$ ) using Cu  $K\alpha$  radiation with a rate of  $0.01^\circ$  ( $2\theta$ )/s.

TEM observations were made by using a Jeol Jem 2010 equipped with an EDX probe and sample preparation was as follows: a drop of the dispersion of the milled catalytic powder in isopropyl alcohol was put on a Lacey carbon grid and the dispersant was removed by evaporation at room temperature.

Diffuse reflectance spectra were obtained on a UV/Vis scanning Jasco spectrometer V-550, equipped with an integrating sphere, using  $\text{BaSO}_4$  as reference. UV-Vis spectra were recorded in the diffuse reflectance mode ( $R$ ) and transformed by a magnitude proportional to the extinction coefficient ( $K$ ) through a Kubelka-Munk function ( $F(R)$ ).



Laser-Raman spectra were performed with a Labram spectrometer (Dilor) interfaced with an Olympus optical microscope. The excitation radiation was a He-Ne laser (632.8 nm) operated at a power of 10 mW. The 10× objective of the microscope was used, so that a spot of about 20  $\mu\text{m}$  at the surface of the sample was measured at once. Spectra were obtained by averaging 10 scans of the Raman shift range between 1200 and 100  $\text{cm}^{-1}$  recorded in 25 s with a spectral resolution of 7  $\text{cm}^{-1}$ . The identity of the spectra obtained at different positions of each sample was systematically verified.

The overall surface acidity of the prepared catalysts was determined by a temperature-programmed desorption of ammonia ( $\text{NH}_3$ -TPD) in a fixed-bed continuous flow micro-reactor system. Before the  $\text{NH}_3$ -TPD measurement, a sample (200 mg) was outgassed in a flow of pure helium (60 ml/min), at 500 °C for 30 min. Subsequently, the sample was cooled down to 100 °C and saturated in a flow of 0.5%  $\text{NH}_3/\text{He}$  (60 ml/min) for about 30 min. Then, the catalyst was purged in a helium flow until a constant baseline level was attained. The ammonia desorption was carried out in the temperature range of 100–500 °C with a linear heating rate of 10  $\text{Kmin}^{-1}$  in a flow of He (60 ml/min). The temperature in the catalyst bed was measured by a K-type thermocouple located in a quartz capillary immersed in the catalyst bed. The molecules desorbing from the samples were monitored on-line by a quadrupole mass-spectrometer (BALZERS QMS 422) connected to the reactor outlet

by a heated line. The  $\text{NH}_3$ -TPD spectra were obtained from the  $m/z = 16$  mass-to-charge signal ratio.

The number and strength of acid sites were evaluated by two-cycle adsorption (TCA) of ammonia from the gas-phase at three different temperatures. The amounts of  $\text{NH}_3$  adsorbed at different partial pressures in the equilibrium bulk phase were measured by using a Micromeritics ASAP 2010 Chemi System apparatus. Prior to adsorption measurements, the sample (about 200 mg) was submitted to He flow under vacuum at 473 K and then was outgassed at 673 K under vacuum for 2h. Then it was cooled down to 308 K in a flow of helium. Successive ammonia doses were sent onto the sample until a final equilibrium pressure of about 40 Torr was reached. The equilibrium pressure was measured after each adsorption step and the amount of  $\text{NH}_3$  adsorbed was calculated. At the end of the first adsorption cycle, the sample was outgassed under vacuum at 308 K for 30 min and a second adsorption cycle was then performed at the same temperature. In the frame of the same analysis, these adsorption/desorption steps were repeated at  $T=373\text{K}$  and  $622\text{ K}$ .

The XPS analyses were performed on a Kratos Axis Ultra spectrometer (Kratos Analytical – Manchester – UK) equipped with a monochromatic  $\text{Al K}_\alpha$  (1486.6 eV) X-ray radiation (powered at 10 mA and 15 kV). The sample powders were pressed into small stainless steel troughs mounted on a multi specimen holder. The analysis chamber was operated under ultrahigh vacuum with a pressure close

to  $5 \times 10^{-9}$  Torr ( $6.67 \times 10^{-7}$  Pa). The angle between the normal to the sample surface and the [multi elements] lens axis was  $0^\circ$ . The hybrid lens magnification mode was used with the slot aperture resulting in an analysed area of  $700 \mu\text{m} \times 300 \mu\text{m}$ . The pass energy was set at 40 eV. In these conditions, the energy resolution gives a full width at half maximum (FWHM) of the Ag  $3d_{5/2}$  peak of about 1.0 eV.

Charge stabilisation was achieved by using the Kratos Axis device. The following sequence of spectra was recorded: survey spectrum, C1s, O1s, and C1s again to check the stability of charge compensation in function of time and the absence of degradation of the sample during the analyses. The binding energy (BE) values were referred to the  $\underline{\text{C}}$ -(C,H) contribution of the C1s peak fixed at 284.8 eV. The peaks were fitted by a non-linear least square fitting program using a weighted sum of Lorentzian and Gaussian component curves after background subtraction in accordance with Shirley and Sherwood [4,5]. The surface atomic concentrations were calculated by correcting the intensities with theoretical sensitivity factors based on Scofield cross section [6]. The following peak intensities were used for the quantitative analysis: O 1s, Si  $2p_{3/2}$ , Ti  $2p_{3/2}$ .

For FT-IR measurements, powder samples were pressed into thin, self-supporting wafers. Spectra were collected at a resolution of  $2 \text{ cm}^{-1}$ , on a Bruker FTIR Equinox 55 spectrophotometer equipped with a MCT detector. Pre-treatments were carried out using a standard vacuum frame, in a IR cell equipped with KBr windows. To remove water and other atmospheric contaminants, wafers were outgassed for

1 hour at 723 K before adsorption of CO at nominal 77 K and  $\text{NH}_3$  at room temperature.

Due to the weakness of the interaction with CO, adsorption is studied at low temperatures: spectra have been recorded at the nominal temperature of liquid nitrogen, by dosing increasing amounts of CO (in the 0.05 – 15 mbar equilibrium pressures range) on samples previously outgassed at 723 K, inside a special quartz IR cell, allowing simultaneously to dose carbon monoxide and to add liquid  $\text{N}_2$ . After each experiment, an evacuation step has been performed to study the reversibility of the interaction.

Being the interaction stronger with ammonia than with CO,  $\text{NH}_3$  has been dosed at room temperature, in the equilibrium pressure range  $1,00 \cdot 10^{-2}$  – 17,0 mbar and then by removing the reversible fraction of the adsorbate via prolonged evacuation.

### **2.3 Transesterification reaction of triglycerides with methanol: materials and methods**

The catalytic screening was performed in small stainless steel vial reactors. The reaction was made by introducing reagents (0.9 g of methanol and 2.0 g of soybean oil) and a weighed amount (0.1 g) of catalyst into each reactor. The reactors were then heated in a ventilated oven. The reactors were constantly agitated inside the oven.

The oven temperature was kept at 50°C for 14 minutes, then increased at a rate of 20°C/min up to 180°C. After one hour, the temperature was quickly decreased by immersion of vials into a cold

bath.

The fatty acids methyl esters (FAME) yields, in the catalytic tests, were determined using the H-NMR technique [7] (Bruker 200 MHZ), i.e., by measuring the ratio of the H-NMR signals related to the methoxylic ( $A_1$ ) and methylenic groups ( $A_2$ ), respectively:

$$Y_{\text{FAME}} = \frac{A_1 / 3}{A_2 / 2} \quad (1)$$

The H-NMR experiments were performed at NMR section of CIMCF (Centro Interdipartimentale Metodologie Chimico-Fisiche – Department of Chemistry – University of Naples (Italy)).

## **2.4 Results and discussion**

### **2.4.1 Evaluation of the surface monolayer coverage of silica by titanium tetra-isopropoxide ( $\text{Ti}(\text{O-Pr}^i)_4$ )**

A critical factor regarding the preparation of supported  $\text{TiO}_2/\text{SiO}_2$  catalysts is the maximum surface coverage of the precursor molecules.

Several factors such as the porosity, size, and morphology of the silica pores may influence the maximum surface coverage of a precursor. Very small pores may be inaccessible to large precursor molecules. Therefore, the maximum surface coverage of precursor molecules is associated with the sterical hindrance effect. Above the maximum surface coverage, extra precursor molecules do not react with the surface hydroxyls and remain on the surface after the solvent is removed. The unreacted precursor molecules either evaporate during calcination at elevated temperatures or remain on the surface and become oxidized into oxide phase.

In order to determine the maximum surface coverage of silica by titanium alkoxide, a deep study of the grafting adsorption behaviour of titanium tetra-isopropoxide ( $\text{Ti}(\text{O-Pr}^i)_4$ ) on the surface of silica support by contacting solutions of increasing concentrations of the mentioned alkoxide, dissolved in dioxane, was carried out.

This approach resulted very interesting to investigate the chemical adsorption of titanium alkoxide until the surface saturation, by using the isotherm obtained, depicted in Fig. 2.1, that was obtained from the data reported in Table 2.1 (Columns 4 and 5).

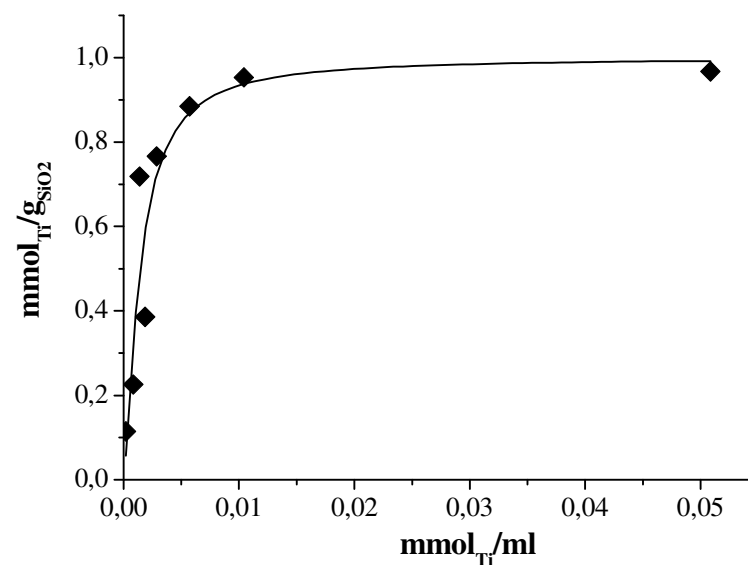


**Fig. 2.1:** Adsorption isotherm of titanium tetra-isopropoxide ( $\text{Ti}(\text{O-Pr}^i)_4$ ) adsorbed by grafting on the surface of  $\text{SiO}_2$ .

As can be seen, the adsorption isotherm can be interpreted as a Langmuir isotherm in line with the following relation:

$$K=(1/C^{\text{eq}})/(\Gamma^{\infty}/\Gamma^{\infty}-\Gamma^{\text{eq}}) \quad (2)$$

By regression analysis experimental points can be well fitted by using the following values of the parameters:  $K = 710,89 \text{ [L/mol]} \cdot \Gamma^{\infty} = 1.02 \text{ mmol}_{\text{Ti}}/\text{gSiO}_2$ . From the latter value, we can deduce that the titanium alkoxide adsorbed monolayer corresponds to about 8.14% by weight of  $\text{TiO}_2$ .

In the adopted preparation, due to the sterical hindrance effect, the maximum surface coverage of the  $\text{Ti}(\text{O-Pr})_4$  precursor in a one-step grafting has been found to be  $\sim 2.2 \text{ Ti atoms/nm}^2$ , which is similar to the maximum trimethylsilyl (TMS) surface coverage of 2.2-2.7 groups/ $\text{nm}^2$  [8]. This value is in a close agreement with the findings of Gao et al. [9], which found that the percentage by weight corresponding to the surface monolayer coverage of silica by titania is 8.10 % by weight of  $\text{TiO}_2$ . Moreover, by comparing the hydroxyls density on the silica surface ( $0.92 \text{ mmol}_{\text{OH}}/\text{gSiO}_2$ ), determined by thermogravimetric analysis (TGA), with the concentration of Ti-atoms ( $\text{mmol}_{\text{Ti}}/\text{gSiO}_2$ ) anchored on the surface in correspondence of the monolayer coating, a stoichiometry of about 1 hydroxyl group (-OH) per 1 atom of titanium (Ti) was deduced.

On the basis of the results achieved, it is possible to classify the titanium silica-supported catalysts in two categories, depending on the content of titanium grafted on  $\text{SiO}_2$ , expressed as “titanium surface density” and defined as the number of titanium atoms per square nanometer of the catalyst ( $\text{atoms}_{\text{Ti}}/\text{nm}^2$ ): sub-monolayers ( $\sim 2 \text{ atoms}_{\text{Ti}}/\text{nm}^2$ ) and monolayers ( $\sim 4\text{-}6 \text{ atoms}_{\text{Ti}}/\text{nm}^2$ ).

Another important observation is the strong affinity of titanium alkoxide with the silica surface, derived from the steep rise in the initial part of the adsorption isotherm. Saturation of the adsorbed alkoxide monolayer is reached at a relatively low alkoxide equilibrium concentration ( $0.01 \text{ mmol}_{\text{Ti}}/\text{ml}$ ).

However, it is interesting to note that, after calcination treatment, not only some of Si–OH groups become reexposed and can further react with more  $\text{Ti}(\text{O–Pr}^i)_4$  precursor molecules but also some of Ti–OH groups of Ti-species anchored in previous grafting steps. Thus, in order to completely cover the surface of silica with titania, the above-mentioned sequence of operations, i.e., grafting, filtering, drying, steaming and calcinating were repeated, under the same conditions, twice more on each sample. This strategy resulted very useful to charge on the surface of silica a sufficient amount of titanium to form a monolayer coating of silica characterized by a highly dispersed active phase, corresponding to both isolated and/or polymeric titanium species, as resulted from the characterization investigation reported in the next paragraphs.

So, a higher loading of  $\text{TiO}_2$  ( $\sim 20\% \text{ wt TiO}_2$ ), which correspond to  $\sim 4 \text{ Ti atoms/nm}^2$ , is reached by employing three grafting steps, as shown from the adsorption results reported in Table 2.2.

As stated above, among the variables involved in the synthesis of this type of catalysts ( $\text{TiO}_2/\text{SiO}_2$ ), also the nature of the solvent used for dispersing the titanium alkoxide before the grafting reaction, plays an important role. By taking into account the results reported in Table 3, the yield of the grafting reaction, i.e. the maximum quantity of titanium alkoxide, expressed as  $\% \text{ wt TiO}_2$ , that is possible to charge



on the silica surface by employing one grafting-step, is almost quantitative by using toluene. This is probably due to the fact that the grafting is an equilibrium reaction and, thus, the use of the parent alcohol as solvent reduces the anchorage efficiency.

## **2.4.2 Characterization results**

### **2.4.2.1 Nitrogen adsorption (BET) measurements**

$\text{SiO}_2$  and the prepared supported  $\text{TiO}_2/\text{SiO}_2$  catalysts were submitted to BET analyses in order to verify the possible effect of titanium loading on the specific surface area of the silica, used as base support. The obtained values are listed in Tables 2.1 and 2.2.

It is interesting to observe for all the prepared samples that the specific surface area of the starting support does not significantly change by charging increasing amounts of  $\text{TiO}_2$ , confirming in this way the possibility to prepare high-surface supported titania catalysts by adopting the grafting preparation method.

Moreover, BET analysis showed that both the type of silica used and the titanium silica-supported catalysts prepared possess a prevalent mesoporous texture characterized by uniform pore sizes (3-4 nm).

In Figs 2.2 and 2.3, the BET adsorption isotherm and pores distribution for silica and 11TS-D catalyst (11 % wt  $\text{TiO}_2$ ) are reported.

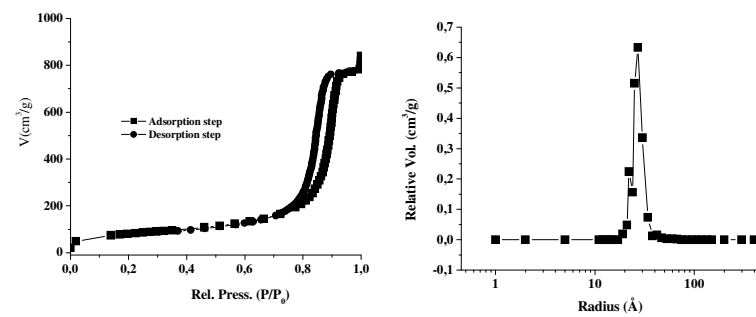


**Fig. 2.2:**  $\text{N}_2$  adsorption/desorption isotherm (left) and pore size distribution (right) of silica (S432 GRACE DAVISON)

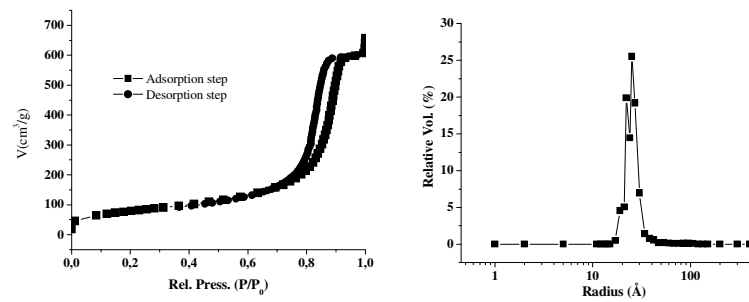


**Fig. 2.3:**  $\text{N}_2$  adsorption/desorption isotherm (left) and pore size distribution (right) of silica supported titania catalyst (20TS-D).

From the comparison between Figs. 2.2 and 2.3, we note that the grafting of titanium alkoxide onto  $\text{SiO}_2$  gives place to solids ( $\text{TiO}_2/\text{SiO}_2$ ) which retain the original mechanical and structural properties of the starting support, but characterized by a chemically different surface with respect to the silica.

#### 2.4.2.2 XRD analyses

All the prepared  $\text{TiO}_2/\text{SiO}_2$  catalysts were submitted to XRD measurements in order to verify the presence of crystallites on the surface of the catalysts and to have an estimation of titanium surface



As can be observed from Fig. 2.4, XRD measurements detected that XRD reflections typical of  $\text{TiO}_2$  (anatase) are completely absent in both the plots reported. This suggests that the grafting of titanium alkoxide on silica allows the establishment of a well-dispersed titanium oxide, and likely the formation of a homogeneous coverage of the active phase as a monolayer.

In other words, XRD analysis reveals the high dispersion of the grafted Ti-species also at high  $\text{TiO}_2$  loadings, which can be reached by employing two and more grafting steps.

#### **2.4.2.3 TEM/EDX analyses**

The homogeneous spreading of titanium oxide on the surface of silica was detected also by both TEM and EDX analyses, in agreement with the XRD observations. Three samples of the series of the prepared catalysts, listed in Tables 2.1 and 2.2, were analysed through TEM analysis, such as: 3.09TS-D, 7.73TS-D and 20TS-D.

In Fig. 2.5 and 2.6, TEM micrographies recorded at two enlargements (600 and 800K) and an EDX punctual analysis, performed at different points of the 3.09TS-D catalyst surface, are reported respectively.

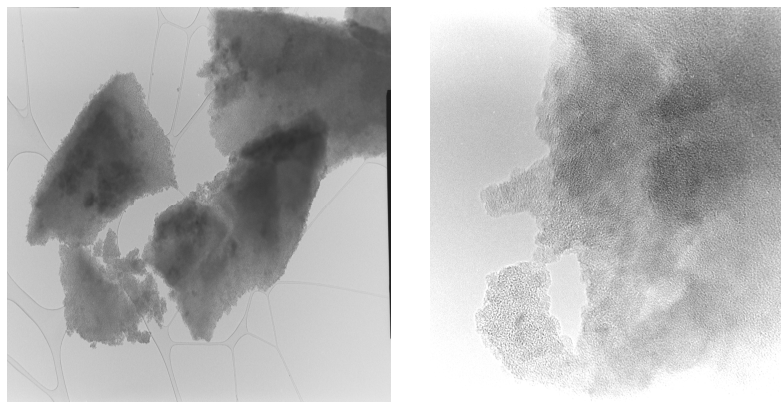


**Fig. 2.5:** TEM micrographies, recorded at 600K (left) and 800 K (right), of 3.09TS-D catalyst.

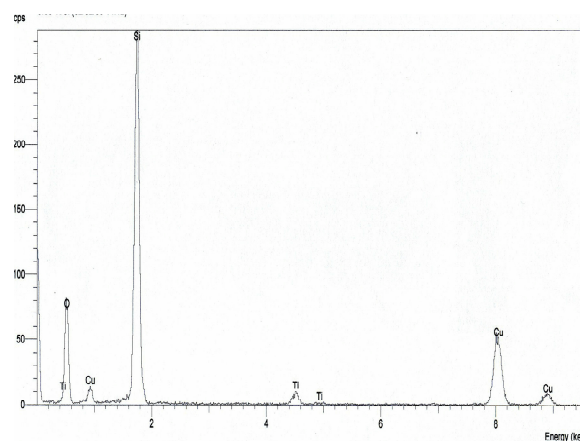


**Fig. 2.6:** EDX spectrum of the 3.09TS-D sample.

TEM observations revealed the absolute absence of well-defined titania crystalline phases, showing that the titanium species are uniformly dispersed on the silica surface. A semi-quantitative EDX analysis gave a value of supported  $\text{TiO}_2$  of about 3.1%, confirming the chemical analysis data obtained by UV-Vis spectroscopic measurements.

In Fig. 2.7 and 2.8, TEM microographies and an EDX punctual analysis, performed at different points of the 7.73TS-D catalyst surface, are reported respectively.

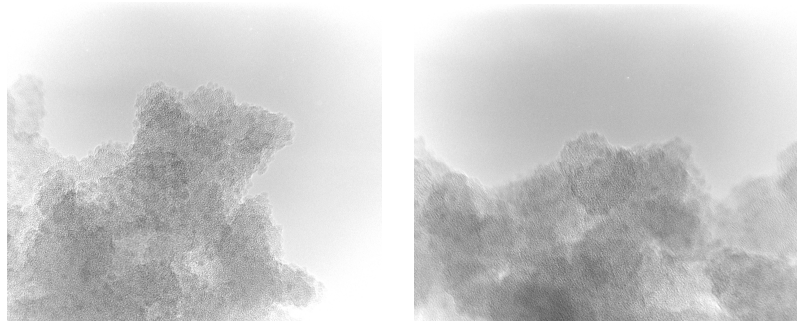


**Fig. 2.7:** TEM microographies, recorded at 600K (left) and 800 K (right), of the 7.73TS-D sample.

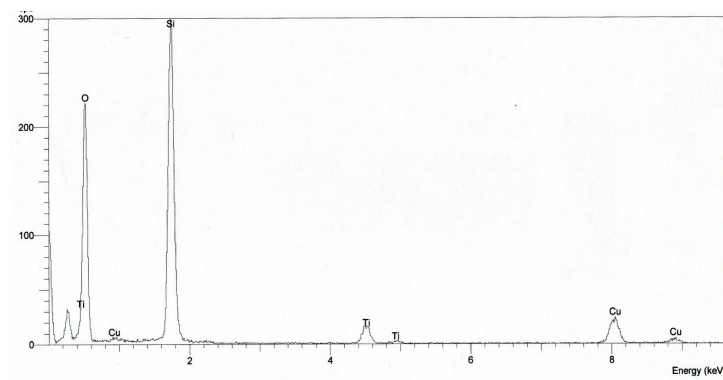


**Fig. 2.8:** EDX spectrum of the 7.73TS-D catalyst.

As shown, the 7.73TS-D catalyst resulted prevalently amorphous to TEM observations. A semi-quantitative EDX analysis gave a value

of supported  $\text{TiO}_2$  of about 7.7%, confirming the atomic composition provided by UV-Vis chemical data.

Similar observations were found for the 20TS-D sample characterized by a higher Ti amount, as can be noted by the following Figs 2.9 and 2.10.

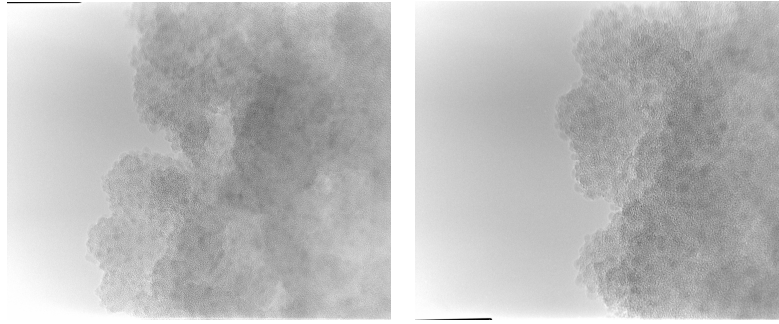


**Fig. 2.9:** TEM microographies, recorded at 600K (left) and 800 K (right), of the 20TS-D sample

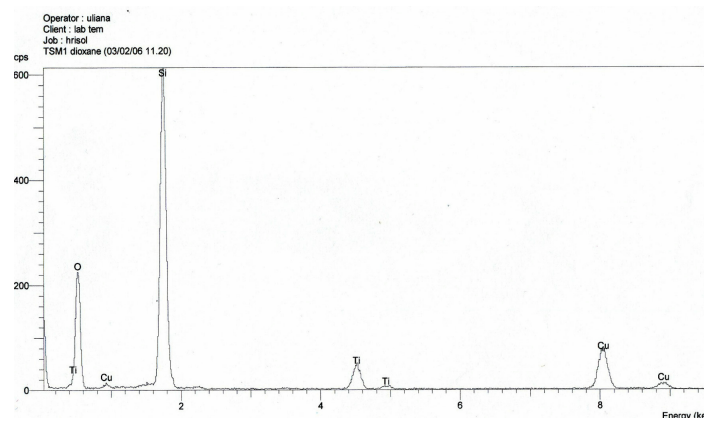


**Fig. 2.10:** EDX spectrum of the 20TS-D catalyst

A good agreement between the UV-Vis chemical analysis data (20 % wt  $\text{TiO}_2$ ) and the semi-quantitative EDX investigation (19.8 % wt  $\text{TiO}_2$ ) was also found in this last case.

These characterization results suggested that the grafted titanium species are homogeneously dispersed on the surface of silica up to the monolayer coverage.

#### **2.4.2.4 UV-Vis Diffuse Reflectance Spectroscopy**

The diffuse reflectance UV-Vis spectra usually provide information about the coordination geometry of the Ti cations (the first coordination sphere) and the ligand environment (the second coordination sphere) under various conditions. It is well known that the Ti cations in tetrahedral coordination show a typical band at ~ 212 nm, due to the ligand-metal charge transfer between  $\text{Ti}^{4+}$  and oxygen ligands, such as  $-\text{O}-\text{H}$ ,  $-\text{O}-\text{Si}$ ,  $-\text{O}-\text{Ti}$ , or  $\text{H}_2\text{O}$ . On the other hand, a shift of the band towards higher wavelengths (~ 260 nm) is usually observed for the Ti cations in octahedral environments [9].

All the  $\text{TiO}_2/\text{SiO}_2$  synthesized catalysts were submitted to DR-UV analysis. The recorded spectra of all the  $\text{TiO}_2/\text{SiO}_2$  prepared are compared in Fig. 2.11. The spectra of bulk  $\text{SiO}_2$  and  $\text{TiO}_2$  anatase are also reported for a useful comparison.



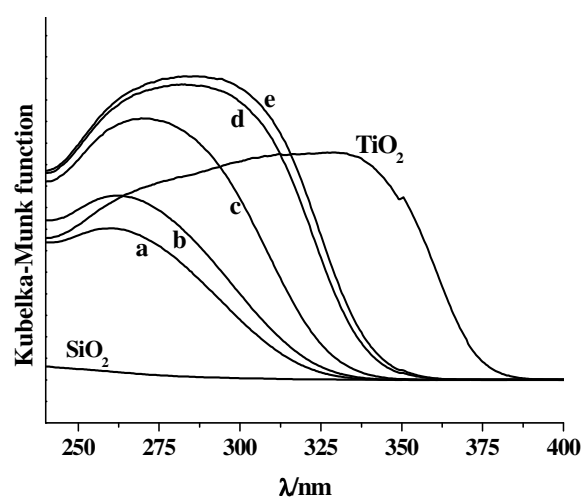


**Fig. 2.11:** DRS UV-Vis spectra of synthesized samples (a-e): a) 0.92TS-D; b) 1.80TS-D; c) 3.09TS-D; d) 7.73TS-D; e) 20TS-D

As can be observed, the absorption of silica in the range 200-500 nm can be considered negligible. In particular, the comparison of UV-Vis results reported in Fig. 2.11 suggested that the supported titania/silica oxides even at low Ti loadings ( $< 7\%$  wt  $\text{TiO}_2$ ) does not contain only isolated  $\text{TiO}_4$  sites, but a small amount of polymerized Ti species may also be present.

It is interesting to note that the maximum ligand–metal charge transfer (LMCT) transitions shifts towards higher wavelengths by increasing  $\text{TiO}_2$  loading, suggesting an increase in the polymerization degree of Ti atoms, in agreement with some findings of literature [10].

These results are in agreement with the ones obtained by FT-IR analysis, according to which the intensity of the  $3747\text{ cm}^{-1}$  due to isolated Si–OH hydroxyls decreases significantly, which indicates the consumption of Si–OH hydroxyls with increasing  $\text{TiO}_2$  loading (more

details are reported in Chapter III). In particular, it is interesting to observe that the 7.73TS-D and 20TS-D catalysts showed a broader absorption band with a shape very similar to that of the bulk  $\text{TiO}_2$  anatase. This suggests that even though the  $\text{TiO}_2$  crystallites are very small and beyond the detection sensitivity of XRD measurements, they may still possess the same electronic property as the pure  $\text{TiO}_2$  anatase phase.

Finally, the decrease of the edge energy of LMCT transitions of Ti atoms by increasing  $\text{TiO}_2$  loading may also be associated to the increase in the number of nearest Ti atoms, which suggests the polymerization of the surface Ti atoms on the silica surface at higher  $\text{TiO}_2$  loadings. The observed shift of the band-gap absorption edge may be explained in terms of quantum effects due to the small titania particles [11].

However, information about the “real” coordination of titanium species is complicated by the coordination of water molecules from the ambient to the titanium sites. The hydration of Ti (IV) sites is also favoured as a consequence of the hydrophilic character of the solid. At last, in all the catalysts, the presence of  $\text{TiO}_2$  clustering can be ruled out because no adsorption at  $\sim 370\text{-}410\text{ nm}$  was detected.

#### **2.4.2.5 Raman analysis of surface Ti species**

The Raman spectra of the dehydrated samples  $\text{TiO}_2/\text{SiO}_2$  are reported in Fig. 2.12.

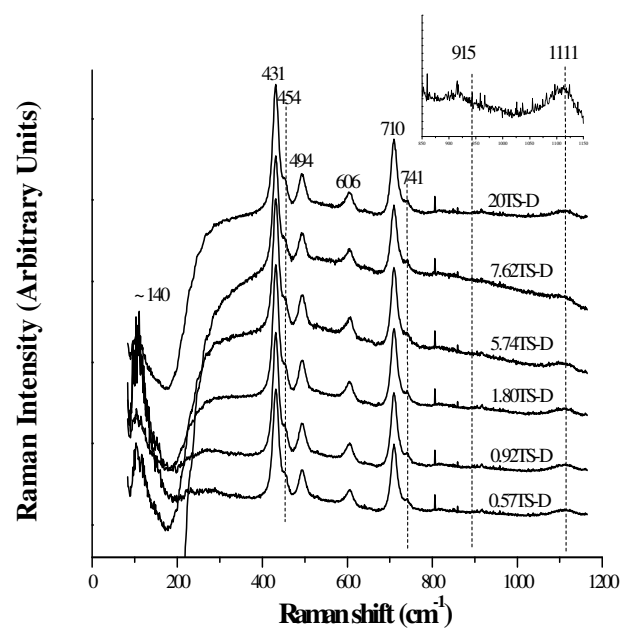


**Fig. 2.12:** Raman spectra of the series of the prepared  $\text{TiO}_2/\text{SiO}_2$  samples.

As can be seen, very sharp bands at  $\sim 431$ ,  $494$ ,  $606$ ,  $710 \text{ cm}^{-1}$  appear as well as less strong Raman features at  $\sim 454$ ,  $741$ ,  $915$  and  $1111 \text{ cm}^{-1}$ . With respect to the typical Raman signals of the silica support, reported in literature at  $\sim 410$ ,  $487$ ,  $607$ ,  $802$  and  $\sim 976 \text{ cm}^{-1}$ , slight shifts were detected in the case of supported  $\text{TiO}_2/\text{SiO}_2$  samples. The bands at  $\sim 494$  and  $606 \text{ cm}^{-1}$  can be assigned to D1 and D2 defect modes which have been attributed to tri- and tetracyclosiloxane rings produced via the condensation of surface hydroxyls [12,13]. The band at  $\sim 430 \text{ cm}^{-1}$  has been assigned to the symmetrical Si-O-Si bending mode [13]. It is interesting to note that the  $\sim 802 \text{ cm}^{-1}$  band, present in the spectra of  $\text{SiO}_2$  [13], shifts downward to  $710\text{--}748 \text{ cm}^{-1}$ , suggesting that some Si-O-Si bridging bonds are affected by the presence of dispersed titanium oxide.

Two new Raman bands are also observed at  $\sim 915$  and  $1111\text{ cm}^{-1}$ . These bands have been assigned to silica vibrations perturbed by the presence of Ti, which are indicative of the formation of Ti-O-Si bridging bonds [14]. The latter value ( $1111\text{ cm}^{-1}$ ) is about  $30\text{ cm}^{-1}$  lower than the one at  $1080\text{ cm}^{-1}$  in [6] but it is very close to the one ( $1115\text{ cm}^{-1}$ ) detected in Ti-silicalites.

This spectroscopic result suggests that the average coordination of Ti cations on the silica surface in the case of our grafted samples is comparable with the one in the Ti silicalite framework. When the  $\text{TiO}_2$  loading reaches 20 % by weight, a weak Raman bands at  $\sim 140\text{ cm}^{-1}$  is observed, indicative of the presence of trace amount of crystalline  $\text{TiO}_2$  (anatase), whose Raman spectrum is reported in Fig. 2.13.

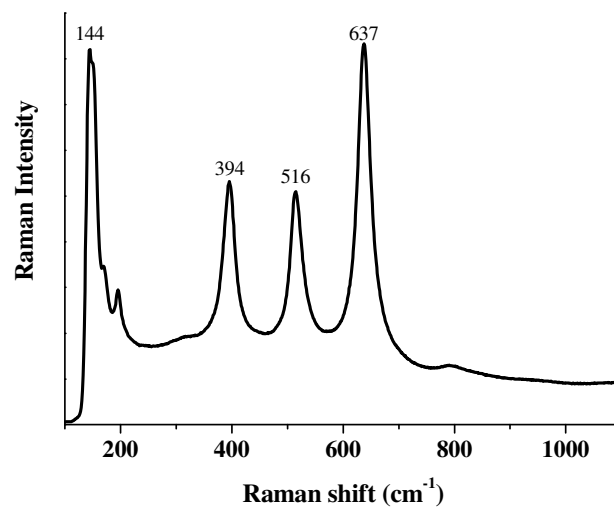


**Fig. 2.13:** Raman spectrum of  $\text{TiO}_2$  anatase

These results indicate that the maximum surface dispersion on  $\text{SiO}_2$  is  $\sim 6\text{ Ti atoms/nm}^2$ . This observation once again demonstrates that Raman spectroscopy is extremely sensitive to the formation of

crystalline  $\text{TiO}_2$  (anatase) particles. On the contrary, XRD experiments cannot detect the presence of  $\text{TiO}_2$  crystallites (anatase) below 30%  $\text{TiO}_2$  loading, suggesting that the  $\text{TiO}_2$  crystallites on  $\text{SiO}_2$  are very small and below the detection sensitivity of the XRD technique ( $<40 \text{ \AA}$ ).

#### 2.4.2.6 Determination of the surface dispersion and structure by XPS analyses

Information about the nature and dispersion of supported titania species are acquired by XPS.

Typical XPS spectra of Ti (2p) together with the nearby O (1s) lines for some of the series of  $\text{TiO}_2/\text{SiO}_2$  samples, listed in Tables 2.1 and 2.2 are depicted in Figs 2.14-2.17.

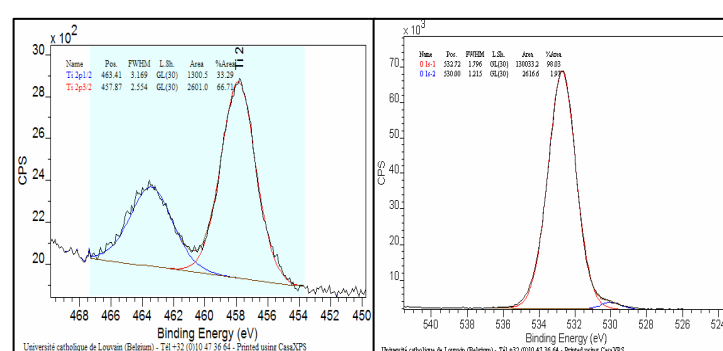


**Fig. 2.14:** Ti 2p (left) and O 1s (right) XPS spectra of 0.92TS-D catalyst

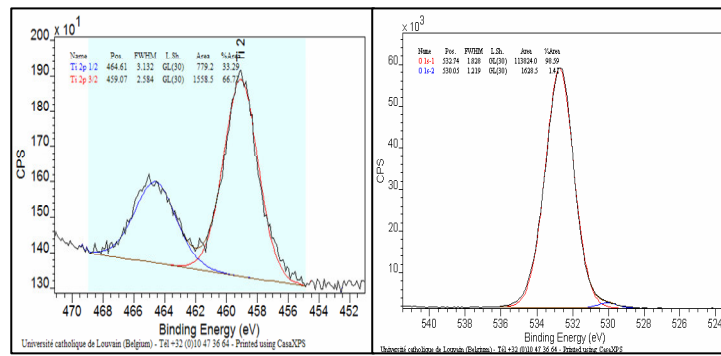


**Fig. 2.15:** Ti 2p (left) and O 1s (right) XPS spectra of 1.80TS-D catalyst

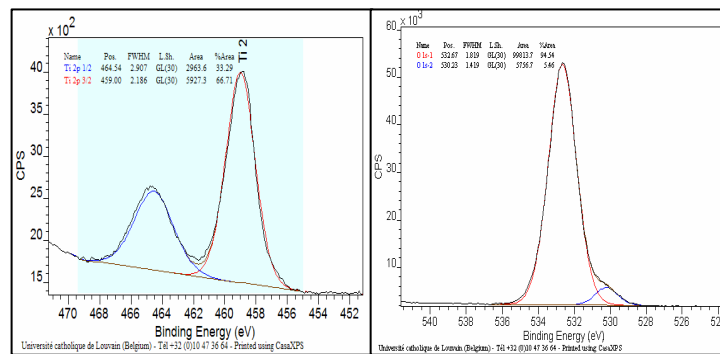


**Fig. 2.16:** Ti 2p (left) and O 1s (right) XPS spectra of 7.62TS-D catalyst

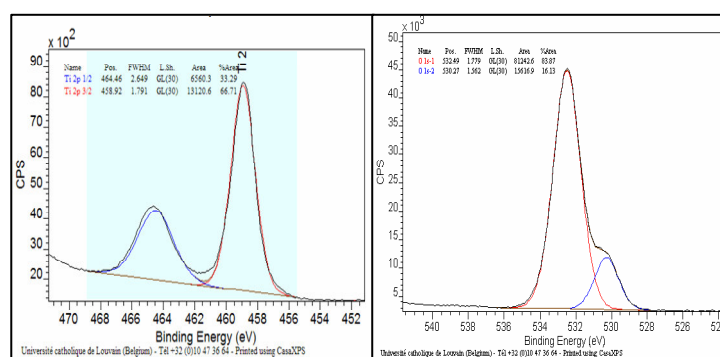


**Fig. 2.17:** Ti 2p (left) and O 1s (right) XPS spectra of 20TS-D catalyst

The surface Ti/Si atomic ratios obtained by XPS analysis are shown in Table 2.4. It can be seen that surface and bulk Ti/Si atomic ratios have approximately a linear relationship up to about 20% wt  $\text{TiO}_2$  ( $n_{\text{Ti}}/n_{\text{Si,bulk}}=0.14$ ). This experimental evidence showed that Ti is evenly spread over all surfaces, internal as external. However, aggregation of Ti-species may occur at high Ti loadings (17-20 % wt  $\text{TiO}_2$ ), giving place to the formation of  $\text{TiO}_2$  nano-particles on the silica surface.

The BEs of Si  $2p_{3/2}$ , Ti  $2p_{3/2}$ , and O  $1s$  for the dehydrated  $\text{TiO}_2/\text{SiO}_2$  samples as well as for the reference compounds,  $\text{SiO}_2$  and  $\text{TiO}_2$  (anatase), are also presented in Table 2.4.

The BEs of O1s of prepared supports displayed an asymmetry towards BE values. The main component at  $532.7 \pm 0.2$  eV is in agreement with the O ( $1s$ ) BE for  $\text{SiO}_2$ . A second one, appearing at lower BE, is at  $530.0 \pm 0.3$  eV higher than O( $1s$ ) in  $\text{TiO}_2$ . This peak, whose position is intermediate between those in  $\text{SiO}_2$  (533.0 eV corresponding to oxygen in Si-O-Si bonds) and  $\text{TiO}_2$  (529.6 eV corresponding to oxygen in Ti-O-Ti bonds), can reasonably be assigned to the oxygen in the Si-O-Ti bridging bonds [14].

The dispersion of  $\text{TiO}_2$  on  $\text{SiO}_2$  was evaluated by taking into account the intensity values. The variation of the intensity ratios,  $I(\text{Ti})/I(\text{Si})$ , as a function of the atomic composition  $n_{\text{Ti}}/n_{\text{Si}}$  for a theoretical monolayer of  $\text{TiO}_2$  on silica has been calculated using the model of Kerkhof and Moulijn [15], and the obtained results are reported as straight line in Fig. 2.18. The corresponding experimental values in the same figure are also reported.

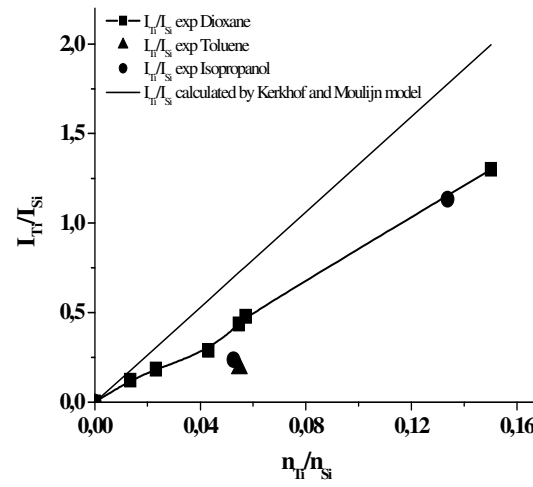


**Fig. 2.18:** XPS intensity ratios as function of the chemical composition ( $\text{Ti/Si}$  ratio)

The agreement between experimental and calculated values appears to be good for the  $\text{TiO}_2/\text{SiO}_2$  sample containing less than 1.80 %  $\text{TiO}_2$  by weight, indicative of a homogeneous distribution of the grafted Ti species with monoatomic thickness.

In addition, it is possible to observe that the catalysts, prepared by dispersing titanium tetra-isopropoxide in toluene and isopropanol, show a lower  $I_{\text{Ti}}/I_{\text{Si}}$  intensity ratio with respect to the corresponding one in dioxane, characterized by the same  $\text{Ti/Si}$  bulk atomic ratio. These results seem to indicate a possible influence of the solvent used on the final surface dispersion.

However, the values obtained in terms of  $I_{\text{Ti}}/I_{\text{Si}}$  are higher than the ones showed by Wang et al. [16], related to  $\text{TiO}_2/\text{SiO}_2$  samples with



similar Ti loadings but prepared by impregnation. On the other hand, the XPS values found here are in agreement with values obtained by Keranen et al. for a series of TiO<sub>2</sub>/SiO<sub>2</sub> catalysts prepared by Atomic Layer Deposition (ALD) [17].

Table 2.4 - XPS results obtained for TiO<sub>2</sub>/SiO<sub>2</sub> catalysts

| Catalysts        | TiO <sub>2</sub><br>Loading<br>(% wt TiO <sub>2</sub> ) | Atomic ratios |                               | Si 2p <sub>3/2</sub><br>(eV) | Ti 2p <sub>3/2</sub><br>(eV) | O 1s (eV)<br>(contribution, %) |
|------------------|---|---------------|-------------------------------|------------------------------|------------------------------|--------------------------------|
|                  |   | Ti/Si<br>XPS  | Ti/Si<br>Chemical<br>Analysis |                              |                              |                                |
| SiO <sub>2</sub> | 0   | -             | -                             | 103.4                        | -                            | 533.0 (100)                    |
| 0.92TS-D         | 0.9   | -             | -                             | 103.5                        | 459.0                        | 532.7 (98), 530.0 (2)          |
| 1.80TS-D         | 1.8   | 0.012         | 0.014                         | 103.4                        | 459.0                        | 532.7 (99), 530.1 (2)          |
| 3.09TS-D         | 3.1   | 0.018         | 0.023                         | 103.6                        | 459.1                        | 532.7 (98), 530.1 (2)          |
| 5.74TS-D         | 5.7   | 0.028         | 0.043                         | 103.5                        | 459.1                        | 532.6 (97), 530.3 (3)          |
| 7.62TS-D         | 7.6   | 0.046         | 0.057                         | 103.4                        | 458.8                        | 532.7 (95), 530.2 (5)          |
| 20TS-D           | 20.   | 0.125         | 0.15                          | 103.3                        | 458.9                        | 532.5 (84), 530.3 (16)         |
| 7TS-Tol          | 7.0   | -             | -                             | 103.5                        | 458.7                        | 532.7 (97), 530.0 (3)          |
| 17.8TS-Tol       | 17.8  | 0.109         | 0.134                         | 103.4                        | 458.9                        | 532.6 (91), 530.1 (9)          |
| 7.30TS-I         | 7.3   | 0.040         | 0.055                         | 103.7                        | 458.4                        | 532.5 (96), 530.6 (4)          |
| TiO <sub>2</sub> | 100   | -             | -                             | -                            | 458.4                        | 529.6 (100)                    |

2.4.2.7 Acidic properties of supported TiO<sub>2</sub>/SiO<sub>2</sub> catalysts

2.4.2.7.1 Determination of the surface acidity by NH<sub>3</sub>-TPD measurements

NH<sub>3</sub>-TPD measurements were carried out to determine the overall surface acidity of the prepared catalysts.

Table 2.5 gathers the total amounts of desorbed ammonia for some of the TiO<sub>2</sub>/SiO<sub>2</sub> catalysts reported in Tables 2.1, 2.2 and 2.3.

Table 2.5 - NH<sub>3</sub>-TPD results for titanium based catalysts

| Catalyst   | Solvent     | S <sub>BET</sub><br>(m <sup>2</sup> /g) | Overall<br>Surface<br>acidity<br>(μmol <sub>NH3</sub> /g) | Overall<br>Surface<br>acidity<br>(μmol <sub>NH3</sub> /m <sup>2</sup> ) |
|------------|-------------|---|---|---|
| 3.09TS-D   | Dioxane     | 284                                     | 64.6  | 0.23  |
| 7.62TS-D   | Dioxane     | 282                                     | 155.8   | 155.8   |
| 20TS-D     | Dioxane     | 279                                     | 234.9   | 0.84  |
| 7.30TS-ISO | Isopropanol | -                                       | 135.3   | -   |
| 17.8TS-TOL | Toluene     | 278                                     | 204.3   | 0.73  |

As shown in Table 2.5, the amount of the acidic sites increases almost linearly by increasing the amount of TiO<sub>2</sub> grafted on silica until reaching the surface monolayer coverage. The NH<sub>3</sub>-TPD profiles obtained are presented in Fig. 2.18.

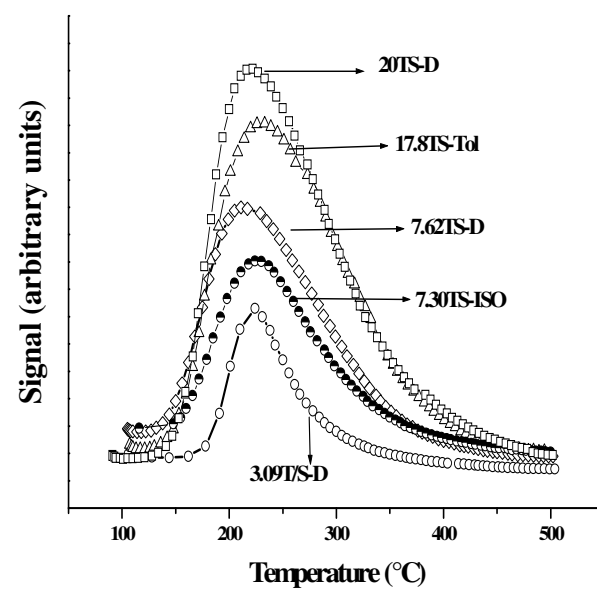


Fig. 2.18:  $\text{NH}_3$ -TPD profiles of  $\text{TiO}_2/\text{SiO}_2$  catalysts

From the profiles shown in Fig. 2.18, it is possible to observe that the loading of titanium gives no apparent impact on the strength of the surface acid sites, independently of the solvent used in the preparation of the catalysts.

#### 2.4.2.7.2 Determination of the strength of surface acidic sites by $\text{NH}_3$ -chemisorption

The number and strength of the surface acidic sites were evaluated by two-cycles adsorption (TCA) of ammonia from the gas-phase at three different temperatures. This type of analysis was performed on the sample, indicated with the acronym 20TS-D (preparation conditions and some related properties are reported in Table 2.2).

Figs 2.19, 2.20 and 2.21 show  $\text{NH}_3$ -adsorption isotherms obtained in two successive cycles for the sample 20TS-D, at three different temperatures ( $T=35\text{K}$ ,  $373\text{K}$ ,  $622\text{K}$ ), respectively.

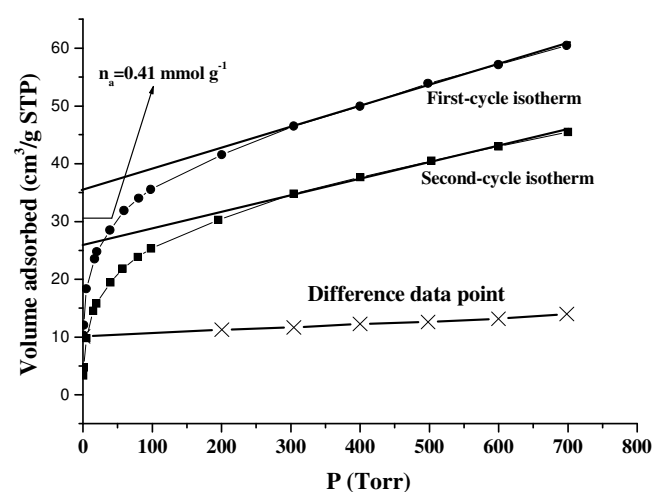


**Fig. 2.19:** Two-cycles adsorption of gaseous ammonia on  $\text{TiO}_2/\text{SiO}_2$  (20 %wt  $\text{TiO}_2$ ) at 308 K.

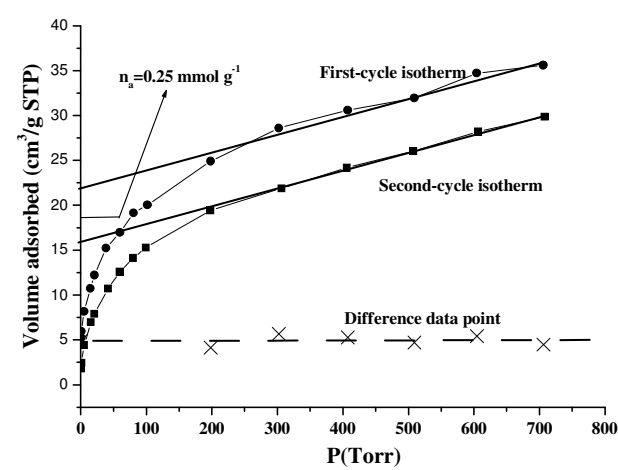


**Fig. 2.20:** Two-cycles adsorption of gaseous ammonia on  $\text{TiO}_2/\text{SiO}_2$  (20 %wt  $\text{TiO}_2$ ) at 373 K.

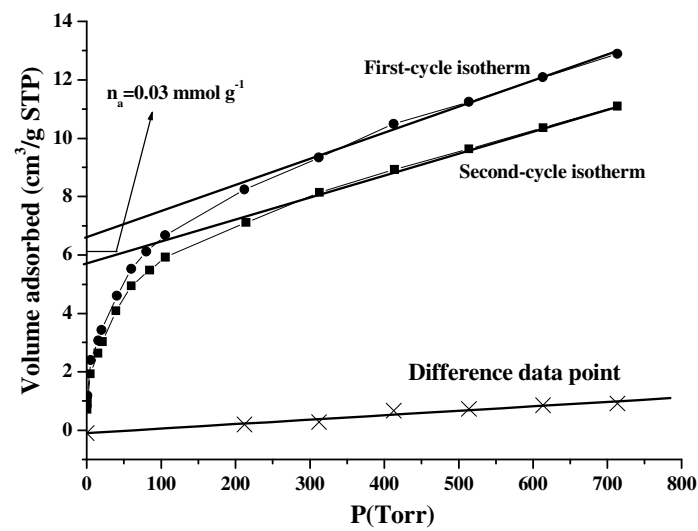


**Fig. 2.21:** Two-cycles adsorption of gaseous ammonia on  $\text{TiO}_2/\text{SiO}_2$  (20 %wt  $\text{TiO}_2$ ) at 622 K.

Independently of the temperature investigated, it is possible to observe that the total amount of ammonia adsorbed increases quickly with increasing bulk pressure in the region of very low-pressures values. This indicates the presence of very active surface sites, which give strong acid-base interactions with ammonia molecules.

For higher-pressure values, the rate of increasing adsorption diminishes and the isotherm becomes quasi-linear. This linearity is described to the physical adsorption on some other surface sites. A linear adsorption part can also be distinguished in the second-cycle isotherm. The slopes of both linear segments are almost identical, which means that further adsorption of ammonia molecules progresses

in much the same way. The two straight lines are suitably extrapolated to zero pressures.

The difference for points at which the curves reach zero pressure determines the maximum irreversible adsorption of NH<sub>3</sub>. In particular, it provides: at T= 308 K the total number of acidic sites (weak, medium and strong); at T=373K the number of medium and strong acid sites; at T= 622K the number of strong acidic sites. The number of acidic sites, determined with the use of the above procedure, for the sample indicated with the acronym 20TS-D are reported in the Table 2.6.

**Table 2.6** - Quantitative determination of number and strenght of acid sites, as determined by NH<sub>3</sub>-chemisorption analysis, for the catalysts 20TS-D

| Weak acid sites<br>(35°C<W.A.S.< 101 °C)<br>(μmol/g <sub>sample</sub> ) | Medium acid sites<br>(101°C<M.A.S.< 350 °C)<br>(μmol/g <sub>sample</sub> ) | Strong acid sites<br>(S.A.S.> 350 °C)<br>(μmol/g <sub>sample</sub> ) |
|---|--|--|
| 200   | 218  | 31   |

The acidic sites are classified as Strong Acid Sites (S.A.S= those ones on which NH<sub>3</sub> is still adsorbed above 350 °C); Medium Acid Sites (M.A.S= those ones on which NH<sub>3</sub> remains adsorbed between 101 °C and 350 °C) and Weak Acid Sites (W.A.S= those ones on which NH<sub>3</sub> remains adsorbed only below 101°C).

#### **2.4.2.7.3 Study of the surface acidity of $\text{TiO}_2/\text{SiO}_2$ catalysts by means of FT-IR measurements of CO and $\text{NH}_3$ adsorption**

The surface properties of  $\text{TiO}_2/\text{SiO}_2$  catalysts were studied by means of FT-IR spectroscopy of adsorbed probe molecules, CO and ammonia, in order to determine the acid strength of the coordinatively unsaturated surface (c.u.s.) titanium cations at the surface of silica.

##### **2.4.2.7.3.1 Hydroxyls spectra of samples outgassed at 723 K**

Figure 2.22 reports hydroxyls spectra, normalized to unit weight to allow comparison, in the  $3800 - 3200 \text{ cm}^{-1}$  range, of samples outgassed at 723 K. A spectrum is also reported, of the commercial silica (Grace S432) used as support.



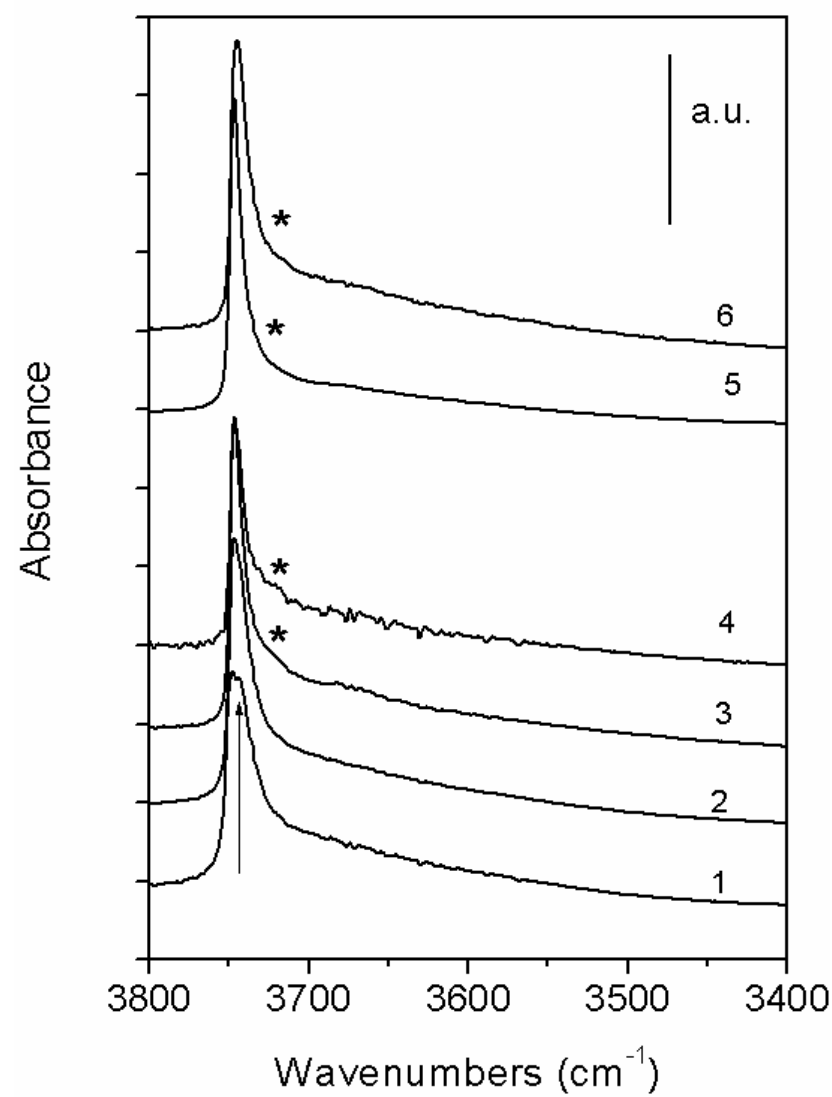
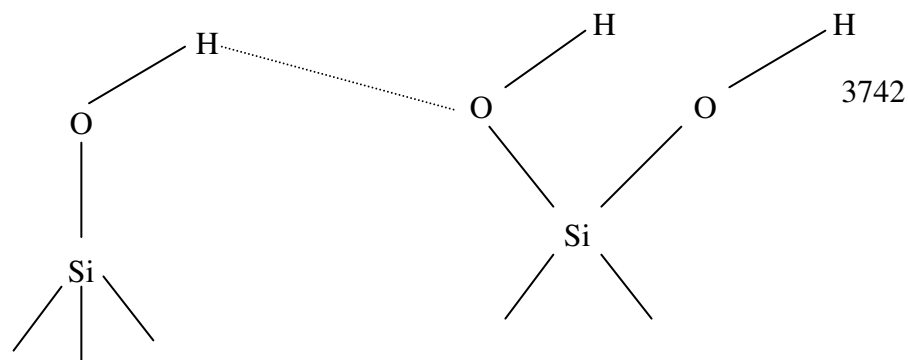


**Fig. 2.22:** FT-IR spectra of samples outgassed at 723 K, in the 3800 – 3200  $\text{cm}^{-1}$  range. Spectra normalized to samples unit area, in order to allow comparison, are reported of samples: silica Grace 432 (curve 1); 3TS-D (curve 2); 7TS-D (curve 3); 18TS-D (curve 4); 7TS-Tol (curve 5) ; 18TS-Tol (curve 6).

All spectra show a prominent band at about  $3745\text{ cm}^{-1}$ , due to isolated silanols, invariably observed at the surface of dehydrated silicas. With

pure silica (curve 1), a component is seen at  $3742\text{ cm}^{-1}$  (arrow), assigned to isolated/geminal silanols couples (Ref: A. Burneau, J.P.Gallas, *The Surface Properties of Silica*, A.P. Legrand Ed. **1999**, 194 and references therein), depicted in Scheme 1. The spectrum also shows a tail on the low frequencies side, due to some heterogeneity of sites, expected for silicas outgassed at 723 K.



**Scheme 1**

When Ti is present, the component at  $3742\text{ cm}^{-1}$  decreases in intensity (starting with sample 3.09TS-D, curve 2), and disappears at higher Ti loadings; with sample (curve 3), corresponding to a nominal monolayer coverage, only the band of free silanols is seen and its intensity does not change much even at higher Ti loadings. The disappearance of the  $3742\text{ cm}^{-1}$  band is probably related a slightly more acidic nature of the species in Scheme I than the free silanols.

The constant intensity of the  $3745\text{ cm}^{-1}$  band strongly suggests that, under the experimental conditions adopted, grafting with titanium

alkoxide occurs preferentially onto silanol-free surface patches, e.g. reactive siloxanes bridges rather than on isolated silanols. This is in agreement with previous results of Brunel et al. (Ref: D. Brunel, A. Cauvel, F. Di Renzo, F. Fajula, B. Fubini, B. Onida, E. Garrone, *New J. Chem.*, **2000**, 24, 807) who reported similar conclusion for the grafting of triethoxymethylaminopropane.

At high titanium loadings (curves 3 – 6), a new component appears at  $3720\text{ cm}^{-1}$  (asterisks), assigned to new Ti-OH species. As the intensity of silanols band at  $3745\text{ cm}^{-1}$  is weakly affected by titanium loading, such new species are likely not to be formed at the expenses of silanols, but to grow onto the grafted phase.

#### **2.4.2.7.3.2 Adsorption of CO at nominal 77 K on $\text{TiO}_2/\text{SiO}_2$ catalysts**

Carbon monoxide is widely used as a probe molecule to detect the presence and the nature of Lewis acidic sites and also of Brønsted sites, *i.e.* acidic hydroxyls, to which it may H-bond.

When the interaction between CO and the adsorbing site is basically of an electrostatic nature, like in the cases above, a hypsochromic shift occurs, with respect to the free CO molecule ( $2143\text{ cm}^{-1}$ ).

The following figures report difference spectra obtained after subtraction of those of the bare samples, depicted in Figure 2.22. Two spectral ranges are considered: that of hydroxyls stretch mode ( $\nu(\text{OH})$ ),

$3800 - 3400 \text{ cm}^{-1}$ , sections (a) of the Figures and that of the  $\text{C}\equiv\text{O}$  stretch mode ( $\nu(\text{CO})$ ,  $2250 - 2050 \text{ cm}^{-1}$ , sections (b) of the Figures).

Figure 2.23 reports spectra normalized to unit weight taken after CO dosage on sample 3.09TS-D: by increasing the CO pressure, a negative band is seen at  $3744 \text{ cm}^{-1}$ , while a broad adsorption forms, centred at  $3666 \text{ cm}^{-1}$ , with a shoulder at ca.  $3600 \text{ cm}^{-1}$ .

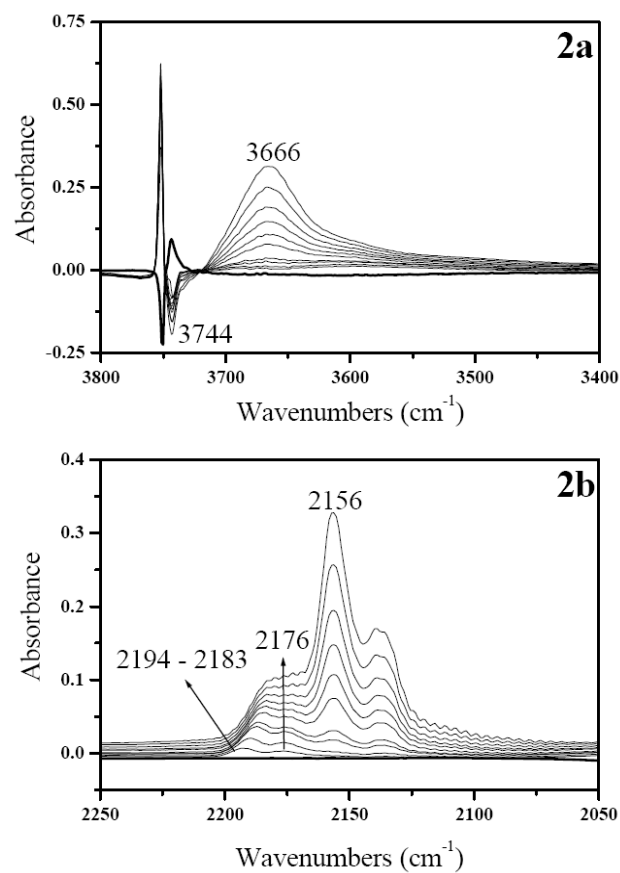


**Fig. 2.23:** FTIR difference spectra of CO adsorbed at nominal 77 K on sample 3.09TS-D, in the hydroxyls stretch range (section a) and in the CO stretch range (section b). Normalized spectra are reported, recorded in the 0.05 – 15 mbar equilibrium pressures range.

These features are due to H-bonding among CO molecules and OH species: those originally absorbing at  $3745\text{ cm}^{-1}$  (isolated silanols) shift to  $3666\text{ cm}^{-1}$  ( $\Delta\nu = 79\text{ cm}^{-1}$ ), as do silanols at the surface of dehydroxylated silicas ( $\Delta\nu = 80\text{ cm}^{-1}$ ), so indicating that the acidity of silanols is not altered by the presence of titanium. The shoulder at  $3600\text{ cm}^{-1}$  is due to more acidic silanols, visible in the spectrum of the bare sample (curve 2 in Figure 2.22) as a tail to band at  $3745\text{ cm}^{-1}$ . The interaction with hydroxyls is reversible, as the original IR spectrum was recovered after prolonged evacuation. The positive peak observed is due to slight changes in temperature brought about by the presence of the gas phase.

The band at  $2156\text{ cm}^{-1}$  (Figure 2.23b) is due to the CO stretch mode of carbon monoxide molecules interacting via H-bonding with silanols: it develops only at higher CO equilibrium pressures, being the interaction weaker than with other acidic sites; the signal at ca.  $2138\text{ cm}^{-1}$  is due to physisorbed CO.

At higher wavenumbers, bands are seen at  $2194\text{ cm}^{-1}$ , shifting to  $2183\text{ cm}^{-1}$  with coverage, and at  $2176\text{ cm}^{-1}$ : with bulk  $\text{TiO}_2$  (anatase), CO adsorption gives rise to well separated bands at 2205 and  $2189\text{ cm}^{-1}$  [18], due to the occurrence of two families of co-ordinatively unsaturated  $\text{Ti}^{4+}$  ions, but with  $\text{TiO}_2$  supported on  $\text{SiO}_2$  different acidic sites are expected. According to K. Hadjiivanov et al. [19], bands at  $2194\text{ cm}^{-1}$  and at  $2176\text{ cm}^{-1}$  are assigned to associated and isolated  $\text{Ti}^{4+}$  sites, respectively, both adsorbing CO in a reversible way.

The shift of the former band, from 2194 to 2183  $\text{cm}^{-1}$ , is interpreted as due to the collective behaviour of CO oscillators adsorbed on associated  $\text{Ti}^{4+}$  sites of an extended phase, as the shift is relatively large as compared to other oxide systems, meaning that adsorption sites can not be considered as isolated  $\text{Ti}^{4+}$  cations. According to Hadjiivanov et al. [18, 19], these sites can be assigned to titanium cations having at least one co-ordinatively unsaturated  $\text{Ti}^{4+}$  cation in the second coordination sphere.

Hadjiivanov and co-workers have shown, by means of adsorption experiments of  $^{12}\text{CO} - ^{13}\text{CO}$  mixtures, that both static and dynamic contributions affect the  $\nu(\text{CO})$  shift [20]: the dynamic interaction brings about a blue-shift, whereas the static interaction lowers the CO frequency.

For the second type of sites, the static shift is very small, which suggests that they represent isolated titanium cations. This is consistent with the small static shift for CO adsorbed on titania-silica systems with a low concentration of titanium cations.

Figures 2.24a and 2.24b report difference spectra obtained with 7.29TS-D sample.

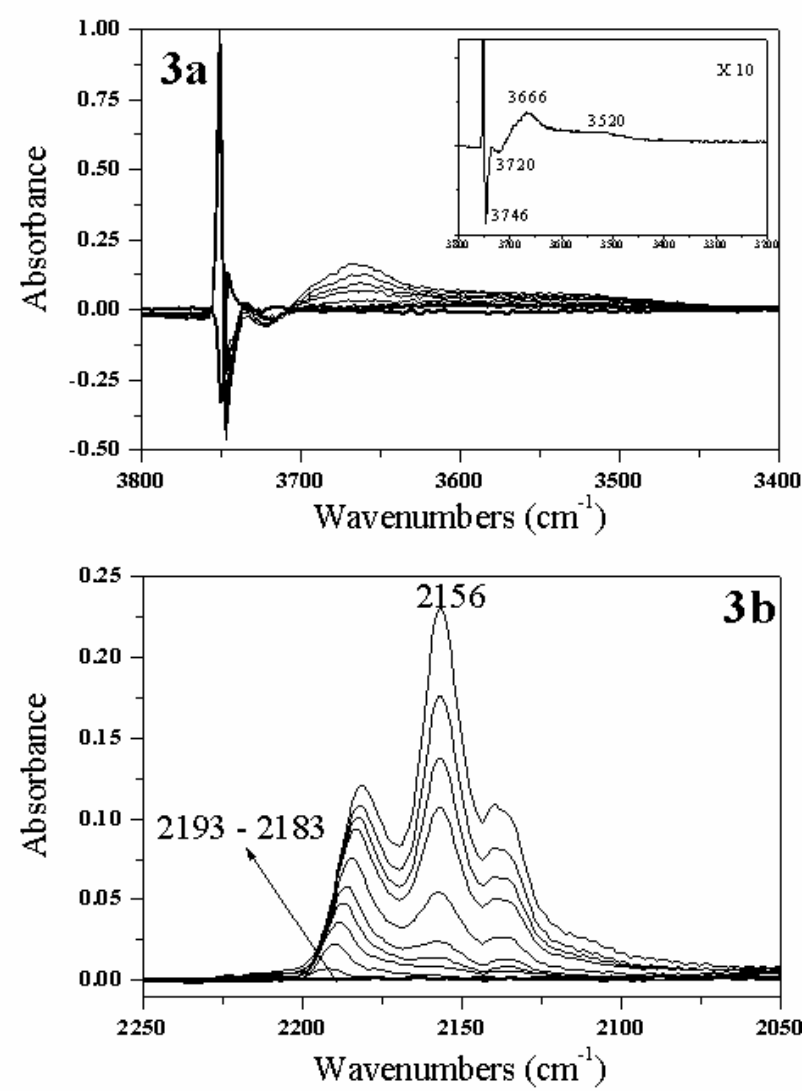


Fig. 2.24: FTIR difference spectra of CO adsorbed at nominal 77 K on sample 7.29TS-D, in the hydroxyls stretch range (section a) and in the CO stretch range (section b). Normalized spectra are reported, recorded in the 0.05 – 15 mbar equilibrium pressures range.

In the  $\nu(\text{OH})$  region (Figure 2.24a), besides the band of isolated silanols shifting from 3746 to 3666  $\text{cm}^{-1}$ , due to the formation

of H-bonding, new species are seen, i.e. a band at  $3720\text{ cm}^{-1}$ , shifting to  $3520\text{ cm}^{-1}$  absent with sample 3TS-D with a lower Ti-loading. Such a feature is better observed in the inset to Figure 2.24a, which reports the last spectrum magnified by a factor of ten: band at  $3720\text{ cm}^{-1}$  can be due to the presence of another kind of hydroxyl groups, i.e. non silica hydroxyls, with higher acid strength with respect to free silanols. The observed shift  $3720 - 3520\text{ cm}^{-1} = 200\text{ cm}^{-1}$  is larger than that of TiOH groups at the surface of pure  $\text{TiO}_2$ , meaning that, probably due to a synergic effect of the silica support, more acidic TiOH species occur. The corresponding CO stretch mode (Figure 2.24b), expected at about  $2165\text{ cm}^{-1}$ , being of low intensity, is probably masked by the other two prominent bands at  $2193 - 2183\text{ cm}^{-1}$  and  $2156\text{ cm}^{-1}$  (Figure 2.24b).

The band at  $2193\text{-}2183\text{ cm}^{-1}$ , as discussed before, is assigned to CO molecules interacting with “associated”  $\text{Ti}^{4+}$  sites and that at  $2156\text{ cm}^{-1}$  to CO interacting via H-bonding with surface SiOH groups. It is worth observing that isolated  $\text{Ti}^{4+}$  sites should be absent in sample 7TS-D, as the corresponding band at  $2176\text{ cm}^{-1}$  is not observed and new TiOH species are formed.

With sample 17.8TS-D, in the O-H stretch region, the same species are observed as on sample 7.29TS-D (figure 2.25a).



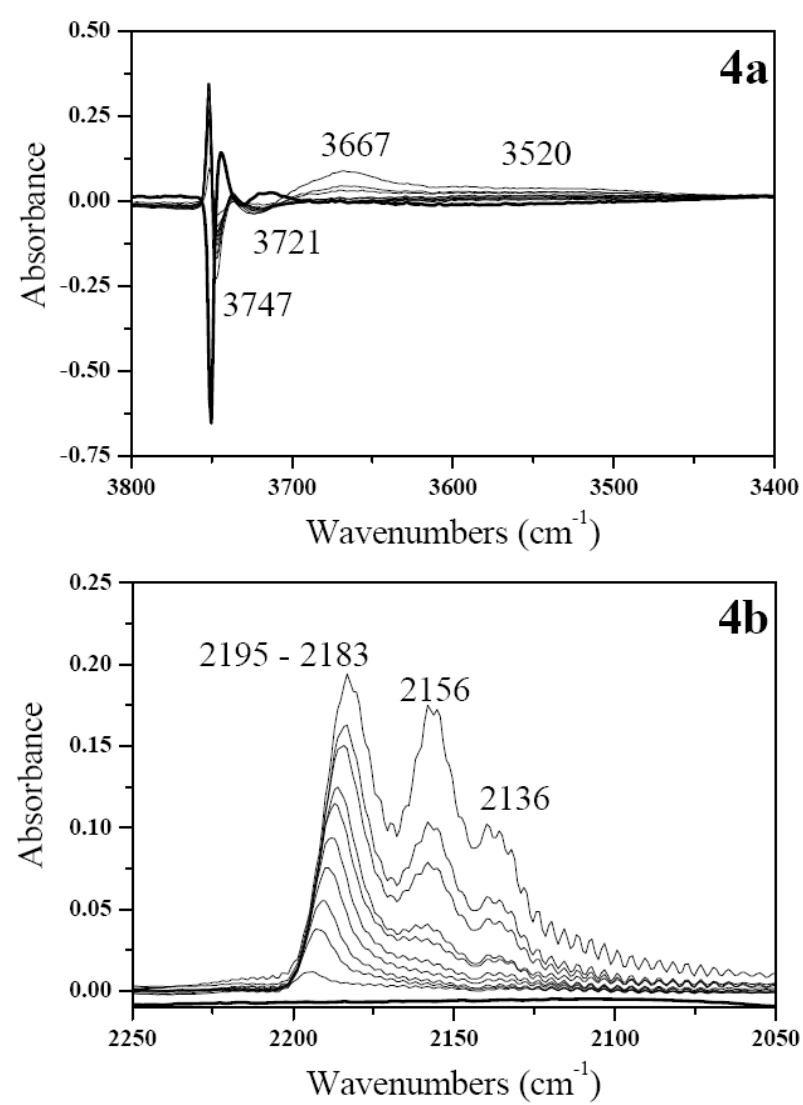


**Fig. 2.25:** FTIR difference spectra of CO adsorbed at nominal 77 K on sample 17.8TS-D, in the hydroxyls stretch range (section a) and in the CO stretch range (section b). Normalized spectra are reported, recorded in the 0.05 – 15 mbar equilibrium pressures range.

The most relevant difference observed after CO dosage on sample 17.8TS-D is observed in the CO stretch range (Figure 2.25b) with an increased intensity is observed of the band at  $2195 - 2183 \text{ cm}^{-1}$ , due to CO on associated  $\text{Ti}^{4+}$  sites, with respect to that of CO adsorbed on hydroxyls ( $2156 \text{ cm}^{-1}$ ). Such a behaviour indicates that by increasing the titanium loading, the hydroxyls population remains more or less constant, whereas an extended titania phase in which vicinal  $\text{Ti}^{4+}$  cations are present is formed. This semi-quantitative evaluation is in agreement with results described in previous papers [22-24], according to which, at low Ti loadings, species with titanium sitting in tetrahedral coordination seem to be prevalent on the catalyst surface until the surface monolayer coating is reached ( $\sim 2.2 \text{ Ti atoms/nm}^2$ ). In contrast, the degree of the polymerization of Ti species increases by further increasing  $\text{TiO}_2$  loading, giving rise to a large amount of octahedral Ti-sites grafted on  $\text{SiO}_2$ .

In order to investigate a possible role of the solvent used during preparation on the surface properties of grafted  $\text{TiO}_2/\text{SiO}_2$  catalysts, CO adsorption at nominal 77 K is reported in Figures 2.26 and 2.27 for samples 7TS-Tol and 18TS-T, respectively, obtained by using toluene instead of dioxane.

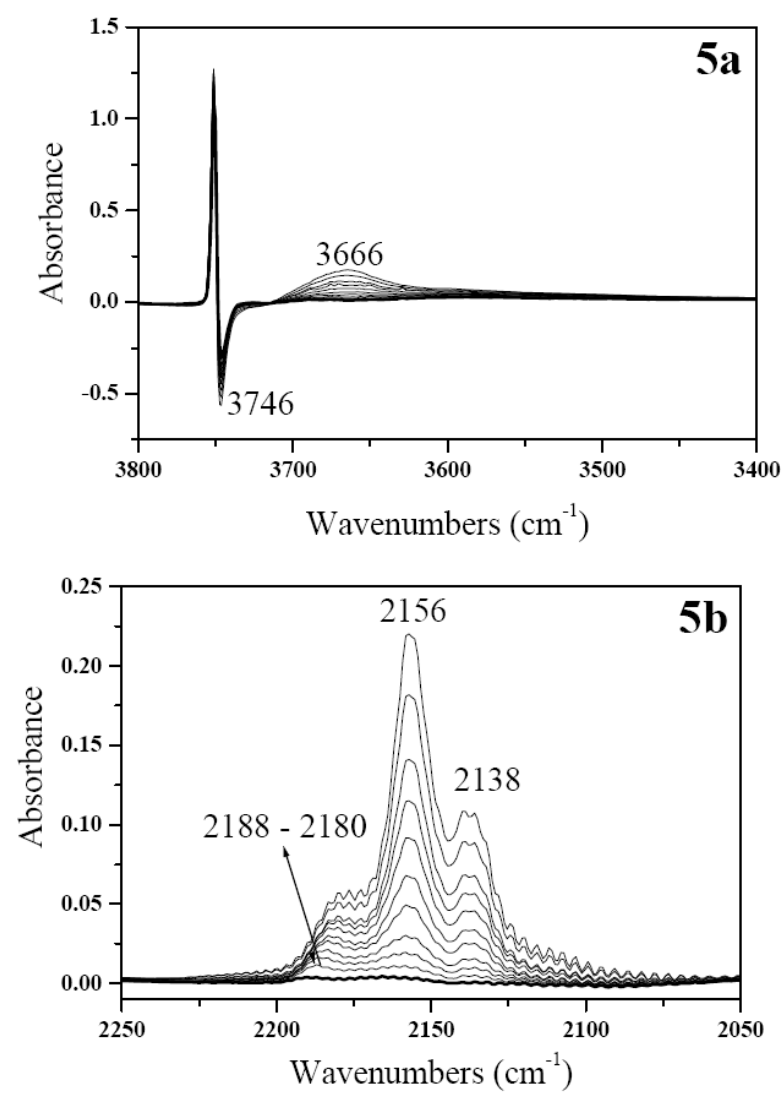


**Fig. 2.26:** FTIR difference spectra of CO adsorbed at nominal 77 K on sample 7TS-Tol, in the hydroxyls stretch range (section a) and in the CO stretch range (section b). Normalized spectra are reported, recorded in the 0.05 – 15 mbar equilibrium pressures range.

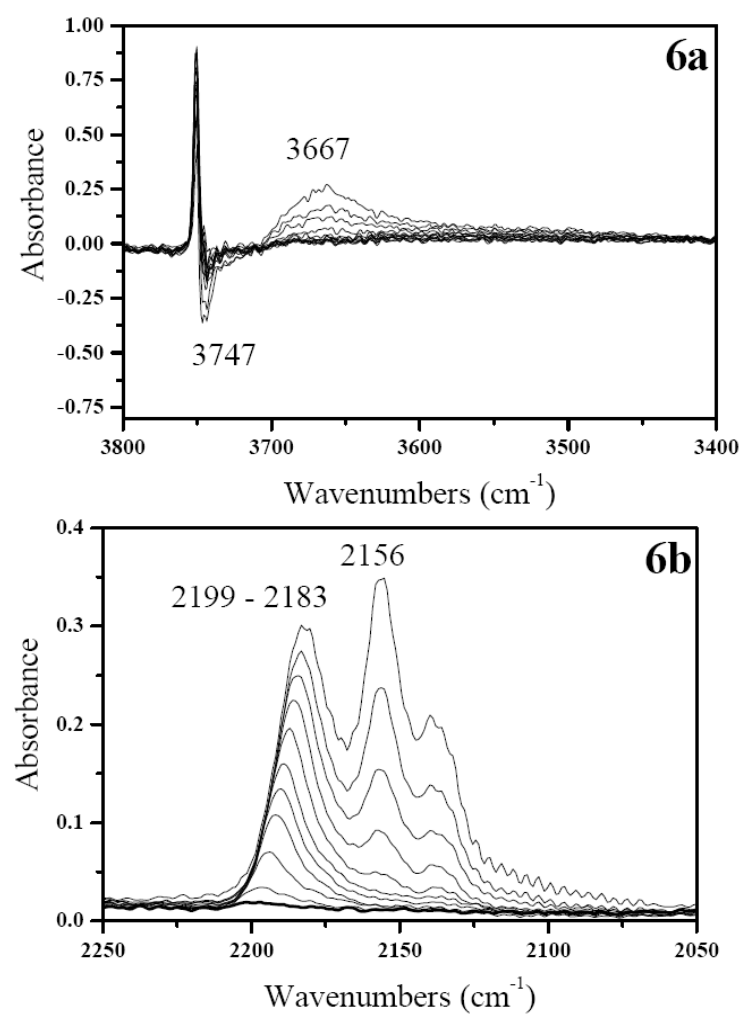


**Fig. 2.27:** FTIR difference spectra of CO adsorbed at nominal 77 K on sample 18TS-Tol, in the hydroxyls stretch range (section a) and in the CO stretch range (section b). Normalized spectra are reported, recorded in the 0.05 – 15 mbar equilibrium pressures range.

With sample 7TS-Tol (Figures 2.26a and 2.26b), in the OH stretch range the band of isolated silanols at 3747  $\text{cm}^{-1}$  is seen to shift to 3667  $\text{cm}^{-1}$  upon CO adsorption; in the CO stretch range, a band at 2188  $\text{cm}^{-1}$

is seen to shift to  $2180\text{ cm}^{-1}$  with coverage and at high CO partial pressure the bands of CO adsorbed on isolated silanols ( $2156\text{ cm}^{-1}$ ) and that of physisorbed CO ( $2138\text{ cm}^{-1}$ ) are seen. With respect to sample 7.09TS-D, with comparable titanium loading, the main difference concerns the absence of TiOH species, as the corresponding band at  $3720\text{ cm}^{-1}$  is not seen.

Similar results are obtained with sample 18TS-Tol (Figures 2.27a and 2.27b), i.e. only the band of isolated silanols is seen in the  $3800 - 3400\text{ cm}^{-1}$ , and those of associated  $\text{Ti}^{4+}$  sites ( $2199 - 2183\text{ cm}^{-1}$ ), besides those at  $2156$  and  $2138\text{ cm}^{-1}$ , assigned above.

The band associated to  $\text{Ti}^{4+}$  sites is observed at slightly higher wavenumbers ( $2199\text{ cm}^{-1}$  against  $2195\text{ cm}^{-1}$ ) with respect to sample 18TS-D having comparable titanium loading, indicating the occurrence of  $\text{Ti}^{4+}$  cations, more exposed at the surface, acting as stronger acidic Lewis sites, with respect to the sample 18TS-D. The use of toluene instead of dioxane as a solvent seems to favour the formation of an extended  $\text{TiO}_x$  phase, with highly uncoordinated  $\text{Ti}^{4+}$  cations, with respect to the formation of TiOH species.

Results described above show that the surface properties of these  $\text{TiO}_2/\text{SiO}_2$  systems differ strongly from those of pure oxides: several studies have shown that CO adsorption on both anatase and rutile  $\text{TiO}_2$  modifications results in the appearance of  $\text{Ti}^{4+}$  carbonyls that are well visible at ambient temperature and under CO equilibrium pressure [25,26].

Two  $\text{Ti}^{4+}$  sites have been reported at the surface of anatase, the maxima of the respective bands located at 2208 ( $\alpha$  sites) and 2192 ( $\beta'$  sites)  $\text{cm}^{-1}$ , at low coverage, shifting to 2206 and 2186  $\text{cm}^{-1}$ , respectively at high coverage [25].

With the present  $\text{TiO}_2/\text{SiO}_2$  catalysts, in contrast, the CO adsorption at ambient temperature was negligible, which evidences that, in general, the solids investigated are characterized by a weaker Lewis acidity than  $\text{TiO}_2$  itself.

Thus, the absence of strong Lewis acid sites on grafted  $\text{TiO}_2/\text{SiO}_2$  catalysts is the main difference, when compared to pure titania. This is an important aspect, influencing significantly the catalytic performances of  $\text{TiO}_2/\text{SiO}_2$  catalysts with respect to  $\text{TiO}_2$  itself, as reported below. In contrast, Lewis acidity appears to be similar to other silica-supported titania catalysts [20] and of titanium silicalite [27].

#### **2.4.2.7.3.3 Adsorption of $\text{NH}_3$ at room temperature on $\text{TiO}_2/\text{SiO}_2$ systems**

Ammonia is probably the most frequently used probe molecule for acidity assessment, as it can interact with both Brønsted acidic sites, by forming ammonium ions, and Lewis acidic sites, by forming acidic-basic adducts.

Its small size allows to probe quantitatively almost all acid sites in micro, meso- and macro-porous oxides [28]. The protonated species (ammonium ions) and the coordinatively bonded ammonia differ,

from a spectroscopic point of view, by their different NH deformation and stretching vibrations. The ammonium ion shows typical absorptions at 1450 and 3300  $\text{cm}^{-1}$ , whereas co-ordinatively bonded ammonia molecules absorb at 1250, 1630 and  $\sim 3330$   $\text{cm}^{-1}$ . In particular, the deformation vibrations (bending modes) at 1450 and 1630  $\text{cm}^{-1}$  are used as most reliable indicators for the presence of protonated and coordinatively bonded ammonia, respectively.

In this work, all the samples have been characterized by means of FTIR spectroscopy of adsorbed ammonia: being the interaction stronger with ammonia than with CO, spectra have been recorded at room temperature, by dosing increasing amounts of ammonia, in the equilibrium pressure range  $1,00 \cdot 10^{-1}$  – 17,0 mbar and then by removing the reversible fraction of the adsorbate via prolonged evacuation.

Figs. 2.28a and 2.28b report normalized spectra taken after dosing about 5 mbar of ammonia on the five samples outgassed at 723 K: spectra are reported after subtraction of the spectra of the bare samples, reported in Figure 2.22.

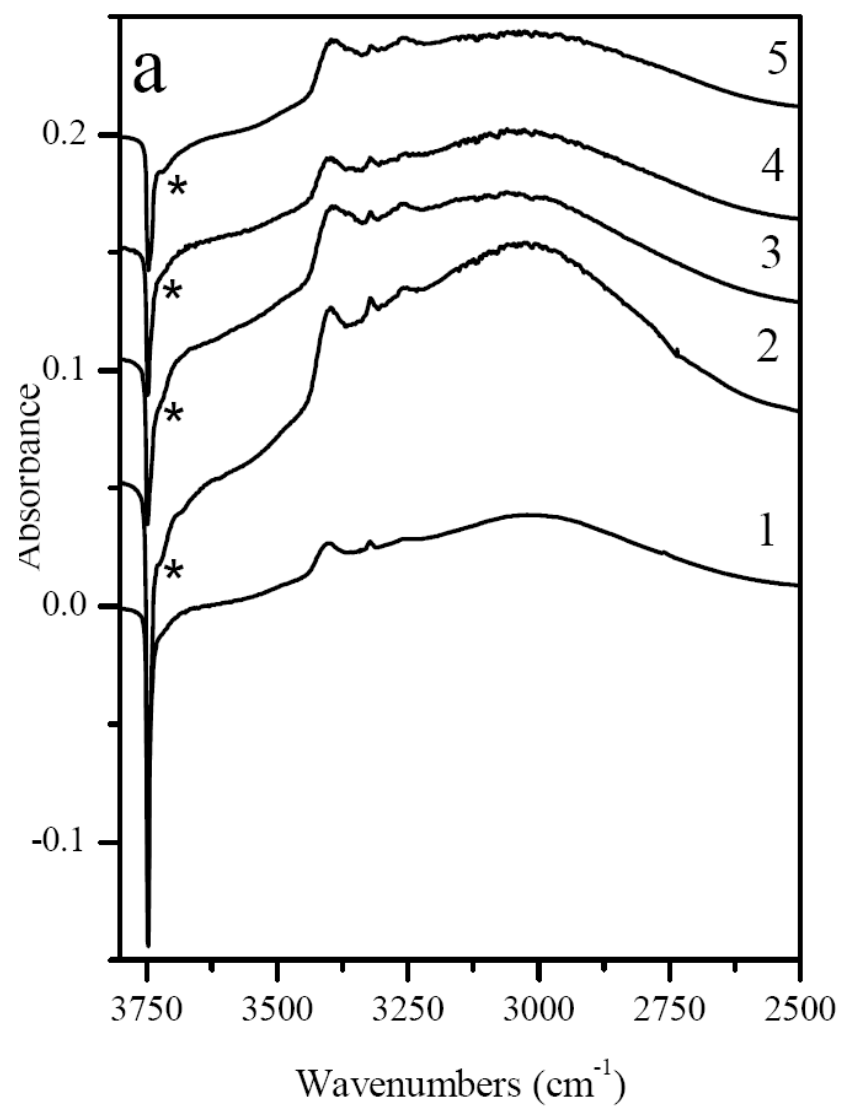


**Figure 2.28:** FT-IR difference spectra recorded after dosing at room temperature about 5 mbar of  $\text{NH}_3$  on samples outgassed at 723 K. Section a): OH stretch region (3800 – 2500  $\text{cm}^{-1}$ ); section b): N-H bending region. Curves 1, 2, 3, 4 and 5 refer to samples 3.09TS-D, 7.29TS-D, 17.8TS-D, 7TS-Tol and 18TS-Tol, respectively.



In the OH stretch range (Figure 2.28a), with all samples a negative band at  $3745\text{ cm}^{-1}$  and a broad absorption with maximum at about  $2990\text{ cm}^{-1}$  are seen: these features are readily assigned to the interaction of isolated silanols ( $3744\text{ cm}^{-1}$ ) with ammonia molecules via the formation of H-bonding. Being the interaction much stronger than with CO, the observed shift is ca.  $750\text{ cm}^{-1}$ , as commonly observed with pure silica.

Besides these features, another negative band is seen at about  $3720\text{ cm}^{-1}$ , with all samples except 3.09TS-D: in agreement with results of CO adsorption, it is assigned to more acidic Ti-OH species.

Figure 2.28b reports the same spectra in the NH bending mode region ( $1700 - 1350\text{ cm}^{-1}$ ): with sample 3.09TS-D, a signal is seen at  $1606\text{ cm}^{-1}$ , assigned to  $\text{NH}_3$  molecules adsorbed on  $\text{Ti}^{4+}$  sites. The shoulder observed at ca.  $1636\text{ cm}^{-1}$  is due to ammonia molecules interacting with isolated silanols via H-bonding: such band, seen only at appreciable ammonia pressure, is reversible upon evacuation at room temperature (spectra not shown). By increasing the titanium loading on samples synthesised in dioxane (curves 2 and 3), the intensity of the band at  $1606\text{ cm}^{-1}$  increases markedly, and a new band is seen at ca.  $1460\text{ cm}^{-1}$ . The latter feature is assigned to the formation of ammonium ions, due to the interaction of ammonia with more acidic TiOH species, absorbing at  $3720\text{ cm}^{-1}$  in the original spectra: this conclusion is supported by the presence of a negative band in the OH stretching region (Figure 2.28a, asterisks). The interaction of

ammonia with such  $\text{TiOH}$  species is only partially reversible after evacuation at room temperature (spectra not reported).

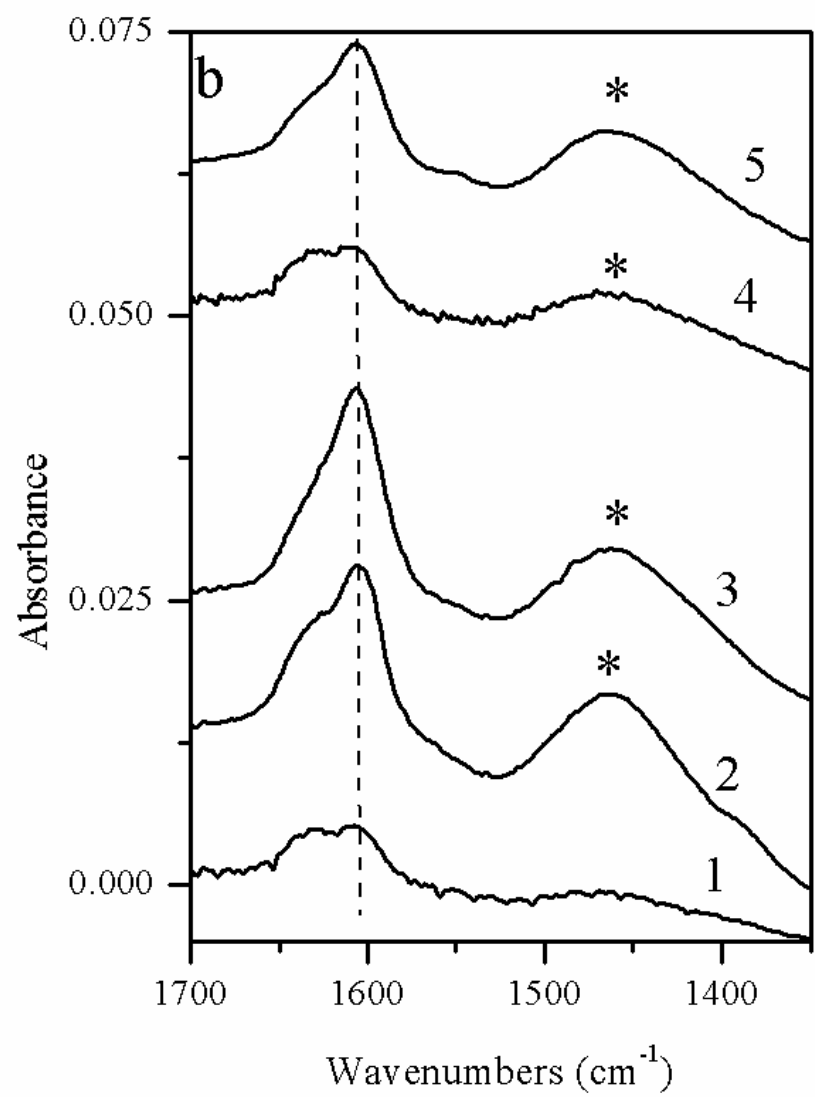


**Figure 2.28:** FT-IR difference spectra recorded after dosing at room temperature about 5 mbar of  $\text{NH}_3$  on samples outgassed at 723 K. section b): N-H bending region. Curves 1, 2, 3, 4 and 5 refer to samples 3.09TS-D, 7.29TS-D, 17.8TS-D, 7TS-Tol and 18TS-Tol, respectively.

No relevant differences were observed for the 7TS-Tol (curve 4) and for 18TS-Tol (curve 5) catalysts, besides the fact that the contribution of more acidic TiOH species is lower with respect to samples having the same titanium content synthesised in dioxane.

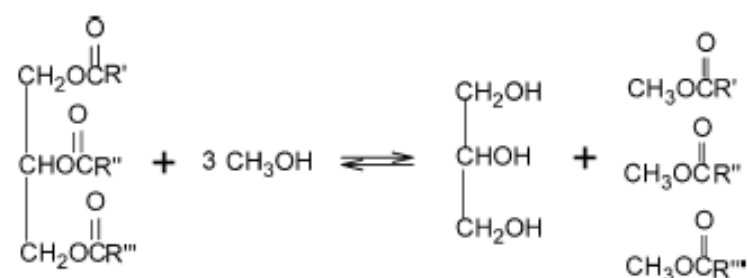
The main results coming from FT-IR spectroscopy of adsorbed CO and  $\text{NH}_3$  on  $\text{TiO}_2/\text{SiO}_2$  catalysts prepared by *grafting* can be synthesized as follows:

- The interaction between titania and silica in silica-supported titania catalysts gives place to supported  $\text{Ti}^{4+}$  sites, characterized by a weaker Lewis acidity than on pure TiO.
- Two kinds of Lewis acid sites, differing in the electrophilic properties of the respective  $\text{Ti}^{4+}$  cations, were detected: a) isolated  $\text{Ti}^{4+}$  sites ( $2177\text{-}2173\text{ cm}^{-1}$ ) mainly at low Ti loading and b) “associated”  $\text{Ti}^{4+}$  sites ( $2194\text{-}2183\text{ cm}^{-1}$ ).
- Hydroxyl groups with higher acid strength, with respect to Si-OH groups of  $\text{SiO}_2$  and to TiOH groups of  $\text{TiO}_2$ , were observed on the surface of 7.29TS-D sample, that was indicated by the shift of the band from  $3721$  to  $3520\text{ cm}^{-1}$  in the FTIR spectrum of adsorbed CO (Fig. 2.24a). This was also confirmed by ammonia adsorption. In fact, the band at  $1465\text{ cm}^{-1}$  (see Fig. 2.28a) rises in intensity in parallel with the appearance of the band at  $3716\text{ cm}^{-1}$ .

### 2.4.3 Catalytic performances of $\text{TiO}_2/\text{SiO}_2$ in the transesterification of refined/edible oils with methanol

#### 2.4.3.1 Literature information on biodiesel production

Biodiesel (fatty acids methyl esters, FAME) has recently become very attractive, because of its environmental benefits and the fact that it is produced from renewable sources [29,30]. Nowadays, most biodiesel is produced by the transesterification of triglycerides of refined/edible type oils using methanol and an alkaline catalyst (NaOH, NaOMe) [29,30]. The occurring reaction is:



As can be seen, glycerol is a by-product of the reaction. Because of present day high cost of petroleum notwithstanding, biodiesel is not competitive with petroleum diesel without subsidies or tax incentives. There are two main factors that affect the cost of biodiesel: the cost of raw materials (fats or oil and alcohols) and the cost of processing [31]. The most commonly used technology for TG transesterification is based on the use of batch plants, in which a basic homogeneous catalyst is used (NaOH or  $\text{NaOCH}_3$ ) and, at the end of the reaction,

the catalyst is neutralized with acetic acid or a mineral acid. A continuous transesterification process would be a good opportunity for reducing the production costs [31]. However, this technology has different unavoidable drawbacks. In the presence of moisture or free fatty acids (FFAs), soaps are formed that favour emulsion between glycerol and oil. Emulsion is also favoured by the presence of unreacted monoglycerides and diglycerides. Therefore, a long settling time is necessary for the separation of the two emulsified phases. Moreover, the recovered glycerol is, normally, impure, because of the presence of salts, soaps, monoglycerides, and diglycerides, and purification represents an additional cost.

The cost of biodiesel could certainly be reduced through the use of a heterogeneous catalyst, instead of a homogeneous one, providing for higher-quality esters and glycerol, which are more easily separated, and there is no need for further expensive refining operations. To this end, the French Institute of Petroleum (IFP) has recently announced the construction of a new 160 000 t/yr biodiesel plant that is based on the use of an heterogeneous catalyst [31,32]. The catalyst proposed by the IFP is a Lewis acid catalyst based on a zinc compound (zinc aluminate [33]). Many other heterogeneous catalysts that are based on both acid [34,35] and basic [35-41] solids have recently been proposed in the literature. In particular, the Mg-Al calcined hydrotalcites, derived from hydrotalcites of general formula  $[\text{Mg}^{2+}(1-x)\text{Al}^{3+}x(\text{OH})_2]x+(\text{CO}_3)^{2-} x/n$ , are solids with interesting basic

properties that have shown good activity in transesterification reactions.

Corma et al. [42], for example, in a patent mainly devoted to the transesterification of triglycerides with glycerol to prepare monoglycerides, also claimed the possibility to use calcined hydrotalcites and magnesium oxides in promoting the transesterification of triglycerides with monoalcohols, even if no examples or experimental data for this reaction are reported in the patent.

Leclercq et al. [36] tested the use of commercial calcined hydrotalcites in the transesterification of rapeseed oil, at 60 °C, with poor results for this catalyst, probably because of the very low temperature adopted in the performed runs.

Cantrell et al. [41], on the contrary, successfully used calcined hydrotalcites in promoting the transesterification of glycerol-tributirrate with methanol.

More recently, Santacesaria et al. [43,44] reported the good performances of calcined hydrotalcites and magnesium oxide in promoting the transesterification reactions that occur in biodiesel preparation.

#### **2.4.3.2 Catalytic screening of $\text{TiO}_2/\text{SiO}_2$ catalysts**

The catalytic performances of the  $\text{TiO}_2/\text{SiO}_2$  samples were tested in the transesterification of refined “neutral” soybean oil with methanol,

that is the reaction on which the biodiesel production is based. The operative conditions adopted are reported at the point 2.2.3.

**Table 2.6** - Catalytic activities of  $\text{TiO}_2/\text{SiO}_2$  in the transesterification of refined/edible oils with methanol

| Catalysts      | Grafting steps | wt % $\text{TiO}_2$ | $\text{S}_{\text{BET}}$ ( $\text{m}^2/\text{g}$ ) | $\text{Y}_{\text{FAME}}$ (%) |
|----------------|----------------|---------------------|---|------------------------------|
| $\text{SiO}_2$ | -              | 0                   | 282   | 2.78                         |
| 0.92TS-D       | 1              | 0.92                | 284   | 46.30                        |
| 1.80TS-D       | 1              | 1.80                | 283   | 52.41                        |
| 3.09TS-D       | 1              | 3.09                | 284   | 64.05                        |
| 5.74TS-D       | 1              | 5.74                | 278   | 59.11                        |
| 7.62TS-D       | 1              | 7.62                | 282   | 64.05                        |
| 11TS-D         | 1              | 11.0                | 278   | 64.19                        |
| 20TS-D         | 3              | 20.0                | -   | 49.00                        |
| 7TS-Tol        | 1              | 7.00                | 268   | 47.57                        |
| 17.8TS-Tol     | 3              | 17.8                | 274   | 44.44                        |
| 7.30TS-I       | 1              | 7.30                | -   | 68.15                        |
| $\text{TiO}_2$ | -              | 100                 | -   | 2.71                         |

Y=Yield; FAME=Fatty Acid Methyl Esters

In Fig. 2.29 the activities are reported as function of the  $\text{TiO}_2$  amount charged on the surface of the catalysts.

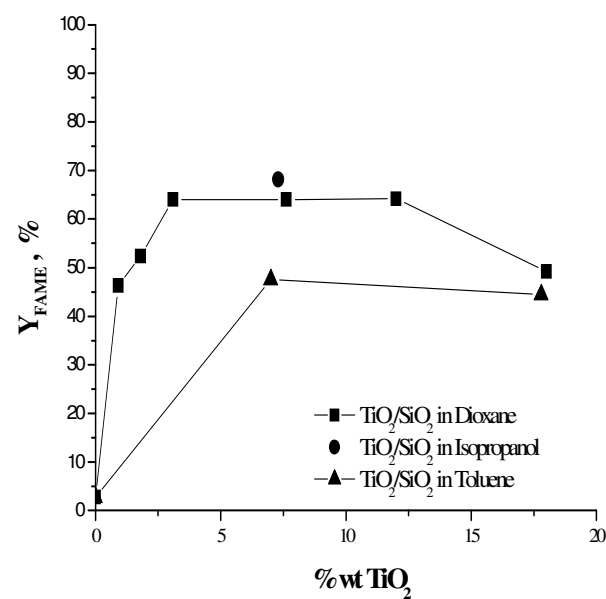


**Fig. 2.29:** Catalytic activity of the  $\text{TiO}_2/\text{SiO}_2$  catalysts in the transesterification of refined/edible oils or fats with methanol

It is interesting to observe from the catalytic results reported in Fig. 2.29 that, for both the series of samples respectively prepared in dioxane and toluene as solvents, the yields increase by increasing the titanium loading (% wt  $\text{TiO}_2$ ) until to reach the monolayer coverage corresponding to about 7 % by weight of  $\text{TiO}_2$ .

By further increasing the amount of titanium grafted on silica, the yield-values moderately decrease for the catalysts prepared in dioxane, while remain quite constant for the ones in toluene. In particular, in all the range of % wt  $\text{TiO}_2$  investigated, the catalysts prepared in toluene have shown lower activity-values than the ones prepared in isopropanol and dioxane. These data show a possible influence of the preparation variables, i.e. titanium loading and solvent, on the



titanium surface environment and, consequently, on the reactivity-properties of  $\text{TiO}_2/\text{SiO}_2$  catalysts.

It is worth that crystalline (anatase)  $\text{TiO}_2$  shows no catalytic activity in the same reactions. This finding is in agreement with the results observed with homogeneous catalysts [29], which suggested that an optimal range in strength exists for Lewis acidic sites, and that very strong Lewis acidic catalysts are less active in transesterification reactions. As matter of fact, the acidic sites have to coordinate the reactant molecules, but not so much in order to release also the products.

This effect appeared more pronounced for 17.8TS-D and 18TS-Tol catalysts, whose FTIR normalized spectra of adsorbed CO showed a larger concentration of “associated”  $\text{Ti}^{4+}$  sites with respect to the solids with smaller amount of supported titania. Moreover, FTIR measurements of  $\text{NH}_3$  adsorbed evidenced for these catalysts an increase of Brønsted acid sites, assigned to the increase of Ti-OH groups with respect to the silica support, as consequence of grafting reaction of titanium isopropoxide. According to these characterizations, lower activities in the transesterification reaction were found for the mentioned solids.

Finally, the results obtained in this work enable to attribute the best catalytic behaviour, showed by 3.09TS-D and 7.29TS-D samples in the transesterification reaction to the higher dispersion of titanium sites, confirmed by the band at  $2176\text{ cm}^{-1}$ , assigned to CO adsorbed onto isolated  $\text{Ti}^{4+}$  sites.

### 2.4.3.3 Comparison of the catalytic performances of $\text{TiO}_2/\text{SiO}_2$ catalysts with other heterogeneous catalytic systems

In the present paragraph, the catalytic performances of one of the  $\text{TiO}_2/\text{SiO}_2$  catalysts listed in Table 2.1, in particular the catalyst indicated with the acronym 3.09TS-D, were compared with those of other heterogeneous catalytic systems, both acidic and basic, such as:  $\text{VOPO}_4 \cdot 2 \text{H}_2\text{O}$  (VOP), prepared according to the literature [45];  $\text{Al}(\text{H}_2\text{O})_{0.18}\text{VO}_{0.82}\text{PO}_4 \cdot 2\text{H}_2\text{O}$  (AlVOP), prepared as reported in [46];  $\text{MgO}$ , supplied by Merck.

The catalytic screening of all the catalysts mentioned above was performed at 180 °C in the transesterification of a “neutral” soybean oil (FFA concentration = 0.2% w/w). At the end of the reaction, all the catalysts were separated from reagents and products by centrifugation. So, additional runs were carried out by re-testing the used catalysts in the same reaction conditions of the first runs. The obtained catalytic results are gathered in Fig. 2.30.

Since at high temperatures the stainless steel internal surface of the vials can catalyze the transesterification reaction [47], also a run without catalyst was performed obtaining about 10% of yield (see Fig. 2.30).

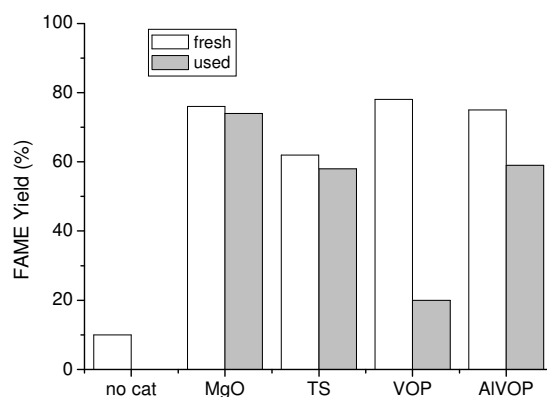


**Fig. 2.30:** Percentage of FAME yields obtained in several cases, such as: (a) without catalyst; (b) MgO; (c) TS; (d) VOP. For (b)-(d) cases, catalytic results referred to both fresh and used catalysts in reaction with neutral oil are showed. (“Neutral” oil = 2.0 g, methanol = 0.88 g, catalyst = 0.1 g, T=180°C).

As can be seen from Fig. 2.30, MgO, VOP and AIVOP catalysts showed the best performances in terms of FAME yields (75-80 %) while TS (3.09TS-D) catalyst gave lower yield (62 %). Moreover, from the results reported in Fig. 2.30, it is interesting to note that VOP catalyst, unlike the other two catalytic systems, i.e. MgO and 3.09TS-D, suffers from a strong deactivation when it is re-used. As shown in a recent work by Di Serio et al. [48], the deactivation of VOP catalyst is due to the methanol which, at the investigate temperature (180 °C), gives place to a slow reduction of the vanadium species ( $\text{V}^{5+} \rightarrow \text{V}^{3+}$ ) on the catalyst surface. The activity can easily be restored by calcination [48].

The deactivation of the VOP active phase can be limited by introducing aluminium in the VOP structure, as occurred in the case of AlVOP catalyst. On the contrary, both MgO and 3.09TS-D catalysts seem more stable to the deactivation phenomenon.

#### 2.4.3.4 Investigation of the stability of $\text{TiO}_2/\text{SiO}_2$ catalysts

In order to investigate the stability of the 3.09TS-D catalyst, the activity was tested also in the presence of high FFA concentrations (10% w/w), but keeping unchanged the other reaction conditions (Oil (FFA = 10% w/w) = 2.0 g, methanol=0.88 g, catalyst =0.1g, T =180°C), and compared with the ones of MgO. The acidic oil was prepared by adding oleic acid to the soybean oil. In the case of acid oil, the relation (1) (see paragraph 2.3) must to be re-arranged in order to take into account also the contribute from the acid oil to the global FAME yield, as reported in the following lines:

$$(3) \quad Y_{FAME} = \frac{n_{FAME}}{3n_o^0 + n_{OA}^0}$$

( $n_o^0$  =initial moles of oil;  $n_{OA}^0$  = initial moles of oleic acid;  $n_{FAME}$  = moles of FAME)

So, we have:

$$(4) \quad Y_{FAME} = \frac{3}{3 + \Gamma} \frac{A_1 / 3}{A_2 / 2}$$

where

$$(5) \quad \Gamma = \frac{w_{\%OA} / 100}{1 - w_{\%OA} / 100} \frac{MW_O}{MW_{OA}}$$

( $w_{\%OA}$ = weight % of initial oleic acid;  $MW_{OA}$ =molecular weight of oleic acid;  $MW_O$  = molecular weight of soybean oil)

When the  $w_{\%OA}$  is 0 (neutral oil), the equation (5) is reduced to equation (6).

A run without catalyst in the presence of high FFA concentration was also conducted.

By comparing the catalytic results referred to the run without catalyst reported in Fig. 2.30 with the ones shown in Fig. 2.31a, it is possible to note that the FAME yield increases a little in the case of transesterification of acidic oil with respect to neutral oil. This increase is due to the occurring of the non-catalytic esterification reaction (a FFA concentration 6.5 % w/w is reached at the end of the reaction) and is also probably due to the catalytic effect of the presence of FFA on the transesterification reaction.

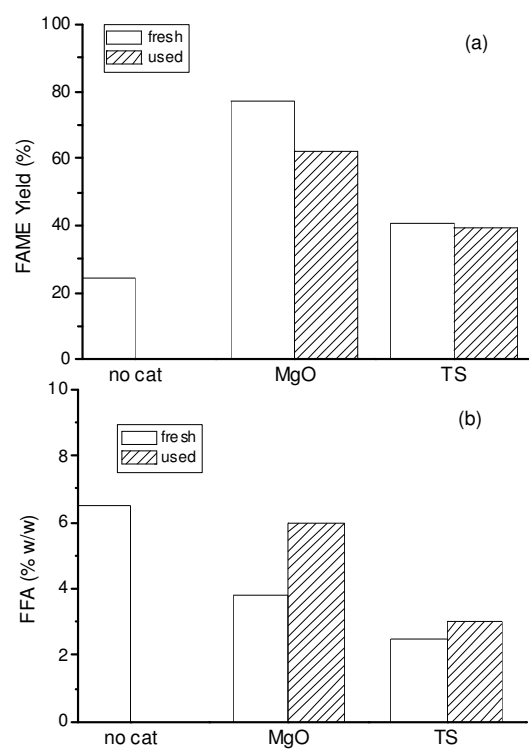


**Fig. 2.31:** (a) FAME yields (%) and (b) final FFA concentrations obtained both without catalyst and in the presence of fresh and used catalysts in reaction with acidic oil (FFA=10 % w/w). (Oil= 2.0g, methanol = 0.88 g, catalyst =0.1 g, T=180°C).

Moreover, as can be seen from the Fig. 2.31, the 3.09TS-D catalyst (TS in the figure) was deactivated in presence of high concentration of FFA but the final value of acidity in the run was much lower than the one obtained in the non catalyzed run (2.5%). These results show that the 3.09TS-D catalyst is also an esterification catalyst. Moreover, even if the TS catalyst in presence of FFA has shown lower performances than with neutral oil, it is a stable catalyst.

As matter of fact, 3.09TS-D catalyst gave quite the same FAME yield and FFA final concentration, when it was re-used in the same reaction condition (see Fig. 2.31a and 2.31b). MgO showed about the same FAME yield in presence of both FFA and neutral oil (see Figs. 2.30 and 2.31a). However, the utilize of this type of solid as catalyst in the biodiesel production presents some drawbacks, such as the formation of Mg soaps as a consequence of the reaction between MgO and FFA, giving place to a final opalescent product. From these preliminary data, the 3.09TS-D catalyst appeared a very promising catalyst for the transesterification of oils containing high FFA concentration.

So, on the basis of the promising results achieved during the catalytic screening, we decided to deep the investigation about the catalytic performances of the titania supported on silica catalyst (TS).

#### **2.4.3.4.1 Effect of the presence of water and temperature reaction**

The deactivation of the 3.09TS-D catalyst in the presence of FFA is probably due to the formation of water during the esterification reaction. In order to investigate this aspect, catalytic runs with different amounts of water were carried out.

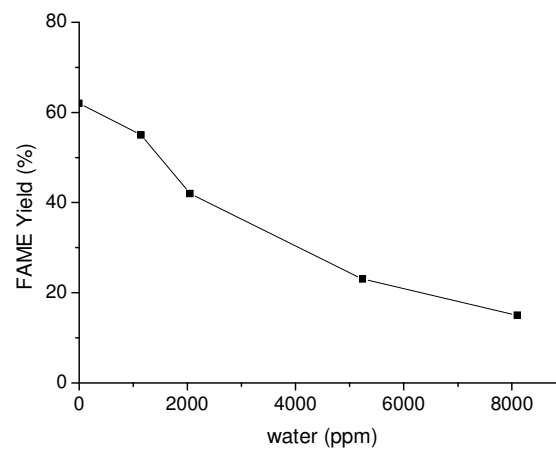


**Fig. 2.32:** Influence of water on the transesterification performances of TS catalyst. (Oil = 2.0g, methanol = 0.88g, catalyst = 0.1g,  $T=180^\circ\text{C}$ .).

From the results reported in Fig. 2.32, it appears evident that water has a strong deactivating effect. These results are in agreement with data observed for the homogeneous Lewis acid catalysts by Di Serio et al. [29] and with the data reported by Hillion et al. [49] for an heterogeneous Lewis acid catalyst (Zinc Alluminate).

Runs at different reaction temperatures were performed to estimate the activation energy of the reaction (see Fig. 2.33).

The corresponding kinetic constants reported in the Arrhenius plot (Fig. 2.34) were determined considering a first order with respect to the glycerides groups because the molar excesses of used methanol, and neglecting the transient of temperature. Data reported in Fig. 2.34 confirmed the necessity of high temperature to obtain reaction rate useful for industrial application of the TS catalyst, being the calculated activation energy of about 96 KJ/mol.



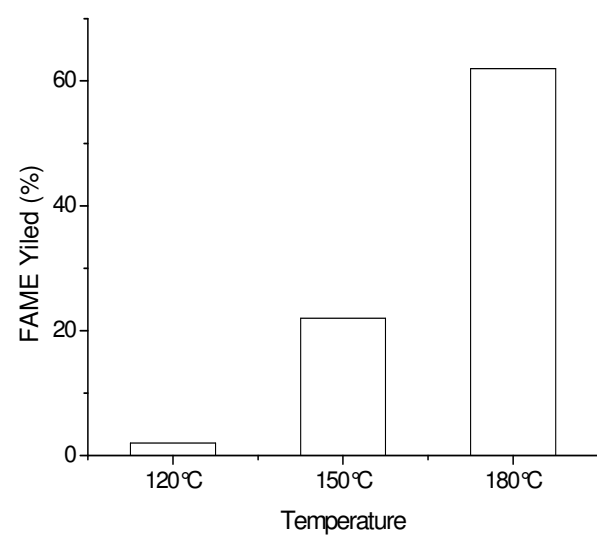


**Fig. 2.33:** Influence of the temperature reaction on the activity (FAME yield). (Oil = 2.0g, methanol = 0.88g, catalyst (TS) = 0.1 g).

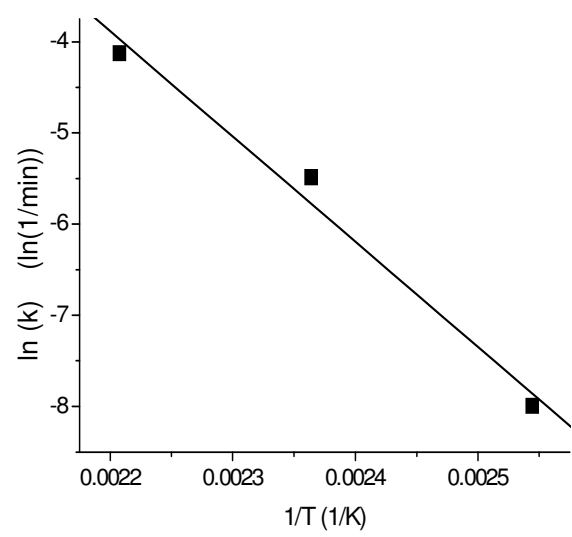


**Fig. 2.34:** Arrhenius plot of kinetic constants. (Oil = 2.0g, methanol = 0.88g, catalyst (TS) =0.1 g).

## 2.5 Conclusions

The results achieved revealed that several and different factors involved in the preparation route influence both the surface properties and the reactivities of the titania supported onto silica catalysts.

In particular, the results obtained from FT-IR measurements of CO and  $\text{NH}_3$  adsorption enable us to establish interesting correlations between the electrophilic nature of supported  $\text{Ti}^{4+}$  sites, e.g. the acid strength of titanium cations, and their catalytic performances in the transesterification reaction of refined oil with methanol.

The interaction between titania and silica in silica-supported titania catalysts gives place to supported  $\text{Ti}^{4+}$  sites, characterized by a weaker Lewis acidity than on pure  $\text{TiO}_2$ . Two kinds of Lewis acid sites, differing in the electrophilic properties of the respective  $\text{Ti}^{4+}$  cations, were detected: a) isolated  $\text{Ti}^{4+}$  sites ( $2177\text{-}2173\text{ cm}^{-1}$ ) mainly at low Ti loading and b) “associated”  $\text{Ti}^{4+}$  sites ( $2194\text{-}2183\text{ cm}^{-1}$ ). Hydroxyl groups with higher acid strength, with respect to Si-OH groups of  $\text{SiO}_2$  and to TiOH groups of  $\text{TiO}_2$ , were observed at the surface of 7TS-D sample, corresponding to a monolayer coverage of silica by Ti-alkoxide molecules.

Finally, the catalytic tests of the prepared  $\text{TiO}_2/\text{SiO}_2$  catalysts showed that isolated  $\text{Ti}^{4+}$  cations have an appropriate Lewis acid strength to catalyze the transesterification of refined oil with methanol.

At last, the *grafting* method by using tetra-isopropoxide as precursor appeared very useful to obtain a good surface dispersion of

the supported Ti species and the most suitable acidity for type and strength.

## 2.6 References

- [1] F.R.D. Snell and L.S. Ettre, *Enciclopedia of Industrial Chemical Analysis*, **1974**, 19, 107, Interscience, New York.
- [2] S. Brunaber, P.H. Emmet, *J.Am. Chem. Soc.*, **1938**, 60, 309.
- [3] D. Dollimore, G.R. Heal, *J. Appl. Chem.*, **1964**, 14, 109.
- [4] D. A. Shirley, *Phys. Rev. B*, **1972**, 4709
- [5] P. M. A. Sherwood, in: D. Briggs, M. P. Seah (Eds.) *Practical Surface Analysis*, Wiley, New York, **1990**, 181).
- [6] J. H. Scofield, *J. Electr. Spectrosc. Relat. Phenom.*, **1976**, 8, 126
- [7] Gelbard, G., Brès, O., Vargas, R.M., Vielfaure, F., Schuchardt, U.F., *JAOCs*, **1995**, 72, 1239.
- [8] I. Grohmann, W. Pilz, G. Walther, H. Kosslick, V.A. Tuan, *Surf. Interface Anal.*, **1994**, 22, 403.
- [9] X. Gao, S.R. Bare, J.L.G. Fierro, M.A. Banares, I.E. Wachs, *J. Phys. Chem. B*, **1998**, 102, 5653.
- [10] E.F. Vansant, P.V.D. Voort, K.C. Vranken, *Stud. Sci. Surf. Catal.*, **1995**, 93.
- [11] B. A. Morrow, A. J. Mcfarlan, *J. Non-Cryst. Solids*, **1990**, 120, 21.
- [12] C. J. Brinker, B. C. Montez, *J. Non-Cryst. Solids*, **1988**, 99, 418.
- [13] P. MacMillan, *Am. Mineral.*, **1986**, 69, 622.

- [14] X. Gao, S.R. Bare, J.L.G. Fierro, M.A. Banares, I.E. Wachs, *J. Phys. Chem. B*, **1998**, 102, 5653.
- [15] F.P.J.M. Kerkhof, J.A. Moulijn, *J. Phys. Chem.*, **1979**, 82, 1612.
- [16] S. Wang et al., *Journal of Mol. Cat. A: Chemical*, **2004**, 214, 273.
- [17] J. Keranen, C. Guimon, E. Iiskola, A. Auroux, L. Niinisto, *Catal. Today*, **2003**, 78, 149.
- [18] K.I. Hadjiivanov, B.M. Reddy, H. Knözinger, *Applied Catalysis A: General*, **1999**, 188, 355.
- [19] K.I. Hadjiivanov, G.N. Vayssilov, *Adv. Catalysis.*, **2002**, 47, 307.
- [20] A. Fernandez, J. Leyrer, A.R. Gonzalez-Elipe, G. Munuera and H. Knözinger, *Journal of Catalysis*, **1988**, 112, 489.
- [21] O.V. Manoilova, J. Dakka, R.A. Sheldon, A. Tsyganenko, *Stud. Surf. Sci. Catal.*, **1995**, 94, 163.
- [22] M. Cozzolino, R. Tesser, M. Di Serio, E. Santacesaria, 2<sup>nd</sup> Concorde meeting proceedings, **2006**, submitted to *Applied Catalysis A: General*.
- [23] M. Cozzolino, R. Tesser, M. Di Serio, M. Ledda, G. Minutillo, E. Santacesaria, *Studies in Surface Science and Catalysis, E. Gaigneaux et al. (Editors)*, **2006**, 162, 299.
- [24] E. Santacesaria, M. Cozzolino, M. Di Serio, A.M. Venezia, R. Tesser, *Applied Catalysis A: General*, **2004**, 270, 177.
- [25] K.I. Hadjiivanov, O. Saur, J. Lamotte, J.C. Lavalley, *Z. Phys. Chem. (Munich)*, **1994**, 187, 281.
- [26] G. Busca, H. O. Saur, J.C. Lavalley, V. Lorenzelli, *Appl. Catal.*, **1985**, 14, 245.
- [27] G. Vayssilov, *Catal. Rev.-Sci Eng.*, **1997**, 39, 209.

- [28] J.A. Lercher, C. Gründling, G. Eder-Mirth, *Catalysis Today*, **1996**, 27, 353.
- [29] M. Di Serio, M. Ledda, M. Cozzolino, G. Minutillo, R. Tesser, and E. Santacesaria, *Ind. Eng. Chem. Res.* **2006**, 45, 3009-3014.
- [30] M. Di Serio, R. Tesser, M. Dimiccoli, F. Cammarota, M. Nastasi, *Journal of Mol. Catalysis A: Chem.*, **2005**, 239(1-2), 111.
- [31] Ma, F.; Hanna, M. Biodiesel production: a review. *Bioresour.Technol.* **1999**, 70, 1.
- [32] Ondrey, G., *Chem. Eng.* **2004**, 10, 13.
- [33] Stern, R.; Hillion, G.; Rouxel, J.-J.; Leporq, S. U.S. Patent No. 5,908,946, June 1, 1999.
- [34] Furuta, S.; Matsushashi, H.; Arata, K., *Catal. Commun.* **2004**, 5, 712.
- [35] Schuchardt, U. F.; Vargas, R. M.; Gelbard, G., *J. Mol. Catal., A: Chem.* **1996**, 109, 37.
- [36] Leclercq, E.; Finiels, A.; Moreau, C., *J. Am. Oil Chem. Soc.* **2001**, 78, 1161.
- [37] Mazzocchia, C.; Modica, G.; Kaddouri, A.; Nannicini, R., *C. R. Chim.* **2004**, 7, 601.
- [38] Hoydonckx, H. E.; De Vos, D. E.; Chan, S. A.; Jacobs, P. A., *Top. Catal.*, **2004**, 27, 83.
- [39] Suppes, G. J.; Dasari, M. A.; Doskocil, E. J.; Mankidy, P. J.; Goff, M. J., *Appl. Catal., A* **2004**, 257, 213.
- [40] Ebiura, T.; Echizen, T.; Ishikawa, A.; Murai, K.; Baba, T., *Appl. Catal., A* **2005**, 283, 111.

- [41] Cantrell, D. G.; Gillie, L. J.; Lee, A. F.; Wilson, K. *Appl. Catal., A* **2005**, 287, 183.
- [42] Corma, A.; Iborra, S.; Miquel, S.; Primo Millo, J., PCT WO No. 98/56747, 1998.
- [43] Siano, D.; Siano, L.; Nastasi, M.; Santacesaria, E.; Di Serio, M.; Tesser, R.; Minutillo, G., from ASER srl, Italian Patent Application No. MI2004A02163, 2004.
- [44] Di Serio, M.; Ledda, M.; Cozzolino, M.; Minutillo, G.; Tesser, R.; Santacesaria, E., *Industrial & Engineering Chemistry Research* 45(9), **2006**, 3009.
- [45] B. A. Morrow, A. J. Mcfarlan, *J. Non-Cryst. Solids*, **1990**, 120, 21.
- [46] C. J. Brinker, B. C. Montez, *J. Non-Cryst. Solids*, **1988**, 99, 418.
- [47] Dasari, M.A., Goff, M.J., Suppes, G.J., *JAOCs*, **2003**, 80, 189.
- [48] Di Serio M, Cozzolino M., Tesser R., Patrono P., Pinzari F., Bonelli B., Santacesaria E., *Applied Catalysis A: General*, **2006**, submitted.
- [49] Hillion G., Le Pennec D., *US Patent Application*, 20050113588A1, **2005**.

# III

## EXPERIMENTAL SECTION

### **Design of the best catalyst ( $\text{TiO}_2/\text{SiO}_2$ ) for the epoxidation reaction of cyclooctene**

#### **Abstract**

The previous chapter (Chapter II) investigated the catalytic performances in the transesterification reaction of a series of  $\text{TiO}_2/\text{SiO}_2$  catalysts, prepared by performing the grafting reaction between  $(\text{Ti-OPr}^i)_4$  and the hydroxyl groups of silica in dioxane. However, in order to investigate the influence of both the solvent used for the grafting reaction and the preparation procedure adopted on the surface structure and reactivity properties of the grafted titanium sites in the epoxidation reactions, we have chosen to focus on the preparation of  $\text{TiO}_2/\text{SiO}_2$  catalysts by using toluene as solvent. Furthermore, the epoxidation reaction of cyclooctene with cumene hydroperoxide was employed to investigate the reactivity of the

catalysts prepared since this reaction is very sensitive to the surface structure of the supported titanium species. As already reported in Chapter II, also in this case the deposition of increasing quantities of  $\text{TiO}_2$  onto silica surface was achieved by chemisorption of titanium alkoxide precursor  $(\text{Ti}(\text{OPr}^i)_4$ , dissolved in toluene, onto surface hydroxyl groups of the support, followed by hydrolysis with steam water and calcination. In addition, a detailed characterization study was conducted in order to collect information about the structural characteristics of the supported titanium species onto silica surface. The catalysts were characterized by chemical analysis, BET surface area measurements, X-ray diffraction (XRD), DRUV-Vis, FT-IR and DRIFT spectroscopy analyses, TEM/EDX and  $\text{NH}_3$ -TPD. The catalytic results obtained highlighted that a homogenous surface dispersion of the grafted titanium on the silica surface is a fundamental requirement to obtain a high stability to prevent leaching phenomena and, consequently, high activity.

### 3.1 Catalysts preparation

The catalysts were prepared by contacting the silica (Grace S432, specific surface area =  $282 \text{ m}^2/\text{g}$ , pore volume =  $1.02 \text{ cm}^3/\text{g}$ , hydroxyl groups =  $0.92 \text{ mmol/g}$ ), calcined at  $773 \text{ K}$  for  $8 \text{ h}$ , with a solution of tetra-isopropoxide  $(\text{Ti}(\text{OPr}^i)_4$ , Aldrich) dissolved in anhydrous toluene.

The reaction was performed in a jacketed glass-reactor of  $200 \text{ cm}^3$  for  $6 \text{ h}$ , under stirring, at boiling temperature of toluene ( $388 \text{ K}$ ). The solid was filtered off, washed with toluene, dried at  $393 \text{ K}$  overnight,



hydrolyzed with steam and, finally, calcined at 773 K for 2 h (in this way burning off the residual alkoxide groups). The amount of adsorbed titanium was determined by the colorimetric analysis suggested by Snell and Ettre [1], by evaluating the quantity of titanium adsorbed on the surface of the catalyst after the grafting reaction. The operative conditions and the adsorption results are listed in Table 3.1.

| <b>Table 3.1:</b> List of the catalysts prepared by <i>grafting</i> titanium alkoxide on SiO <sub>2</sub> and related properties - Amount of the support (SiO <sub>2</sub> ) = 4g |  |  |                          |                             |   |  |
|---|--|--|--------------------------|-----------------------------|---|--|
| Catalysts   | Ti(O-Pr) <sup>i</sup> <sub>4</sub><br>initial<br>amount<br>(g) | TiO <sub>2</sub><br>anchored<br>(mmol <sub>Ti</sub> /gSiO <sub>2</sub> ) | % wt<br>TiO <sub>2</sub> | Titanium<br>adsorbed<br>(%) | S <sub>BET</sub><br>(m <sup>2</sup> /g) | Pore<br>volume<br>(cm <sup>3</sup> /g) |
| SiO <sub>2</sub>  | -  | -  | -                        | -                           | 282                                     | 1.02                                   |
| TS1   | 0.04   | 0.035  | 0.3                      | 100                         | -                                       | -                                      |
| TS2   | 0.2  | 0.176  | 1.4                      | 100                         | 280                                     | 0.99                                   |
| TS3   | 0.4  | 0.352  | 2.8                      | 100                         | 283                                     | 0.81                                   |
| TS4   | 0.6  | 0.528  | 4.2                      | 100                         | -                                       | -                                      |
| TS-M (1 step)   | 1.04   | 0.716  | 5.7                      | 78                          | 280                                     | 0.23                                   |
| TS-D (2 steps)  | 1.04   | 1.184  | 9.5                      | 64                          | 276                                     | 0.26                                   |
| TS-T (3 steps)  | 1.04   | 1.383  | 11.1                     | 50                          | 278                                     | 0.27                                   |

From the values reported in Table 3.1, it is possible to note that the adsorption of titanium tetra-isopropoxide was almost total, at low titanium coverage.

Therefore, in order to reach a monolayer coating of the silica surface, we used an excess of the grafting reagent compared to the monolayer and repeated the grafting procedure three times. More precisely, an amount of alkoxide corresponding to about 1.5 times the hydroxyls density on silica was used in each grafting step. The solid obtained after the first step of the grafting reaction was filtered, washed with toluene and oven-dried at 120 °C for 12 h. The solid was then submitted to a flux of steam for 2 h, at 150 °C, in order to eliminate the residual alkoxide groups by hydrolysis. Finally, the obtained solid was calcined at 500 °C for 2 h.

However, as underlined in the *Chapter II*, after calcination, some of OH groups, both Si-OH and Ti-OH species, became re-exposed on the surface of catalysts. So, in order to completely cover the surface of silica with titania, the above-mentioned sequence of operations, i.e., grafting, filtering, drying, steaming and calcinating were repeated, under the same conditions, twice more on each sample. This strategy resulted very useful to charge on the surface of silica a sufficient amount of titanium to form a monolayer coating of silica characterized by a highly dispersed active phase, corresponding to both isolated and/or polymeric titanium species.

### 3. 2 Techniques used in catalyst characterization

Different techniques were used for catalysts characterization, such as: BET measurements, X-ray diffraction (XRD), TEM/EDX, Diffuse reflectance spectroscopic analyses (DRIFT and DRUV), Temperature Programmed Desorption (TPD).

The specific surface area ( $S_{\text{BET}}$ ), porous volume and pore size distribution analyses were performed as exposed in the protocol presented at the point 2.2.

X-ray diffraction patterns (XRD) were carried out as presented at the point 2.2.

TEM observations were carried out under the same analytical conditions reported at the point 2.2.

Diffuse reflectance spectra were obtained following the experimental protocol presented at the point 2.2.

FTIR and DRIFT were recorded by using a Nicolet AVATAR 360 instrument, equipped with an accessory for the diffuse reflectance. Samples were powdered and diluted 1% by weight with KBr. Adsorbed water was completely removed “in situ” by heating at 673 K under vacuum ( $10^{-5}$  mbar).

Thermal programmed desorption (TPD) measurements were carried out by using ammonia as probe molecule. Samples of about

100 mg were first calcined in situ at 673 K for 1 h under air flow in order to remove adsorbed water. After cooling, the samples were subsequently contacted with a stream of Helium ( $1000 \text{ cm}^3/\text{min}$ ), containing 1000 ppm of  $\text{NH}_3$ , until to reach a saturation level. The ammonia desorption was performed under Helium flow from 373 to 773 K (heating rate= $10 \text{ K/min}$ ).

The amount of titanium has been determined by using a colorimetric method [1], after dissolution with a concentrated sulphuric acid solution, diluting and then treating with  $\text{H}_2\text{O}_2$ .

### 3.3 Catalytic tests in the epoxidation of reaction

Epoxidation of cyclooctene (Fluka 98%) with cumene hydroperoxide (Fluka 80% by weight in cumene) has been performed in a  $100 \text{ cm}^3$  three necks glass vessel equipped with a Liebig condenser and an internal cooling coil. The reaction temperature was kept constant, at 355 K, by putting the vessel in a thermostatted bath. To  $22 \text{ cm}^3$  of cyclooctene, 0.3 g catalyst was normally added, then  $10 \text{ cm}^3$  cumene hydroperoxide was slowly added with a syringe.

The reaction mixture was kept in temperature under a nitrogen atmosphere for 3 h. Unreacted hydroperoxide was determined by iodometric titration [2] at the end of the reaction. The epoxide formed was determined with the method suggested by Dearbon et al. [3]. After 3 h of reaction, yields per cent to epoxide, referred to the initial amount of peroxide, were determined. Selectivities were determined as:  $\text{selectivity} = 100 \times [\text{formed epoxide (mol)} / \text{consumed peroxide (mol)}]$ .

### 3.4 Results and discussion

#### 3.4.1 Catalyst preparation

By comparing the amount of the anchored metal on the surface of the  $\text{TiO}_2/\text{SiO}_2$  supported oxides with the one corresponding to the “theoretical”  $\text{TiO}_2$  monolayer on silica ( $\Gamma^\infty = 1.02 \text{ mmol}_{\text{Ti}}/\text{g}_{\text{SiO}_2}$ ), determined by performing a study about the chemical adsorption of titanium alkoxide on silica (see paragraph 2.4.1), it is possible to deduce that the solids, reported in Table 3.1 and indicated with the acronyms TS1, TS2, TS3 and TS4, can be considered as sub-monolayer catalysts.

In order to obtain a greater coverage of the silica surface, catalysts with a greater amount of  $\text{TiO}_2$  were prepared by grafting an amount of  $\text{TiO}_2$  corresponding about to mono-layer (TS-M), double-layer (TS-D) and tri-layer (TS-T) coatings. In particular, TS-D and TS-T catalysts were prepared by submitting the monolayer catalyst (TS-M) to the operations of grafting, hydrolysis and calcination described above, 1 and 2 times respectively. The related properties are reported in Table 3.1 also.

#### 3.4.2 Catalyst characterization

##### 3.4.2.1 Nitrogen adsorption (BET) measurements

$\text{SiO}_2$  and the prepared catalysts have been submitted to BET analyses in order to verify the possible effect of titanium loading on the specific surface area of the silica, used as base support.

The obtained values are listed in Table 3.1. It is interesting to observe for all the prepared samples that the specific surface area does

not change significantly with titanium loading, confirming in this way the possibility to prepare by grafting high-surface supported titania catalysts. On the contrary, a considerable decrease of pore volume, compared with the one of the starting support, can be noted for all the sub-monolayer catalysts until to reach the monolayer coverage. No variations were observed for  $\text{TiO}_2$  loadings higher than the monolayer coating.

#### **3.4.2.2 X-ray diffraction analysis**

All the prepared catalysts were submitted to X-ray diffraction analyses (XRD) in order to verify the presence of crystallites and to have an estimation of  $\text{TiO}_2$  dispersion.

The absence of  $\text{TiO}_2$ -crystallites was observed in all the XRD patterns of the  $\text{TiO}_2/\text{SiO}_2$  prepared samples, which resulted mainly amorphous. These results suggested that the  $\text{TiO}_2$  particles on  $\text{SiO}_2$  are very small and below the detection sensitivity of the XRD technique ( $<40\text{\AA}$ ). Only the TS-T catalyst showed the characteristic peak of  $\text{TiO}_2$  anatase at  $2\theta=25^\circ$ . The amount of  $\text{TiO}_2$  crystalline-phase, present in TS-T sample, has been calculated taking into account as reference the anatase peak with the higher intensity value and considering  $\text{ZrO}_2$  as reference compound. This has been made in agreement with the method reported in literature [4]. Physical mixtures of anatase  $\text{TiO}_2$ ,  $\text{SiO}_2$  and  $\text{ZrO}_2$ , containing a fixed amount of  $\text{ZrO}_2$  (5 % wt) and increasing quantities of titania (2, 5, 10, 15, 20 % wt), were prepared and then submitted to XRD analysis. A calibration straight line was constructed by reporting the amount of

$\text{TiO}_2$ , present in each sample, as function of the ratio between the area of the characteristic anatase peak at about  $2\theta=25^\circ$  and that one of  $\text{ZrO}_2$  peak at about  $2\theta=28^\circ$ . A quantity of the TS-T sample (0.2 g), containing 5% wt of  $\text{ZrO}_2$ , was then submitted to XRD analysis. The corresponding XRD plot is reported in Figure 3.1, as well as the XRD plots of both  $\text{TiO}_2$  anatase, used as reference, and  $\text{ZrO}_2$ .

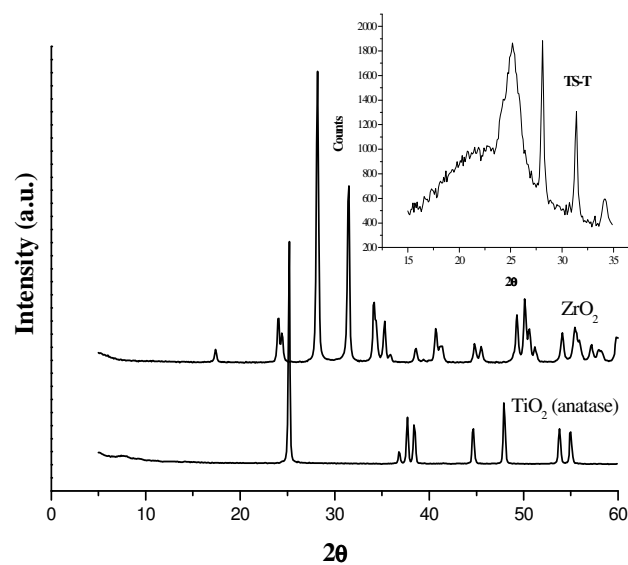


**Figure 3.1:** XRD plots of:  $\text{TiO}_2$ ,  $\text{ZrO}_2$  and TS-T samples

As can be seen from Figure 3.1, the reflex at about  $2\theta=25^\circ$  appeared as a broad peak. This means that the sizes of crystallites are very small. These last ones were determined along with the crystallographic direction 101, using the Scherrer formula:

$$\bar{d}_{hkl} = \frac{K\lambda}{B_d \cos \theta}$$



where: K= Scherrer constant;  $\lambda$ = wavelength;  $B_d$  = FWHM (Full Width Half Maximum);  $\theta$  = Bragg angle

Crystallites size was about 45 Å, a value quite close to the instrumental sensitivity limit.

A further effort was devoted to study the influence of calcination temperature on the quantity of TiO<sub>2</sub> crystalline phase and sizes of crystallites. At this purpose, the TS-T sample was calcined at different temperatures and then submitted to XRD analysis after each step of calcination. The obtained values are reported in Table 3.2.

**Table 3.2:** Influence of calcination temperature on the amount of TiO<sub>2</sub> crystalline phase and on crystallites size by XRD

| Temperature<br>of calcination<br>treatment<br>(°C) | % wt<br>TiO <sub>2</sub> *<br>(crystalline) | <i>d<sub>hkl</sub></i> (Å) |
|--|---|----------------------------|
| 500  | 1.8   | 42                         |
| 600  | 1.9   | 44                         |
| 700  | 2.0   | 47                         |
| 800  | 2.6   | 50                         |

\*The percentage of crystalline TiO<sub>2</sub> is referred to the total grafted titanium amount (%wt of TiO<sub>2</sub>)

As can be seen from the values reported in Table 3.2, the low amount of crystalline TiO<sub>2</sub>, observed also in the case of the catalyst calcined at higher temperatures, and the slight changes of crystallites

size confirm the stability of Si–O–Ti bond and, consequently, a good surface dispersion of the Ti species grafted on silica.

### 3.4.2.3 Morphological analyses by TEM and EDX

TEM observations and EDX analyses were conducted on TS3 and TS-T catalysts, corresponding to a sub- and tri-layer of  $\text{TiO}_2$  grafted on silica, respectively. In Figure 3.2, both TEM analysis and EDX spectrum, related to TS3 catalyst, are reported.

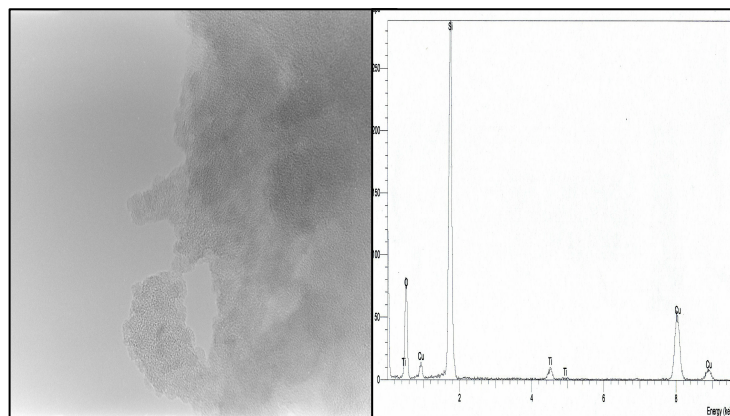


**Figure 3.2:** TEM micrograph (800K) (left) and EDX spectrum (right) of TS-3 catalyst

Both the catalysts TS-3 and TS-T resulted quite completely amorphous to the morphological observations. The presence of well-defined crystalline  $\text{TiO}_2$ -phases on the surface of the support was not revealed.

These results suggest that the titanium grafted remains homogeneously dispersed onto the silica support, even after repeating three times the grafting operation of titanium alkoxide on silica.

A semi-quantitative EDX analysis gave a value of Ti corresponding, for both the analysed catalysts, to chemical analysis data.

### 3.4.2.4 FTIR spectroscopic analysis

#### 3.4.2.4.1 Analysis of $3200\text{--}2700\text{ cm}^{-1}$ spectral range

Some  $\text{TiO}_2/\text{SiO}_2$  samples were submitted to FTIR analysis, before to be submitted to the calcination treatment.

In Figure 3.3 we report the infrared spectra recorded in the range  $3100\text{--}2800\text{ cm}^{-1}$  for TS1, TS2 and TS3 catalysts.

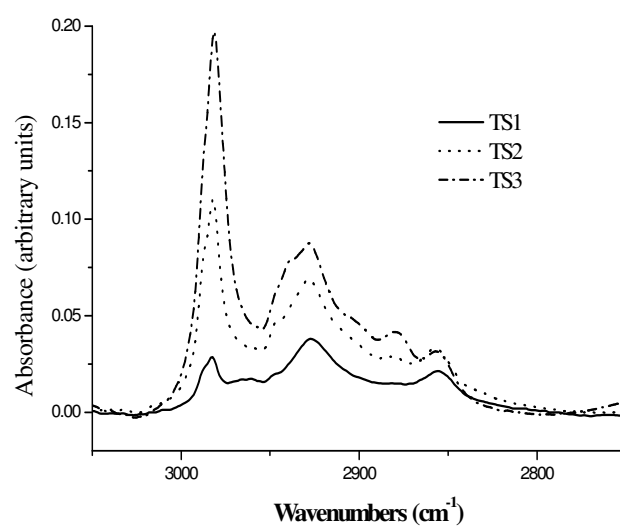


**Figure 3.3:** Infrared spectra (spectral range:  $3100\text{--}2800\text{ cm}^{-1}$ ) of TS1, TS2 and TS3 samples

The spectra showed four bands at  $2981$ ,  $2929$ ,  $2880$ ,  $2857\text{ cm}^{-1}$ , assigned to symmetric and asymmetric vibrational stretching C–H of  $\text{CH}_3$  groups [5].

The bands corresponding to the vibrational stretching C–C of isopropilic groups and of  $\text{CH}_3$  wagging in the range  $1260\text{--}1145\text{ cm}^{-1}$ , and the ones characteristic of vibrational stretching C–O in the range  $1150\text{--}1050\text{ cm}^{-1}$  did not appear in the spectra obtained since completely overlapped by the strong bands characteristic of vibrational stretching Si–O–Si in the range  $1000\text{--}1300\text{ cm}^{-1}$ .

Figure 3.4 shows the area of the examined peaks as function of molar ratio Ti/Si for the sub-monolayer catalysts: TS1, TS2, and TS3.

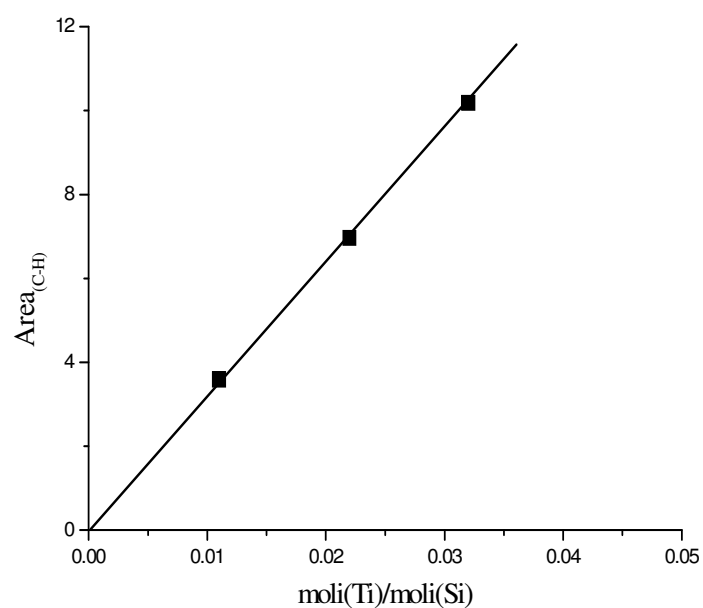


**Figure 3.4:** Area of infrared signals recorded in the range  $3100\text{--}2800\text{ cm}^{-1}$  ( $A_{\text{C-H}}$ ) as function of the molar ratio Ti/Si for the sub-monolayer catalysts

A linear correlation between the area and the molar ratio Ti/Si was found. This suggests that the grafting stoichiometry remains constant at least for the catalysts with a titanium load lower than the one corresponding to the monolayer coverage.

### 3.4.2.4.2 Analysis of spectral range 4000-3500 $\text{cm}^{-1}$

In Figure 3.5 the spectra of silica and of sub-monolayer  $\text{TiO}_2/\text{SiO}_2$  catalysts, recorded in the range 4000-3500  $\text{cm}^{-1}$  after calcination, are reported.

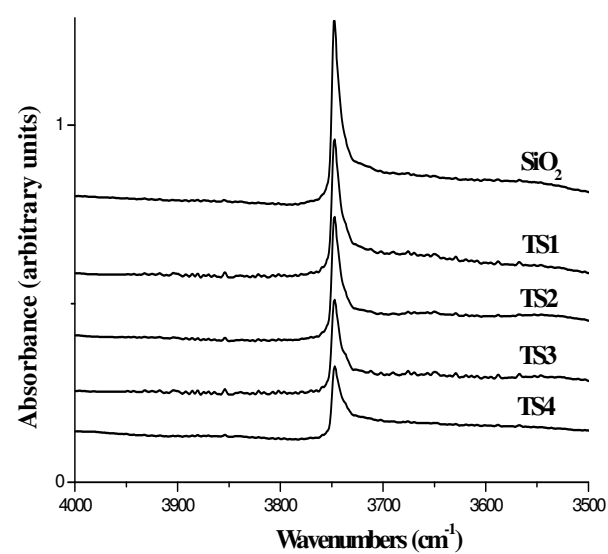


**Figure 3.5:** Infrared spectra (spectral range: 4000-3700  $\text{cm}^{-1}$ ) of the support ( $\text{SiO}_2$ ) and TS1, TS2, TS3 and TS4.

From the Figure 3.5, it is interesting to observe the decreasing of the intensity of the peak at 3747  $\text{cm}^{-1}$ , attributed to the isolated surface silanols (single  $\text{Si}-\text{OH}$  groups and geminal  $\text{Si}(\text{OH})_2$  groups). This trend can be related to the consumption of  $\text{Si}-\text{OH}$  hydroxyls during the deposition of titanium oxide on the silica support.

In Figure 3.6 the profile of the ratio between the area of the peak characteristic of vibrational stretching of residual  $\text{O}-\text{H}$  groups of titania-supported silica catalysts and the one of the same peak of the silica support, is reported as function of the molar ratio  $\text{Ti}/\text{Si}$ .

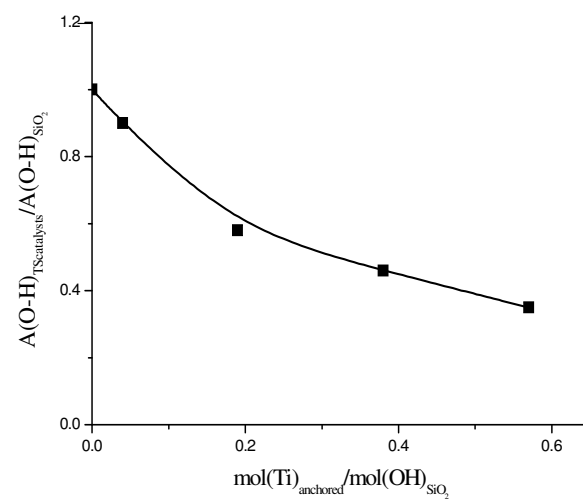


**Figure 3.6:**  $A(\text{O-H})_{\text{TS catalysts}} / A(\text{O-H})_{\text{SiO}_2}$  as function of  $\text{mol(Ti)}_{\text{anchored}} / \text{mol(OH)}_{\text{SiO}_2}$

As can be seen from the Figure 3.6, no linear correlation was observed. This is a consequence of the decrease of titanium dispersion since aggregates of  $\text{TiO}_2$  occur during the calcination treatment. For this reason, only for sub-monolayer catalysts (TS1 and TS2 catalysts), the stoichiometry values obtained would correspond to the exact stoichiometry of grafting reaction, that resulted to be about 2.5 (i.e., due to the heterogeneous character of the surface, two or three titanium atoms can be linked to one silicon atom).

This value was calculated according with the following equation (1):

$$\text{Stoichiometry} = (1 - \text{molOH}_{\text{SiO}_2\text{residual}}) / (\text{molOH}_{\text{SiO}_2\text{initial}}) / (\text{molTi}_{\text{anchored}} / \text{molTi}_{\text{initial}}) \quad (1)$$

### 3.4.2.4.3 Determination of $\text{TiO}_2$ dispersion by DRIFT analysis in the spectral range $1400\text{-}700\text{ cm}^{-1}$

DRIFT analysis has been performed on the following catalysts: TS1, TS2, TS4, TS-M, TS-D and TS-T.

Two of the spectra obtained, related to TS1 and TS-T samples, are reported in Figures 3.7 and 3.8, showing the following signals: a large band with a maximum at  $\sim 1100\text{ cm}^{-1}$  attributed to the asymmetric vibrational stretching Si-O-Si, characteristic of  $\text{SiO}_4$  units with tetrahedral coordination; a shoulder at  $\sim 1200\text{ cm}^{-1}$ , related to the asymmetric vibrational stretching Si-O $^-$ ; a peak at  $\sim 800\text{ cm}^{-1}$  attributed to the corresponding symmetric vibrational stretching and, finally, a peak at  $\sim 950\text{ cm}^{-1}$  characteristic of symmetric vibrational stretching Si-O-Ti. This last peak resulted crucial in order to determine, almost from a semi-quantitative point of view, the dispersion of  $\text{TiO}_2$  over the silica.

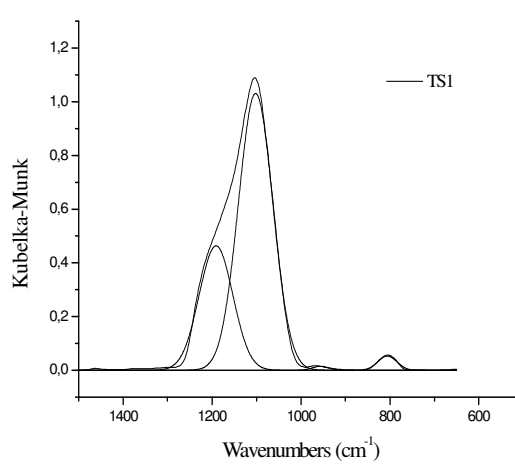


**Figure 3.7:** DRIFT spectrum of TS1 catalyst

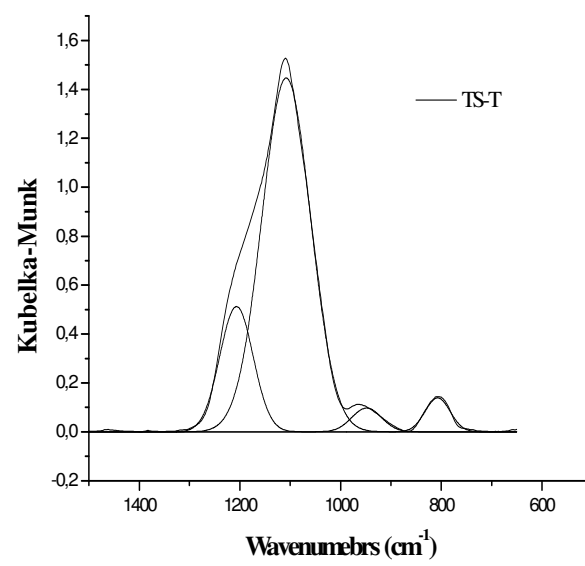


**Figure 3.8:** DRIFT spectrum of TS-T catalyst

It is possible to have an estimation of catalyst dispersion by comparing the area of the band at  $\sim 950 \text{ cm}^{-1}$  with the one of the band at  $\sim 1200 \text{ cm}^{-1}$ . The ratio between the two mentioned areas,  $A_{(\text{Si-O-Ti})}$  and  $A_{(\text{Si-O-Si})}$ , calculated by a gaussian deconvolution of the four peaks mentioned above, could be an index of the catalyst dispersion.

The values obtained for each sample are reported in Table 3.3.



**Tab. 3.3:** Data resulted from the gaussian deconvolution of the four peaks examined by FT-IR analysis

| TS1                 |       | TS2                 |       | TS4                 |       |
|---------------------|-------|---------------------|-------|---------------------|-------|
| Adsorption          |       | Adsorption          |       | Adsorption          |       |
| band                | Area  | band                | Area  | band                | Area  |
| (cm <sup>-1</sup> ) |       | (cm <sup>-1</sup> ) |       | (cm <sup>-1</sup> ) |       |
| 1191                | 43.8  | 1198                | 37.2  | 1206                | 29.0  |
| 1102                | 99.6  | 1103                | 137.3 | 1108                | 117.4 |
| 956                 | 0.68  | 952                 | 6.12  | 953                 | 3.01  |
| 805                 | 2.83  | 806                 | 8.33  | 808                 | 5.31  |
| TSM                 |       | TSD                 |       | TST                 |       |
| Adsorption          |       | Adsorption          |       | Adsorption          |       |
| band                | Area  | band                | Area  | band                | Area  |
| (cm <sup>-1</sup> ) |       | (cm <sup>-1</sup> ) |       | (cm <sup>-1</sup> ) |       |
| 1205                | 46.9  | 1207                | 37.2  | 1206                | 42.4  |
| 1104                | 153.6 | 1103                | 137.3 | 1107                | 175.6 |
| 946                 | 5.15  | 944                 | 6.12  | 948                 | 7.18  |
| 807                 | 9.41  | 806                 | 8.33  | 807                 | 8.60  |

In order to obtain a rough evaluation of titania dispersion on the carrier, the A<sub>(Si-O-Ti)</sub>/A<sub>(Si-O-Si)</sub> ratio is reported as function of molar ratio Ti/Si in Figure 3.9.

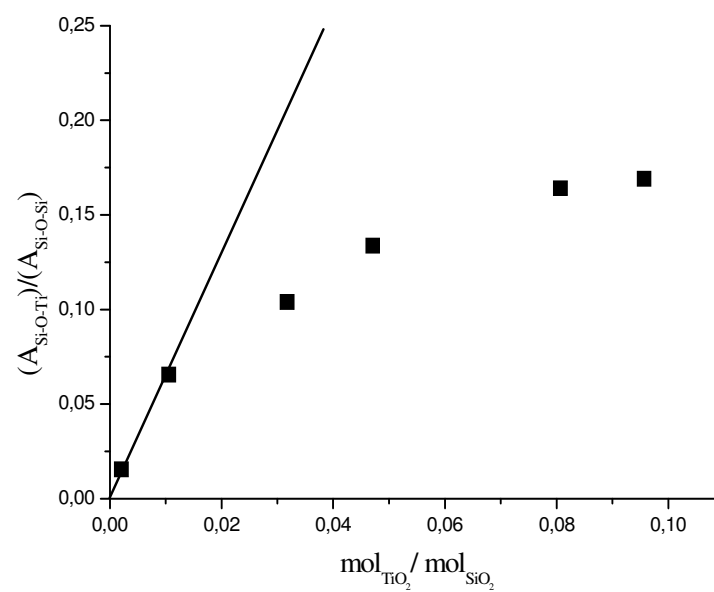


**Figure 3.9:**  $A_{(\text{Si-O-Ti})}/A_{(\text{Si-O-Si})}$  as function of molar composition

No linear increase of the ratio of areas with the molar ratio Ti/Si is observed. This indicates that the dispersion decreases by increasing the titanium content, probably as consequence of titanium aggregation.

A similar trend was obtained in a previous work [6] by submitting to XPS analyses  $\text{TiO}_2/\text{SiO}_2$  catalysts, prepared by grafting  $\text{Ti}(\text{O-Pr}^i)_4$  on a silica with a higher surface area (Aldrich,  $S_{\text{BET}}=450 \text{ m}^2/\text{g}$ ).

This can be seen in Figure 3.10 where the dispersion values calculated from DRIFT and XPS experimental data are reported and compared.

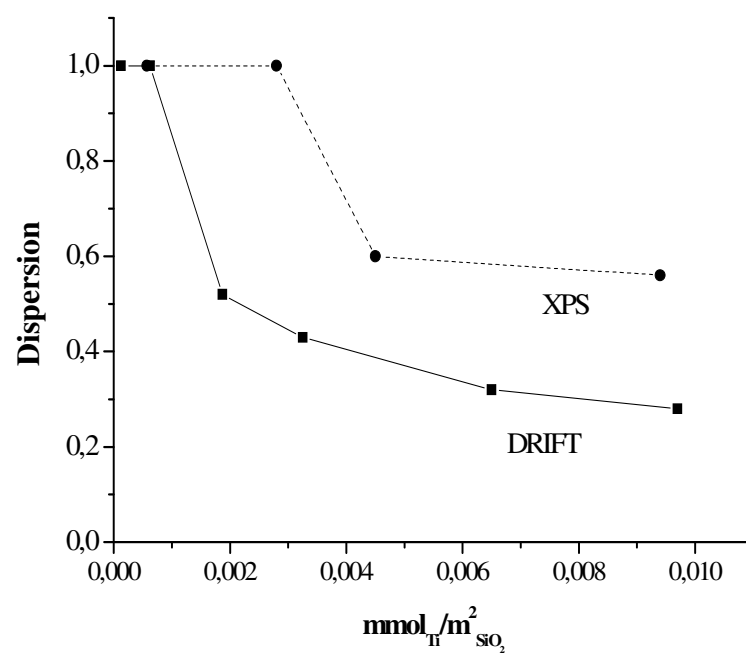


**Figure 3.10:** Comparison between the dispersion values calculated from DRIFT and XPS data for  $\text{TiO}_2/\text{SiO}_2$  catalysts (S432 Grace  $\text{SiO}_2$ ,  $282 \text{ m}^2/\text{g}$ ) and  $\text{TiO}_2/\text{SiO}_2$  catalysts (Aldrich  $\text{SiO}_2$ ,  $450 \text{ m}^2/\text{g}$ ), respectively.

The lower DRIFT dispersion-values are due to the lower surface area of the starting support. Both the XPS and DRIFT analyses revealed that there is a limit to the quantity of  $\text{TiO}_2$  that can be anchored with a unitary dispersion, depending probably on the specific surface area of the support. The value obtained by DRIFT analysis is about  $0.002 \text{ mmol}_{\text{Ti}}/\text{m}^2_{\text{SiO}_2}$ , corresponding to  $\sim 2 \text{ Ti}_{\text{atoms}}/\text{nm}^2_{\text{catalyst}}$ .

#### 3.4.2.5 Diffuse reflectance UV-Vis spectroscopy analysis

The DR-UV spectra are usually considered to provide information about the coordination geometry of the Ti cations (the first

coordination sphere) and the ligand environment (the second coordination sphere) under various conditions.

It is well known that the Ti cations in tetrahedral coordination show a typical band at  $\sim 212$  nm, due to the ligand-metal charge transfer between  $\text{Ti}^{4+}$  and oxygen ligands, such as  $-\text{O}-\text{H}$ ,  $-\text{O}-\text{Si}$ ,  $-\text{O}-\text{Ti}$ , or  $\text{H}_2\text{O}$ . On the other hand, a shift of the band towards higher wavelengths ( $\sim 260$  nm) is usually observed for the Ti cations in octahedral environments.

All the  $\text{TiO}_2/\text{SiO}_2$  catalysts were submitted to DR-UV analysis. The DRUV spectra of all the  $\text{TiO}_2/\text{SiO}_2$  prepared samples are compared in Figures 3.11 e 3.12.

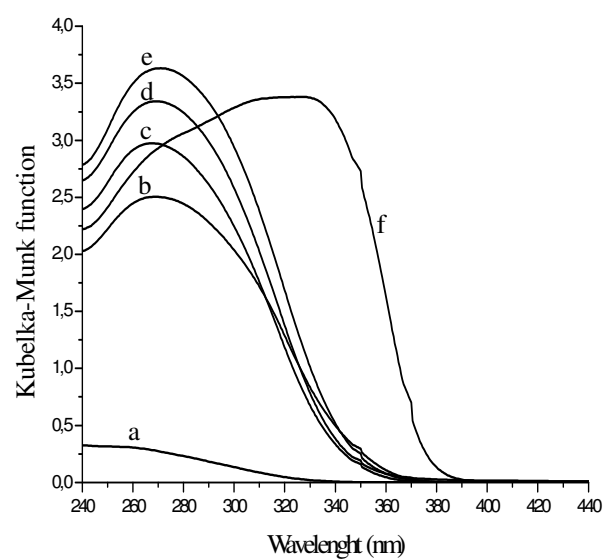


**Figure 3.11:** DR-UV spectra: (a)  $\text{SiO}_2$ , (b) TS1; (c) TS3; (d) TS4; (e) TS-M; (f)  $\text{TiO}_2$  (anatase)

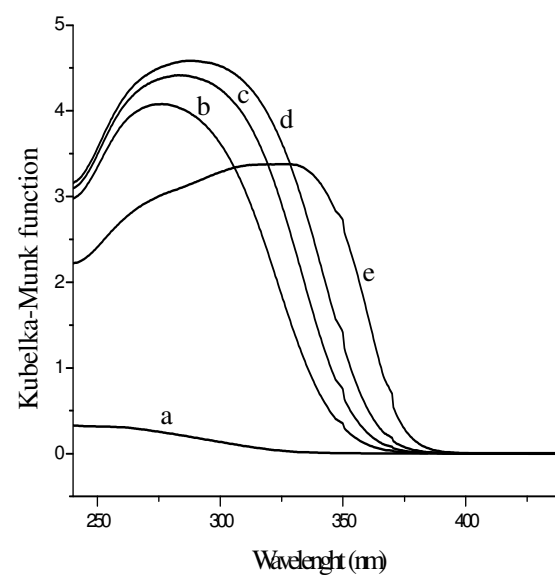


**Figure 3.12:** DR-UV spectra: (a)  $\text{SiO}_2$ , (b) TS-M; (c) TS-D; (d) TS-T; (e)  $\text{TiO}_2$  (anatase)

The DR-UV spectrum of bulk  $\text{TiO}_2$  anatase is also included in both the figures for a useful comparison. The absorption of silica in the range 200-500 nm can be considered negligible.

In particular, the comparison of UV-Vis results reported in Figure 3.11 suggested that the supported titania/silica oxides even at low Ti loadings ( $< 6\%$  wt  $\text{TiO}_2$ ) does not contain only isolated  $\text{TiO}_4$  sites, but a small amount of polymerized Ti species may also be present.

By considering the spectra reported in Figure 3.12, it is interesting to note that the maximum ligand–metal charge transfer (LMCT) transitions shifts towards higher wavelengths by increasing  $\text{TiO}_2$  loading, suggesting an increase in the polymerization degree of Ti atoms [7].

These results are in agreement with the ones obtained by FT-IR analysis, according to which the intensity of the  $3747\text{ cm}^{-1}$  due to isolated Si–OH hydroxyls decreases significantly, which indicates the consumption of Si–OH hydroxyls with increasing  $\text{TiO}_2$  loading. In particular, it is interesting to observe that the TS-D and TS-T samples, prepared by repeating two and three times the titanium alkoxide grafting step respectively, have shown a broader absorption band with a shape very similar to the one of the bulk  $\text{TiO}_2$  anatase. This suggests that, even though the  $\text{TiO}_2$  crystallites are very small and beyond the detection sensitivity of XRD measurements, they may still possess the same electronic property as the pure  $\text{TiO}_2$  anatase phase. Finally, the decrease of the edge energy of LMCT transitions of Ti atoms with increasing  $\text{TiO}_2$  loading may also be associated to the increase in the number of nearest Ti atoms, which suggests the polymerization of the surface Ti atoms on the silica surface at higher  $\text{TiO}_2$  loadings. The observed shift of the band-gap absorption edge may be explained in terms of quantum effects due to the small titania particles [8].

#### **3.4.2.6 Temperature programmed desorption (TPD) analyses**

Silica and two of  $\text{TiO}_2/\text{SiO}_2$  prepared samples were submitted to TPD analyses by using ammonia as probe molecule, in order to evaluate the modification of the acidic surface properties of the starting support by the deposition of the active species on its surface. The results obtained are reported in Table 3.4.

Table 3.4: NH<sub>3</sub>-TPD results of some TiO<sub>2</sub>/SiO<sub>2</sub> catalysts

| Catalysts        | Amount of<br>Titanium<br>(mmol <sub>Ti</sub> /gSiO <sub>2</sub> ) | Overall<br>Surface<br>Acidity<br>(μmol <sub>NH3</sub> /g) | T <sub>M</sub><br>(°C) |
|------------------|---|---|------------------------|
| SiO <sub>2</sub> | -   | 57.4  | 205                    |
| TS-M             | 0.716   | 211   | 215                    |
| TS-T             | 1.383   | 276   | 215                    |

From the values reported in Table 3.4, it can be observed that the deposition of titanium species increases strongly the total number of the acid sites on the surface of silica. On the contrary, by considering the related values of temperature (T<sub>M</sub>) in correspondence of the maximum of the NH<sub>3</sub> desorption, the strenght of acid sites remains almost constant. In particular, the obtained results suggested the presence of acid sites of medium strenght.

3.4.3 Catalytic performances in the epoxidation reaction of TiO<sub>2</sub>/SiO<sub>2</sub> catalysts

It is well known from the literature that the catalytic performances of titanium oxide appears to be completely modified by the interaction with the silica support, which is associated to the changes in the molecular structure and coordination environment.

The peculiar catalytic performance of the highly dispersed TiO<sub>2</sub>/SiO<sub>2</sub> catalysts in comparison with TiO<sub>2</sub> crystallites was previously demonstrated for liquid-phase epoxidation reactions with hydrogen peroxide and alkyl hydroperoxide [9]. The pure TiO<sub>2</sub> phase

in not active for the epoxidation reaction, while the highly dispersed  $\text{TiO}_2/\text{SiO}_2$  catalysts exhibit high reactivity and high selectivity to epoxide [9]. Two fundamental requirements in order to obtain good catalytic performances and high stability are: high dispersion of the catalytically active component within the matrix (site isolation) and stability to leaching [10-12].

In the present work, the catalytic performances of  $\text{TiO}_2/\text{SiO}_2$  prepared catalysts have been tested in the epoxidation reaction of cyclooctene with cumene hydroperoxide. Cyclooctene is an interesting test reagent because of the high stability of the corresponding oxide. The results obtained are gathered in Table 3.5 where yields (%) to epoxide and related selectivities are reported, as well as the chemical composition of the catalysts, expressed as  $\text{mmol}_{\text{Ti}}/\text{g}_{\text{SiO}_2}$ .

**Table 3-5:** Catalytic results in the epoxidation reaction of cyclooctene with cumene hydro-peroxide

| Catalysts | Anchored<br>metal<br>( $\text{mmol}_{\text{Ti}}/\text{g}_{\text{SiO}_2}$ ) | Yields               | Selectivity<br>(%) |
|-----------|--|----------------------|--------------------|
|           |  | to<br>epoxide<br>(%) |                    |
| TS2       | 0.176  | 3.8                  | 7.3                |
| TS3       | 0.352  | 11.6                 | 28.2               |
| TS-M      | 0.716  | 31.3                 | 70.8               |
| TS-T      | 1.383  | 21.2                 | 36.3               |

In Figure 3.13, the conversion and the selectivity are reported as function of the molar composition of the  $\text{TiO}_2/\text{SiO}_2$  catalysts.



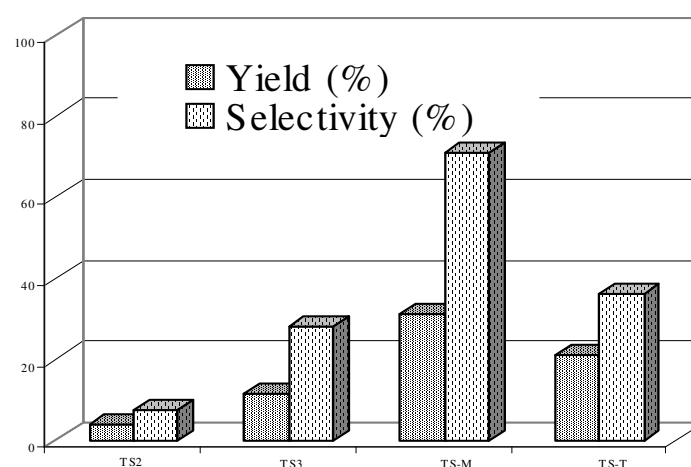


**Figure 3.13:** Activity and Selectivity of  $\text{TiO}_2/\text{SiO}_2$  catalysts in the epoxidation reaction of cyclooctene with cumene hydroperoxide

As can be seen from Figure 3.13, both activities and selectivities are affected by Ti loading. In particular, the results obtained showed an increase of both the activity and selectivity by increasing  $\text{TiO}_2$  loading until to reach the surface monolayer coating, and then a decreasing by depositing on the silica surface a greater amount of  $\text{TiO}_2$ . This behaviour could be related to the structural environment of the surface-supported Ti species. At low Ti coverage, supported  $\text{TiO}_2/\text{SiO}_2$  oxide-based catalysts mainly show tetrahedral titanium sites, that correspond to the Lewis acid sites, considered the active species in the epoxidation reactions.

By further increasing the  $\text{TiO}_2$  loading, an increasing of the degree polymerization of Ti species occurs, giving place to a large amount of octahedral Ti sites grafted on  $\text{SiO}_2$  of greater size. These last ones showed a lower activity in the epoxidation reaction. On the contrary, they seem to favour the decomposition of the hydroperoxide, giving

place to lower selectivities. This is in agreement with what observed experimentally and reported in Figure 3.13.

A comparison activity-selectivity between the two systems, i.e.  $\text{TiO}_2/\text{SiO}_2$  catalysts ( $\text{SiO}_2$ , 282  $\text{m}^2/\text{g}$ ) and  $\text{TiO}_2/\text{SiO}_2$  catalysts ( $\text{SiO}_2$ , 450  $\text{m}^2/\text{g}$ ) [6], is reported in Figure 3.14.

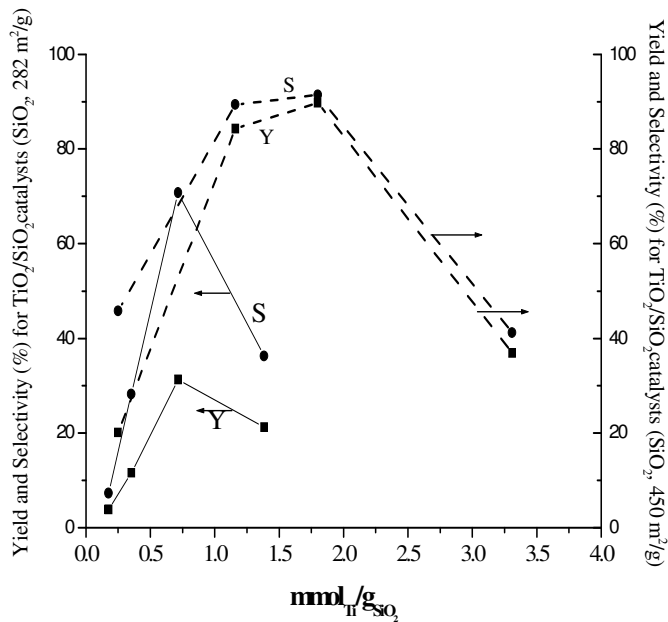


**Figure 3.14:** Comparison yield-selectivity vs molar composition between two systems:  $\text{TiO}_2/\text{SiO}_2$  catalysts ( $\text{SiO}_2$ , 282  $\text{m}^2/\text{g}$ ) and  $\text{TiO}_2/\text{SiO}_2$  catalysts ( $\text{SiO}_2$ , 450  $\text{m}^2/\text{g}$ ) [8].

It is interesting to note that the two catalytic systems investigated showed a maximum in terms of both yield and selectivity in correspondence of different values of the molar composition, corresponding to the monolayer  $\text{TiO}_2$  coverage for both the catalytic systems.

These results suggest that the surface area of the starting support determines significantly the maximum surface coverage of titanium oxide species on silica and, consequently, the dispersion capacity. The higher yield-values observed in the case of the  $\text{TiO}_2/\text{SiO}_2$  system characterized by a higher surface area [6] are due to the higher amount of supported Ti active sites.

### 3.5 Conclusions

The experimental evidences achieved and reported in this chapter suggested that grafting titanium alkoxide on the silica surface in toluene occurs easily and quantitatively for low coverage degree, giving place to highly dispersed titanium forming a monolayer. This aspect has been confirmed both by XRD and TEM analyses, which showed a homogeneous dispersion of the grafted titanium species resulted until to reach the monolayer coverage. The attempt to obtain multilayer coatings of silica by repeating more times the grafting operation brings to the formation of amorphous agglomerates characterized by a lower surface  $\text{TiO}_2$  dispersion, as indicated by DRIFT analyses from a semi-quantitative point of view. However, textural analyses carried out by BET method showed that the specific surface area does not change significantly with titanium loading, confirming in this way the possibility to prepare by grafting high-surface supported titania catalysts.

All these observations are in agreement with what observed by testing the catalytic performances of  $\text{TiO}_2/\text{SiO}_2$  catalysts in the epoxidation reaction of cyclooctene with cumene hydroperoxide. The

trend of the catalytic data showed that both the activity and selectivity may be influenced by the coordination environment of the surface titanium. Finally, the experimental results suggest that a homogeneous surface titanium is a fundamental requirement to obtain a high stability in order to prevent leaching phenomena and, consequently, good catalytic performances.

At last, the surface area and the concentration of the hydroxyl groups of the  $\text{SiO}_2$  are considered crucial to achieve good dispersion of the active sites and good catalytic performances in the epoxidation reaction.

### 3.6 References

- [1] F.R.D. Snell and L.S. Ettre, *Encyclopedia of Industrial Chemical Analysis*, 1974, 19, 107, Interscience, New York.
- [2] V.R. Kokatnur, M. Jelling, *J. Am. Chem. Soc.*, **1941**, 63, 1432.
- [3] E.C. Dearbon, R.M. Fuoss, A.K. MacKenzie, R.G. Shepherd Jr., , *Ind. Eng. Chem.*, **1953**, 45 (12), 2715.
- [4] J.R. Anderson, K.C. Pratt, “Introduction to characterization and testing of catalysts”, Academic Press.
- [5] K. Witke, A. Lachowicz, W. Bruser, Z. Zeigan, *Anorg. All. Chem.*, **1980**, 465, 193
- [6] P. Iengo, G. Aprile, M. Di Serio, D. Gazzoli, E. Santacesaria, *Appl. Catal. A: General*, **1999**, 178, 97.
- [7] X. Gao, I.E. Wachs, *Catal. Today*, **1999**, 51, 233.
- [8] G. Lassaletta, A. Fernandez, J.P. Espinos, A.R. Gonzalez-Elipe, *J. Phys. Chem.*, **1995**, 99, 1484.

- [9] R.A. Sheldon, *J. Mol. Catal.*, **1980**, 7, 107.
- [10] R. Hutter, T. Mallat, A. Baiker, *J. Chem. Soc. Faraday Trans.*, **1995**, 91, 1261.
- [11] R. Hutter, T. Mallat, A. Baiker, *J. Catal.* **1973**, 31, 427.
- [12] T. Maschmeyer, F. Rey, G. Sanker, J.M. Thomas, *Nature*, **1995**, 378, 159.



# **PART B**

**Supported vanadium oxide  
based catalysts  
for the ODH reactions**





# IV

## INTRODUCTION

### **Abstract**

Supported vanadium oxide based catalysts are very complex inorganic materials that play an important role in heterogeneous catalysis in both the gas and the liquid phase. They are active in a wide range of applications. Their synthesis and molecular design require a profound knowledge of solution chemistry, solid-state and inorganic chemistry, and their application as catalysts results from the specific interaction between the support oxide and the vanadium oxide.

This review/chapter reports an in-dept investigation about the current knowledge available in literature about the supported vanadium oxide based catalysts. Great attention will be addressed to the several aspects concerning this group of supported metal oxide catalysts, ranging from the preparation methods, characterization techniques of molecular structures of vanadium oxides on the surface

of different inorganic oxides/supports to the catalytic performances in the ODH reactions.

The understanding of the fundamental relationships between the molecular structure of the different supported vanadium oxide species and their catalytic behaviour in reactions of interest in industrial field, such as the oxidative dehydrogenation (ODH) reactions of both alkanes to alkenes and alcohol to aldehydes, represent the main goal of this chapter.

## 4.1 Introduction

Vanadium was discovered in 1801 in Mexico by the Spanish mineralogist A.M. del Rio, who considered it to be present in a particular brownish lead mineral [1–3]. He named the new element erythronium. However, the French chemist H.V. Collet-Descotils incorrectly declared that this new element was only impure chromium. Later on, in 1830, the Swedish chemist N.G. Sefström rediscovered the element and named it in honour of Vanadis, the old Norse name for the Scandinavian goddess Freyja—a fertility goddess—because of its beautiful multi-coloured compounds. In 1831, vanadium was unambiguously identified as the originally named erythronium element of del Rio and the lead mineral is now known as vanadinite ( $\text{Pb}_5(\text{VO}_4)_3\text{Cl}$ ). The most dominant non-metallurgical use of vanadium is in catalysis, which represents about 5% of the annual production of vanadium. Table 4.1 summarizes some industrial catalytic processes based on vanadium oxides [4].

Table 4.1: Industrial catalytic processes using vanadium oxides

| Industrial processes   | Catalyst material  |
|--|--|
| Oxidation of SO <sub>2</sub> to SO <sub>3</sub> in the production of sulfuric acid | V <sub>2</sub> O <sub>5</sub>                                    |
| Oxidation of benzene to maleic anhydride   | V <sub>2</sub> O <sub>5</sub>                                    |
| Oxidation of naphthalene to phthalic anhydride                                     | V, Mo oxides   |
| Oxidation of butene to phthalic anhydride  | V, P oxides  |
| Selective reduction of NO <sub>x</sub> with NH <sub>3</sub>                        | V <sub>2</sub> O <sub>5</sub> /WO <sub>3</sub> /TiO <sub>2</sub> |
| Oxidative dehydrogenation of alkanes to alkenes                                    | V/support  |

Vanadium oxide based catalysts are used in the manufacture of important chemicals (e.g. sulphuric acid, phthalic anhydride) and in the reduction of environmental pollution (e.g. nitrogen oxides from flue gas of power plants) and is the most important metal used in metal oxide catalysis [4]. The importance of vanadium in supported metal oxide catalysis is further underlined by Figure 4.1.

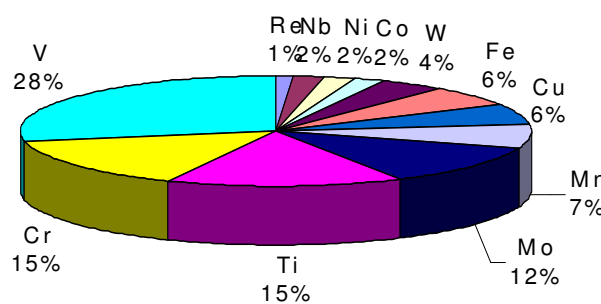


Figure 4.1: Overview of the importance of vanadium in supported metal oxide catalysis. The numbers are based on an extensive open literature search in the period 1967-2000.

This figure summarizes the number of papers (expressed as a percentage of the total number of papers) of several transition metals in the field of metal oxide catalysis, which can be found in the open

literature [5]. Most catalysts based on vanadium oxide consist of a vanadium oxide phase deposited on the surface of an oxide support, such as  $\text{SiO}_2$ ,  $\text{Al}_2\text{O}_3$ ,  $\text{TiO}_2$  and  $\text{ZrO}_2$ . Supporting a metal oxide on the surface of another oxide was initially proposed to improve the catalytic activity of the active metal oxide phase due to a gain in surface area and mechanical strength [7,15]. The support was considered as inert substance that provided a high surface to carry the active metal oxide component or to improve the mechanical strength of the catalyst material. However, during the last decade catalyst scientists have unambiguously shown that the activity and selectivity of supported metal oxide catalysts are significantly affected by the properties of the support oxide material. This is generally known as the “metal oxide–support effect”, although its exact origin and mechanism of operation is still unclear. For this reason, fundamental knowledge about the chemistry of supported vanadium oxides is required because of key importance in heterogeneous catalysis and spectroscopic tools are necessary to built up this knowledge.

The goal of this chapter is to discuss the chemical phenomena taking place at the supported metal oxide-support interface for each stage of the life span of a heterogeneous catalyst.

Such information is crucial not only for developing relevant structure/composition-activity/selectivity relationships, but also for understanding the underlying principles of designing supported metal oxides for a particular catalytic application. Thus, the discussion based on the most emphasized aspects shown in literature will be formulated on three different levels:

- a) “Catalyst design” of supported vanadium oxide catalysts
- b) Spectroscopic characterization of the supported vanadium oxide catalysts as function of the support type/composition and vanadium oxide loading
- c) Discussion of the catalytic performances in order to determine the catalytic activity/selectivity of the supported vanadium oxide catalysts as function of the support type/composition and vanadium oxide loading.

## **4.2 Preparation methods of supported vanadium oxide catalysts**

The preparation of supported metal oxide catalysts is a very important step because it significantly affects the three most important characteristics of the final catalyst product, i.e., its catalytic activity, catalyst selectivity, and catalyst lifetime [5].

Despite the large number of patents and applications about catalyst preparation, the field of “catalyst design” can be still considered in continuous developing. It involves the precise control over the nature (oxidation state, coordination environment, dispersion, etc) of the supported active site at the molecular level in a reproducible manner. This far from easy, and future research has to be directed toward a better understanding of the basic aspects of catalyst preparation through the use of *in situ* and *operando* microscopic and spectroscopic techniques. In this respect, it is important to recall the definition of catalyst preparation by Richardson [6]. Catalyst preparation is thus defined as the strategy domain in chemical industries. It is also a field

with great potential because important improvements in catalyst performance can be obtained by simply fine-tuning the different preparation steps of a specific catalyst.

There are two main stages in the preparation of supported metal oxides catalysts. In a first stage, the active metal component precursor is deposited on the oxidic support. The second stage consists of a transformation of the deposited metal precursor into a metal oxide dispersed at the support surface. This transformation process can be achieved by a heat treatment of the precursor material in oxygen or in air, often referred to as calcination step (formation of supported metal oxides).

Supported vanadium oxide based catalysts can be prepared via several methods.

**(a) Impregnation**

The most simple and widely used deposition method is impregnation which refers to a procedure whereby a certain volume of an aqueous or non aqueous solution containing the specific metal component precursor is totally adsorbed into the pores of an inorganic oxide. Two important impregnation procedures can be distinguished. If the support is dipped into an excess amount of solution, the process is called **wet impregnation**. More precise control over the vanadium oxide loading is achieved with a technique called **dry impregnation**, **pore volume impregnation** or **incipient wetness impregnation**. In this case, the support is contacted with a solution of appropriate concentration, corresponding in quantity to the total known pore volume of the support, or slightly less. This allows precise control of

the concentration of the active vanadium oxide component on the support. However, the maximum loading obtainable in a single impregnation step is limited by the solubility of the reagent and if necessary multiple impregnation steps should be applied.  $V_2O_5$  has a low solubility in aqueous and non-aqueous solutions and therefore, many authors prepare their supported vanadium oxide catalysts by impregnating the support with either an aqueous solution of, e.g.  $NH_4VO_3$  or  $NH_4VO_3$  dissolved in aqueous oxalic acid [4]. The impregnation process is followed by a drying and heating step in which the vanadium oxide compound is chemically anchored onto the support oxide. This is illustrated in Figure 4.2 (a).

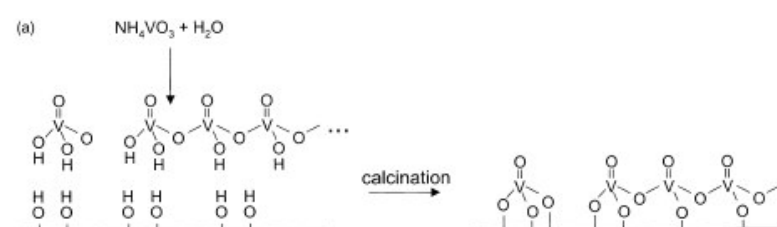


**Figure 4-2 (a):** Synthesis method for the preparation of supported vanadium oxide catalyst: impregnation with an aqueous solution of  $NH_4VO_3$ , followed by calcination in oxygen.

Non-aqueous impregnation methods use vanadyl acetylacetonate ( $VO(acac)_2$ ) as vanadium compound or  $VO(OC_2H_5)_3$  or  $VO(OC_3H_7)_3$  in methanol or another organic solvent [7,8]. The latter method is illustrated in Figure 4.2 (b). After the impregnation step the material is calcined in air at high temperatures (e.g. 500 °C) and surface anchored vanadium oxides are formed.

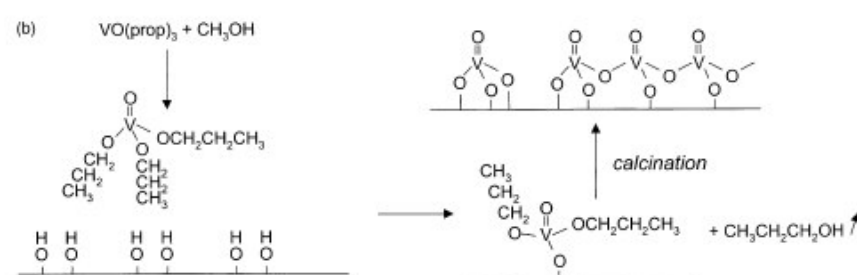


**Figure 4.2 (b):** Synthesis method for the preparation of supported vanadium oxide catalyst: impregnation with  $\text{VO}(\text{OC}_3\text{H}_7)_3$  in methanol, followed by calcination in oxygen or in air and release of propanol.

### (b) Grafting

Grafting is defined as the removal from solution of a compound containing vanadium through interaction with hydroxyl groups on the surface of an inorganic support. Many authors have used a solution of  $\text{VOCl}_3$  in  $\text{CCl}_4$  or in benzene to obtain a dispersed  $\text{VO}_x$  phase on various inorganic oxides [9,10]. Several authors pointed out that grafting techniques lead to more dispersed catalysts that are stable when an opportune support is used. Grafting in non-aqueous solutions of methanol or toluene by extraction of the active species by interaction with the hydroxyl groups of the support [11-23] have been mainly employed with vanadium alkoxides, in particular with vanadyl triethoxide  $\text{VO}(\text{OEt})_3$ , vanadyl trisopropoxide  $\text{VO}(\text{OPr}^i)_3$ , or vanadyl triisobutoxide  $\text{VO}(\text{OBu}^i)_3$ , respectively. Multi-step grafting followed by calcination is often used to obtain a monolayer of vanadium oxide on the surface of a support oxide.



In the preparation of heterogeneous catalysts, gas phase techniques have gained interest in the recent years as a route of developing new catalysts [24]. In general, liquid phase deposition can be regulated by controlled reagent concentration and washing and drying procedures whereas in the gas phase, the key factors are the character of precursor, the reaction temperature and the number of active surface hydroxyl sites. Other advantages include the absence of the solvents, decreased number of work stages and enhanced reactivity of the less reactive precursor complexes [25].

An example of gas-phase technique is the **Atomic Layer Deposition** (ALD), which has been successfully used in the preparation of series of V/SiO<sub>2</sub> and V/Al<sub>2</sub>O<sub>3</sub> catalysts from a volatile vanadyl acetylacetonate precursor.

A related technique is **Chemical Vapor Deposition** (CVD), which makes use of a volatile inorganic or organo-metallic compound that is deposited at the surface of a support oxide by reaction with the support hydroxyl groups. Interesting vanadium precursor compounds for this preparation method are VCl<sub>4</sub> and VOCl<sub>3</sub>, and their interaction with SiO<sub>2</sub>, TiO<sub>2</sub> and Al<sub>2</sub>O<sub>3</sub> has been studied in detail [4]. In particular, ALD as applied to thin film processing and modification of porous surfaces can be categorize as a special form of CVD. The functional principle of ALD technique relies on systematic use of surface saturation through self-controlled chemisorption of the volatile metal precursors on surface sites of the support. Controlled reaction conditions are achieved by stabilizing the surface deposition sites on the support by heat treatment and by removing any physisorbed or

unreacted molecules after each reaction by inert gas purge [25]. The growth rate of the surface layer is, within the so-called ALD temperature window [26], highly reproducible and not so dependent on the deposition parameters, e.g. the reaction temperature, vapor pressure and concentration of the precursors [25]. An ideal ALD process is thus providing “adsorption control” in heterogeneous catalyst preparation.

Although many different synthesis methods have been used in preparing supported vanadium oxide, many authors found to contain essentially the same vanadium oxide configurations after prolonged calcination treatments [26]. However, it is important to point out that the adopted preparation method influences the amount of supported vanadium oxides, which can be deposited on a particular support oxide without the formation of crystalline  $V_2O_5$ . In this way, the preparation method may affect the vanadium oxide dispersion on the surface of the oxide support.

### **4.3 Characterization methods for supported vanadium oxides**

The characterization of the molecular structures of supported vanadium oxides is rather involved, since deposition of this metal oxide on an inorganic oxide can result in:

- 1) isolated vanadium ions;
- 2) dimeric or polymeric species;
- 3) chains of vanadium ions building up a two dimensional over-layer of supported vanadium oxides;

- 4) three-dimensional vanadium oxides (e.g.  $V_2O_5$ ), crystalline or not; and
- 5) mixed metal oxide phases with the support (e.g.  $ZrV_2O_7$ ), or a combination of the above-mentioned molecular structures.

Different vanadium oxide configurations are shown in Figure 4.3.

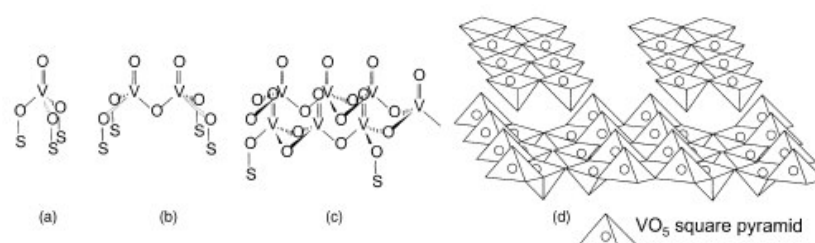


**Figure 4.3:** Possible molecular configurations for supported vanadium oxides (with S the support cation): (a) isolated vanadium oxide species; (b) dimeric vanadium oxide species; (c) two-dimensional vanadium oxide chains; (d)  $V_2O_5$  crystals.

Useful characterization techniques, which can provide detailed information about the molecular structure of supported vanadium oxides, must be capable of discriminating between these different vanadium oxide configurations and of quantifying the individual oxidation states [4]. The spectroscopic techniques used in the literature for studying supported vanadium oxides are summarized in Table 4.3 [27], together with the information about detectable oxidation states, dispersion, coordination and quantitative determination. It is clear from Table 4.2 [27] that no characterization technique will be capable of providing all the information needed for a complete characterization. Thus, successful characterization of vanadium oxides in heterogeneous catalysts requires a multi-technique

approach in order to get innovation on the road of the ‘rational design’ of catalysts, which offers the prospect of improved formulations for existing catalysts, and more effective and selective catalysts created from scratch [28].

Among the numerous characterization techniques used in heterogeneous catalysis, Raman spectroscopy has gained great attention in the development of catalysts in the last fifty years. An interesting example of this is represented, as reported in the following lines, by the considerable number of Raman studies focused on the structure of the monolayer vanadium oxide layer on titania (anatase) catalytic systems. These belong to an important class of commercial catalysts used for selective oxidation and ammonoxidation of aromatics and methylaromatics as well as for the removal of pollutant nitrogen oxides by reaction with ammonia. In addition, they find use as catalysts for oxidation in air of methanol to formaldehyde.

Several Raman studies have focused on the nature of structural changes as function of vanadia loading and concentration [29,30]. These studies, focused in the region of V–O stretching mode, revealed at the highest loadings the presence of a sharp intense Raman band at  $997\text{ cm}^{-1}$ , which primarily due to the formation of bulk  $\text{V}_2\text{O}_5$  on the  $\text{TiO}_2$  surface and is not catalytically interesting species. For the bands that appear at lower vanadia loadings, curve deconvolution of this frequency region is necessary to get a clear perspective on the number of Raman bands [30]. Starting with the lowest loading (1.3%), a sharp band at  $\sim 1030\text{ cm}^{-1}$ , and two broad bands at  $\sim 1025\text{ cm}^{-1}$  and  $915\text{ cm}^{-1}$  are observed. With increasing in loading level, two new bands appear

at  $850\text{ cm}^{-1}$  and  $960\text{ cm}^{-1}$ , along with a shift of the band at  $915\text{ cm}^{-1}$  to  $940\text{ cm}^{-1}$ .

A model of vanadyl species on the titania surface has been proposed based on these Raman spectra.

Discussing the assignment of the high frequency bands, it is important to point out that both the bands between  $1020$  and  $1030\text{ cm}^{-1}$  have been assigned to V=O stretch of monomeric vanadyls on the  $\text{TiO}_2$  surface. The higher frequency component at  $\sim 1030\text{ cm}^{-1}$  is due to the isolated vanadyl species, whereas the band at  $\sim 1025\text{ cm}^{-1}$  is from vanadyl species in close proximity, though still monomeric in nature. Although the nature of O bridging between V=O and  $\text{TiO}_2$  could not be elucidated from the Raman spectra, NMR spectroscopic studies suggest that the symmetry is greater than the two-fold, suggesting the possibility of  $-\text{TiO}_3-\text{V}=\text{O}$  [31-33]. Another possibility is  $-\text{TiO}_4-\text{V}=\text{O}$ , because there are four-fold oxygen sites on the (001)  $\text{TiO}_2$  plane [30].

The second group of the bands around  $915\text{-}955\text{ cm}^{-1}$  become prominent at higher vanadium loadings and are assigned to V=O stretches of end groups in oligomeric vanadate ions on the  $\text{TiO}_2$  surface.

With increasing loadings, the level of polymerization increases, leading to an increase in the frequency of this band. These assignments are consistent with the Raman spectra of polyvanadates ions in solution, which show an increase in frequency of the V=O stretch from  $\sim 900$  to  $\sim 1000\text{ cm}^{-1}$  as more V–O–V linkages are formed.

The band at  $960\text{ cm}^{-1}$  observed at the highest loadings has been assigned to the V=O stretch of the internal vanadium in the oligomeric species. Finally, the bands around  $840\text{-}850\text{ cm}^{-1}$  are assigned to the V–O–V bending motion of the vanadate species.

**Table 4.2:** Experimental techniques for characterizing catalysts and adsorbed species [27]

| Techniques                               | Acronym | Type of information                                       |
|--|---------|---|
| Low-energy electron diffraction          | LEED    | Two-dimensional structure and registry with metal surface |
| Auger electron spectroscopy              | AES     | Elemental analysis  |
| X-ray photoelectron spectroscopy         | XPS     | Elemental analysis and valence state                      |
| Ion scattering spectroscopy              | ISS     | Elemental analysis  |
| Ultraviolet photoelectron spectroscopy   | UPS     | Electronic structure                                      |
| Electron energy loss spectroscopy        | EELS    | Molecular structure                                       |
| Infrared spectroscopy                    | IR      | Molecular structure                                       |
| Raman spectroscopy                       | RS      | Molecular structure                                       |
| X-ray diffraction                        | XRD     | Bulk crystal structure                                    |
| Extended X-ray absorption fine structure | EXAFS   | Bond distance and coordination number                     |
| Transmission electron spectroscopy       | TEM     | Crystal size, shape, morphology and structure             |

## 4.4 Factors influencing the dispersion of the surface vanadium oxide species

### 4.4.1 The support effect

Among the supported metal oxide catalysts, supported vanadium oxides represent a relevant example of the interaction between the vanadium oxide and the support surface.

It is well known [4] that the support characteristics (e.g. chemical composition) have a tremendous impact on the properties of the supported vanadium oxide species. This metal oxide-support effect – in the hydrated, dehydrated state as well under reaction conditions – is not well studied and therefore not well understood both at molecular and electronic level. In general, the function of the oxide support (*e.g.*,  $\text{SiO}_2$ ,  $\text{Al}_2\text{O}_3$ ,  $\text{TiO}_2$ , *etc*) in supported metal oxide catalysts is to tailor the catalytic performance of the active metal oxide component (*e.g.*, oxides of V, Mo, Cr, *etc*) by increasing the number of exposed active sites and/or modifying their molecular structures/physico-chemical properties.

Surface vanadium oxide species exhibit very different reactivity properties depending on the specific oxide support used. For example, the reactivity trends of surface vanadium oxide species as function of oxide support were determined for [34]:

methanol oxidation:  $\text{V}_2\text{O}_5/\text{ZrO}_2$ ,  $\text{V}_2\text{O}_5/\text{TiO}_2 \gg \text{V}_2\text{O}_5/\text{Al}_2\text{O}_3 \gg \text{V}_2\text{O}_5/\text{SiO}_2$ ;

CO oxidation:  $\text{V}_2\text{O}_5/\text{ZrO}_2 > \text{V}_2\text{O}_5/\text{TiO}_2 > \text{V}_2\text{O}_5/\text{Al}_2\text{O}_3$ ;

the SCR of  $\text{NO}_x$ :  $\text{V}_2\text{O}_5/\text{ZrO}_2 > \text{V}_2\text{O}_5/\text{TiO}_2 > \text{V}_2\text{O}_5/\text{Al}_2\text{O}_3 > \text{V}_2\text{O}_5/\text{SiO}_2$



These trends imply that it is possible to alter the catalytic properties of vanadium oxide catalysts by changing and modifying the oxide support. The basis for these trends lies in the change at the molecular level of the bridging V–O–Support bonds between the active surface vanadium oxide species and the support cations, where the support cations possess different electronegativities. Consequently, molecular engineering of the active surface vanadium oxide species can be realized by modifying the bridging V–O–S bonds, where the electronegativity of the support cation varies [4].

The electronegativity is usually used to predict the direction and approximate extent of the polarity of a covalent bond. The absolute electronegativity  $\chi$  is defined as an average of the ionization potential (the energy required to remove an electron from an atom) and the electron affinity /the energy released by gain of one electron), and is further related to the electron chemical potential by the Equation (4.1):

$$\mu = (\partial E / \partial N)_Z = -\chi \quad (4.1)$$

where N is the total number of an atom or molecule, E is the total electronic energy and Z is the nuclear charge. The physical importance of electronegativity differences determine the charge transfer that occurs on bond formation.

It is well known that the partial charge  $\delta$  on an atom in a molecule or a polyatomic ion is a useful parameter in evaluating the effectiveness of the atom as an electron donor or acceptor. It is defined as the ratio of the change in electronegativity in forming the

compound to the unit charge change, and the partial charges will add to zero from a neutral molecule. Oxygen in most compounds usually possess a negative value (electron donor), and with a relatively low negative partial charge of oxygen, the molecule or ion becomes more acidic or less effective as an electron-pair donor. Therefore, the comparison of oxygen partial charge  $\delta_O$  in a metal oxide compound as well as its electronegativity can be used to predict the change in the electron density when the ligand of the central cation changes. In contrast, the V(V) cation usually possesses a positive partial charge, which demonstrates its ability as an electron-pair acceptor.

The electronegativities and partial charges of some V-containing model clusters are calculated and presented in Table 4.3.

**Table 4.3:** Electronegativities and partial charges in some V-containing model clusters

| Molecules/clusters                                   | $S$  | $\delta_O$ | $\delta_V$ |
|--|------|------------|------------|
| VO(OH) <sub>3</sub>                                  | 3.06 | −0.20      | 0.22       |
| VO(OH) <sub>2</sub> (OCH <sub>3</sub> )              | 2.94 | −0.24      | 0.17       |
| VO(OH) <sub>2</sub> (OCH <sub>3</sub> ) <sub>2</sub> | 2.88 | −0.26      | 0.15       |
| VO(OCH <sub>3</sub> ) <sub>3</sub>                   | 2.83 | −0.27      | 0.13       |
| VO[OSi(OH) <sub>3</sub> ] <sub>3</sub>               | 3.01 | −0.22      | 0.20       |
| VO[OTi(OH) <sub>3</sub> ] <sub>3</sub>               | 2.89 | −0.260     | 0.15       |
| VO[OZr(OH) <sub>3</sub> ] <sub>3</sub>               | 2.72 | −0.31      | 0.08       |

S= Sanderson's relative electronegativity

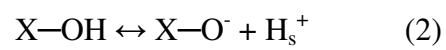
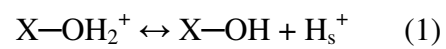
As the OH<sup>−</sup> ligand of the VO(OH)<sub>3</sub> cluster is substituted by CH<sub>3</sub>O<sup>−</sup>, the electronegativity and the positive partial charge on vanadium ( $\delta_V$ )

on the clusters decreases, while the oxygen negative partial charge  $\delta_{\text{O}}$  becomes more negative. This trend indicates that the change of the ligand around the central cation can greatly affect its local chemical environment. Similarly, when using model Ti, Zr, Si hydroxyl clusters as ligands for V(V) cation, the resulting electronegativity is a strong function of the electronegativity of the bridged metal cations ( $\text{Si} > \text{Ti} > \text{Zr}$ ). This trend reveals that for vanadium oxide compounds, the electron density around both the oxygen and vanadium atoms varies with ligands that possess different electronegativities. Decreasing the electronegativity of the support cations increases the electron density (the negative partial charge  $\delta_{\text{O}}$ ) of the bridging oxygen of the V–O–S bond, which is associated with the significant increase in TOFs for methanol oxidation over the corresponding supported vanadia catalysts. This is the molecular basis for modification of catalytic properties of supported vanadium oxide catalysts.

#### **4.4.2 The effect of vanadium oxide loading**

Apart from the role of the inorganic oxide used as support, the molecular structure of vanadium oxide species on amorphous support oxides can be influenced also by the vanadium oxide loading [35]. Several authors have shown that the surface vanadium oxide molecular structures depend on the net pH at which the oxide surface possesses no surface charge (point of zero charge, pzc). The net surface pH at pzc or the isoelectric point (IEP) of a specific support is mainly determined by its composition ( $\text{SiO}_2$ ,  $\text{Al}_2\text{O}_3$ ,  $\text{ZrO}_2$ ,  $\text{TiO}_2$  and  $\text{MgO}$ ). Under hydrated conditions, the surface of an amorphous oxide

is covered by a thin water film and its hydroxyl population is subject to pH-dependent equilibria reactions:



where X= Si, Al, Zr, Ti o Mg;  $\text{H}_s^+$  e  $\text{H}^+$  represent the surface and solution proton, respectively. The lower the IEP of the amorphous oxide, the more the equilibria of the reactions (1)–(3) are driven to the right. The higher the  $\text{H}^+$  concentration near the surface, the more the equilibrium reactions in aqueous solutions are driven towards the formation of more polymerized vanadium oxide species. When the vanadium oxide loading increases, two effects come into play:

- (1) the pH near the surface is lowered due to the presence of acidic vanadium oxides, and decreases with increasing vanadium oxide loading;
- (2) the dispersion depends on the available surface area as well as the availability of surface hydroxyl groups.

Both factors influence the chemistry of vanadium in the same direction, i.e. toward the formation of surface polyvanadates. In other words, the following sequence is observed for increasing vanadium oxide loading: orthovanadate ( $\text{VO}_4$ )  $\rightarrow$  pyrovanadate ( $\text{V}_2\text{O}_7$ )  $\rightarrow$

metavanadate  $(VO_3)_n \rightarrow$  decavanadate  $(V_{10}O_{28}) \rightarrow$  vanadium pentoxide ( $V_2O_5$ ), as illustrated in Fig. 4.3:

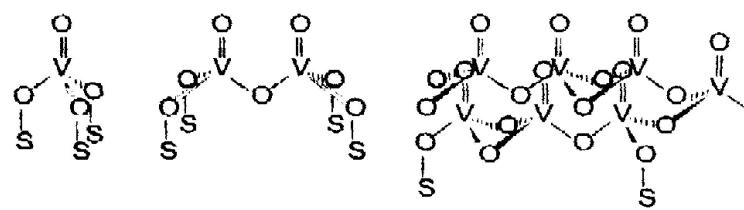


**Fig. 4.3:** Molecular structures of surface vanadium oxide species

Effect (2) also implicates that high surface area supports, such as alumina and silica or titania/silica, will give rise to relatively less polymerized vanadium oxide species ( $V_{10}O_{28}$ ) at high vanadium oxide loadings because more surface area is available to accommodate monovanadate species. The effect of the presence of additives, such as  $P_2O_5$  and  $K_2O$ , can alter the IEP of the supports or form vanadium phosphate or potassium vanadate compounds, and consequently, change the vanadium oxide speciation.

Figure 4.4 illustrates this trend by showing the Raman spectra of dehydrated  $V/Al_2O_3$  catalysts with an increasing amount of vanadium oxide. It can be seen that the Raman band at  $930\text{ cm}^{-1}$ , due to the presence of polymeric vanadium oxides, gradually increases with increasing vanadium oxide loading. At very high vanadium oxide loadings, a fraction of the supported vanadium oxide species are present in an octahedral coordination ( $VO_6$  units), which can aggregate to form amorphous and crystalline  $V_2O_5$  clusters.

A final remark should be made about the formation of mixed metal oxides upon heating of supported vanadium oxide catalysts. It has been shown that  $\text{MgV}_2\text{O}_7$  and  $\text{ZrV}_2\text{O}_7$  can be formed when V/MgO and V/ $\text{ZrO}_2$  catalysts, respectively are calcined in air [4].

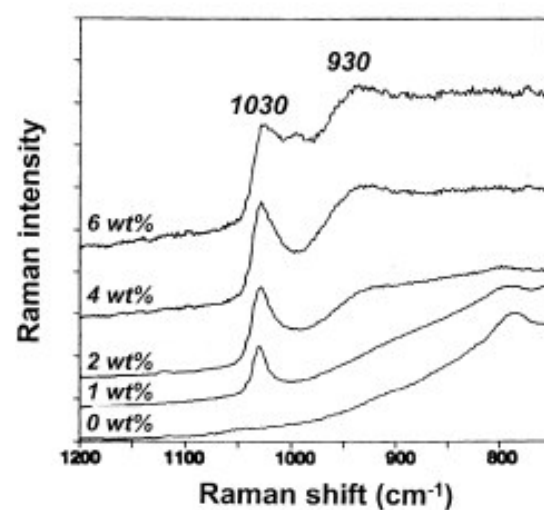


**Figure 4.4** Raman spectra of calcined V/ $\text{Al}_2\text{O}_3$  catalysts as a function of vanadium oxide loading [4].

#### 4.5 Structural properties of highly dispersed supported vanadium oxide species

The molecular structure of supported vanadium oxide species on various supports have been extensively investigated by combined spectroscopic techniques, mainly Raman, DRIFT, UV-vis DRS and XPS. These techniques resulted very useful to estimate the “surface monolayer coverage”.

The surface monolayer coverage is defined as the maximum amount of vanadium oxide, amorphous or bi-dimensional layer, that is

possible to charge on the surface of an oxide. An estimation can be obtained from experimental and structural calculations [37]. By taking into account the length of V–O bond of crystalline vanadium pentoxide ( $\text{V}_2\text{O}_5$ ), the surface monolayer coverage is estimated to be  $10 \text{ VO}_x/\text{nm}^2$  for a bi-dimensional layer characterized by polyvanadates and to be  $2.5 \text{ VO}_x/\text{nm}^2$  for monomeric isolated units. However, the experimental data must be considered very approximated because the structure of the surface vanadium pentoxide is similar to that of crystalline vanadium pentoxide.

Among the several available characterization techniques, the RAMAN spectroscopy revealed particularly efficient to identify the nature of the surface vanadium species, both dispersed and aggregated. Recent works reported that the surface monolayer coverage resulted to be  $7\text{--}8 \text{ VO}_x/\text{nm}^2$  [37] for different supports, such as  $\text{TiO}_2$ ,  $\text{ZrO}_2$ ,  $\text{Al}_2\text{O}_3$ ,  $\text{Nb}_2\text{O}_5$ ,  $\text{CeO}_2$ , expected for the silica support as the surface monolayer coverage resulted to be  $0.7 \text{ VO}_x/\text{nm}^2$ . This is probably due to the lower density and reactivity of the surface hydroxyl groups present onto silica surface. The characterization results revealed that the surface molecular structures of vanadium oxide species on the modified supports are a strong function of the environmental conditions [36]. In the dehydrated state, only the isolated  $\text{VO}_4$  species are present up to monolayer coverage of  $\sim 12 \text{ wt\% V}_2\text{O}_5$  ( $\sim 2.6 \text{ V atoms/nm}^2$ ). Hydration dramatically change the molecular structure of surface vanadium oxide species. Full hydration results in maximum polymerization to form chain and/or two-dimensional  $\text{VO}_5/\text{VO}_6$  polymers, most likely through V–OH–V

bridges, which are structurally similar to the  $V_2O_5 \cdot nH_2O$  gels. Methanol chemisorption at high temperatures ( $120^\circ\text{C}$ ) results in isolated, four-fold coordinated V(V)-methoxy species, which may serve as the intermediate complex for methanol oxidation to redox products.

However, in recent years, much attention has been paid to the design and synthesis of multilayered  $V_2O_5/MO_x/SiO_2$  catalysts. In the case of these systems, the silica support is initially modified with a monolayer of surface metal oxide species ( $TiO_2$ ,  $ZrO_2$  or  $Al_2O_3$ ), and the surface vanadium oxide species is subsequently dispersed on the top of the surface metal oxide species as the second surface layer, as schematically shown in Figure 4.5.

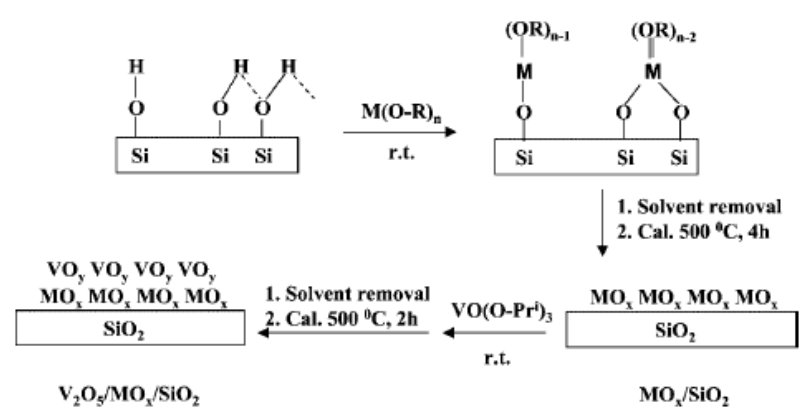


**Figure 4.5:** Schematic drawing for the preparation procedure for multilayered  $V_2O_5/MO_x/SiO_2$  catalysts



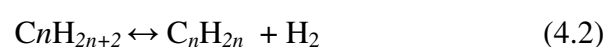
TPR and methanol oxidation were employed as chemical probe reactions to examine the reducibility and reactivity/selectivity properties of these multilayered surface metal oxide catalysts. The characterization results revealed that the molecular structures of the surface vanadium oxide species on these modified supports ( $\text{MO}_x/\text{SiO}_2$ ) are a strong function of environmental conditions. In these multilayered catalytic systems, the surface V cations preferentially interact with the surface titanium/zirconium/aluminium oxide species on the silica surface [36]. This preferential interaction is thought to be partially with the higher basicity of the surface M–OH hydroxyls than the Si–OH hydroxyls, which results in a higher reactivity of the M–OH hydroxyls with the V-isopropoxide precursor molecules during the catalyst preparation.

Several investigations [4, 36] confirmed that the reducibility and the catalytic properties of the surface vanadium oxide species are significantly altered by the modification of the silica surface. A significant example is represented by the fact that the methanol oxidation  $\text{TOF}_{\text{redox}}$  of these multilayered  $\text{V}_2\text{O}_5/\text{MO}_x/\text{SiO}_2$  systems generally increases by more than an order of magnitude relative to the  $\text{V}_2\text{O}_5/\text{SiO}_2$  catalysts. These reactivity enhancements for methanol oxidation are associated with the change of the Si(IV)– $\text{O}^-$  oxygenated ligands by the less electronegative M– $\text{O}^-$  ligands, which strongly suggests that the basis for the support effect lies in the increase of the electron density of the bridging oxygen of the V–O–support bond. No apparent correlation, however, was found between the TPR reducibility and methanol oxidation reactivity of the  $\text{V}_2\text{O}_5/\text{MO}_x/\text{SiO}_2$

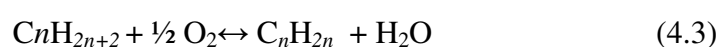
catalysts, which is most likely associated with their different reaction mechanism [36].

#### **4.6 Reactivity/Selectivity properties of vanadium oxide catalysts in the Oxidative Dehydrogenation (ODH) reactions**

It seems that nowadays, for conversion of light alkanes, the oxidative dehydrogenation (ODH) reaction is more promising than direct dehydrogenation. In reality, for light alkanes ( $C_2$  to  $C_4$ ), the thermodynamic of the reaction



is such that the alkane is favoured by the equilibrium in the low temperatures and at atmospheric pressure [38]. Reactions are endothermic (e.g., for n-butane  $\Delta H_r$  is about 134 kJ/mol) and in order to shift the equilibrium to product formation, reactions must be carried out at relatively high temperatures (from 500 to 650°C). In addition, the number of molecules is higher on the product side and consequently operation at high pressures, which is usually preferred in industrial practice, would shift the equilibrium towards the unfavourable direction. The use of high temperatures in catalytic dehydrogenation presents several disadvantages. The difficulty in controlling undesirable reactions that decrease selectivity (such as cracking of hydrocarbons) and coke formation over the catalyst, which decreases activity, are the most significant. For all these reasons, reactions of alkanes with oxygen:



are excellent alternatives in the synthesis of alkenes. The formation of a very stable product such as water makes this reaction very thermodynamically favourable. Thus, in principle, practically complete conversion can be attained even at low temperatures and high pressures, bringing enormous advantages from the economic and process engineering points of view. However, in such conditions selectivity also presents limitations.

Notwithstanding all the above-mentioned advantages over dehydrogenation, ODH (as well as the majority of other catalytic-oxidation processes) has some drawbacks [38]: due to its exothermic character it may require special care in reactor operation, some feed composition ranges can be explosive (leading to limitations in feed compositions or to multiple air inlets), and the desired product must be sufficiently stable in the reaction conditions in order to be removed from the product stream before it decomposes or undergoes other subsequent reactions. Indeed, selective oxidation of alkanes is a great challenge due to the nature of the chemical bonds involved. Many side reactions with oxygen are possible, requiring highly selective catalysts. In many cases such reactions are much more thermodynamically favourable than the desired ODH reactions, but the secondary products usually have no economic interest when compared to the high value of hydrogen, produced as a co-product in the conventional dehydrogenation process. Thus, ODH reactions with high yield are a great challenge in catalysis. The key-aspect of the technology is, therefore, the development of catalysts capable of activating only C–H bonds of the alkane molecule in a flow of

oxygen. This problem become of great importance in light of the petrochemical industry's tendency to be based in the future on the direct use of alkanes as raw materials instead of alkenes [39].

Several review have discussed oxidation catalysts containing vanadium, but none is specifically concerned with the oxidehydrogenation reactions. However, an interesting work reported in literature by Mademov and Corberan [39] summarized publishing data on catalytic performances of different vanadium-containing oxides in the ODH of C<sub>2</sub>-C<sub>5</sub> alkanes.

The analysis of the structure-activity relationships showed that various species characterized by a different reactivity exist on the surface of these catalysts. There are some indications that tetrahedral vanadium species (VO<sub>4</sub>) are the most favourable for alkane oxidehydrogenation. This model makes use of the concept of site isolation and the effect of metal-oxygen bond strenght on the selectivity. Its intrinsic activity seems to be largely dependent on the structure of the nearest surrounding and, therefore, can be modified by changing the nature and the number of neighbouring ions. Although the reaction mechanism is generally accepted to be through the redox cycle between V<sup>5+</sup> and V<sup>4+</sup>, opposite relationships between catalysts activity /selectivity and reducibility have been established, even for the same catalytic system. Very probably, there should be a correlation between the catalytic property and the redox property of the VO<sub>4</sub> and V<sub>2</sub>O<sub>7</sub> units. Suggesting that a certain extent of reduction is needed for the selective dehydrogenation of the alkane, the selective site can be represented as a reduced site V<sub>2</sub>O<sub>7</sub> unit in which the

oxygen bridging two vanadium ions is removed ( $V^{4+} \square V^{4+}O^{2-}M^{n+}$ ). This site is able to activate an alkane molecule by abstracting one hydrogen atom with the oxygen bridging  $V^{4+}$  and  $M^{n+}$  cations, but not to hold an alkyl or adsorbed alkene very strongly due to the reduced electron-accepting property of the  $V^{4+}$  ion. Under the same reaction conditions,  $VO_4$  groups are expected to reduce to a smaller extent as their oxygen ions are more difficultly removed than those in  $V_2O_7$  units. An optimum extent of reduction and a good selectivity can be achieved either by carrying out the reaction under more severe conditions or by using a more reactive alkane. No clear interpretation regarding the mode of alkane activation can be derived from a survey of the literature. This and some other aspects of the reaction mechanism need further studies at a molecular level.

#### 4.7 Conclusions

The literature survey reported in this chapter has shown that supported vanadium oxide catalysts are very complex inorganic materials that play an important role in most of heterogeneous catalytic processes. Their synthesis and catalytic design require a profound knowledge of both the solid-state chemistry and inorganic chemistry. Their application in heterogeneous catalysis results from the specific interaction between the support and the vanadium oxide. Insight into the preparation of supported vanadium oxides at the molecular level would be very important to an understanding of the different steps involved.

It is also evident from this review/chapter that the support characteristics (i.e., structure and chemical composition) have a tremendous impact on the properties of the supported vanadium oxide catalysts. This support–effect results in the formation of specific, often not-well defined, molecular structures of metal oxides with, for example, special redox properties. A better insight into the formation and local structure of these molecular structures can be only obtained by applying a battery of complementary characterization techniques, preferably under *in situ* conditions. Thus, future research has to be directed towards the use of an intelligent combination of preferably *in situ* spectroscopic techniques delivering both molecular and electronic information about the supported vanadium oxides.

#### 4.8 References

- [1] R.J.H. Clark, *The chemistry of titanium and vanadium*, Elsevier, Amsterdam, **1968**.
- [2] F.A. Cotton, G. Wilkinson, *Advanced Inorganic Chemistry*, A Comprehensive Text, 4th ed., Wiley, New York, 1980.
- [3] N.N. Greenwood, A. Earnshaw, *Chemistry of the Elements*, Pergamon Press, Oxford, **1984**.
- [4] Bert M. Weckhuysen, Daphne E. Keller, *Catalysis Today*, 2003, 78, 25.
- [5] B.M. Weckhuysen, P. Van Der Voort, G. Catana (Eds.), *Spectroscopy of Transition Metal Ions on Surfaces*, Leuven University Press, 2000 (The literature search is based on a Chemical Abstract search in the period 1967–2000).

- [6] J. T. Richardson, “Principles of Catalyst development”, Plenum. New York, 1989.
- [7] M. Baltes, O. Collart, P. Van Der Voort, E.F. Vansant, *Langmuir*, **1999**, *15*, 5841.
- [8] P. Van Der Voort, M. Baltes, E.F. Vansant, *Catalysis Today*, **2001**, *68*, 121.
- [9] A. Wokaun, M. Schraml-Marth, A. Baiker, *J. Catal.*, **1989**, *116*, 595.
- [10] P. Iengo, M. Di Serio, M. Di Serio, V. Solinas, E. Santacesaria, *Applied Catalysis A: General*, **1998**, *167*, 85-101.
- [11] A. Comite, A. Sorrentino, G. Capanelli, M. Di Serio, R. Tesser, E. Santacesaria, *J. Mol. Catal. A Chem.*, **2003**, *198*, 151.
- [12] P. Iengo, M. Di Serio, V. Solinas, D. Gazzoli, G. Salvio, E. Santacesaria, *Applied Catalysis A: General*, **1998**, *170*, 225.
- [13] P. Iengo, G. Aprile, M. Di Serio, D. Gazzoli, E. Santacesaria, *Appl. Catal. A General.*, **1999**, *178*, 97.
- [14] R. Monaci, E. Rombi, V. Solinas, A. Sorrentino, E. Santacesaria, G. Colon, *Appl. Catal. A General*, **2001**, *214*, 203.
- [15] V. Iannazzo, G. Neri, S. Galvagno, M. Di Serio, R. Tesser, E. Santacesaria, *Appl. Catal. A General*, **2003**, *246*, 49.
- [16] E. Santacesaria, A. Sorrentino, R. Tesser, M. Di Serio, A. Ruggiero, *J. Mol. Catal. A Chem*, **2003**, *204–205*, 617.
- [17] E. Santacesaria, A. Sorrentino, M. Di Serio, R. Tesser, *Studies in Surface Science and Catalysis 143*, Ed. E. Gaigneaux et al., Elsevier, **2002**, 77.

- [18] E. Santacesaria, M. Cozzolino, M. Di Serio, A.M. Venezia, R. Tesser, *App. Catal. A: General* **2004**, 270, 177.
- [19] M. Cozzolino, R. Tesser, M. Di Serio, M. Ledda, G. Minutillo, E. Santacesaria, *Studies in Surface Science and Catalysis*, E. Gaigneaux et al. (Editors), **2006**, 162, 299.
- [20] M. Cozzolino, R. Tesser, M. Di Serio, E. Gaigneaux, P. Eloy, E. Santacesaria, *Studies in Surface Science and Catalysis*, E. Gaigneaux et al. (Editors), **2006**, 162, 299.
- [21] M. Cozzolino, R. Tesser, M. Di Serio, E. Santacesaria, 2<sup>nd</sup> Concorde meeting proceedings, **2006**, submitted to publication to *Applied Catalysis A: General*.
- [22] M. Cozzolino, R. Tesser, M. Di Serio, P. D’Onofrio, E. Santacesaria, 3<sup>rd</sup> Concorde meeting (Seville), **2006**, to submit to *Catalysis Today*.
- [23] B. Bonelli, M. Cozzolino, R. Tesser, M. Di Serio, M. Piumetti, E. Garrone, E. Santacesaria, **2006**, submitted to *Journal of Catalysis*.
- [24] S. Haukka, E.-L. Lakomaa, V. Lujala, T. Suntola, *Stud. Surf. Science Cat.*, **1995**, 91, 957.
- [25] J. Keränen, A. Auroux, S. Ek, L. Niinistö, *Applied Catalysis A: General*, **2002**, 228, 213.
- [26] T. Machej, J. Haber, A.M. Turek, I.E. Wachs, *Appl. Catal.*, **1991**, 70, 115.
- [27] National research Council (1992), *Catalysis Looks at the Future*, National Academy Press, Washington.
- [28] Bert M. Weckhuysen, *Nature*, **2006**, 439, 458.



- [29] M. A. Vuurman, I.E. Wachs, A.M. Hirt, *J. Phys. Chem.*, **1991**, 95, 9928.
- [30] G.T. Went, L.J. Leu, A.T. Bell, *J. Catalysis*, **1992**, 134, 479.
- [31] H. Eckert, I.E. Wachs, *J. Phys. Chem.*, 93, 6796.
- [32] Weckhuysen, B. M. (ed.) *In-Situ Spectroscopy of Catalysts*, Am. Sci., Stevenson Ranch, CA, 2004.
- [33] Weckhuysen, B. M. *Chem. Commun.* **2002**, 97.
- [34] G. Deo, I.E. Wachs and J. Haber, *Crit. Rev. Surf. Chem.*, **1994**, 4, 141.
- [35] G. Deo, I.E. Wachs, *J. Phys. Chem.*, **1991**, 95, 5889.
- [36] X. Gao, I.E. Wachs, *Topics in Catalysis*, **2002**, 18, 243.
- [37] A. Khodakov, B. Olthof, A.T. Bell, E. Iglesia, *J. Catal.*, **1999**, 181, 205.
- [38] L.M. Maidera and M.F. Portela, *Catalysis Reviews*, 2002, 44(2), 247.
- [39] E.A. Mademov, V. Cortes Corberan, *Applied Catalysis A: General*, 1995, 127, 1.



**PART B**

**EXPERIMENTAL**

**SECTION**



# V

## EXPERIMENTAL SECTION

### ODH of n-butane to butenes by supported vanadium based catalysts

#### Abstract

The present chapter focused on the study of the Oxidative Dehydrogenation reaction (ODH) of n-butane to butenes on supported vanadium based catalysts. For this purpose, many different vanadium based catalysts have been prepared and tested in the target reaction, by investigating the influence of several factors, such as: vanadium loading, type of support and synthesis procedure. The catalysts were prepared both by impregnation and grafting for a useful comparison. In particular, the grafting procedure was studied by contacting solutions of increasing concentrations of vanadyl tri-isopropoxide, dissolved in dioxane, with two different supports:  $\text{SiO}_2$  and  $\text{TiO}_2/\text{SiO}_2$ . Grafting adsorption behaviour was studied using the isotherms obtained in the two cases. On silica we obtained an isotherm with two different recognisable plateaux. On the contrary, in the adsorption on  $\text{TiO}_2/\text{SiO}_2$  the system followed the Langmuir adsorption law with a

saturation value at about 7% of adsorbed  $V_2O_5$ . By greatly increasing the vanadyl concentration multi-layer adsorption seems to occur. In this latter case, catalysts obtained after calcination resulted less dispersed. Each point of both the mentioned isotherms corresponds to a catalyst with more or less dispersed vanadium. All these catalysts were characterised by using many different techniques (XRD, DRUV, DRIFT, RAMAN and XPS) and tested in the ODH of butane. In particular, we observed that vanadium dispersed catalysts are more active and selective. From the observation of the adsorption isotherms, it is possible to decide the best conditions for preparing well dispersed catalysts, with a relatively high vanadium loading, and thus more active and selective.

### **5.1 Introduction to the ODH of *n*-butane to butenes**

The wide availability and low price of light alkanes (about one half of that of the corresponding alkenes) and the fact that they are generally environmentally non-aggressive products, have provided incentives for their use as raw materials in the chemical industry [1]. A notable example of utilization of alkanes is their conversion to unsaturated hydrocarbons, which are currently produced in steam crackers (e.g., ethylene, propylene, isobutene, butadiene, etc.), because the present-day chemical industry depends heavily on the use of olefins as starting materials. Indeed, the petrochemical industry's tendency seems to be the direct use of alkanes as raw materials instead of alkenes, due to the great abundance of natural gas and liquefied petroleum gas (LPG). Consequently, more recent studies and research, in an effort to meet future needs for chemical products, fibers and

polymers, have focused on functionalization of paraffins instead of conversion of olefins. In fact, efforts must be directed towards using cheaper raw materials.

A relevant example concerns styrene production via the butane–butadiene process. Since raw materials are responsible for about 80% of the cost of styrene production, a potentially interesting process would be to start from butane, available in large amounts and at low prices, which would be selectively oxidized to butadiene, leading by dimerization to 4-vinylcyclohexene and subsequent oxidation to styrene [1]. However, such a process is not yet included in the main uses of butane.

*n*-Butane, which can be recovered from LPG by distillation, has at present a variety of industrial uses: steamcracking yields ethylene and propylene, catalytic dehydrogenation yields butenes and butadiene, acid-catalyzed isomerization provides *i*-butane and *i*-butene (used to produce MTBE), and maleic anhydride or acetic acid are obtained through catalytic or non-catalytic oxidations, respectively. In the mid-1960s, among other large-scale catalyzed reactions, dehydrogenations of butane to butenes and/or butadiene and ethylbenzene to styrene became prominent [1-8]. In 1991, among the 147 billion pounds of organic products obtained via catalytic processes by the 50 top chemical industries in the United States, 9.8% were produced by dehydrogenation.

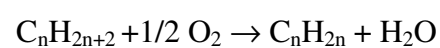
The importance of butadiene synthesis is due to the fact that it is one of the basic petrochemical products. It is used in the manufacture of butadiene–styrene rubber (one of the major rubbers for manufacture of tyres), other synthetic rubbers (e.g., latex, polybutadiene rubber,

etc.), plastics with special mechanical properties (e.g., polystyrene, ABS polymers, etc.), and as raw material in a wide variety of chemical synthesis. The worldwide production of butadiene in 1983 amounted to  $5.03 \times 10^6$  t (in North America the total was  $1.20 \times 10^6$  t) and the trend has been for this production to increase.

Essentially two processes were used in the United States for butadiene synthesis: a two-phase process departing from *n*-butane (Philips process), wherein butenes were converted into butadiene in the second phase, or a single-stage process using *n*-butane and *n*-butenes (Houdry Catadiene process). Butenes from refining units or from other sources also could be converted into butadiene through a single stage process. These processes were applied quickly to synthetic rubber manufacture in the United States at the beginning of the Second World War when natural-rubber sources were suddenly cut.

There are two possible ways for converting the alkane: direct dehydrogenation and ODH.

Thermal dehydrogenation processes for olefin production are highly endothermic and require complex tube furnaces. In addition, excess steam (about 50% by volume) is necessary to slow coke formation, and the effluent contains other products in addition to the desired olefins. Catalytic dehydrogenation has several drawbacks. Thus, ODH reaction that can be schematized as follows:





is very attractive mainly due to the absence of thermodynamic limitations (concerning the equilibrium) and need for heat transfer, allowing operation at much lower reaction temperatures (1,2). From the economic and engineering process point of view, significant advantages can be obtained. The ODH reaction of n-butane is quite complex and the involvement of several consecutive-parallel reactions for formation of dehydrogenation (C<sub>4</sub>s) and total oxidation (CO<sub>x</sub>) products is generally accepted [8-10]. However, the formation of other organic oxygen-containing products is also very common. Consequently, the maximum yields obtained are still smaller than those achieved in processes of dehydrogenation of paraffins. Nonetheless, a comparison between the two processes should consider several aspects, all affecting the overall economics. According to the literature [11], n-butane (and isobutane) ODH will compete with dehydrogenation processes for synthesis of olefins with high purity when certain conditions are reached:

- the possibility of getting high alkane conversions and high yields of olefins at relatively low temperatures;
- absence of oxygenated products (organic acids, aldehydes) which may make it necessary to use expensive anticorrosion materials;
- stable catalytic behaviour over long periods.

An intense research effort has been directed to look for highly efficient catalysts. However, the complexity of the reactions, associated with the large number of factors that determine their behaviour, has seriously complicated the task. Moreover, and despite

the large number of studies found in the open literature, some important aspects, such as the nature of the active sites, the kinetics and mechanism of the reaction, the hydrocarbon activation process and the factors that determine selectivity, are not sufficiently clear. It nevertheless seems evident that the acid–base surface properties of mixed oxides are an important selectivity-determining factor [9,10]. This has led to the use of promoters, especially alkali or alkaline-earth metals [12,13], for the purpose of modifying the surface basicity in strong favour of C<sub>4</sub> formation.

In order to reach the high performance levels that will be the key for definitive industrial application, different technological approaches also should be attempted. These include the use of new or recent technologies. For instance, the use of circulating bed reactors (CBRs)—in which the catalyst is reoxidized by oxygen in a regeneration zone after passing through the reaction stage where the hydrocarbon is oxidized—is interesting and even promising. The use of this configuration arises from the fact that a higher oxygen partial order was found for total oxidation. So higher C<sub>4</sub> yields from butane would be achieved in the absence of oxygen in the gas phase, i.e., in a redox mode using lattice oxygen with periodic regeneration. This can be done in practice by using multiple reactors or mobile or fluidized bed catalytic reactors.

One of the best illustrations of this is offered by the design of some recent industrial reactors in which the circulating catalyst is considered as an oxidant reactant that is reduced in situ in a butane stream and reoxidized later on in an external regenerator [14,15]. Dupont's circulating fluidized-bed technology is also promising and

has been used for maleic anhydride production (121). Recently, a fluidized bed reactor was patented for oxidation and oxydehydrogenation of hydrocarbons [16].

Another extremely interesting technology, which has been studied intensively and developed during the last decade, is that of membrane reactors. A large part of the research on membrane reactors has focused on equilibrium shift by selective removal of one particular product and was applied, for instance, in dehydrogenation reactions [17]. The other main field for its application uses the membrane to feed a reactant in a controlled way to the reaction zone, where several reactions may occur. A typical example is the selective oxidation of hydrocarbons. For butane ODH an inert ceramic membrane reactor with V/Mg/O catalysts has been used, allowing fine control of oxygen distribution along the bed [18]. A subsequent theoretical study, with simulation runs, explained the differences observed experimentally in the conversion-selectivity behaviour of fixed beds and IMRs [19]. These reactors present several advantages over conventional FBRs. In particular, higher selectivities are obtained (because oxygen partial pressure can be maintained sufficiently low in the entire reactor). The heat produced is also more evenly distributed along the bed, considerably decreasing formation of hot-spots and therefore leading to more stable and safe operation. Thus, the life of a catalyst charge can be increased too.

Another interesting reactor configuration is illustrated in the recent US patent by Mazanec et al. [20]. In it, an electrochemical process is used for extracting oxygen from an oxygen-containing gas by using a membrane module, which is then transferred to another zone

containing a gas that consumes oxygen, e.g., a hydrocarbon. It is possible that in the near future the combination of both factors, i.e., a highly efficient and economical reactor configuration with a catalyst of excellent performance level, will provide the key for definitive industrial implementation of butane and other ODH processes as an alternative to conventional direct dehydrogenation.

## 5.2 Experimental

### 5.2.1 Supports preparation

As described in the Chapter II (paragraph 2.1), a commercial silica (Grace S432, Specific surface area=320 m<sup>2</sup>/g, Pore volume=1.02 cm<sup>3</sup>/g, Hydroxyls density =0.92 mmol/g) was used as a base support.

A commercial TiO<sub>2</sub> support (anatase, Aldrich with 80 m<sup>2</sup>/g of specific surface area) was also used for some comparisons.

Two different attempts were made for preparing TiO<sub>2</sub>/SiO<sub>2</sub> supports. In one case, the support was prepared by contacting the silica, calcined at 500 °C for 8h, with a solution of titanium tetra-isopropoxide (Fluka) dissolved in dioxane, at room temperature.

Details about the preparation of these supports are reported in Chapter II at the point 2.1. The operative conditions adopted and the adsorption results are reported in Table 2.1 (Part A-Chapter II).

In another case, toluene was used as a solvent and the grafting reaction was performed in a jacketed glass-reactor of 300 cm<sup>3</sup> by contacting the silica support with the alkoxide solution and keeping the reactor at the boiling temperature (115 °C) of toluene for 6 hours (see paragraph 2.1.1). The operative conditions adopted for preparing

this kind of  $\text{TiO}_2/\text{SiO}_2$  support and some related properties are summarized in Table 2.2.

### 5.2.2 Catalysts preparation by impregnation

Two different impregnation procedures were used for preparing vanadium based catalysts, that are respectively: “wet impregnation” and “incipient wetness impregnation” techniques. In the first case, the support was dipped into an excess amount of  $\text{NH}_4\text{VO}_3$  solution dissolved in aqueous oxalic acid [21,22]. This preparation procedure was adopted for preparing supported vanadium oxide catalysts on some different supports, such as: commercial  $\text{SiO}_2$  (Grace S432),  $\text{TiO}_2$  (anatase Aldrich) and  $\text{TiO}_2/\text{SiO}_2$  prepared by coating silica with titanium alkoxide, as previously described. Details on the adopted operative conditions for the catalysts prepared with this procedure are reported in Table V.1. After the impregnation step, the solid was oven-dried, at 120 °C, overnight and calcined in air at 500 °C for 2h. A more precise control over the vanadium oxide loading, that is necessary for a high loading charge, can be achieved with the “incipient wetness impregnation”, where the support is contacted with a volume of the solution of appropriate concentration, corresponding to about the total volume necessary for filling completely the pores of the support. Only one catalyst has been prepared following this procedure impregnating  $\text{TiO}_2/\text{SiO}_2$  with vanadyl tri-isopropoxide dissolved in dioxane. After the impregnation step, the solid was oven-dried, at 120 °C, overnight and calcined in air at 500 °C, for 2h. More details on the adopted conditions are reported always in Table V.1.

Table V.1: Operative conditions adopted for the preparation of vanadium based catalysts by impregnation

| Precursor/solvent/support   | Acronym                              | % wt<br>V <sub>2</sub> O <sub>5</sub> | Precursor<br>(g) | Oxalic<br>acid<br>(g) | Volume of<br>solvent<br>(cm <sup>3</sup> ) | Amount of<br>support<br>(g) |
|---|--------------------------------------|---------------------------------------|------------------|-----------------------|--|-----------------------------|
| NH <sub>4</sub> VO <sub>3</sub> /H <sub>2</sub> O/SiO <sub>2</sub>                      | 5V <sub>imp</sub> /SiO <sub>2</sub>  | 5                                     | 0.374            | 0.420                 | 30   | 6                           |
| NH <sub>4</sub> VO <sub>3</sub> /H <sub>2</sub> O/SiO <sub>2</sub>                      | 30V <sub>imp</sub> /SiO <sub>2</sub> | 30                                    | 2.316            | 2.566                 | 30   | 6                           |
| NH <sub>4</sub> VO <sub>3</sub> /H <sub>2</sub> O/SiO <sub>2</sub>                      | 5V <sub>imp</sub> /TiO <sub>2</sub>  | 5                                     | 0.386            | 0.428                 | 30   | 6                           |
| NH <sub>4</sub> VO <sub>3</sub> /H <sub>2</sub> O/(TiO <sub>2</sub> -SiO <sub>2</sub> ) | 5V <sub>imp</sub> /TSM               | 5                                     | 0.386            | 0.428                 | 30   | 6                           |
| VO(OR) <sub>3</sub> /DIOS/(TiO <sub>2</sub> -SiO <sub>2</sub> ) <sup>a</sup>            | 11.6V <sub>imp</sub> /TSM            | 11.6                                  | 0.323            | -                     | 2.5  | 1.04                        |
| NH <sub>4</sub> VO <sub>3</sub> /H <sub>2</sub> O/MgO <sup>b</sup>                      | 30V <sub>imp</sub> /MgO              | 30                                    | 2.316            | -                     | 30   | 6                           |

<sup>a</sup>This catalyst has been prepared by “incipient wetness impregnation”.

<sup>b</sup>This catalyst has been prepared without oxalic acid.

### 5.2.3 Catalysts preparation by grafting

Two types of catalysts were prepared by grafting, one using SiO<sub>2</sub> as a support and the other one using highly dispersed TiO<sub>2</sub>/SiO<sub>2</sub> supports: TSm (7.29 %wt TiO<sub>2</sub>) and TSM (17.8 %wt TiO<sub>2</sub>). The supports indicated with the acronyms TSm and TSM correspond, respectively, to the titanium tetra-isopropoxide monolayer and multilayer coverage of silica and were prepared by adopting the synthesis procedure reported in Chapter II at the point 2.1. In both the cases, a given amount of solid was contacted with solutions of vanadyl tri-isopropoxide (VO[O-*i*Pr]<sub>3</sub>, Aldrich 99.999%, d=0.963g/ml) dissolved in anhydrous dioxane of increasing concentrations. The grafting reaction was performed for 5h in a well stirred jacketed glass reactor, under inert helium atmosphere. The solids obtained were filtered, washed with dioxane, oven-dried at 120 °C overnight, heated at 200 °C and then calcined at 500 °C. Residual alkoxide groups were eliminated by burning. In Tables V.2/3/4, the operative conditions used for preparing V<sub>2</sub>O<sub>5</sub>/SiO<sub>2</sub>, V<sub>2</sub>O<sub>5</sub>/TSm and V<sub>2</sub>O<sub>5</sub>/TSM catalysts, respectively, are summarised and the related adsorption results are reported. The amounts of vanadium adsorbed on silica have been determined by analysing residual vanadium on the mother solutions contacting the solid, using atomic absorption (AAS) spectroscopy (see Appendix).

**Table V.2** - Operative conditions used for the preparation of a series of V/SiO<sub>2</sub> catalysts by grafting different amounts of VO(O-<sup>i</sup>Pr)<sub>3</sub> in 50 cm<sup>3</sup> of dioxane.

| Acronym                 | Alkoxide<br>initial<br>amount<br>VO(O- <sup>i</sup> Pr) <sub>3</sub><br>(g) | Amount<br>of SiO <sub>2</sub><br>(g) | Metal<br>residual<br>amount<br>(mmolV/ml) | Vanadium<br>adsorbed<br>(%) | Supported<br>Vanadium<br>oxide<br>(% wt V <sub>2</sub> O <sub>5</sub> ) |
|-------------------------|---|--------------------------------------|---|-----------------------------|---|
| 0.16V/SiO <sub>2</sub>  | 0.013   | 3.005                                | 0.000                                     | 100.0                       | 0.16  |
| 0.49V/SiO <sub>2</sub>  | 0.039   | 2.987                                | 0.000                                     | 100.0                       | 0.49  |
| 0.90V/SiO <sub>2</sub>  | 0.081   | 3.322                                | 0.000                                     | 100.0                       | 0.90  |
| 1.27V/SiO <sub>2</sub>  | 0.114   | 3.237                                | 0.0003                                    | 97.0                        | 1.27  |
| 1.84V/SiO <sub>2</sub>  | 0.154   | 2.961                                | 0.0007                                    | 94.8                        | 1.84  |
| 2.07V/SiO <sub>2</sub>  | 0.205   | 3.323                                | 0.0017                                    | 90.0                        | 2.07  |
| 3.81V/SiO <sub>2</sub>  | 0.344   | 3.034                                | 0.0028                                    | 90.7                        | 3.81  |
| 5.41V/SiO <sub>2</sub>  | 0.487   | 3.006                                | 0.0041                                    | 90.2                        | 5.41  |
| 7.24V/SiO <sub>2</sub>  | 0.649   | 3.020                                | 0.0051                                    | 90.5                        | 7.24  |
| 8.55V/SiO <sub>2</sub>  | 0.782   | 2.851                                | 0.0105                                    | 83.8                        | 8.55  |
| 11.89V/SiO <sub>2</sub> | 1.149   | 2.866                                | 0.0191                                    | 79.8                        | 11.89   |



**Table V.3** - Operative conditions used for the preparation of a series of V/TSm catalysts by grafting different amounts of VO(O-<sup>i</sup>Pr)<sub>3</sub> in 50 cm<sup>3</sup> of dioxane.

| Acronym   | Initial<br>alkoxide<br>concentration<br>(mmol <sub>V</sub> /ml) | Equilibrium<br>alkoxide<br>concentration<br>(mmol <sub>V</sub> /ml) | Alkoxide<br>concentration<br>on the support<br>(mmol <sub>V</sub> /g <sub>supp</sub> ) | Theoretical<br>vanadium<br>oxide<br>(% wt V <sub>2</sub> O <sub>5</sub> ) | Supported<br>vanadium<br>oxide<br>(% wt V <sub>2</sub> O <sub>5</sub> ) |
|-----------|---|---|--|---|---|
| 0.94V/TSm | 0.006224  | 0.000032  | 0.1032   | 1.00  | 0.94  |
| 2.00V/TSm | 0.013214  | 0.000040  | 0.2196   | 2.00  | 2.00  |
| 3.10V/TSm | 0.027837  | 0.005777  | 0.3488   | 4.22  | 3.10  |
| 3.22V/TSm | 0.022560  | 0.001260  | 0.3549   | 4.00  | 3.22  |
| 3.49V/TSm | 0.043960  | 0.020060  | 0.3839   | 6.00  | 3.49  |
| 4.51V/TSm | 0.012907  | 0.027300  | 0.4958   | 8.00  | 4.51  |

**Table V.4** - Operative conditions used for the preparation of a series of V/TSM catalysts by grafting different amounts of VO(O-<sup>i</sup>Pr)<sub>3</sub> in 50 cm<sup>3</sup> of dioxane.

| Acronym   | Alkoxide<br>initial<br>amount<br>VO(O- <sup>i</sup> Pr) <sub>3</sub><br>(g) | Amount of<br>support<br>(g) | Metal residual<br>amount<br>(mmol <sub>V</sub> /ml) | Vanadium<br>adsorbed<br>(%) | Supported<br>vanadium oxide<br>(% wt V <sub>2</sub> O <sub>5</sub> ) |
|-----------|---|-----------------------------|---|-----------------------------|--|
| 1.34V/TSM | 0.043   | 1.177                       | 0.000020  | 100.0                       | 1.34   |
| 1.84V/TSM | 0.055   | 1.112                       | 0.000020  | 100.0                       | 1.84   |
| 2.43V/TSM | 0.065   | 0.997                       | 0.000023  | 100.0                       | 2.43   |
| 2.90V/TSM | 0.093   | 1.162                       | 0.000024  | 99.5                        | 2.90   |
| 4.78V/TSM | 0.158   | 1.219                       | 0.000101  | 99.6                        | 4.78   |
| 5.92V/TSM | 0.229   | 1.379                       | 0.000796  | 95.4                        | 5.92   |
| 7.06V/TSM | 0.217   | 1.036                       | 0.001756  | 90.5                        | 7.06   |
| 11.1V/TSM | 0.333   | 1.040                       | 0.001991  | 93.1                        | 11.08  |

#### 5.2.4 Techniques used in catalysts characterisation

Supports and catalysts were characterised by using different techniques such as: X ray diffraction (XRD), diffuse reflectance spectroscopic analysis (DRIFT and DRUV) and Laser-Raman Spectroscopy (LRS).

Textural analyses were carried out by using a Thermoquest Sorptomatic 1990 Instrument (Fisons Instruments) and by determining the nitrogen adsorption/desorption isotherms at 77 K. The samples were thermally pretreated under vacuum overnight up to 473 K (heating rate = 1 K/min). Specific surface area and pore distributions were determined by using the BET and Dollimore-Heal methods.

XRD analyses were carried out by using a Philips diffractometer. The scans were collected at the range of 5-80° (2 $\theta$ ) using CuK $\alpha$  radiation with a rate of 0.01° (2 $\theta$ )/second.

Diffuse reflectance spectra were obtained on a Shimatzu AV2101 spectrophotometer. FTIR and DRIFT spectra were made by using a Nicolet AVATAR 360 instrument. Samples were powdered and diluted 1% by weight with KBr. Adsorbed water was completely removed “in situ” by heating at 400°C in a vacuum (10<sup>-5</sup> mbar).

Raman spectra were obtained using the Brucker RFS100 (Nd-Yag line laser resolution on 32cm<sup>-1</sup>, power 0.5W) on calcined samples.

The X-ray photoelectron spectroscopy analyses were performed with a VG Microtech ESCA 3000 Multilab, equipped with a dual Mg/Al anode. The spectra were excited by the non-monochromatised Mg K $\alpha$  source (1254.4 eV) operated at 14 kV and 15 mA. The analyser operated in the constant analyser energy (CAE) mode. For the individual peak energy regions a pass energy of 20 eV across the hemispheres was used. Survey spectra were measured at 50 eV pass energy. The samples, analysed as prepared, were pelletised and then mounted on double-sided adhesive tape. The pressure in the analysis chamber was in the range of  $10^{-8}$  Torr during data collection. The binding energies of the supports were referenced with respect to the energy of the C 1s peak at 285.1 eV arising from adventitious carbon. The binding energy of the supported catalysts was referenced with respect to the Si 2p binding energy of the carriers, which was 104.3 eV for the pure silica and 103.5 eV for the TSM. The invariance of the peak shapes and widths at the beginning and at the end of the analyses indicated the absence of differential charging. The peaks were fitted by a non-linear least square fitting program using a weighted sum of Lorentzian and Gaussian component curves after background subtraction in line with Shirley and Sherwood [37,38].

The binding energy values are quoted with a precision of  $\pm 0.15$  eV. Surface atomic concentration was evaluated from peak areas using appropriate sensitivity factors built into the VG instrument software. Intensity ratio calculations were performed according to the Kerkhof and Moulijn model [23] using photoelectron cross sections by Scofield [24], electron mean free path by Seah [25], and the values of

bulk density ( $2.6 \text{ g/cm}^3$ ) and surface area ( $280 \text{ m}^2/\text{g}$ ) of the silica support.

The amounts of titanium loading have been determined by using a colorimetric method [26], after dissolution of titanium with a concentrated sulphuric acid solution, diluting and then treating with  $\text{H}_2\text{O}_2$ . Vanadium load in the prepared catalysts was determined by atomic adsorption spectroscopy, after dissolution in concentrated sulphuric acid.

### 5.2.5 Catalytic tests

Kinetic runs were performed at atmospheric pressure by using a quartz tubular micro-reactor. The reactor was fed with the inert gas Helium (Sol 99%) mixed with the reagents butane (Sol 99.99%) and oxygen (Sol 99%). All the experiments were performed at  $T=500^\circ\text{C}$  changing the catalyst weight (0.015-0.05 g) and the total feed flow rate (50-200  $\text{cm}^3/\text{minute}$ ) but keeping the  $\text{O}_2/\text{C}_4\text{H}_{10}$  ratio (1.7) and related the partial pressures constant ( $P_{\text{C}_4\text{H}_{10}} = 7.69 \text{ KPa}$ ,  $P_{\text{O}_2} = 13.04 \text{ KPa}$ ). The activities were determined by analysing with an online gas-chromatograph from the composition of the mixture at the outlet of the reactor. An HP 5890A Series II gas-chromatograph equipped with two different columns (Carboxen 1006 PLOT and Chrompack fused silica PLOT  $\text{Al}_2\text{O}_3/\text{KCl}$ ), one connected to the thermoconductivity detector (TCD), to analyse residual  $\text{O}_2$ , CO and  $\text{CO}_2$ , and the other connected to the flame ionization detector (FID) to analyse unreacted

butane and other formed hydrocarbons. The temperature was programmed to stay at 50°C for 5 minutes, then increasing at 5°C/minute up to 100 °C and subsequently at 10°C/minute up to 200°C. The experimental apparatus adopted is depicted in Fig. 5.1.

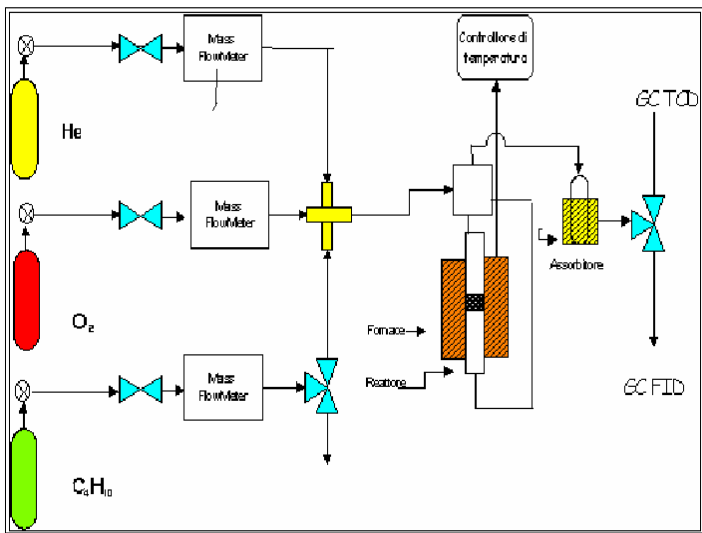


Fig. 5.1: Experimental apparatus adopted for the catalytic tests

5.3 RESULTS AND DISCUSSION

System V/SiO<sub>2</sub>: Chemical adsorption isotherm of vanadyl tri-alkoxide on silica

The amounts of vanadium adsorbed on silica have been determined by analysing residual vanadium on the mother solutions contacting the solid, using atomic absorption spectroscopy (AAS). Adsorbed

vanadium has been determined by comparing the initial concentration with the concentration found after adsorption and relating this value to the amount of used silica. The obtained results are reported in Table 5.2. From the adsorption data determined, it was possible to draw the adsorption isotherm reported in Fig. 5.2.

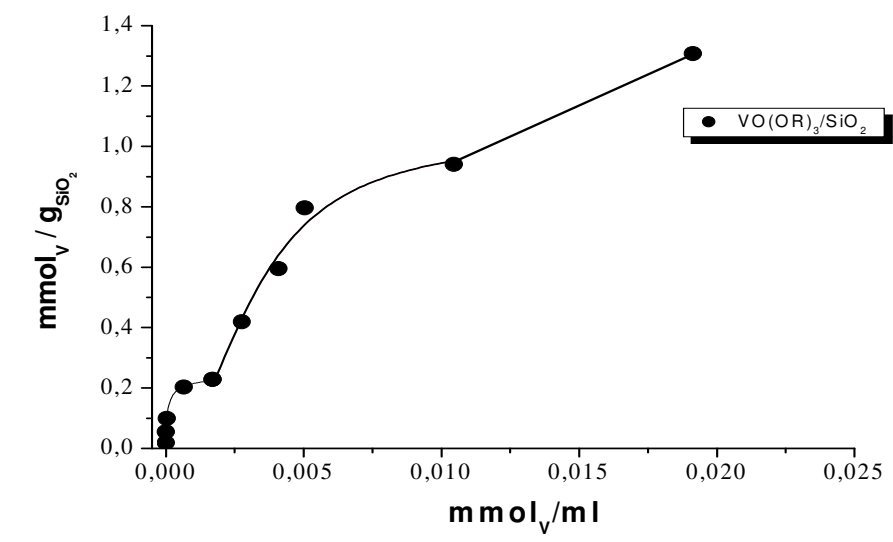
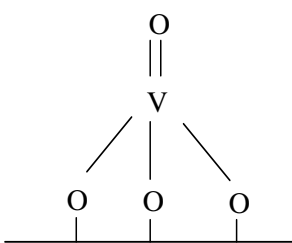


**Fig. 5.2:** Adsorption isotherm of VO(O-<sup>i</sup>Pr)<sub>3</sub> on the silica surface obtained by *Grafting*



As can be seen from Fig. 5.2, two saturation values can be observed at 0.25 mmol/g<sub>SiO<sub>2</sub></sub> (corresponding to about 2.0% by weight of V<sub>2</sub>O<sub>5</sub>) and 0.9 mmol/g<sub>SiO<sub>2</sub></sub> (corresponding to about 8.0% by weight of V<sub>2</sub>O<sub>5</sub>), respectively. It is possible, then, to observe a further increase of adsorbed vanadium by further increasing the degree of the silica coverage by vanadyl alkoxide. The first plateaux, probably, corresponds to the reaction of hydroxyls having higher affinity for vanadyl alkoxide. The interaction of the other hydroxyls is lower and lower, as can be deduced from the lower slope of the isotherm reaching the second plateaux. The adsorption observed after the second plateaux is probably due to the interaction of vanadium on the surface with vanadium complexes in solution, like the interactions occurring in the formation of aggregates in homogeneous phase. According to the observation reported in the literature [28], for very low coverage degree on silica, isolated species of the type:



are prevalent.

Moreover, in the literature [28], is also reported that the monolayer on silica corresponds to a very low value of the sites density of about 0.7 VO<sub>x</sub>/nm<sup>2</sup>. This value is quite low if compared with the one of 7-8VO<sub>x</sub>/nm<sup>2</sup>, normally, obtained for the adsorption on other oxides such

as:  $\text{Al}_2\text{O}_3$ ,  $\text{TiO}_2$ ,  $\text{ZrO}_2$ , ecc. This low saturation level has been interpreted as the consequence of the low density and reactivity of the hydroxyls on the silica surface. The first plateau of Fig. 5.2 seems to be related to the monolayer even if the obtained value of  $0.47 \text{ VO}_x/\text{nm}^2$  for the alkoxide adsorption is moderately lower than  $0.7 \text{ VO}_x/\text{nm}^2$ , found by other authors for the adsorption of  $\text{V}_2\text{O}_5$ . However, this value is reasonable considering that vanadium alkoxide molecules have a size greater than  $\text{V}_2\text{O}_5$ .

The second plateau ( $\sim 1.88 \text{ VO}_x/\text{nm}^2$ ) could be interpreted as the adsorption of dimers or trimers of the vanadium alkoxides molecules, that are prominent in solution, on the less reactive hydroxyls. The formation of oligomers of increasing molecular weight, directly on the surface, is probably responsible of the increase of the adsorption observed at the highest concentration values. However, a correct interpretation of the described isotherm is not easy and is worth to be further deepened.

**System V/TiO<sub>2</sub>/SiO<sub>2</sub>: chemical adsorption isotherm of vanadyl tri-isopropoxide on TiO<sub>2</sub>/SiO<sub>2</sub> support.**

Besides the silica support, the adsorption of vanadyl tri-isopropoxide was also investigated on the surface of silica-supported titania oxides, previously prepared by grafting. In this case, the chemical adsorption of vanadyl alkoxide was carried out on two types of  $\text{TiO}_2/\text{SiO}_2$  supports: TSm (monolayer, 7.29 %wt  $\text{TiO}_2$ ) and TSM (17.8 %wt  $\text{TiO}_2$ ), both prepared by grafting. This study was developed

by contacting different amounts of vanadyl alkoxide, dissolved in dioxane as solvent, with a given amount of the support. In both cases, the adsorbed amount of vanadium on  $\text{TiO}_2/\text{SiO}_2$  support, at different concentrations of vanadyl tri-isopropoxide, has been determined by comparing the initial concentration of the solution with the residual one, analysed by the atomic absorption spectroscopy (AAS). The obtained results are reported in Table 5.3 for the support TSm and in Table 5.4 for the support TSM.

The corresponding adsorption isotherms are depicted, respectively, in Fig. 5.3 and 5.4.

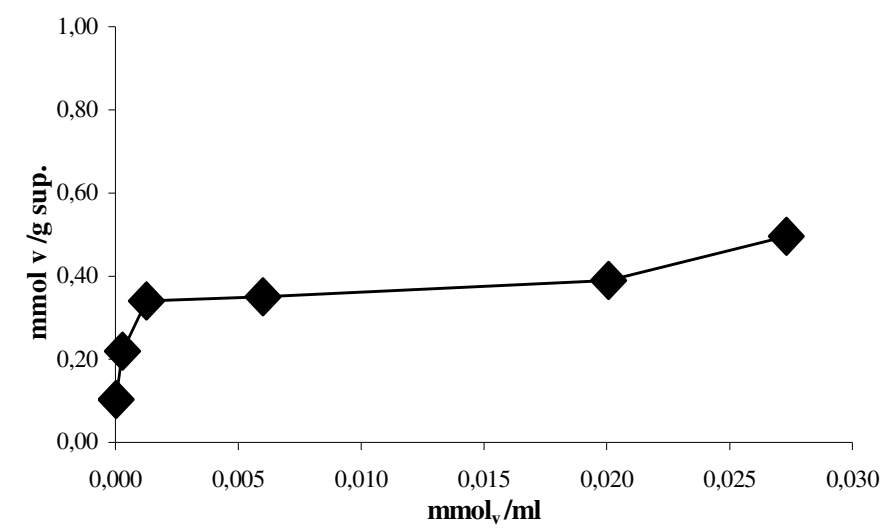


**Fig. 5.3:** Adsorption isotherm of  $\text{VO}(\text{O-}^i\text{Pr})_3$  on the surface of TSm

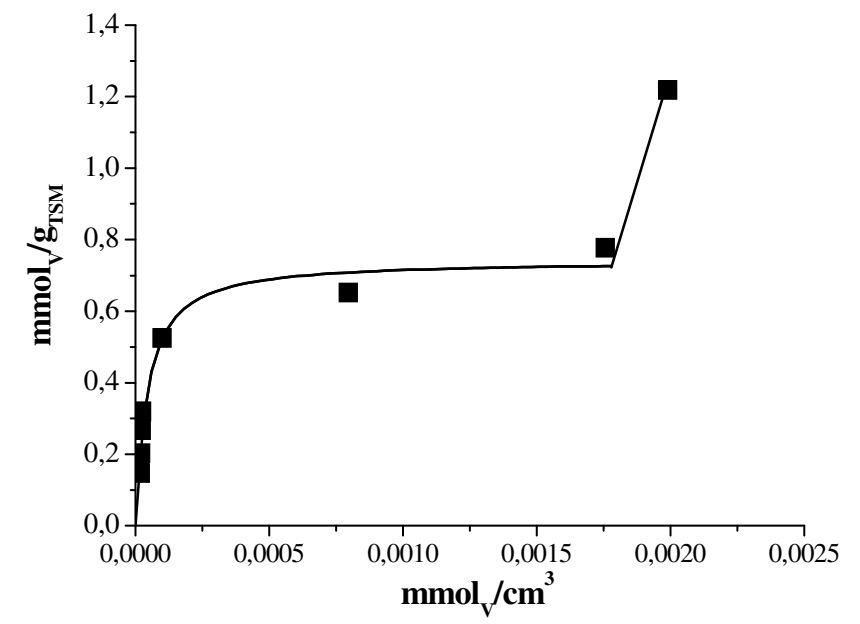


**Fig. 5.4:** Adsorption isotherm of  $\text{VO}(\text{O}^i\text{Pr})_3$  on the surface of TSM

By comparing from a qualitative point of view the isotherms, reported in Fig. 5.3 and 5.4, with the one obtained onto the silica surface, it is possible to note the greater affinity of the vanadyl triisopropoxide for a  $\text{TiO}_2$  surface. This can be more appreciated from the Fig. 5.5.

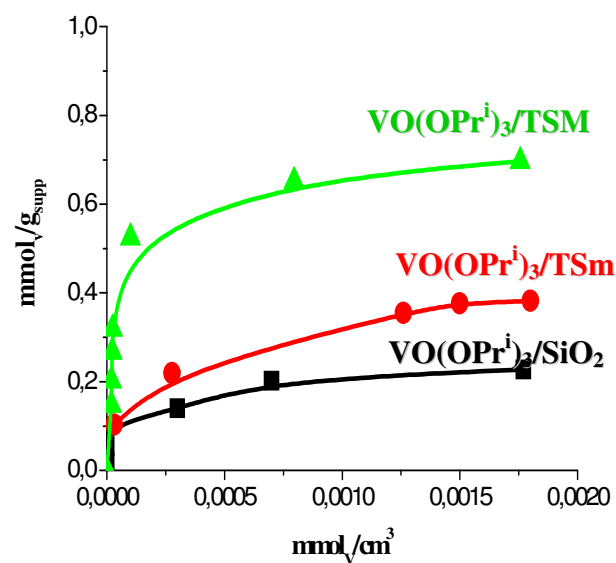
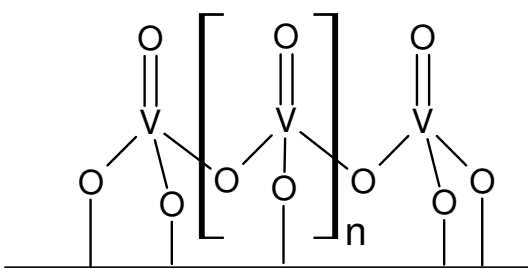


**Fig. 5.5:** Comparison between the chemical adsorption isotherms of vanadyl alkoxides on:  $\text{SiO}_2$ , TSm and TSM.

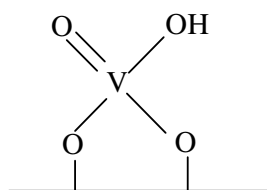
The steep rise of the curves obtained on  $\text{TiO}_2$  surface denotes a strong interaction between the adsorbate and the adsorbent in agreement with the findings reported in the literature [29,30]. The curves reported in Fig. 5.4 can be interpreted with the Langmuir isotherm with the exclusion of the last point and the obtained parameters are:

$K=2.19 \times 10^4$  (L/mol) and  $\Gamma^\infty = 0.77$  mmols<sub>V</sub>/g<sub>TSM</sub>. The great affinity of the vanadyl alkoxide for TiO<sub>2</sub> surface is shown by the large value obtained for  $K$  that is about 30 times the value obtained for the interaction between titanium tetra-isopropoxide and silica surface. The saturation value, corresponding to the monolayer, occurs for a surface density of  $1.67 \text{ VO}_x/\text{nm}^2$ , that is about 7% by weight of V<sub>2</sub>O<sub>5</sub>. This value is comparable with the one ( $2.3 \text{ VO}_x/\text{nm}^2$ ) given by Khodakov et al. [31] for the theoretical monovanadate monolayer. Also in this case, the difference between the two values can be justified considering the greater molecular size of the vanadyl tri-alkoxide with respect to V<sub>2</sub>O<sub>5</sub>. It is interesting to observe that the overall stoichiometry for the monolayer is about 2OH/V.

This means that we can have on the surface a mixture of oligomeric species of the type:



with the already seen monomeric species or alternatively a monomeric isolated specie of the type:



It is interesting to observe that also in this case by further increasing the vanadyl tri-isopropoxide concentration the adsorption increases over the monolayer. This can be interpreted again by assuming the possibility of aggregation by vanadium (on the surface)-vanadium (in solution) interaction. The plot of Fig. 5.4 clearly shows the optimal experimental condition for obtaining the maximum vanadium load, corresponding to the monolayer but avoiding the occurrence of further vanadium-vanadium aggregation occurring at high vanadium alkoxide concentration.

### Catalysts and supports characterization

#### *X rays diffraction analyses*

Prepared catalysts and supports have been submitted to XRD analyses in order to verify the presence of crystallites and to have an estimation of the solids dispersion. In Fig. 5.6, for example, XRD plots obtained for respectively pure  $V_2O_5$  and  $V_2O_5$  impregnated on silica at two different levels of concentrations (30% and 5% by weight) are reported. As can be seen, crystalline  $V_2O_5$  is evident in the samples of pure  $V_2O_5$  and in the samples containing 30% of  $V_2O_5$ .



For the lowest amount of  $V_2O_5$  the catalyst shows a relatively good dispersion. The absence of crystallites of  $V_2O_5$  has been observed for all the catalysts prepared by grafting on both  $SiO_2$  and  $TiO_2-SiO_2$ , independently of the amount of vanadium loaded. For catalysts of  $TiO_2-SiO_2$  impregnated with 11.6% of  $V_2O_5$ , an increase of the intensity of the anatase reflex, at  $25^\circ$ , can be observed with respect to a catalyst prepared by grafting containing a comparable amount of  $V_2O_5$ . This phenomenon has already been observed [32], that is, when vanadium is not uniformly dispersed on the surface it promotes the formation of anatase crystallites during the catalyst calcination.

By concluding catalysts containing amounts of  $V_2O_5$  lower than 10 % by weight don not show crystallites of this compound, in particular those prepared by grafting. Therefore, XRD analysis cannot give information about the molecular dispersion of  $V_2O_5$  on the surface.

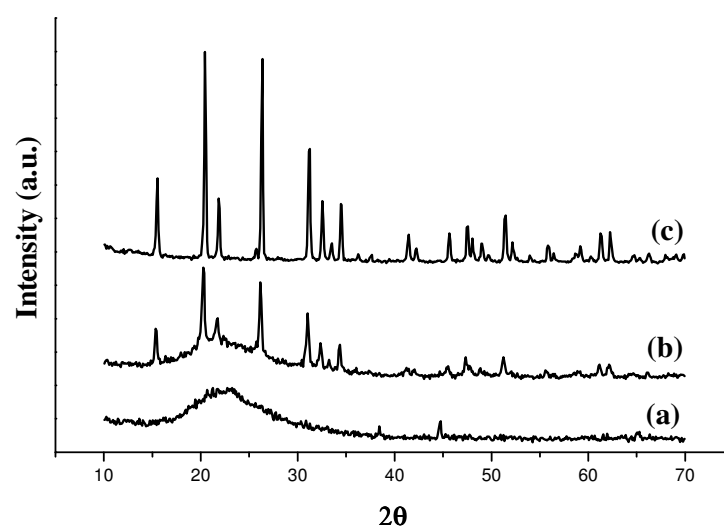


**Fig. 5.6:** XRD spectra of vanadia catalysts supported on  $SiO_2$  by impregnation

and pure  $V_2O_5$ : (a)  $5V_{imp}/SiO_2$ ; (b)  $30V_{imp}/SiO_2$ ; (c) pure  $V_2O_5$ .

### ***Diffuse Reflectance UV Spectroscopy (DR-UV) analysis***

Almost all the prepared catalysts have been submitted, after calcination, to DR-UV examination. It is interesting to observe, first of all, that the  $V_2O_5$  DR-UV spectrum is strongly influenced by the support, as can be seen in Fig. 5.7 where spectra obtained for pure  $V_2O_5$ ,  $V_2O_5$  (30% by weight) impregnated on  $SiO_2$ ,  $MgO$  and  $TiO_2$  respectively, are reported. The spectra of the supports have been subtracted.

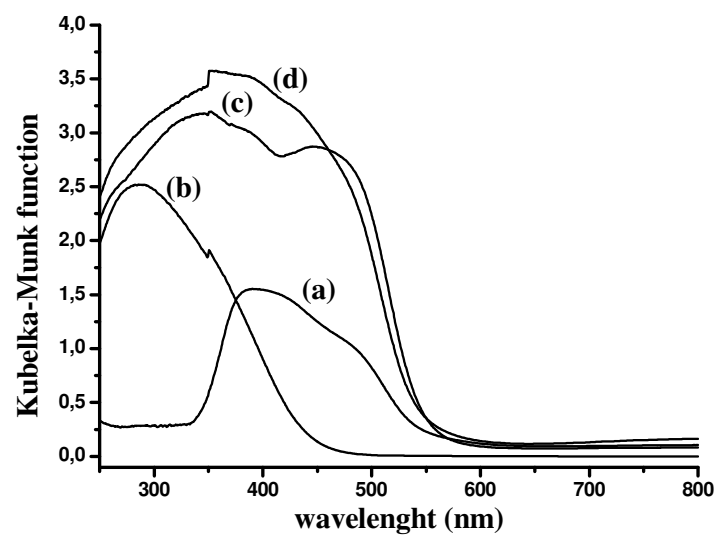


**Fig. 5.7:** DR-UV spectra of vanadia catalysts supported by impregnation over different supports: (a)  $30V_{imp}/TiO_2$ ; (b)  $30V_{imp}/MgO$ ; (c)  $V_2O_5$ ; (d)  $30V_{imp}/SiO_2$ .

In this figure spectra obtained for pure  $V_2O_5$  and  $V_2O_5$  on  $SiO_2$  (c and d) are quite similar, while, the reflectance band is strongly shifted to the right for  $V_2O_5$  on  $TiO_2$  and on the left for MgO. The band with a maximum at about 300-350 nm is, normally, attributed to vanadium not isolated with tetrahedral coordination [33-36], while, the band with a maximum at 400nm has been attributed to  $V^{5+}$  species in square-pyramidal coordination [34] and the band with maximum at 480 nm has been assigned to  $V^{5+}$  in distorted octahedral coordination [34]. Pure  $V_2O_5$  and  $V_2O_5$  on  $SiO_2$  show all the three types of the mentioned coordination, while, for  $V_2O_5$  supported on  $TiO_2$  by impregnation,  $V^{5+}$  species in square-pyramidal coordination seems to be prevalent with respect to distorted octahedral coordination, while, vanadium with tetrahedral coordination is completely absent. On the contrary, for  $V_2O_5$  supported, by impregnation, on MgO tetrahedral coordination is prevalent with respect to square-pyramidal one and  $V^{5+}$  in distorted octahedral coordination is completely absent. The amount of supported  $V_2O_5$  clearly affects the intensity of the band, as it can be appreciated in Fig. 5.7 and Fig. 5.8, where, the spectra obtained for different amounts of  $V_2O_5$  grafted on respectively  $SiO_2$  and  $TiO_2$ - $SiO_2$ , are reported. Also in this case, the spectra of the supports have been subtracted. As it can be seen, the influence of the support, previously observed is confirmed, that is, we can observe a large band, from 250 to 550 nm, on  $SiO_2$  denoting the presence of vanadium, probably aggregated,

with different types of coordination, and a narrower band from 325 to 480 nm, related to more dispersed sites of vanadium with a prevalent square-pyramidal coordination on  $\text{TiO}_2\text{-SiO}_2$ . It is important to remark that for vanadium grafted on titania coating silica ( $\text{TiO}_2/\text{SiO}_2$ ), DR-UV bands show the formation of more homogeneous sites with respect to catalysts prepared by impregnating vanadium on  $\text{TiO}_2$ . As a matter of fact, the DR-UV band at 480 nm is not evident for the catalysts prepared by grafting, therefore, the presence of  $\text{V}^{5+}$  in distorted octahedral coordination is very low, in particular at low vanadium coverage degree. This means that titania coating silica has properties that are somewhat different from the ones of the surface of pure titania (anatase). This has been confirmed, as it will be seen later, by the XPS analysis in which it will be shown that the presence of silica increases the ionicity of the Ti-O bond grafted on the surface. The absence of bands in the range 600-800 nm is justified by the absence of  $\text{V}^{4+}$ .

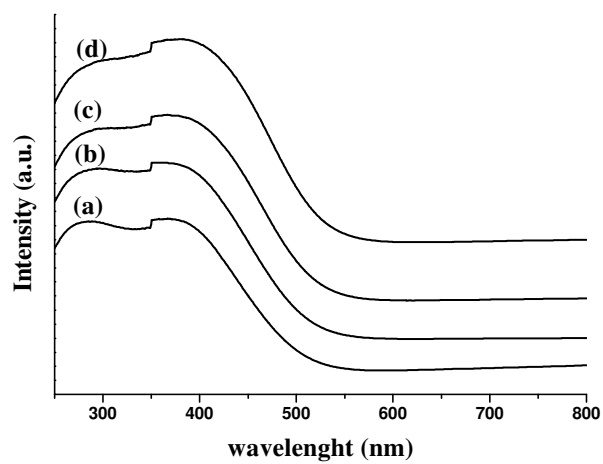


**Fig. 5.7:** A comparison of DR-UV spectra obtained for the vanadia catalysts grafted on silica: (a) V/SiO<sub>2</sub> (4); (b)V/SiO<sub>2</sub> (6); (c) V/SiO<sub>2</sub> (7); (d) V/SiO<sub>2</sub> (11).

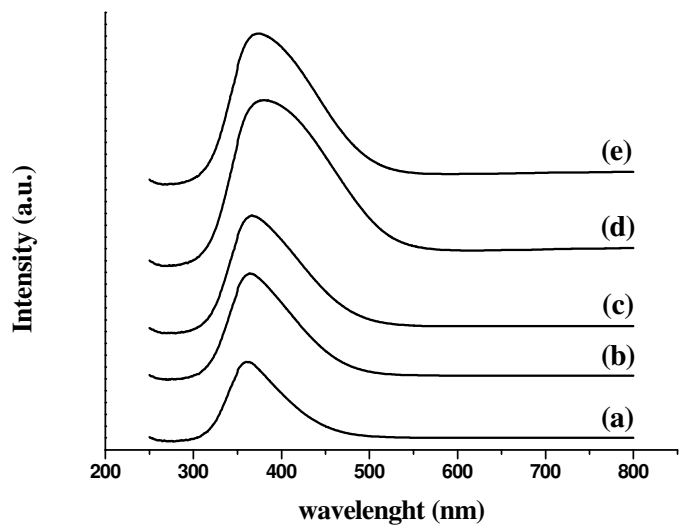


**Fig. 5.8:** A comparison of DR-UV spectra obtained for the vanadia catalysts grafted on silica: (a) V/SiO<sub>2</sub> (4); (b)V/SiO<sub>2</sub> (6); (c) V/SiO<sub>2</sub> (7); (d) V/SiO<sub>2</sub> (11).

**DRIFT analysis**

DRIFT analysis has been performed on selected catalyst samples. The spectra, respectively obtained for silica support and for the catalyst containing 30% by weight of  $V_2O_5$  ( $30V_{imp}/SiO_2$ ) impregnated on silica, have shown a band in the range  $500-600\text{ cm}^{-1}$  characteristic of V-O-V bonds. This suggests the presence of polyvanadylic species. It is interesting also to observe the presence of a small band at  $1026\text{ cm}^{-1}$  corresponding to V=O bond typical of crystalline  $V_2O_5$ . This last observation is in agreement with the X-ray analysis showing the presence of  $V_2O_5$  crystallites on the surface of silica for high vanadium load. The large band with maximum at about  $1100\text{ cm}^{-1}$  is related to the asymmetric vibrational stretching Si-O-Si [38-40]. The conclusion, in agreement with the literature [28], is that  $V_2O_5$  on silica gives place to aggregation favouring the formation of crystalline structures for high vanadium load. Instead, the spectra obtained for two different catalysts, prepared by grafting vanadyl triisopropoxide on  $TiO_2-SiO_2$  support, differing for the amount of grafted vanadia ( $4.78V/TSM$  4.78 % wt  $V_2O_5$ ,  $11.1V/TSM$  11.1 % wt  $V_2O_5$ ) have shown a new band appears in the range  $960-990\text{ cm}^{-1}$ , corresponding to polyvanadylic species of low nuclearity [42]. The bands in the range  $550-800\text{ cm}^{-1}$ , characteristic of V-O-V bonds increase, with vanadium load, in correspondence with an increase of vanadium aggregation. More details about the attribution of the bands

can be found in previous papers and related references there reported [42-45].

#### ***Raman spectroscopy***

Almost all the catalysts obtained by grafting of the type V/TSM have been submitted to Raman spectroscopy analysis. Catalysts containing less than 3% by weight of  $V_2O_5$  did not provide adsorption peaks being that the signal was too low. For greater amounts of  $V_2O_5$ , a well observable peak at  $1030\text{ cm}^{-1}$  appears together with a broad band at  $920\text{-}930\text{ cm}^{-1}$ , as can be seen in Fig. 5.9. The peak at  $1030\text{ cm}^{-1}$  corresponds to monomeric  $V^{5+}$  isolated species [46-48], while, the band at  $920\text{-}930\text{ cm}^{-1}$  is related to polymeric species like metavanadate [46,47]. The absence of  $V_2O_5$  crystallites is confirmed by the absence of a characteristic peak at  $994\text{ cm}^{-1}$  [48-50], although this peak could be overlapped. However, XRD analysis confirms the absence of crystalline structure also for the sample containing more vanadium (11.%  $V_2O_5$  wt, spectrum d).

It is possible to have an estimation of the catalysts dispersion by comparing the area of respectively the peak appearing at  $1030\text{ cm}^{-1}$  and the one of the band at  $920\text{-}930\text{ cm}^{-1}$ . The ratio between the two mentioned area could be an index of the amount of isolated species with respect to the aggregated ones. For the run (b) the area of the band at  $920\text{-}930\text{ cm}^{-1}$  cannot be estimated, while, the ratio is about 2.12 for run (c) corresponding to the alkoxide monolayer coverage

(5.92% wt  $V_2O_5$ ). The ratio decreases for a greater amount of vanadium grafted becoming 1.18 for the sample (d) (11.1 % wt  $V_2O_5$ ). This suggests that the catalysts are rich of isolated species at low coverage, while, a mixture of monomeric and polymeric species exists by increasing vanadium load. However, as proposed by several authors, aggregated species retain linear or planar structures, because, a monolayer of  $V_2O_5$  is formed, as it results from the data reported in Fig. 5.6, notwithstanding all the samples have been calcined. Multilayer structures can be formed, as we have seen, when very concentrated solutions are used in the grafting operation or the grafting is repeated more times. These findings are in good agreement with the observations of other authors, concerning the property of vanadium oxide in spreading on  $TiO_2$  surface [27].

It is interesting to observe in spectra (b,c,d) the bands at 250 and 640  $cm^{-1}$ , that are related to respectively the stretching and bending of the V-O-Ti bonds. The presence of these bonds confirms the good dispersion of vanadium catalysts obtained by grafting. V-O-Ti bonds are prevalent for lower vanadium load with respect to V-O-V bonds and their contribution decreases with the load.



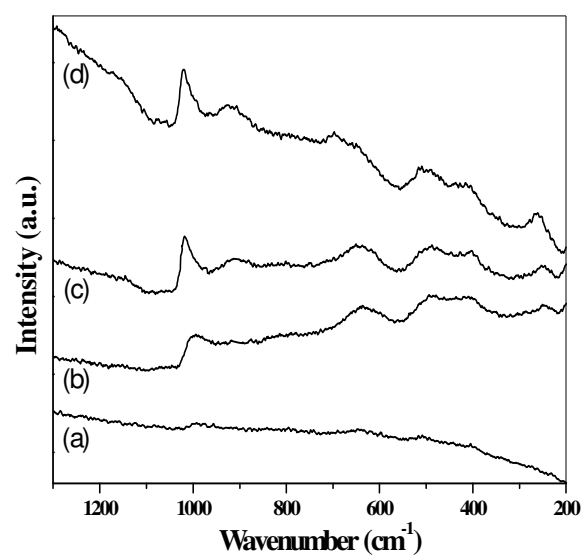


**Fig. 5.9:** A comparison of Raman spectra obtained for the V/TSM catalysts prepared by grafting: 2.92V/TSM (2.92% wt  $V_2O_5$ ); (b) 4.78V/TSM (5) (4.78% wt  $V_2O_5$ ); (c) 5.92V/TSM (5.92% wt  $V_2O_5$ ); (d) 11.1V/TSM (11.1% wt  $V_2O_5$ ).

#### *XPS analysis on $V/SiO_2$ and $V/TiO_2/SiO_2$ catalysts*

Information about the relative dispersion of supported vanadia species as well as indications about the oxidation degree of vanadium in the  $V/SiO_2$  and  $V/TiO_2/SiO_2$  catalysts can be derived from XPS results respectively reported in Tab. 5.5 and Tab. 5.6. The XPS results of the O 1s line for the silica-supported catalysts ( $V/SiO_2$ ) could be divided into two bands centred at  $529.6 \pm 0.3$  eV (vanadium bonded oxygen) and  $533.0 \pm 0.1$  eV (Si-O in the  $SiO_2$  lattice) (Tab. 5.5). In the case of  $V_2O_5/TiO_2/SiO_2$  catalysts (see Tab. 5.6) the main O 1s component, at  $533.1 \pm 0.2$  eV, is in agreement with the O1s BE for

SiO<sub>2</sub>, while both vanadia and titania are thought to contribute to the second one at  $530.5 \pm 0.3$  eV. The V 2p<sub>3/2</sub> BEs of  $516.4 \pm 0.4$  eV for silica (Tab. 5.5) and for titania/silica (Tab. 5.6) supports can be regarded as due to the presence of vanadium species in an oxidation state between V<sup>+4</sup> and V<sup>+5</sup> in the samples [51] with prevalence of the V<sup>+4</sup> component. The presence of V<sup>+4</sup> ions can attributed to the exposure of the samples to X-ray radiation [52]. The invariance of Ti 2p<sub>3/2</sub> BEs along with Vanadium content on V/TSM catalyst, reported in Tab. 5.6, suggests that vanadium does not modify the strength of interaction between the initially deposited TiO<sub>2</sub> and the main support, SiO<sub>2</sub> [52]. Moreover the lowering of n<sub>Ti</sub>/n<sub>Si</sub> ratio along with the increase of vanadium load indicates that the vanadium presence slightly favours the agglomeration of TiO<sub>2</sub> species [44] and that the vanadium is preferentially deposited over the titania. This effect is higher for the 11.6V<sub>imp</sub>/TSM catalyst, that was obtained by vanadyl tri-isopropoxide impregnation with respect to the 11.1V/TSM obtained by the grafting technique. Indeed, 11.6V<sub>imp</sub>/TSM has a vanadium load comparable with the one of 11.1V/TSM catalyst, but lower n<sub>Ti</sub>/n<sub>Si</sub> ratio. Moreover, the XRD analysis of the 11.6V<sub>imp</sub>/TSM catalyst, shows the presence of anatase crystallites that are, on the contrary, absent on the surface of the 11.1V/TSM catalyst prepared by grafting.

Tab. 5.5 - XPS results for the V<sub>2</sub>O<sub>5</sub>/SiO<sub>2</sub> catalysts

| Catalyst  | Vanadium<br>amount<br>(% wt<br>V <sub>2</sub> O <sub>5</sub> ) | XPS: BE (eV)        |                      | Atomic ratios                           |   | XPS: BE of O(1s)<br>(eV) (contribution, %) |
|---|--|---------------------|----------------------|---|---|--|
|   |  | V 2p <sub>3/2</sub> | Si 2p <sub>3/2</sub> | XPS:<br>n <sub>V</sub> /n <sub>Si</sub> | Chemical<br>Analysis :<br>n <sub>V</sub> /n <sub>Si</sub> |  |
| SiO <sub>2</sub>                                    | -  | -                   | 104.3                | -                                       | .   | 533.0 (100)                                |
| V <sub>2</sub> O <sub>5</sub> /SiO <sub>2</sub> (4) | 1.27   | 516.7               | 104.3                | 0.008                                   | 0.009   | 529.5 (5), 533.0 (95)                      |
| V <sub>2</sub> O <sub>5</sub> /SiO <sub>2</sub> (5) | 1.84   | 516.7               | 104.3                | 0.017                                   | 0.012   | 529.7 (5), 533.0 (95)                      |
| V <sub>2</sub> O <sub>5</sub> /SiO <sub>2</sub> (6) | 2.07   | 516.6               | 104.3                | 0.011                                   | 0.015   | 529.4 (5), 533.0 (95)                      |
| V <sub>2</sub> O <sub>5</sub> /SiO <sub>2</sub> (8) | 5.41   | 517.9               | 104.3                | 0.023                                   | 0.037   | 529.6 (10), 533.1 (90)                     |
| V <sub>2</sub> O <sub>5</sub> /SiO <sub>2</sub> (9) | 7.24   | 516.8               | 104.3                | 0.013                                   | 0.060   | 529.9 (4), 533.0 (96)                      |

Tab. 5.6 - XPS results for the V/TSM catalysts

| Catalyst     | XPS: BE (eV)           |                         | XPS :<br>n <sub>Ti</sub> /n <sub>Si</sub> | Chemical<br>Analysis :<br>n <sub>Ti</sub> /n <sub>Si</sub> | Atomic ratios                            |  |  |   |   | XPS: BE of O(1s) (eV)<br>(contribution, %) |
|--------------|------------------------|-------------------------|---|--|--|--|--|---|---|--|
|              | V<br>2p <sub>3/2</sub> | Ti<br>2p <sub>3/2</sub> |   |  | XPS :<br>n <sub>V</sub> /n <sub>Si</sub> | Chemical<br>Analysis:<br>n <sub>V</sub> /n <sub>Si</sub> | XPS :<br>n <sub>V</sub> /n <sub>Ti</sub> | Chemical<br>Analysis :<br>n <sub>V</sub> /n <sub>Ti</sub> | XPS:<br>n <sub>V</sub> /(n <sub>Si</sub> +n <sub>Ti</sub> ) |  |
| TSM          | -                      | 459.5                   | 0.12                                      | 0.17   | -  | -  | -  | -   | 0   | 538.8 (16), 533.2 (84)                     |
| 1.34V/TSM    | 516.4                  | 459.4                   | 0.11                                      | 0.17   | 0.03                                     | 0.010  | 0.26                                     | 0.06  | 0.009   | 530.4 (15), 533.3 (85)                     |
| 2.90V/TSM    | 516.1                  | 459.4                   | 0.11                                      | 0.17   | 0.03                                     | 0.025  | 0.33                                     | 0.15  | 0.021   | 530.4 (16), 533.3 (84)                     |
| 4.78V/TSM    | 516.5                  | 459.4                   | 0.11                                      | 0.17   | 0.04                                     | 0.040  | 0.39                                     | 0.23  | 0.034   | 530.7 (22), 533.2 (78)                     |
| 11.1V/TSM    | 516.1                  | 459.3                   | 0.10                                      | 0.17   | 0.05                                     | 0.100  | 0.53                                     | 0.61  | 0.086   | 530.4 (15), 533.1 (85)                     |
| 11.6Vimp/TSM | 516.2                  | 459.4                   | 0.08                                      | 0.17   | 0.04                                     | 0.110  | 0.50                                     | 0.65  | 0.094   | 529.8 (16), 532.3 (84)                     |

In order to obtain a rough evaluation of vanadia dispersion on the carriers, the XPS experimental ratios  $n_v/(n_{Si} + n_{Ti})$  and  $n_v/n_{Si}$  are reported as a function of  $n_v/(n_{Ti}+n_{Si})$  and  $n_v/n_{Si}$ , obtained by chemical analysis, in Fig. 5.10. For both series prepared by the grafting technique, no linear increase of the surface ratios with the chemical ratios is observed. However a large concentration of the vanadium species is achieved on the surface of the titania/silica support. This means that at least for  $V_2O_5$  concentration up to 4.78 wt% a high dispersion of vanadium species occurs on the titania doped silica, in agreement with the findings of the literature [50]. For the  $SiO_2$  support we observe, on the contrary, that except for the sample with quite low vanadium loading (1.27 % wt  $V_2O_5$ ) the surface is depleted of vanadium. The samples containing higher amount of vanadium show a constant value of the  $n_v/n_{Si}$  ratio corresponding to a lower and lower dispersion. The obtained value of the XPS  $n_v/n_{Si}$  ratio for high Vanadium content ( $n_v/n_{Si} = 0.37$ ) is in good agreement with the value obtained by Keranen et al. for the catalysts prepared by Atomic Layer Deposition (ALD) [51].

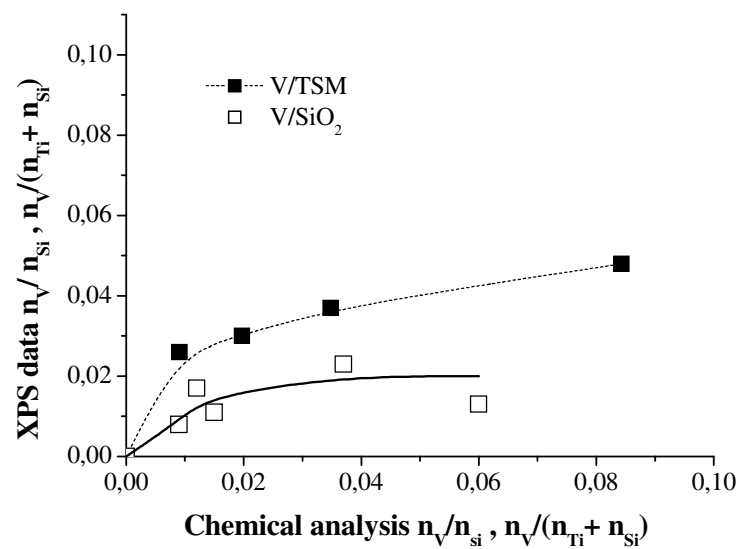


**Fig. 5.10:** XPS vanadium-to-silicon (—) and XPS vanadium to (silicon/titanium) (---) intensities surface ratio of V/SiO<sub>2</sub> and V/TiO<sub>2</sub>/SiO<sub>2</sub> catalysts, respectively.

**Kinetic runs in the Oxidative Dehydrogenation (ODH) of butane**

All the prepared catalysts have been submitted to catalytic tests of the Oxidative dehydrogenation reaction of n-butane to butenes. The obtained results are summarised in Tables 5.7, 5.8 and 5.9.

Table 5.7 - Results of catalytic test reaction for the catalysts prepared by impregnation

| Catalysts                            | V <sub>2</sub> O <sub>5</sub><br>(% wt) | W<br>(g) | Overall<br>feed rate<br>F <sub>t</sub><br>(cm <sup>3</sup> /min) | W/F <sub>t</sub><br>(g <sub>cat</sub> *s)/mol | Conv.<br>%<br>C <sub>4</sub> H <sub>10</sub> | Conv.<br>%<br>O <sub>2</sub> | Selectivities % |                 | Molar products distribution     |  |  |                                   |      |                 |  |
|--------------------------------------|---|----------|--|---|--|------------------------------|-----------------|-----------------|---------------------------------|--|--|-----------------------------------|------|-----------------|--|
|                                      |   |          |  |   |  |                              | C <sub>4</sub>  | CO <sub>x</sub> | 1-C <sub>4</sub> H <sub>8</sub> | 2-C <sub>4</sub> H <sub>8</sub><br>cis | 2-C <sub>4</sub> H <sub>8</sub><br>trans | 1,3-C <sub>4</sub> H <sub>6</sub> | CO   | CO <sub>2</sub> | C <sub>1</sub> +C <sub>2</sub> +C <sub>3</sub> |
| 30V <sub>imp</sub> /SiO <sub>2</sub> | 30                                      | 0.05     | 150  | 492.0   | 7.7  | 25.4                         | 15.0            | 83.0            | 9.4                             | 2.5                                    | 2.2                                      | 0.9                               | 49.8 | 33.2            | 2.0  |
| 5V <sub>imp</sub> /TiO <sub>2</sub>  | 5                                       | 0.05     | 150  | 496.9   | 3.2  | 3.9                          | 51.1            | 47.2            | 28.3                            | 9.4                                    | 9.1                                      | 4.3                               | 19.8 | 27.4            | 1.9  |
| 30V <sub>imp</sub> /MgO              | 30                                      | 0.05     | 150  | 529.2   | 9.9  | 17.2                         | 66.6            | 30.6            | 23.3                            | 10.4                                   | 12.7                                     | 20.2                              | 8.8  | 21.8            | 1.5  |
| 30V <sub>imp</sub> /MgO <sup>#</sup> | 30                                      | -        | -  | 530.0   | 8.0  | -                            | 70.0            | 30.0            | 28.0                            | 12.0                                   | 14.0                                     | 16.0                              | -    | -               | -  |
| 5V <sub>imp</sub> /TSM               | 5                                       | 0.01     | 150  | 144.0   | 3,1  | 4,7                          | 73,3            | 25,1            | 23,7                            | 20,2                                   | 17,4                                     | 12,0                              | 12,1 | 13,0            | 0.7  |

<sup>#</sup> Data from [34]

**Table 5.8:** Results of catalytic test reaction for the catalysts V/SiO<sub>2</sub> prepared by grafting

| Catalyst<br>type       | V <sub>2</sub> O <sub>5</sub><br>(% wt) | W<br>(g) | Overall<br>feed rate<br>F <sub>i</sub><br>(cm <sup>3</sup> /min) | W/F <sub>i</sub><br>(g <sub>cat</sub> *s)/mol | Conv.<br>%<br>C <sub>4</sub> H <sub>10</sub> | Conv.<br>%<br>O <sub>2</sub> | Selectivities<br>% |                 | Molar products distribution     |  |  |                                   |      |                 |  |
|------------------------|---|----------|--|---|--|------------------------------|--------------------|-----------------|---------------------------------|--|--|-----------------------------------|------|-----------------|--|
|                        |   |          |  |   |  |                              | C <sub>4</sub>     | CO <sub>x</sub> | 1-C <sub>4</sub> H <sub>8</sub> | 2-C <sub>4</sub> H <sub>8</sub><br>cis | 2-C <sub>4</sub> H <sub>8</sub><br>trans | 1,3-C <sub>4</sub> H <sub>6</sub> | CO   | CO <sub>2</sub> | C <sub>1</sub> +C <sub>2</sub> +C <sub>3</sub> |
| 1.27V/SiO <sub>2</sub> | 1.27                                    | 0.15     | 100  | 2269.7  | 3.9  | 1.1                          | 73.1               | 23.2            | 30.6                            | 19.2                                   | 16.8                                     | 6.4                               | 4.2  | 19.9            | 3.8  |
|                        | 1.27                                    | 0.15     | 50   | 4539.8  | 8.3  | 4.2                          | 55.3               | 41.4            | 24.2                            | 13.5                                   | 11.7                                     | 5.9                               | 9.1  | 32.4            | 3.3  |
| 2.07V/SiO <sub>2</sub> | 2.07                                    | 0.10     | 100  | 1497.9  | 4.7  | 7.3                          | 68.8               | 28.1            | 28.5                            | 17.9                                   | 15.3                                     | 7.0                               | 8.5  | 19.6            | 3.1  |
|                        | 2.07                                    | 0.10     | 50   | 2995.9  | 9.2  | 14.4                         | 61.1               | 35.6            | 25.5                            | 14.8                                   | 12.6                                     | 8.2                               | 11.7 | 23.9            | 3.3  |
| 3.81V/SiO <sub>2</sub> | 3.81                                    | 0.10     | 150  | 1001.6  | 3.7  | 3.2                          | 80.2               | 17.5            | 34.2                            | 20.7                                   | 18.1                                     | 7.3                               | 1.6  | 15.9            | 2.3  |
|                        | 3.81                                    | 0.10     | 50   | 3004.7  | 11.5   | 9.6                          | 57.2               | 40.6            | 25.4                            | 12.7                                   | 11.0                                     | 8.0                               | 16.3 | 24.4            | 2.2  |



Table 5.9: Results of catalytic test reaction for the catalysts V/TSM prepared by grafting

| Catalyst<br>type | V <sub>2</sub> O <sub>5</sub><br>(% wt) | W<br>(g) | Overa<br>ll<br>feed<br>rate<br>F <sub>t</sub><br>(cm <sup>3</sup> /<br>min) | W/F <sub>t</sub><br>(g <sub>cat</sub> *s)/m<br>ol | Conv.<br>C <sub>4</sub> H <sub>10</sub><br>% | Conv.<br>O <sub>2</sub><br>% | Selectivities<br>% |                 | Molar products distribution     |  |  |                                       |      |                 |  |     |
|------------------|---|----------|---|---|--|------------------------------|--------------------|-----------------|---------------------------------|--|--|---------------------------------------|------|-----------------|--|-----|
|                  |   |          |   |   |  |                              | C <sub>4</sub>     | CO <sub>x</sub> | 1-C <sub>4</sub> H <sub>8</sub> | 2-C <sub>4</sub> H <sub>8</sub><br>cis | 2-C <sub>4</sub> H <sub>8</sub><br>trans | 1,3-<br>C <sub>4</sub> H <sub>6</sub> | CO   | CO <sub>2</sub> | C <sub>1</sub> +C <sub>2</sub> +C <sub>3</sub> |     |
| 1.35V/TSM        | 1.35                                    | 0.01     | 100   | 224.9   | 5.3  | 13.8                         | 65.7               | 32.2            | 20.9                            | 18.2                                   | 15.1                                     | 11.4                                  | 15.7 | 16.5            | 2.1  |     |
|                  | 1.35                                    | 0.01     | 50  | 449.8   | 9.5  | 20.1                         | 53.8               | 44.2            | 16.3                            | 15.0                                   | 11.5                                     | 11.0                                  | 22.8 | 21.3            | 2.1  |     |
|                  | 1.35                                    | 0.05     | 150   | 529.2   | 14.8   | 31.2                         | 41.5               | 57.1            | 11.6                            | 11.3                                   | 9.2                                      | 9.4                                   | 32.7 | 24.4            | 1.4  |     |
|                  | 1.35                                    | 0.05     | 50  | 1587.6  | 37.5   | 80.1                         | 17.9               | 81.0            | 4.2                             | 4.9                                    | 3.9                                      | 5.0                                   | 47.2 | 33.8            | 1.0  |     |
| 2.92V/TSM        | 2.92                                    | 0.01     | 70  | 100.9   | 3.9  | 8.8                          | 74.1               | 24.1            | 24.9                            | 20.6                                   | 17.4                                     | 11.2                                  | 10.6 | 13.5            | 0.9  |     |
|                  | 2.92                                    | 0.01     | 60  | 216.3   | 7.6  | 12.5                         | 61.8               | 36.8            | 19.2                            | 16.2                                   | 14.4                                     | 11.9                                  | 18.8 | 18.0            | 1.4  |     |
|                  | 2.92                                    | 0.01     | 50  | 252.4   | 9.3  | 15.2                         | 55.8               | 43.0            | 16.8                            | 15.1                                   | 12.8                                     | 11.1                                  | 22.1 | 20.9            | 1.2  |     |
|                  | 2.92                                    | 0.05     | 150   | 1481.8  | 41.8   | 91.1                         | 12.4               | 86.8            | 2.8                             | 3.3                                    | 2.6                                      | 3.6                                   | 51.0 | 35.8            | 0.8  |     |
| 4.78V/TSM        | 4.78                                    | 0.008    | 200   | 61.7  | 4.5  | 12.7                         | 71.9               | 25.8            | 25.2                            | 18.5                                   | 16.6                                     | 11.5                                  |      | 12.1            | 13.7   | 1.5 |
|                  | 4.78                                    | 0.01     | 180   | 116.8   | 10.8   | 24.2                         | 50.6               | 48.6            | 15.9                            | 13.3                                   | 11.6                                     | 9.9                                   |      | 25.8            | 22.8   | 0.8 |
|                  | 4.78                                    | 0.01     | 150   | 140.1   | 12.9   | 28.9                         | 44.2               | 55.1            | 13.4                            | 11.6                                   | 9.9                                      | 9.2                                   |      | 29.7            | 25.3   | 0.8 |

|           |      |      |     |       |      |      |      |      |      |      |      |     |      |      |     |
|-----------|------|------|-----|-------|------|------|------|------|------|------|------|-----|------|------|-----|
|           | 4.78 | 0.01 | 50  | 247   | 20.4 | 40.4 | 28.3 | 70.3 | 8.4  | 7.3  | 6.3  | 6.3 | 36.5 | 33.8 | 1.4 |
| 5.92V/TSM | 5.92 | 0.01 | 200 | 66.9  | 3.7  | 13.3 | 55.2 | 43.9 | 18.8 | 14.9 | 12.9 | 8.5 | 21.5 | 22.4 | 1.0 |
|           | 5.92 | 0.02 | 180 | 138.8 | 11.1 | 19.4 | 36.9 | 62.6 | 12.5 | 9.4  | 8.6  | 6.5 | 32.6 | 29.9 | 0.4 |
|           | 5.92 | 0.02 | 150 | 166.6 | 12.7 | 19.9 | 32.3 | 67.2 | 10.7 | 8.4  | 7.5  | 5.7 | 34.7 | 32.5 | 0.5 |
|           | 5.92 | 0.02 | 100 | 249.9 | 19.3 | 38.3 | 21.6 | 77.8 | 6.8  | 5.7  | 5.1  | 4.0 | 40.0 | 37.8 | 0.7 |
|           | 5.92 | 0.01 | 50  | 267.5 | 33.6 | 45.9 | 10.2 | 89.4 | 3.0  | 2.9  | 2.5  | 1.9 | 24.3 | 65.1 | 0.3 |
| 11.1V/TSM | 11.1 | 0.01 | 200 | 61.7  | 11.1 | 28.8 | 26.6 | 72.9 | 9.9  | 6.7  | 6.1  | 4.0 | 41.7 | 31.2 | 0.5 |
|           | 11.1 | 0.01 | 180 | 98.8  | 12.2 | 26.0 | 21.9 | 77.5 | 8.1  | 5.7  | 5.1  | 3.0 | 42.8 | 34.7 | 0.5 |
|           | 11.1 | 0.01 | 50  | 247.0 | 13.1 | 40.6 | 18.9 | 80.6 | 6.7  | 5.0  | 4.4  | 2.7 | 46.3 | 34.3 | 0.5 |
|           | 11.1 | 0.01 | 150 | 118.6 | 32.1 | 76.6 | 6.1  | 93.4 | 1.8  | 1.8  | 1.5  | 0.9 | 52.7 | 40.7 | 0.6 |

In Tab. 5.7 are reported the performances obtained by the catalysts prepared by impregnation and related operative conditions. In Tab. 5.8, the performances and related operative conditions for the catalysts prepared by grafting vanadyl tri-isopropoxide directly on silica, are reported. At last, in Tab. 5.9 the performances obtained by catalysts in which vanadium was grafted on  $\text{TiO}_2/\text{SiO}_2$  support are reported.

From data reported in Tab. 5.7 it is possible to observe a dramatic effect of the support on the activities and selectivities of vanadium based catalysts in the ODH of butane in agreement with the observations of many different authors reported in the literature [53]. In particular, the catalysts  $\text{V}/\text{SiO}_2$  containing a large amount of vanadia (30% by weight) and for this reason low dispersed give place to very low activities and selectivities. The two  $\text{V}/\text{MgO}$  catalysts, reported in Tab. 5.7, are one prepared by us and another one correspondent to the performances reported by the literature [54] for a comparison. As can be seen, both the catalysts containing 30% by weight of  $\text{V}_2\text{O}_5$  have very similar behaviour and show a low activity but a good selectivity. The low activity can be explained with the low dispersion of these catalysts for the high vanadium load. The good selectivity induced by the presence of  $\text{MgO}$  is a well known phenomenon largely described in the literature [53]. Then, it is interesting to compare the performances of the catalysts  $\text{V}/\text{TiO}_2$  and  $\text{V}/\text{TSM}$  having the same vanadium loading of 5% wt. As can be seen,  $\text{V}/\text{TSM}$  is much more active and selective than  $\text{V}/\text{TiO}_2$  giving the same conversion for a lower residence time and a much higher selectivity to butenes. This means that  $\text{TiO}_2$ , deposited by grafting on

silica, in a highly dispersed form, has a beneficial effect on the ODH of butane for what concerns both activity and selectivity. In conclusion, dispersed  $\text{TiO}_2$  of the TSM support is a good environment for vanadia catalysts, as already reported in the literature. Therefore, the behaviour of V/TSM catalysts is, worth to be deepened. At this purpose, in the present thesis we have studied in detail also the effect of surface vanadium dispersion was in detail investigated by testing the catalysts prepared by grafting vanadyl tri-isopropoxide on TSM and the obtained performances have been compared with catalysts prepared in the same way by using  $\text{SiO}_2$  support.

From kinetic results reported in Tab. 5.8, related to the runs performed on the V/ $\text{SiO}_2$  catalysts, prepared by grafting, it is possible to note that activities are very low if compared with the ones related to the V/TSM, and containing the same amount of vanadium. The selectivities, on the contrary, are very high and this seems to be related to the high dispersion of vanadium sites. In fact V/ $\text{SiO}_2$  prepared by impregnation and containing 30% wt  $\text{V}_2\text{O}_5$  has shown a much lower selectivity. The activity of the dispersed catalysts can be roughly related to the vanadium load. The selectivity is poorly affected by the vanadium load, in the examined range (1.27-3.81% wt  $\text{V}_2\text{O}_5$ ). However, selectivity decrease, as usually, with the conversion as it can be seen from the data reported in Tab. 5.8.

All the V/TSM type catalysts have been tested in the ODH of butane. In Fig. 5.11 the conversion obtained for different overall residence times and for each catalyst are reported for a useful comparison.

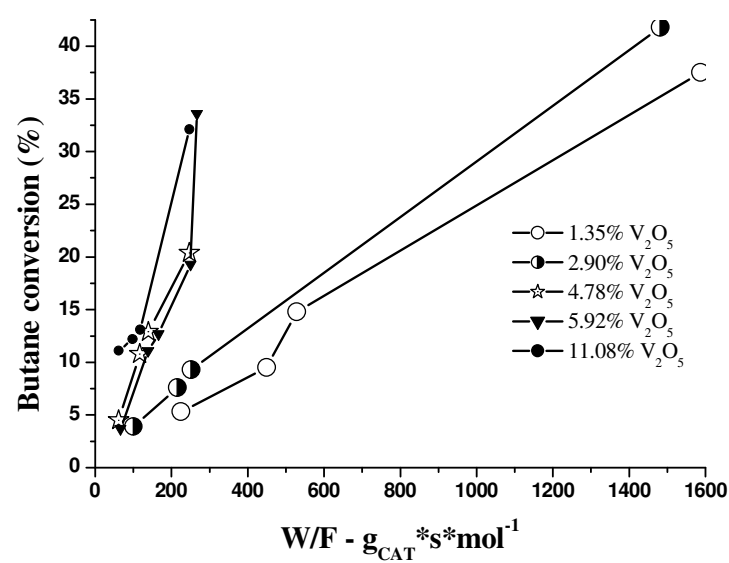


**Fig. 5.11:** A comparison of the activities of the V/TSM catalysts obtained by grafting

As can be seen, activity is strictly related to the amount of vanadium load but, catalysts containing amounts of V<sub>2</sub>O<sub>5</sub> greater than the 4.78% show much lower selectivities, as it is showed in Fig. 5.12, where, selectivities for all the mentioned catalysts are reported as a function of the conversion.

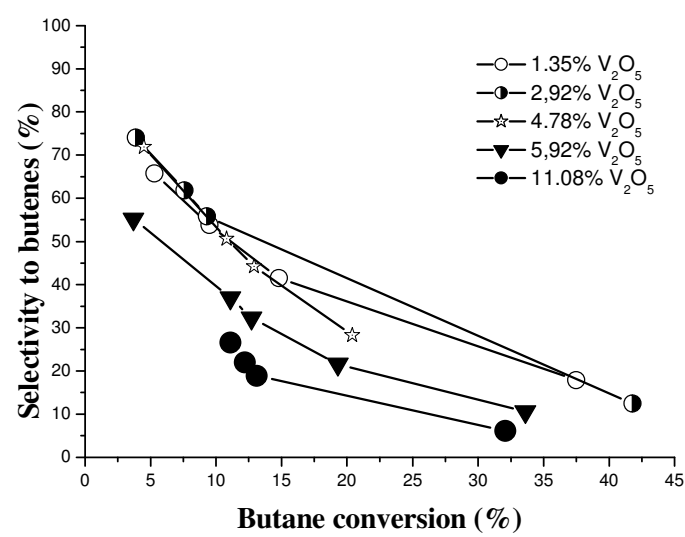


**Fig. 5.12:** A comparison of the selectivities of the V/TSM catalysts obtained by grafting

By calculating the overall butane consumption rates from the runs reported in Fig. 5.11 and putting these values as a function of the vanadium load we obtained a roughly correlation, as showed by the straight line reported in Fig. 5.13. The rate of butane consumption, therefore, is roughly proportional to the amount of vanadium load, but as the selectivity, after an upper limit, largely decreases with this variable, the trend of yields to butenes shows a maximum in correspondence of the catalyst 4.78V/TSM containing an amount of vanadium moderately less than a monolayer, as can be appreciated always in Fig. 5.13. Moreover, catalyst 4.78V/TSM has shown much higher activity and comparable selectivity with respect to the catalysts  $5V_{imp}/TSM$ , prepared by impregnation and containing the same amount of vanadium. Catalysts prepared by impregnation are

evidently less dispersed and the activity loss is a consequence of the lower dispersion.

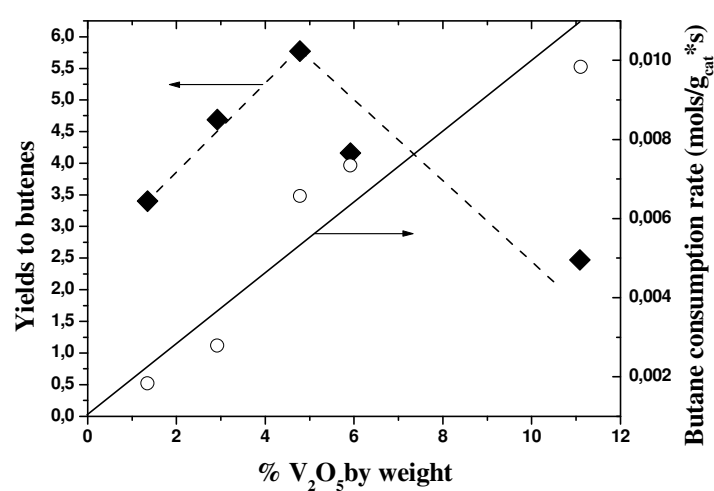


**Fig. 5.13:** A comparison of the yields of the V/TSM catalysts obtained by grafting, runs at  $W/F=200$  ( $\text{g}_{\text{cat}} \cdot \text{s})/\text{mol}_{\text{TOT}}$ ; on the same plot also the butane consumption rates for catalyst containing different vanadium load are reported.

## 5.4 Conclusions

Some different and new insights have been achieved in this experimental part of the thesis, devoted to investigate the catalytic behaviour of supported vanadium based catalysts. For example, the beneficial effect in the use of  $\text{TiO}_2/\text{SiO}_2$  support, prepared by grafting titanium alkoxide on silica, for preparing vanadium catalysts, has been well assessed. In particular, we observed that in this support silica increases the ionicity of the Ti-O bonds. This favours the successive grafting of vanadyl tri-isopropoxide with a more defined structure, giving place after calcination to a relatively uniform class of catalytic

sites that are, very probably, responsible for the higher selectivities observed. In fact, of the three different sites reported in the literature for vanadia catalysts, i.e., vanadium not isolated with tetrahedral coordination,  $V^{5+}$  species in square-pyramidal coordination and  $V^{5+}$  in distorted octahedral coordination, only one has been found largely prevalent in the catalysts prepared by grafting, corresponding to square-pyramidal coordination.

Another important aspect is vanadium dispersion favouring the selectivity, probably, for the same reason, i.e., increasing the uniformity of the catalytic sites. By concluding, sites with square-pyramidal coordination seems to be the most selective ones. Catalysts preparation by grafting allows to increase the density of these sites, while, preparation by impregnation gives place to a broad site distribution and lower selectivity as a consequence.

The dramatic effect of the type of support on the catalysts performances has then been further confirmed. In particular, the aggregation of vanadium oxide directly grafted on silica is demonstrated by both the low activities shown by these catalysts and by the presence of sites of different types on the surface.

At last, by observing the results reported in Figs. 5.4 and 5.13, it is possible to define an optimal procedure of catalyst preparation in order to obtain the best performances in terms of both activity and selectivity. The best catalyst resulted the one prepared by grafting and containing 4.78 % wt  $V_2O_5$  on TSM support. This catalyst retains the high dispersion, characteristic of the sub-monolayer systems, with related selectivity and gives place, therefore, to the maximum yield.



By increasing further the vanadium loading the activity increases but the selectivity strongly decreases for the appearance of other different active sites.

At last, it is also important to point out that the grafting technique gives place to catalysts that are strictly comparable, for what concerns dispersion, with the ones obtainable with the Atomic Layer Deposition technique [50].

## 5.5 References

- [1] Luis M. Madeira and Manuel F. Portela, CATALYSIS REVIEWS, 44(2), 247–286 (2002).
- [2] Kung, H.H., Advances in Catalysis; Eley, D.D., Pines, H., Haag, W.O., Eds.; Academic Press: New York, 1994; Vol. 40, 1–38.
- [3] Hucknall, D.J. Selective Oxidation of Hydrocarbons; Academic Press: London, 1974.
- [4] Grasselli, R.K. Selective Oxidation and Ammoxidation of Olefins by Heterogeneous Catalysis. J. Chem. Ed. 1986, 63 (3), 216–221.
- [5] Thomas, J.M.; Thomas, W.J. Principles and Practice of Heterogeneous Catalysis; VCH: Weinheim, Germany, 1997.
- [6] Satterfield, C.N. Heterogeneous Catalysis in Practice; McGraw-Hill: New York, 1980.
- [7] Figueiredo, J.L.; Ramoa Ribeiro, F. Catalise Heterogenea; Fundacao Calouste Gulbenkian: Lisboa, Portugal, 1989.
- [8] Matar, S.; Mirbach, M.J.; Tayim, H.A. Catalysis in Petrochemical Processes; Kluwer Academic Publishers: Dordrecht, 1989.

- [9] Chaar, M.A.; Patel, D.; Kung, M.C.; Kung, H.H. , J. Catal. 1987, 105 (2), 483–498.
- [10] Blasco, T.; Nieto, J.M.L.; Dejoz, A.; Vasquez, M.I., J. Catal. 1995, 157 (2), 271–282.
- [11] Cavani, F.; Trifirò, F., Catalysis; **1994**, 11, 246–317.
- [12] Grabowski, R.; Grzybowska, B.; Samson, K.; Sloczynski, J.; Stoch, J.; Wcislo, K., Appl. Catal. A: Gen. 1995, 125 (1), 129–144.
- [13] Zazhigalov, V.A.; Bacherikova, I.V.; Komashko, G.A.; Pyatnitskaya, A.I.; Haber, J.; Stoch, J., Appl. Catal. A: Gen. 1996, 134 (2), 225–237.
- [14] Contractor, R.M.; Garnett, D.I.; Horowitz, H.S.; Bergna, H.E.; Patience, G.S.; Schwartz, J.T.; Sisler, G.M., Studies in Surface Science and Catalysis; Corberan, V.C., Bello’n, S.V., Eds.; Elsevier: Amsterdam, 1994; Vol. 82, 233–242.
- [15] Emig, G.; Uihlein, K.; Hacker, C.-J., Studies in Surface Science and Catalysis; Corberan, V.C., Bellon, S.V., Eds.; Elsevier: Amsterdam, 1994; Vol. 82, 243–251.
- [16] Hagemeyer, A., Schweinzer, J., Watzenberger, O., US Patent 5,866,737, February 2, 1999.
- [17] Saracco, G.; Specchia, V., Catal. Rev.—Sci. Eng. 1994, 36 (2), 305–384.
- [18] Tellez, C.; Menendez, M.; Santamaria, J., AIChE J. 1997, 43 (3), 777–784.
- [19] Tellez, C.; Menendez, M.; Santamaria, J., *Chem. Eng. Sci.*, 1999, 54 (13), 2917–2925.

- [20] Mazanec, T.J.; Cable, T.L.; Frye, J.G., Jr.; Kliewer, W.R., US Patent 6,019,885, February 1, 2000.
- [21] M. Inomata, A. Myiamoto, and Y. Murakami, *J. Chem. Soc Chem. Commun.*, (1979) 1009.
- [22] Angelici A. Lemonidou, *Appl. Catal. A: General*, 216 (2001) 277-284.
- [23] F.P.J.M. Kerkhof and J.A. Moulijn, *J. Phys. Chemistry*, 82 (1979) 1612.
- [24] J. H. Scofield, *J. Electr. Spectrosc. Relat. Phenom.*, 8 (1976) 126
- [25] M. P. Seah, *Surf. Interf. Anal.*, 20 (1993) 243
- [26] S. Brunaber, P.H. Emmet, *J. Am. Chem. Soc.*, 60 (1938) 309.
- [27] B.M. Weckhuysen, D.E. Keller, *Catal. Today*, 78 (2003) 25-46.
- [28] I.E. Wachs, B.M. Weckhuysen, *Appl. Catal., A: General*, 157 (1997) 67-90.
- [29] D.J. Cole, C.F. Cullis, D.J. Hucknall, *J. Chem. Soc., Faraday Trans*, 172 (1976) 2744.
- [30] M. Gasior, I. Gasior, B. Grzybowska, *Appl. Catal.*, 10 (1984) 87.
- [31] A. Khodakov, B. Olthof, A.T. Bell, E. Iglesia; *Journal of Catalysis*, 181 (1999) 205-216.
- [32] V. Iannazzo, G. Neri, S. Galvagno, M. Di Serio, R. Tesser, E. Santacesaria; *Applied Catalysis A: General*, 246 (2003) 49-68.
- [33] J.G. Eon, R. Olier and J. C. Volta, *J. Catal.*, 145 (1994) 318.
- [34] G. Busca, G. Martra, A. Zecchina, *Catalysis Today* 56 (2000) 361-370

- [35] T. Lindbald, B. Rebenstorf, Z.G. Yan and S.L.T. Anderson, Appl. Catal. A: General, 112 (1994) 187.
- [36] P. Concepcion, J.M. Lopez Nieto and J. Perez-Pariente, J. Mol. Catal. A: Chemical, 99 (1995) 173.
- [37] M. Taramasso, G. Perego and B. Notari, U.S. Patent 4.410.501
- [38] M.R. Boccun, K.M. Rao, A. Zecchina, G. Leofanti and G. Petrini, Stud. Surf. Catal. Vol. 48, p. 133, Elsevier, Amsterdam, 1989.
- [39] A. Duran, C. Serna, V. Fornes and J.M. Fernandez-Navarro, J. Non-Cryst. Solids, 82 (1986) 69.
- [40] A. Duran, J.M. Fernandez-Navarro, P. Casariego, J. Non-Cryst. Solids, 82 (1986) 69.
- [41] G.T. Went, L.J. Leu, A.T. Bell, J. Catal. 134 (1992) 479-491.
- [42] A. Comite, A. Sorrentino, G. Capanelli, M. Di Serio, R. Tesser, E. Santacesaria; J. Mol. Catal. A: Chem. 198 (2003) 151-165.
- [43] R. Monaci, E. Rombi, V. Solinas, A. Sorrentino, E. Santacesaria, G. Colon; Applied Catalysis A: General 214 (2001) 203-212.
- [44] V. Iannazzo, G. Neri, S. Galvagno, M. Di Serio, R. Tesser, E. Santacesaria; Applied Catalysis A: General 246 (2003) 49-68.
- [45] E. Santacesaria, A. Sorrentino, R. Tesser, M. Di Serio, A. Ruggiero, J. Mol. Catal. A: Chemical 204-205 (2003) 617-627.
- [46] J.M. Jehng, I.E. Wachs, Catal. Lett. 13 (1992) 9.
- [47] L.J. Burchman, G. Deo, X. Gao, I.E. Wachs, Top. Catal. 11-12 (2000) 85.
- [48] X. Gao, S.R. Bare, B.M. Weckuysen, I.E. Wachs, J. Phys. Chem. B 102 (1998) 10842.

- [49] I.E. Wachs, *Catal. Today* 27 (1996) 437.
- [50] N.E. Quaranta, J. Soria, V. Cortes Corberan, and J.L. Fierro, *J. Catal.* 171 (1997) 1-13.
- [51] J. Keranen, C. Guimon, E. Iiskola, A. Auroux, L. Niinisto, *Catal. Today* 78 (2003) 149-157.
- [52] S.T. Oyama, G.T. Went, K.B. Lewis, A.T. Bell, G.A. Somorjai, *J. Phys. Chem. B* 93 (1989) 6786.
- [53] L. M. Maidera, M. F. Portela, *Catalysis Reviews*, 44(2), 247-286 (2002).
- [54] Angelici A. Lemonidou, *Appl. Catal. A: General*, 216 (2001) 277-284.



# VI

## EXPERIMENTAL SECTION

### **Catalytic screening of the ODH of methanol to formaldehyde by supported vanadium based catalysts**

#### **Abstract**

In the present chapter, a catalytic screening of the oxidative dehydrogenation (ODH) of methanol to formaldehyde was carried out on supported vanadium based catalysts.

According to literature, the catalytic evolution of methanol is informative of the surface structure and behaviour of the catalyst and, in fact, it has been widely used as a test reaction. A wide range of by-products (e.g. dimethyl ether, dimethoxymethane, methyl formate, carbon oxides, hydrocarbons) can be obtained depending on both the redox properties and the acidity of the catalyst which, in turn, depend on the interaction between the active phase and the support. Thus, motivated to better understand the relationships between the surface properties and the catalytic performances of vanadia catalysts in the

ODH of methanol, but first of all, motivated to develop a detailed kinetic analysis of the reaction, we decided to perform our work in two steps:

- 3) catalytic screening of the reaction by using different vanadia based catalysts prepared by *grafting*.
- 4) a kinetic study, which has been carried out on a nanostructured-vanadium catalyst, selected in the previous screening (see Chapter VII).

The influence of the preparation method on the surface structure, acidic properties and catalytic activity was demonstrated by examining also the corresponding conventionally impregnated catalysts. The catalysts were characterized by chemical analysis, BET, TPD, RAMAN and XPS spectroscopies and tested in the ODH of methanol to formaldehyde. The main findings of this work showed that the surface dispersion of vanadia species is an important parameter to obtain good performances both in terms of activity and selectivity. A positive trend of selectivity with conversion was observed for all the catalysts of the  $V_{\text{graf}}/\text{TSM}$  series and attributed to the reaction sequence: methanol  $\rightarrow$  dimethoxymethane  $\rightarrow$  formaldehyde.

## 6.1 Introduction

In our rapidly developing world, the production of new synthetic materials is flourishing and, consequently, the demand for bulk chemicals is increasing tremendously. An interesting example is given by formaldehyde ( $\text{CH}_2\text{O}$ ), a base-chemical of major industrial



importance and employed as building-block to produce a large number of products, used in daily life. In spite of fluctuations in the world economy, the growth of formaldehyde has been steady and is expected to continue [1]. The main industrial use of this chemical is in the production of urea-phenolic and melamine resins, which are used in the manufacture of chipboard and plywood. Other applications are in the production of paints, explosives, fertilizers, textiles, cosmetics and papers.

The majority of today's formaldehyde production comes from the partial oxidation of methanol. The industrial processes can be divided in: silver-catalyzed and metal oxide catalyzed processes [1,2]. Most of the newly built formaldehyde plants are based on iron-molybdate (Fe-Mo) catalysts, due to near complete methanol conversion (exceeding 99.9%) as well as very high formaldehyde selectivity (~95%) and due to the stringent environmental regulations being imposed. In this process, all of the formaldehyde is produced by the exothermic partial oxidation of methanol, essentially at atmospheric pressure and temperatures of 250 – 400 °C. Overall plant yields are 88-92% [2].

However, in the last years, interest towards other catalytic systems able to promote the formaldehyde production under more easily controlled conditions has strongly increased. For this reason, the ODH of methanol has been thoroughly investigated in literature [3-12].

Good catalytic performances in terms of both activity and selectivity have also been documented in supported metal oxide catalysts. In particular, supported vanadium oxide based catalysts, widely employed by the chemical industry in various selective

oxidation reactions as well as the selective catalytic reduction of NO<sub>x</sub> by ammonia, have also been found to promote the ODH of alcohols under mild conditions of both T and P, allowing to achieve high activities and high formaldehyde selectivity, to prevent coke formation and, therefore, to extend catalyst lifetime [7]. Moreover, the formation of a very stable product such as water makes this reaction very favourable from thermodynamic point of view. Then, the presence of oxygen limits coking and extends, therefore, catalyst lifetime. All these factors make the ODH of methanol to formaldehyde by supported vanadium oxide catalysts a stimulating scientific challenge [13].

As stated above, the selective oxidation of methanol to formaldehyde represents an important industrial process. On the other hand, a wide range of products (e.g. dimethyl ether, dimethoxymethane, methyl formate, carbon oxides, hydrocarbons) can be obtained depending on both the redox properties and the acidity of the catalyst. Consequently, the catalytic evolution of methanol, either in the presence or in the absence of oxygen, is informative of the surface structure and behaviour of the catalyst, and in fact it has been widely used as a test reaction. For this reason, it is common to state that the partial methanol oxidation is a “structure sensitive” reaction [7].

Among the binary transition metal oxides, vanadium pentoxide, V<sub>2</sub>O<sub>5</sub>, is one of the few which allow significant selectivities in formaldehyde synthesis from methanol oxidative dehydrogenation, being particularly active in the partial oxidation of methanol. This

reaction has been investigated on pure  $V_2O_5$  from several points of view. Bhattacharyya et al. [4], for example, investigated the reaction kinetics of formaldehyde synthesis on bulk vanadia in the temperature range 254-280 °C and proposed a kinetic law consistent with a Mars-van Krevelen-type redox mechanism where the rates of both steps are first order with respect to the reactants, methanol and oxygen. Other examples are reported in literature [5-12]. However, serious efforts have been made to improve the catalytic performances of vanadium pentoxide based catalysts.

First, to enhance the surface area of vanadia to be used as a catalyst for methanol partial oxidation, several researchers tried to support on high-surface metal oxide.

So, the behaviour of vanadia supported on various oxide carriers has been investigated. Roozenboom et al. [5] found that, for “monolayer-type” oxide-supported vanadia catalysts, the activity in methanol oxidation follows the trend  $V_2O_5/TiO_2$  (anatase) >  $V_2O_5/ZrO_2$  >  $V_2O_5/CeO_2$  >  $V_2O_5/\gamma-Al_2O_3$  >  $V_2O_5$ , but the selectivity to formaldehyde follows nearly the inverse trend. More recently, Deo and Wachs [12] found that, at 503 K,  $V_2O_5$ - $TiO_2$  (anatase) allows very high activities and also very high selectivities to formaldehyde. They also found that the addition of a second component to the  $V_2O_5$ - $TiO_2$  (anatase) catalyst can further modify the catalytic properties. They stated that the further addition of W, Nb and Si does not significantly modify the catalytic activity (TOF of vanadium) while the addition of K and P causes the decrease of the TOF. The addition

of P also causes a decrease in formaldehyde selectivity and an increase in dimethyl ether production.

A review proposed by Forzatti et al. [7] on the behaviour of supported vanadia based catalysts in the oxidation of methanol highlighted that a key factor allowing high selectivities in formaldehyde is the absence of very nucleophilic oxygen species able to attack the carbonyl carbon atom of formaldehyde. On the contrary, the existence of surface oxygen species with sufficient nucleophilicity allows formaldehyde to be strongly adsorbed in the form of dioxymethylene, which eventually results in methyl formate with high selectivities. However, the data provided in this paper also suggest that the electronic interaction of vanadium oxide species with semiconductor solids or with transition metal cations allows electron exchanges which favourably affect the catalytic activity.

So, literature information show clearly that the activity of vanadium pentoxide in the oxidation of methanol is strongly influenced by the nature of the support/oxide used. In particular, on the basis of the data concerning studies conducted with the aim to investigate the effect of the operative conditions adopted to perform the reaction, it seems to be evident that the selectivity towards the reaction products is affected not only by the nature of the support but also by vanadium loading, contact time, reaction temperature, feed composition and conversion level and so on. Apart from the role of the support, the importance of the preparation method on the final catalyst behavior has been largely discussed in literature [14-17]. At this purpose, catalyst preparation by using the liquid-phase grafting

technique has gained interest in the recent years as a useful route for obtaining well dispersed catalysts [18,19].

In line with this background, we decided to investigate the catalytic performances of supported vanadium based catalysts not only in the ODH of butane to butenes, as showed in the Chapter V, but also in the ODH of methanol to formaldehyde. We will try to provide a fundamental understanding of the relationships between the structural features and reactivity properties of supported vanadia-based catalysts. For this purpose, many different vanadium catalysts supported on different oxides, such as  $\text{SiO}_2$ ,  $\text{TiO}_2$  and  $\text{TiO}_2/\text{SiO}_2$  (TSm), have been prepared either by impregnation or liquid-phase metal alkoxide grafting for a useful comparison. All the catalysts prepared have been characterized by using many different techniques and tested in the ODH of methanol.

## 6.2 Supports and catalyst preparation

The wet impregnation procedure here adopted to prepare some of vanadium based catalysts has been described at the point 5.2.2. The support, indicated with the acronym TSm, was prepared by contacting the silica, calcined at  $500^\circ\text{C}$  for 8h, with a solution of titanium tetra-isopropoxide (Fluka) dissolved in dioxane, at room temperature. Details about its preparation are reported in the Chapter II. Anyway, the operative conditions adopted and the adsorption results are reported in Table 6.1. Two types of catalysts were prepared by grafting, one using  $\text{SiO}_2$  and the other one using  $\text{TiO}_2/\text{SiO}_2$  (TSm) as a support. In the latter case, a given amount of solid was contacted with

solutions of increasing concentration of vanadyl tri-isopropoxide ( $\text{VO}[\text{O-iPr}]_3$ , Aldrich 99.999%,  $d=0.963\text{g/ml}$ ) dissolved in anhydrous dioxane. The grafting reaction was performed for 5h in a well stirred jacketed glass reactor, under inert helium atmosphere. The solids obtained were filtered, washed with dioxane, oven-dried at  $120\text{ }^\circ\text{C}$  overnight, heated at  $200\text{ }^\circ\text{C}$  and then calcined at  $500\text{ }^\circ\text{C}$ . The operative conditions used for preparing  $\text{V}_{\text{graf}}/\text{SiO}_2$  and  $\text{V}_{\text{graf}}/\text{TiO}_2/\text{SiO}_2$  catalysts, respectively, are reported in Table 6.1. The adsorbed vanadium was determined by atomic absorption spectroscopy.

**Table 6.1:** Operative conditions used for the preparation of the support TSm and V-based catalysts.

| Precursor/solvent/support  | Acronym                                 | Prep.<br>Method | Amount<br>of<br>Precursor<br>(g) | Amount<br>of<br>oxalic acid<br>(g) | Volume<br>of<br>solvent<br>(cm <sup>3</sup> ) | Amount<br>of<br>support<br>(g) |
|--|---|-----------------|----------------------------------|------------------------------------|---|--------------------------------|
| NH <sub>4</sub> VO <sub>3</sub> /H <sub>2</sub> O/SiO <sub>2</sub> | 5V <sub>imp</sub> /SiO <sub>2</sub>     | Impreg.         | 0.374                            | 0.420                              | 30  | 6                              |
| NH <sub>4</sub> VO <sub>3</sub> /H <sub>2</sub> O/SiO <sub>2</sub> | 5V <sub>imp</sub> /TiO <sub>2</sub>     | Impreg.         | 0.386                            | 0.428                              | 30  | 6                              |
| Ti(O-Pr) <sup>i</sup> <sub>4</sub> /Dioxane/SiO <sub>2</sub>       | TSm                                     | Grafting        | 10.787                           | -                                  | 400   | 24                             |
| VO(O-Pr) <sup>i</sup> <sub>3</sub> /Dioxane/SiO <sub>2</sub>       | 5.41V <sub>grat</sub> /SiO <sub>2</sub> | Grafting        | 0.487                            | -                                  | 50  | 3                              |
| VO(O-Pr) <sup>i</sup> <sub>3</sub> /Dioxane/TSm                    | 0.94V <sub>grat</sub> /TSm              | Grafting        | 0.076                            | -                                  | 50  | 3                              |
| VO(O-Pr) <sup>i</sup> <sub>3</sub> /Dioxane/TSm                    | 2.00V <sub>grat</sub> /TSm              | Grafting        | 0.161                            | -                                  | <b>50</b>                                     | <b>3</b>                       |
| VO(O-Pr) <sup>i</sup> <sub>3</sub> /Dioxane/TSm                    | 3.10V <sub>grat</sub> /TSm              | Grafting        | 0.275                            | -                                  | 50  | 3                              |
| VO(O-Pr) <sup>i</sup> <sub>3</sub> /Dioxane/TSm                    | 3.23V <sub>grat</sub> /TSm              | Grafting        | 0.340                            | -                                  | 50  | 3                              |
| VO(O-Pr) <sup>i</sup> <sub>3</sub> /Dioxane/TSm                    | 3.49V <sub>grat</sub> /TSm              | Grafting        | 0.537                            | -                                  | 50  | 3                              |
| VO(O-Pr) <sup>i</sup> <sub>3</sub> /Dioxane/TSm                    | 4.69V <sub>grat</sub> /TSm              | Grafting        | 0.645                            | -                                  | 50  | 3                              |
| VO(O-Pr) <sup>i</sup> <sub>3</sub> /Dioxane/TSm                    | 5.37V <sub>grat</sub> /TSm              | Grafting        | 0.873                            | -                                  | 50  | 3                              |

### 6.3 Techniques used in catalyst characterization

All the catalysts prepared have been characterized by using BET, TPD, RAMAN and XPS spectroscopies.

Details about the experimental conditions of the techniques mentioned above have been reported in Chapter II.

### 6.4 Methods, Techniques and Operating conditions used in the catalytic runs

Kinetic runs were performed in a stainless steel tubular reactor with an internal diameter of 1 cm, kept isothermal with a fluidized bed of sand. Liquid methanol was fed, by a syringe pump, into a vaporizer chamber kept at 250 °C and was then sent, after the addition of a stream of oxygen and helium, into a stainless steel coil kept at the same temperature of the reactor. The composition of the gases at the outlet of the reactor was gas-cromathographically analyzed by withdrawing a sample with an on-line sampling valve kept at 170°C. The GC used was an HP 5890 instrument, with a Restek RT-Q-Plot 30 m × 0.32 mm column. Helium was used as the carrier gas. The conditions used for the analyses were as follows: temperature held at 50°C for 2 min, increased at a rate of 5°C/min to 100°C and then at a rate of 20°C/min to 180°C for 5 min, and finally kept at this temperature for 5 min. A TCD detector kept at 250°C was used.

Table 6.2 reports the GC-factors determined for each component of the reaction mixture.



**Table 6-2:** Components of the reaction mixture and related GC-factors

| Component  | T <sub>R</sub> (min) | Factors |
|--|----------------------|---------|
| O <sub>2</sub>                                   | 1.92                 | 0.7     |
| CO <sub>2</sub>                                  | 2.32                 | 0.51    |
| H <sub>2</sub> O                                 | 5.50                 | 2.45    |
| CH <sub>2</sub> O                                | 8.50                 | 0.71    |
| CH <sub>3</sub> OH                               | 10.36                | 1       |
| (CH <sub>3</sub> ) <sub>2</sub> O                | 11.10                | 1.14    |
| HCOOCH <sub>3</sub>                              | 14.00                | 0.28    |
| CH <sub>2</sub> (OCH <sub>3</sub> ) <sub>2</sub> | 17.50                | 0.68    |

Samples of powdered catalyst, generally 0.3 g, were placed inside the reactor on a bed of glass wool. Two thermocouples located immediately upon and under the catalytic bed allowed the validity of the isothermal conditions to be controlled within  $\pm 1$  °C. In the figures 6.1 and 6.2, a schematic representation of the experimental apparatus and details of the reactor used is reported, respectively.

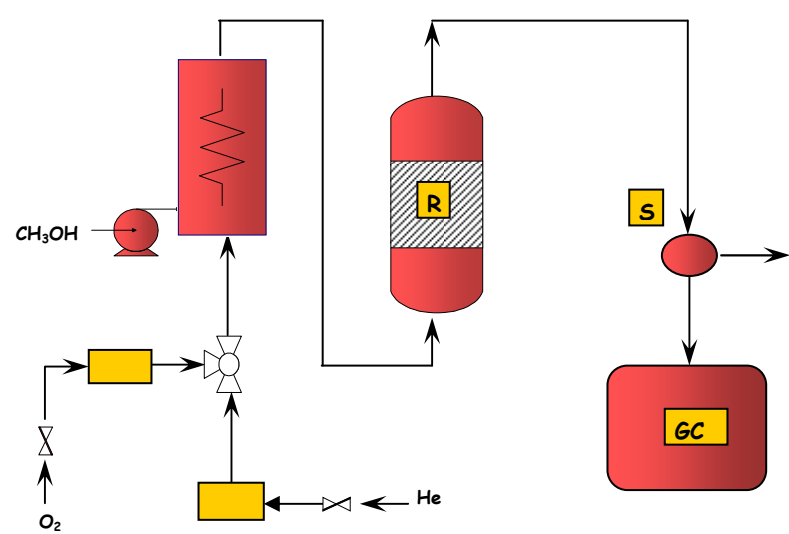


**Figure 6.1:** Schematic representation of the lab-scale plant used for the ODH of methanol to formaldehyde. R= reactor; S= sample valve; GC= gas-cromatograph.

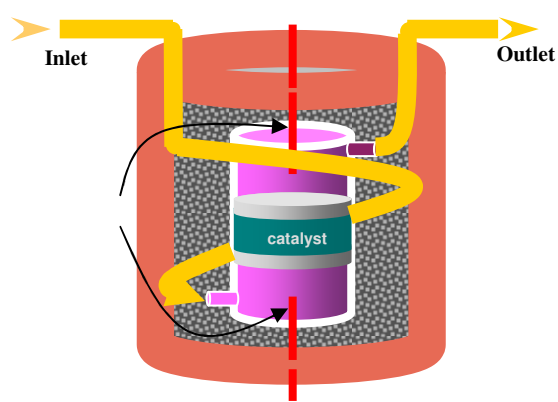


**Figure 6.2:** Schematic drawing of the packed-bed tubular reactor used for the ODH of methanol to formaldehyde. R= reactor; S= sample valve; GC= gas-cromatograph.

The catalytic runs were conducted at atmospheric pressure (1 atm), by keeping constant the residence time and by changing the reaction temperature from 140 to 240 °C. Table 6.3 gathers the operative conditions adopted for the catalytic screening.

**Table 6.3:** Operative conditions used for the catalytic tests (Methaol:Oxygen:Helium = 20:20:60 (mol%))

| Catalyst weight (g) | Helium Flow (ml/min) | Oxygen Flow (ml/min) | Methanol Flow (ml/h) | W/F (g <sub>cat</sub> *h/mol <sub>MetOH</sub> ) |
|---------------------|----------------------|----------------------|----------------------|---|
| 0.5                 | 22.3                 | 7.4                  | 0.8                  | 25.3  |

Results are reported in terms of the methanol conversion and product yields. The methanol conversion is defined as

$$C = \frac{\text{(number of moles of methanol reacted)}}{\text{(number of moles of methanol fed)}}$$

while the yields of the *i*-th product is defined as

$$Y_i = \frac{\text{(number of moles of product } i \text{ formed)}}{\text{(number of moles of methanol fed)}}$$

## 6.5 Results and discussion

### 6.5.1 Catalysts and supports characterization

#### 6.5.1.1 Chemical composition and surface area/porosity determinations

The physico-chemical properties of the supports and vanadium oxide catalysts are listed in Table 6.4. The catalysts are labelled  $XV_p/M$ , where X corresponds to the % by weight of vanadium, V to vanadium, p to the preparation method (imp=impregnation, graf=grafting) and M to the support. No marked effect of the deposition of titanium oxide on the specific surface area of the silica was detected in the case of the support TSm, while, in the case of the vanadium-based catalysts, a decrease in  $S_{BET}$  was observed. The vanadium surface densities are calculated as number of vanadium atoms per square nanometer of catalyst ( $V/nm^2_{cat}$ ) to facilitate a comparison of the samples prepared on different surface area supports [15]. The vanadium contents of the samples are quite smaller than the theoretical monovanadate monolayer coverage of  $2.3 VO_x/nm^2$  [15].

#### 6.5.1.2 Dispersion and structure analysis by XPS

Information about the relative dispersion of supported vanadia species as well as indications about the oxidation degree of vanadium in the catalysts were acquired by XPS.

Andersson [16] has reported the V  $2p_{3/2}$  line positions for several vanadium oxides by standardizing the spectra to the O 1s signal at 529.6 eV. According to this standardization method, the reference V

$2p_{3/2}$  peak positions for  $V_2O_5$ ,  $V_6O_{13}$ ,  $V_2O_4$  and  $V_2O_3$  could be fixed at 516.9, 516.6, 515.9 and 515.7 eV, respectively. The V  $2p_{3/2}$  BEs of  $516.6 \pm 0.3$  eV for the titania/ silica-supported samples indicated the presence of vanadium species mainly in the oxidation state of +4/+5. Only for the catalysts  $5V_{\text{graf}}/\text{SiO}_2$ , a higher V  $2p_{3/2}$  BE value of  $\sim 517.3$  eV was detected.

The XPS spectra of the O 1s line for the silica-supported catalyst,  $5V_{\text{graf}}/\text{SiO}_2$ , could be divided into two bands centred at 530.0 eV (vanadium bonded oxygen) and 532.5 eV (Si-O in the  $\text{SiO}_2$  lattice) [19]. The relative high Ti  $2p_{3/2}$  peak position (459.1 eV) due to the formation of Ti-O-Si bridging bonds [19] in the  $\text{TiO}_2/\text{SiO}_2$  support (Table 6-2) was shifted towards the bulk Ti  $2p_{3/2}$  value ( $458.7\text{eV} \pm 0.2\text{eV}$ ) in the  $V_{\text{graf}}/\text{TSM}$  samples. Along with the decrease in XPS Ti/Si ratio (Table 6.2), this indicated the occurrence of some titania agglomeration during the calcination procedure, not observed by XRD measurements because the crystallite sizes are below the XRD detection threshold limit.

Table 6.4 – Physico-chemical properties of the prepared catalysts and supports

| Catalysts                               | S <sub>BET</sub><br>m <sup>2</sup> /g | NH <sub>3</sub> -TPD |       | XPS: BE (eV)         |                      |                     | Atomic ratio                   |                                | XPS                                  |
|---|---------------------------------------|----------------------|-------|----------------------|----------------------|---------------------|--------------------------------|--------------------------------|--------------------------------------|
|   |                                       | V/nm <sup>2</sup>    | data  | Si 2p <sub>3/2</sub> | Ti 2p <sub>3/2</sub> | V 2p <sub>3/2</sub> | XPS<br>V/Si (Ti/Si)            | Chem. Anal.<br>V/Si (Ti/Si)    | BE of O 1s (eV)<br>(contribution, %) |
|   |                                       |                      |       |                      |                      |                     |                                |                                |                                      |
| SiO <sub>2</sub>                        | 282                                   | -                    | -     | 104.3                | -                    | -                   | -                              | -                              | 533.0 (100)                          |
| 5V <sub>imp</sub> /SiO <sub>2</sub>     | 267                                   | 1.24                 | -     | -                    | -                    | -                   | -                              | -                              | -                                    |
| 5.41V <sub>graf</sub> /SiO <sub>2</sub> | 260                                   | 1.38                 | 79.3  | 103.3                | -                    | 517.3               | 0.01                           | 0.04                           | 530.0 (3), 532.5 (97)                |
| TiO <sub>2</sub>                        | 7                                     | -                    | -     | -                    | 458.4                | -                   | -                              | -                              | 529.6 (100)                          |
| 5V <sub>imp</sub> /TiO <sub>2</sub>     | 5                                     | -                    | -     | -                    | -                    | -                   | -                              | -                              | -                                    |
| TSm <sup>a</sup>                        | 280                                   | -                    | 154.0 | 103.4                | 459.1                | -                   | (0.04)                         | (0.06)                         | 530.1 (4), 532.6 (96)                |
| 0.94V <sub>graf</sub> /TSm              | 286                                   | 0.24                 | -     | 103.4                | 458.8                | 516.5               | 0.004 (0.04) 0.06 <sup>b</sup> | 0.007 (0.06) 0.13 <sup>b</sup> | 530.0 (5), 532.7 (95)                |
| 3.23V <sub>graf</sub> /TSm              | 257                                   | 0.75                 | -     | 103.5                | 458.2                | 516.5               | 0.03 (0.05) 0.67 <sup>b</sup>  | 0.02 (0.06) 0.43 <sup>b</sup>  | 529.2 (5), 531.6 (95)                |
| 4.69V <sub>graf</sub> /TSm              | 240                                   | 1.29                 | 253.5 | 103.6                | 458.7                | 516.9               | 0.01 (0.03) 0.41 <sup>b</sup>  | 0.04 (0.06) 0.73 <sup>b</sup>  | 530.0 (6), 532.8 (94)                |
| 5.37V <sub>graf</sub> /TSm              | 200                                   | 1.78                 | -     | 103.4                | 458.9                | 516.6               | 0.02 (0.04) 0.70 <sup>b</sup>  | 0.40 (0.06) 0.73 <sup>b</sup>  | 530.1(6), 532.7 (94)                 |

6.5.1.3 Nature of the surface species by Raman spectroscopy

The surface analysis was completed by Raman spectroscopy to investigate the vanadia species interaction with the carriers. Both for the impregnated and grafted silica supported catalysts, identical support bands at wavenumbers 274, 355, 457, 559, 779 and 1126  $\text{cm}^{-1}$  appeared. In addition, a sharp but low intensity Raman peak at 1030  $\text{cm}^{-1}$ , assigned to the isolated monomeric vanadia species, was detected together with a broad band centred at  $\sim 920 \text{ cm}^{-1}$ , arose from the polymeric units of the surface vanadia. This can be observed from the Raman spectra depicted in Figure 6.3. It has to be pointed out that only some of the series of catalysts supported onto silica surface have been then tested in the ODH of methanol.

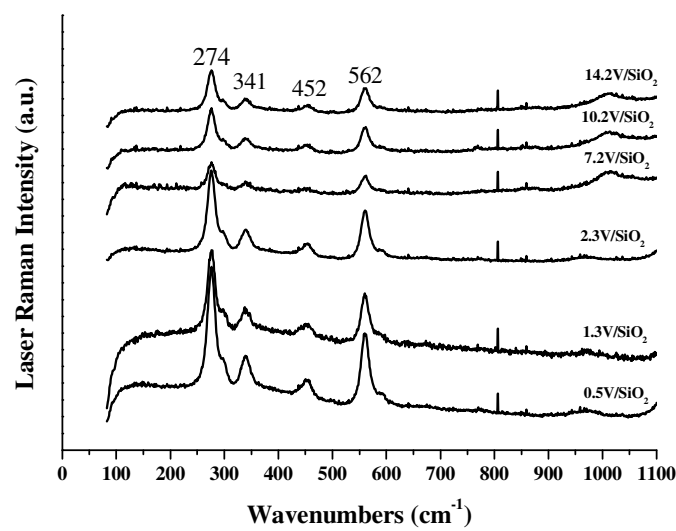
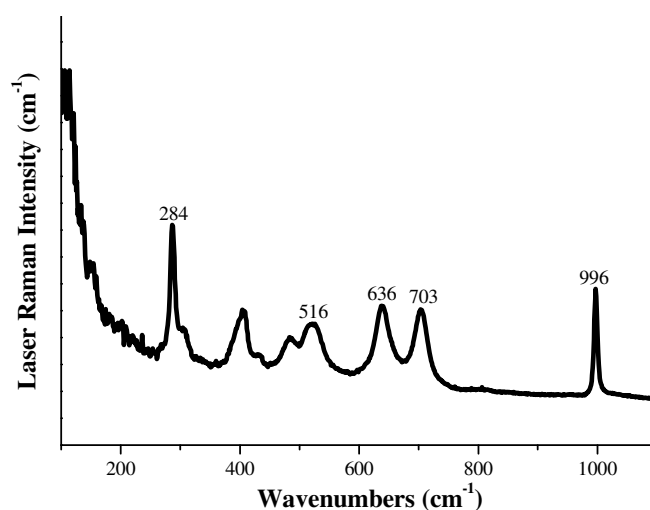


Figure 6.3: Raman spectra for the series of V/SiO<sub>2</sub> catalysts

This indicates that the deposition of vanadia on the silica surface gives place to a class of vanadia species with different surface structure-properties ranging from the isolated vanadium species to the amorphous aggregated ones, independently on the preparation method used. However, the formation of vanadium oxide crystallites was detected for the sample  $5V_{\text{imp}}/\text{TiO}_2$  because a strong peak at  $996\text{ cm}^{-1}$  appeared in the corresponding Raman spectrum, in addition to support bands at 397, 519, 639 and  $788\text{ cm}^{-1}$ , as showed in Figure 6.4.



**Figure 6-4:** Raman spectrum of  $V_{\text{imp}}/\text{TiO}_2$  catalyst

Interesting information were obtained by the Raman surface analysis, reported in Figure 6.5, that were carried out on some catalysts of the series  $V_{\text{graf}}/\text{TSm}$ . As can be seen, the presence of only the signal at  $1030\text{ cm}^{-1}$  for low vanadium loadings (3.5%wt  $\text{V}_2\text{O}_5$ ) was detected. The additional appearance of a broad band at  $920\text{--}930\text{ cm}^{-1}$  occurs for a vanadium loading greater than the monolayer. No  $\text{V}_2\text{O}_5$



crystallites were detected. Finally, it has been found very broad bands at lower wavenumbers, that could be assigned to the surface vanadia-titania interaction [18,19].

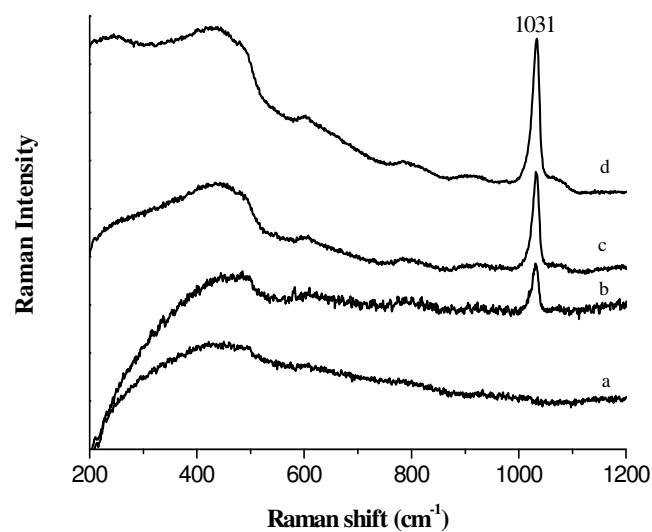


**Figure 6.5:** Raman spectra of the series of V/TSm catalysts: (a) 0.94 % wt V<sub>2</sub>O<sub>5</sub>; (b) 3.23 % wt V<sub>2</sub>O<sub>5</sub>; (c) 4.69 % wt V<sub>2</sub>O<sub>5</sub>; (d) 5.37 % wt V<sub>2</sub>O<sub>5</sub>.

#### 6.5.1.4 Analysis of the acidity of the catalysts by NH<sub>3</sub>-TPD

The TSm support and two vanadium-based catalysts, 5.41V<sub>graf</sub>/SiO<sub>2</sub> and 4.69V<sub>graf</sub>/TSm, supported on SiO<sub>2</sub> and TSm respectively, were submitted to NH<sub>3</sub>-TPD measurements in order to evaluate the effect of vanadia deposition on the number and strength of the surface acid sites.

From Table 6.6 it is evident that the catalyst  $4.69V_{\text{graf}}/\text{TSm}$  is characterized by a greater acidity than  $5.41V_{\text{graf}}/\text{SiO}_2$ . These data show the influence of the nature of the support on the acid properties of the final catalyst. Moreover, it has been observed that the deposition of vanadia on the surface of  $\text{TiO}_2/\text{SiO}_2$  increases the acidity of the starting support without changing the strenght of the acid sites, as the  $T_{\text{MAX}}$  of ammonia desorption ( $T_{\text{MAX}}=213^\circ\text{C}$ ) does not change as a consequence of grafting vanadium species. This is shown in Fig. 6.6 where the  $\text{NH}_3$ -TPD profiles obtained for the TSm support and the  $4.69V_{\text{graf}}/\text{TSm}$  catalyst are reported.

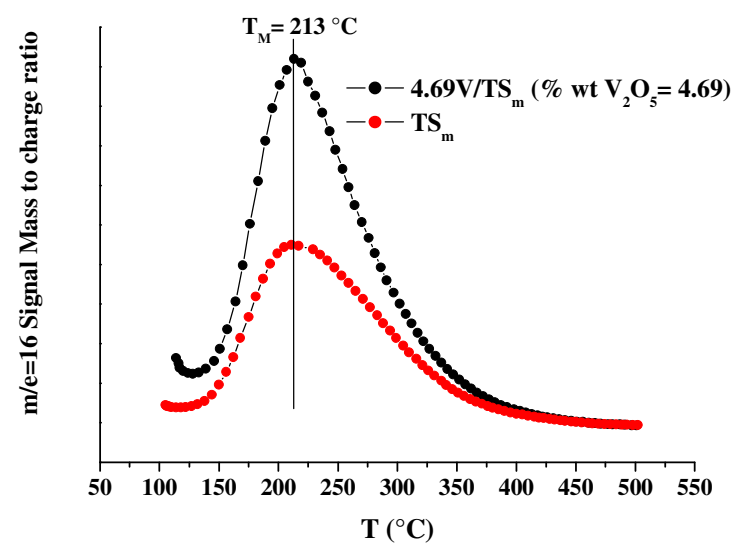


Fig. 6.6:  $\text{NH}_3$ -TPD profiles for the support  $\text{TS}_m$  and the catalyst  $4.69V/\text{TS}_m$

**6.5.2 Catalytic performances obtained in the ODH of methanol to formaldehyde**

The kinetic data collected for the several catalysts tested in the ODH of methanol have been gathered in Tables 6.5/6.6/6.7.

**Table 6.5:** Kinetic data collected for the catalysts prepared by *Impregnation*

| Catalyst                                | VO <sub>x</sub> /nm <sup>2</sup> | W/F<br>(g <sub>cat</sub> *h)/mol <sub>MeOH</sub> | T (°C) | Conv.% | Selettività % |      |       |                 | Resa (%)<br>Aldeide | TON   |
|---|----------------------------------|--|--------|--------|---------------|------|-------|-----------------|---------------------|-------|
|   |                                  |  |        |        | FAld          | MF   | DMM   | CO <sub>2</sub> |                     |       |
| <b>5V<sub>imp</sub>/SiO<sub>2</sub></b> | 1.24                             | 25.4   | 160    | 4.54   | —             | 2.35 | 97.65 | —               | —                   | 3.25  |
|   | 1.24                             | 25.4   | 180    | 9.63   | 9.21          | 2.13 | 88.66 | —               | 0.89                | 6.90  |
|   | 1.24                             | 25.4   | 200    | 15.31  | 11.18         | 2.17 | 86.65 | —               | 1.71                | 10.97 |
|   | 1.24                             | 25.4   | 220    | 31.89  | 24.95         | 4.58 | 70.10 | 0.27            | 7.96                | 22.85 |
|   | 1.24                             | 25.4   | 250    | 63.84  | 28.19         | 7.58 | 61.96 | 2.27            | 18.00               | 26.85 |
| <b>5V<sub>imp</sub>/TiO<sub>2</sub></b> | 46,3                             | 25.5   | 160    | 3.18   | 22.52         | 4.28 | 72.44 | 0.76            | 0.72                | 2.25  |
|   | 46,3                             | 25.5   | 180    | 11.45  | 22.23         | 3.44 | 73.44 | 0.90            | 2.55                | 8.12  |
|   | 46,3                             | 25.5   | 200    | 24.87  | 38.34         | 4.34 | 56.94 | 0.38            | 9.54                | 17.63 |
|   | 46,3                             | 25.5   | 220    | 36.77  | 36.00         | 6.37 | 57.07 | 0.56            | 13.24               | 26.06 |
|   | 46,3                             | 25.5   | 250    | 86.43  | 84.82         | 9.21 | 11.38 | 1.59            | 73.31               | 61.27 |

**Table 6.6:** Kinetic data collected for the catalysts prepared by *Grafting* (V/TSm series)

| Catalyst                   | VO <sub>x</sub> /nm <sup>2</sup> | W/F<br>(g <sub>cat</sub> *h)/mol <sub>MeOH</sub> | T (°C) | Conv.% | Selectivity % |       |       |                 | Yield (%)<br>FAld | TON    |
|----------------------------|----------------------------------|--|--------|--------|---------------|-------|-------|-----------------|-------------------|--------|
|                            |                                  |  |        |        | FAld          | MF    | DMM   | CO <sub>2</sub> |                   |        |
| 0.94V <sub>graf</sub> /TSm | 0.22                             | 25.3   | 180    | 3.50   | —             | 3.57  | 96.43 | —               | —                 | 13,28  |
|                            | 0.22                             | 25.3   | 200    | 13.67  | 3.66          | 1.64  | 94.71 | —               | 0.5               | 51.89  |
|                            | 0.22                             | 25.3   | 245    | 32.19  | 22.24         | 7.56  | 70.08 | 0.12            | 7.16              | 122.33 |
| 3.23V <sub>graf</sub> /TSm | 0.75                             | 25.6   | 180    | 28.72  | 7.79          | 3.73  | 88.48 | —               | 2.24              | 31.56  |
|                            | 0.75                             | 25.6   | 200    | 47.42  | 26.63         | 10.02 | 63.36 | —               | 12.63             | 52.12  |
|                            | 0.75                             | 25.6   | 225    | 61.48  | 72.58         | 18.47 | 7.86  | 1.09            | 44.62             | 67.56  |
|                            | 0.75                             | 25.6   | 245    | 89.27  | 87.94         | 4.12  | —     | 7.93            | 78.51             | 98.11  |
| 4.69V <sub>graf</sub> /TSm | 1.49                             | 25.3   | 140    | 18.97  | 11.03         | 2.66  | 76.20 | 10.10           | 2.09              | 14.53  |
|                            | 1.49                             | 25.3   | 160    | 31.69  | 24.71         | 5.37  | 62.96 | 6.95            | 7.83              | 24.28  |
|                            | 1.49                             | 25.3   | 180    | 32.70  | 57.35         | 12.94 | 20.11 | 9.59            | 18.76             | 25.04  |
|                            | 1.49                             | 25.3   | 195    | 48.79  | 72.77         | 14.77 | 5.92  | 6.55            | 35.50             | 37.38  |
|                            | 1.49                             | 25.3   | 220    | 99.32  | 89.73         | 1.66  | —     | 8.61            | 89.12             | 119.31 |
|                            | 1.49                             | 25.3   | 240    | 99.65  | 83.23         | 1.43  | —     | 15.33           | 82.94             | 119.56 |
|                            | 1.49                             | 25.3   | 260    | 99.12  | 71.79         | 1.86  | —     | 26.35           | 71.16             | 119.12 |

FALD: Formaldehyde; MF: Methyl formate; DMM: Dimethoxymethane.

| <b>Table 6.7:</b> Kinetic data collected for the 5.41V <sub>grat</sub> /SiO <sub>2</sub> catalyst prepared by <i>Grafting</i> |                                  |  |        |        |                 |      |       |                 |                   |      |
|---|----------------------------------|--|--------|--------|-----------------|------|-------|-----------------|-------------------|------|
| Catalyst  | VO <sub>x</sub> /nm <sup>2</sup> | W/F<br>(g <sub>cat</sub> *h)/mol <sub>MeOH</sub> | T (°C) | Conv.% | Selectivity (%) |      |       |                 | Yield (%)<br>FAld | TON  |
|   |                                  |  |        |        | FAld            | MF   | DMM   | CO <sub>2</sub> |                   |      |
| 5.41 V <sub>grat</sub> /SiO <sub>2</sub>  | 1.55                             | 25.4   | 140    | 1.39   | 27.76           | 3.65 | 68.59 | 0               | 0.38              | 0.93 |
|   | 1.55                             | 25.4   | 180    | 2.63   | 28.25           | 4.03 | 67.72 | 0               | 0.74              | 1.74 |
|   | 1.55                             | 25.4   | 200    | 3.14   | 27.52           | 4.85 | 67.63 | 0               | 0.86              | 2.08 |
|   | 1.55                             | 25.4   | 220    | 8.09   | 15.89           | 2.54 | 81.17 | 0.41            | 1.29              | 5.36 |
|   | 1.55                             | 25.4   | 240    | 11.35  | 16.87           | 4.09 | 77.86 | 1.18            | 1.92              | 7,51 |

Depending on the operative conditions adopted, the main products observed were formaldehyde and dimethoxymethane while lower amounts of methyl formate and CO<sub>2</sub> were also found. In Fig. 6.7, a comparison of the conversion, obtained with the catalysts containing an increasing amount of vanadium on the same support TSm, is reported. At a fixed temperature, the increase in vanadium content results in an increase of methanol conversion.

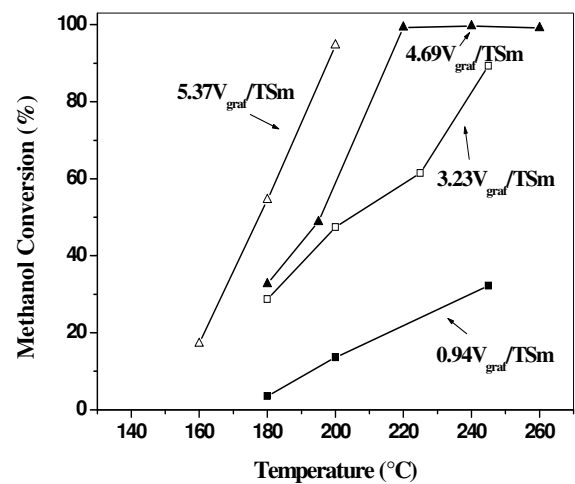


**Figure 6.7** – Methanol conversion as function of temperature for different vanadium loadings supported on the surface of the support TSm

Figure 6.8 reports the trend of selectivity to formaldehyde as a function of methanol conversion. An increase in selectivity is found in correspondence to an increase in conversion. This unusual trend derives from the observation that the first reaction product was dimethoxymethane which is then converted to formaldehyde by the reverse equilibrium reaction with water. In fact, at low temperature,

the main product is dimethoxymethane, while, increasing the temperature, an increase in formaldehyde formation was observed.

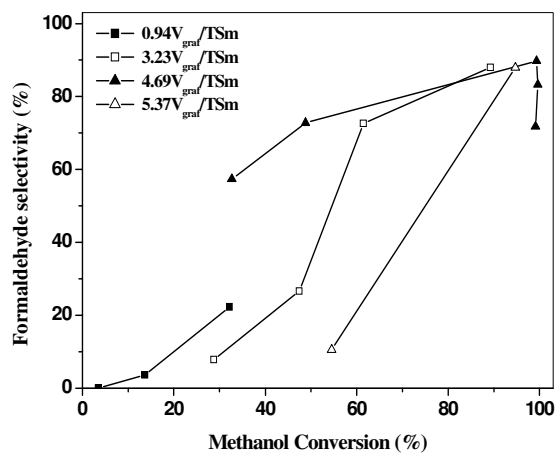


**Figure 6.8** – Formaldehyde selectivity as function of methanol conversion for different catalysts with vanadium loadings supported on the surface of the support TSm.

The catalytic behaviour described below is shown in Fig 6.9 in which the product distribution, for a run on the catalyst 4.69V<sub>grat</sub>/TSm, is reported.



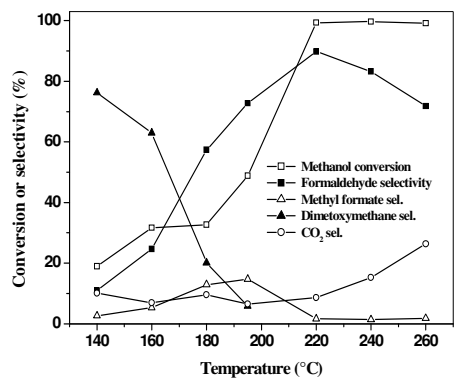


**Fig. 6.9:** Example of products distribution in the ODH reaction obtained for the catalyst 4.69V<sub>graf</sub>/TSm.

At temperature higher than 220 °C, when methanol conversion is nearly complete, formaldehyde total oxidation occurs and an increase in CO<sub>2</sub> production was observed. Finally, in Fig. 6.10, a comparison of the performances in terms of conversion and selectivity, between different catalysts at two temperatures, is reported. All the catalysts reported have a vanadium content of about 5% wt. From the results reported in Fig. 6.10, it is evident that the catalyst 5.37V<sub>graf</sub>/TSm gives the best performances of activity and selectivity mainly if we consider that it presents about the same vanadium density (1.78 V<sub>at</sub>/nm<sup>2</sup>) of the two other 5.41V<sub>graf</sub>/SiO<sub>2</sub> and 5V<sub>imp</sub>/SiO<sub>2</sub>. This trend becomes more pronounced at a higher temperature.

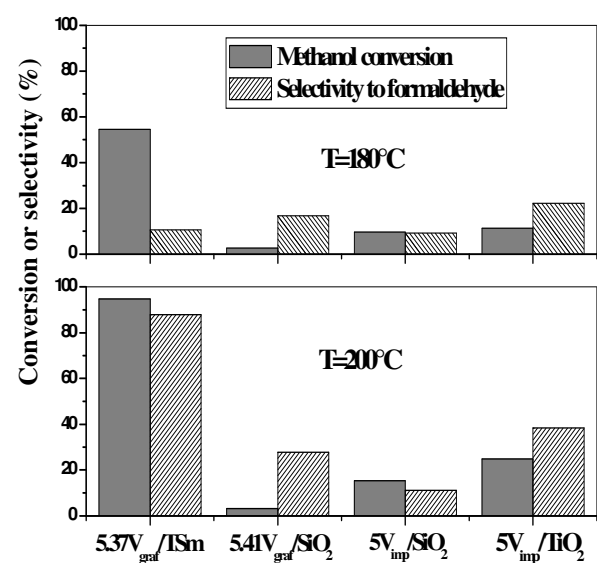


**Fig. 6.10:** Comparison of catalytic performances of different catalysts with similar vanadium loading.

**6.5.2.1 Comparison with a typical industrial catalyst**

An iron-molybdate catalyst (Fe-Mo), used in industrial field to produce formaldehyde by the ODH of methanol, was also tested in our lab-scale plant in order to compare its catalytic performances with those of the catalyst that resulted the best one from the catalytic screening in terms of both activity and selectivity. Table 6.8 and Table 6-9 report the operative conditions used in industrial field and in our lab-scale plant, respectively. The results of the catalytic tests are reported in Table 6-10.

**Table 6.8:** Industrial operative conditions used for the catalytic tests of the Fe-Mo catalyst

| <i><b>Feed</b></i><br><b>composition</b><br><b>(% mol)</b> | <b>SV</b><br><b>g<sub>MeOH</sub>/(Kg<sub>CAT</sub>*h)</b> | <b>T (°C)</b> |
|--|---|---------------|
| CH <sub>3</sub> OH = 5-11%                                 | 800-1200<br>↓<br>W/F ≈ 25-40                              | 250-300       |
| O <sub>2</sub> = 7-12%                                     |   |               |
| Water ≈ 3%   |   |               |
| Inert = balance  |   |               |

**Table 6.9:** Feed composition used to test in our lab-scale plant the Fe-Mo catalyst

| <b>Feed composition</b><br><b>(% mol)</b> | <b>Catalytic tests with</b><br><b>water</b> | <b>Catalytic tests without</b><br><b>water</b> |
|---|---|--|
| CH <sub>3</sub> OH                        | 10  | 10   |
| O <sub>2</sub>                            | 10  | 10   |
| H <sub>2</sub> O                          | 2   | —  |
| Inert (He)                                | balance                                     | balance  |

**Table 6.10:** Catalytic results obtained for the industrial catalyst (Fe-Mo)

| Catalyst                        | W/F<br>(g <sub>cat</sub> *h)/mol <sub>MeOH</sub> | SV<br>(g <sub>MeOH</sub> /kg <sub>cat</sub> *h) | T<br>(°C) | Conv.% | Selectivity (%) |      |      |       |                 | Yield<br>(%)<br>F |
|---------------------------------|--|---|-----------|--------|-----------------|------|------|-------|-----------------|-------------------|
|                                 |  |   |           |        | F               | MF   | DMM  | DME   | CO <sub>2</sub> |                   |
| Industrial catalyst             | 40.0   | 800   | 250       | 95.08  | 90.87           | 0.48 | —    | —     | 8.64            | 86.39             |
|                                 | 40.0   | 800   | 280       | 97.79  | 92.78           | 0.12 | —    | —     | 7.1             | 90.74             |
|                                 | 35.6   | 900   | 250       | 95.74  | 80.77           | 0.62 | —    | 16.03 | 2.59            | 77.32             |
|                                 | 35.6   | 900   | 280       | 97.81  | 92.53           | 0.19 | —    | 3.40  | 3.88            | 90.51             |
|                                 | 35.6   | 900   | 300       | 99.03  | 92.58           | 0.19 | —    | 3.36  | 3.88            | 91.68             |
| (H <sub>2</sub> O) <sup>a</sup> | 35.6   | 900   | 280       | 98.43  | 94.41           | 0.16 | —    | 2.64  | 2.78            | 92.92             |
|                                 | 31.8   | 1000  | 180       | 48.81  | 89.01           | 0.36 | 7.61 | —     | 3.01            | 44.45             |
|                                 | 31.8   | 1000  | 280       | 97.40  | 90.80           | 0.29 | —    | 5.99  | 2.92            | 88.44             |
|                                 | 10.06  | 3200  | 280       | 97.23  | 86.74           | 0.34 |      | 11.71 | 1.21            | 84.34             |

<sup>a</sup> The catalytic test has been conducted by introducing water in the feed.

The comparison of the catalytic performances between the Fe-Mo catalyst and the catalyst 4.69V/TSm, prepared by adopting the *grafting* procedure, can be well appreciated considering the results reported in Table 6.11.

Table 6.11: 4.69V/TSm vs Fe-Mo catalyst

<sup>a</sup> The test has been conducted by introducing water in the feed

| Catalyst                        | W/F<br>(g <sub>cat</sub> *h/mol <sub>Me</sub><br>OH) | T<br>(°C) | Con<br>v.<br>% | Selectivity % |      |         |      |                 | Y <sub>FAld</sub><br>(%) |
|---------------------------------|--|-----------|----------------|---------------|------|---------|------|-----------------|--------------------------|
|                                 |  |           |                | FAld          | MF   | DM<br>M | DME  | CO <sub>2</sub> |                          |
| Flox<br>Catalyst                | 31.8   | 280       | 97.40          | 90.80         | 0.29 | —       | 5.99 | 2.92            | 88.44                    |
| (H <sub>2</sub> O) <sup>a</sup> | 35.6   | 280       | 98.43          | 94.41         | 0.16 | —       | 2.64 | 2.78            | 92.92                    |
| 4.69<br>V <sub>graft</sub> /TSm | 32.2   | 220       | 99.28          | 87.84         | 1.65 | —       | —    | 10.51           | 87.19                    |
| (H <sub>2</sub> O) <sup>a</sup> | 32.2   | 220       | 99.58          | 91.56         | 0.11 | —       | —    | 8.33            | 91.17                    |

As can be noted from the data reported in Table 6.11, both the catalysts show high methanol conversion levels and high formaldehyde selectivities at the operative conditions reported. Moreover, the presence of water seems to improve the catalytic behaviour in both the cases. This experimental evidence confirmed literature data [20], according to which the presence of water in the feed limits the formation of CO<sub>2</sub>, giving place to an increase of the selectivity to formaldehyde. Indeed, the steam has the advantage to burn the coke deposited on the surface of the catalyst, enhancing in this way the activity and, first of all, the selectivity of the system towards the production of formaldehyde.

In Figure 6.11, the catalytic performances of the catalysts mentioned above are reported. They refer only to the tests conducted by introducing water in the feed.

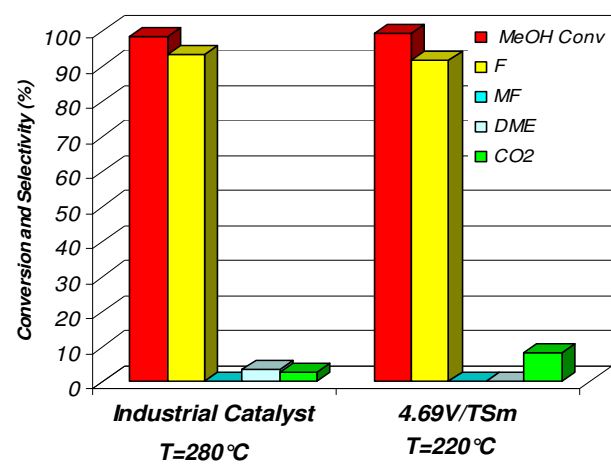


Figure 6.11: Comparison of the catalytic performances

As can be seen, the catalyst 4.69V/TSm, tested in the ODH of methanol to formaldehyde by adopting operative conditions very close to those used in industrial plant, resulted more active than the industrial catalyst, as it showed comparable conversion levels and formaldehyde selectivities at lower operative temperature (220 °C).

By concluding, the results obtained by comparing the catalytic performances of our best catalyst with those of a typical catalyst used in industrial field, seem to be very promising for an industrial development of a new generation of catalysts, characterized by supported vanadium oxide as active phase.

## 6.6 Conclusion

The study of the catalytic performances in the ODH of methanol to formaldehyde of supported vanadium based catalysts, characterized by different supports/oxides and different vanadium loadings, and prepared by using both impregnation and grafting procedures, allowed us to gain information about the nature of the active sites involved in the process studied. This has been done with the aim to understand the relationships between the structure of supported vanadium sites and their catalytic performances. With respect to this, the ODH of methanol to formaldehyde resulted very suitable, as the catalytic evolution of methanol is informative of the surface structure and behaviour of the catalyst. In fact, it is common to state that the partial methanol oxidation is a “structure sensitive” reaction.

The results obtained showed that several factors may influence the activity of vanadium based catalysts. They may be classified in two groups:

- c) Vanadium loading, preparation procedure and nature of the support, for what concerns the catalysts.
- d) Reaction temperature and feed composition, for what concerns the reaction operative conditions. For example, we noted that a small amount of water (2%), fed together with the other reactants, enhances both the activity and formaldehyde selectivity.

Thus, it is very important to tune both the catalysts properties and the operative conditions to obtain good catalytic results, specially

in terms of formaldehyde selectivity. On the contrary, the selectivity to formaldehyde seems to be mainly influenced by the level of the methanol conversion achieved.

Indeed, this study pointed out that the *grafting* method is very useful to prepare well-dispersed catalysts, an indispensable condition to design active and selective catalysts for the ODH reaction of methanol. In fact, the catalyst prepared according to the suggested procedure gave the best results when compared with the impregnated catalyst, characterized by the same amount of active species. A positive trend of selectivity with conversion was observed for all the catalysts of the  $V_{\text{graf}}/\text{TSM}$  series and attributed to the reaction sequence: methanol  $\rightarrow$  dimethoxymethane  $\rightarrow$  formaldehyde.

## 6.7 References

- [1] G. Reuss, W. Disteldorf, O. Grundler, A. Hilt, *Formaldehyde* in: *Ullman Encyclopedia of Industrial Chemistry* 5<sup>th</sup> ed., A11, 619.
- [2] H.R. Gerberich et al., *Formaldehyde Kirk-Othmer Encyclopedia of Chemical Technology*, Wiley, New York, **1994**, 11, 929.
- [3] J.M. Tatibouët, *Applied Catalysis A: General* 148, (1997) 213-252
- [4] S.K. Bhatthacharyya, K. Janikiram and N.D. Ganguli, *J. Catal.*, **1967**, 8, 128.
- [5] F. Roozenboom, P.D. Cordingley and P.J. Gellings, *J. Catal.*, **1981**, 68, 464.
- [6] J.M. Tatibouët and J.E. Germain, *C. R. Acad. Sci. Paris*, **1979**, 289 (II), 305.



- [7] P. Forzatti, E. Tronconi, A.S. Elmi, G. Busca, *Appl. Catal. A*, **1997**, *157*, 387.
- [8] G.K. Boreskov, B.I. Popov, V.N. Bibin and E.S. Kozishnikova, *Kinet. Cata.*, **1967**, *9*, 796.
- [9] N. Pernicone, *J. Less Common Metals*, **1974**, *36*, 289.
- [10] B.M. Weckhuysen, I.E. Wachs, *Handbook of Surfaces and Interfaces of Materials*, *1*, 613.
- [11] J. Kuenski, A. Baiker, M. Glinski, P. Dollenmeire and A. Wokaun, *J. Catal.*, **1986**, *101*, 1.
- [12] G. Deo, I.E. Wachs, *J. Catal.*, **1995**, *146*, 323.
- [13] M. Cozzolino, R. Tesser, M. Di Serio, M. Ledda, G. Minutillo, E. Santacesaria, *Studies in Surface Science and Catalysis, E. Gaigneaux et al. (Editors)*, **2006**, *162*, 697.
- [14] M. Gasior, I. Gasior, B. Grzybowska, *Appl. Catal.*, **1984**, *10*, 87.
- [15] A. Khodakov, B. Olthof, A.T. Bell, E. Iglesia; *Journal of Catalysis*, **1999**, *181*, 205.
- [16] S.L.T. Andersson, *J. Chem. Soc., Farad. Trans.*, **1979**, *75*, 1356.
- [17] X. Gao, S.R. Bare, J.L.G. Fierro, M.A. Banares, I.E. Wachs, *J. Phys. Chem. B*, **1998**, *102*, 5653.
- [18] J. Keranen, C. Guimon, E. Iiskola, A. Auroux, L. Niinistö, *Cat. Today*, **2003**, *78*, 149.
- [19] J.M. Jengh, I.E. Wachs, *Catal. Lett.*, **1992**, *13*, 9.
- [20] M. Quian, M.A. Liauw, G. Emig, *Appl. Catal. A*, **2003**, *238*, 211.



# **PART C**

**Kinetic study  
of the ODH of alcohols to  
aldehydes  
on V/TiO<sub>2</sub>/SiO<sub>2</sub> catalysts**



# VII

## EXPERIMENTAL SECTION

### **Kinetics of the oxidative dehydrogenation (ODH) of methanol to formaldehyde on nano-structured V/TiO<sub>2</sub>/SiO<sub>2</sub> based catalyst**

#### **Abstract**

The data obtained from the catalytic screening of the ODH of methanol to formaldehyde by supported vanadium based catalysts prepared by both impregnation and grafting, reported in Chapter VI, demonstrated that the activity depends mainly on the catalyst preparation procedure, the amount of vanadium anchored on the surface of the support and the reaction temperature, while the selectivity to formaldehyde (the main product observed) is influenced only by the conversion level. In particular, the catalysts prepared by grafting resulted more active than the impregnated ones. Moreover, for the grafted catalysts, the activity increases with increasing the

vanadium loading, while the selectivity depends only on the conversion and seems to be independent on the amount of titania anchored on the surface of silica. Thus, the catalytic screening highlighted that the key-factors determining the activity are: vanadium loading and surface dispersion of grafted vanadium and titanium species.

Therefore, in order to draw a complete picture of the catalytic mechanism of the Oxidative Dehydrogenation of methanol to formaldehyde by supported vanadium based catalysts, a detailed kinetic analysis of the reaction was carried out on a nano-structured supported vanadium oxide catalyst, selected in a preliminary catalytic screening.

The chosen vanadium catalyst, supported on  $\text{TiO}_2/\text{SiO}_2$  support, has been prepared by grafting vanadyl alkoxide, dissolved in dioxane, and characterized by BET, XRD, Raman, XPS and SEM analyses. An exhaustive set of experimental runs has been conducted in an isothermal packed bed tubular reactor by investigating several operative conditions, such as: temperature, contact time, methanol/oxygen feed molar ratio and water feed concentration.

Depending on the operative conditions adopted, the main products observed were formaldehyde and dimethoxymethane while lower amounts of methyl formate and  $\text{CO}_2$  were also found. At low contact time, the main reaction product was dimethoxymethane which was then converted into formaldehyde through the reverse equilibrium reaction with water. As a confirmation of this observation, a peculiar behaviour was detected consisting in an increase of selectivity to

formaldehyde by increasing methanol conversion. The obtained experimental data of methanol conversion and selectivity towards products were modelled by means of an integral reactor model and the related kinetic parameters were determined by non-linear regression analysis. The adopted reaction rate expressions was of the Mars van Krevelen – Langmuir Hinshelwood type and a good agreement was found between the model theoretical prediction and the experimental data. A reaction mechanism and a detailed reaction scheme (*rake-type*) were proposed for methanol ODH on a nano-structured catalyst that were able to interpret correctly the collected experimental observations.

## 7.1 Introduction

The catalytic data reported in the chapter VI underlined how the supported vanadium based catalysts are very able to promote the ODH of methanol to formaldehyde under mild conditions of both temperature (140-260 °C) and pressure (1 atm), allowing to achieve high activity and high selectivity, to prevent coke formation and, therefore, to improve the catalyst lifetime.

We have found that the different catalytic properties of vanadia catalysts may be related to the surface structure of vanadium species and, generally, a good surface vanadium dispersion is one of the key-factors to design very active and selective catalysts.

For what concerns the products-distribution, depending on the operative conditions adopted, the main products observed were formaldehyde and dimethoxymethane, as well as lower amounts of

methyl formate and  $\text{CO}_2$ . An expected increase of methanol conversion resulted by increasing vanadium loading, from 1% up to 5% of  $\text{V}_2\text{O}_5$  by weight. On the contrary, an unusual trend consisting in an increase of selectivity to formaldehyde as a function of methanol conversion, was observed. This trend may be explained by considering that the first reaction product was dimethoxymethane which is then converted to formaldehyde by the reverse equilibrium reaction with water. This observation has been supported by the experimental screening results, according to which, at low temperature and conversion, the main product was dimethoxymethane, while, by increasing the temperature, an increase in formaldehyde formation was detected. At temperature higher than  $220^\circ\text{C}$ , when methanol conversion is nearly complete, formaldehyde oxidation occurs and an increase in  $\text{CO}_2$  production was observed. This scenario, provided by the screening, seems to confirm the structure-sensitivity of methanol oxidation, largely discussed in literature, according to which different products can be obtained by varying the catalyst nature and reaction conditions [1]. Thus, a good knowledge of the reaction mechanism is necessary to elaborate a correct interpretation of variations of the catalytic behaviour. In spite of the large number of papers devoted to investigate the influence of the surface properties and the interaction between the active phase and the support on the catalyst behavior, very few works reported a detailed kinetics model able to describe the products distribution. According to the literature [2], the selective oxidation of methanol to formaldehyde over metal-oxide based catalysts follows a Mars-van-Krevelen type redox mechanism, in



which the oxidation proceeds by a reduction of an oxidized surface site, which is subsequently re-oxidized with gas-phase molecular oxygen [3]. Several authors have studied the kinetics of the methanol partial oxidation to formaldehyde over a Fe-Mo catalyst and only a limited number of papers were addressed towards vanadium oxide catalysts. However, most of the previous works was focused only on the formation of formaldehyde and not much attention was paid to the formation of side products, such as carbon dioxide, dimethylethere (DME) and dimethoxymethane (DMM). Moreover, all the kinetic data reported in the literature were measured at low methanol concentrations (maximum 6%) [4].

Jiru et al. [5] suggested a redox mechanism similar to the one adopted by Mars and van Krevelen [6] for the description of the oxidation of aromatic hydrocarbons over vanadium pentoxide. Edward et al. [7] studied this reaction in a recycle reactor over a Fe-Mo catalyst, and they showed that mass and heat transfer limitations disguise the obtained kinetic data at temperatures exceeding 280 °C.

Furthermore, in another paper, Jiru et al. [8] studied the influence of the reaction products on the reaction rate. They found that the formaldehyde concentration affects the reaction rate, while the water concentration does not. On the other hand, Pernicone et al. [9] observed a significant effect of water vapor, decreasing the reaction rate. Santacesaria et al. [10] studied the methanol partial oxidation in a well-mixed (CSTR) reactor at temperatures below 250 °C to avoid transport limitations. They used different criteria to select the most suitable kinetic model to describe the oxidation of methanol to

formaldehyde over an iron molybdate catalyst. Their criteria were in order of importance: (a) the values of the parameters must have physical significance, (b) the model must fit the experimental runs and (c) the number of parameters must be increased only when significant improvements are obtained in satisfying the preceding criteria. They confirmed the redox mechanism for this reaction. Moreover, they observed that the presence of water lowers the rate of reaction by reducing the number of available active centers on the catalyst.

Furthermore, they found that the amount of dimethoxymethane (DMM) decreased with an increase in the residence time, which could be explained by taking into account the gas phase equilibrium according to the following reaction:



Edwards et al. [7] investigated the partial oxidation of methanol in a mixed flow reactor at atmospheric pressure using lean methanol–air mixtures. Steady-state reaction rates were obtained over a commercial iron molybdate catalyst at temperatures ranging from 170 to 367 °C. Their work contributed further to the knowledge on the reaction kinetics, with particular emphasis on the role of the adsorbed methoxyl intermediates. Furthermore, they suggested that, at low methanol partial pressures, the rate equation of Mars and van Krevelen may be satisfactory, but for high conversions the effect of water must be included.

Pernicone et al. [9] found a marked inhibiting effect of water on the reaction rate for the formaldehyde formation, especially at low water partial pressures. Their experimental results could be explained in terms of competitive adsorption of water and methanol on the free active catalyst surface. Surface acidity seemed to be important and the competitive adsorption could be explained on the basis of a higher basicity of water than methanol. They concluded that the influence of water on the formaldehyde formation rate could not be observed by other researchers who used a recycle reactor or CSTR reactor because of the relatively high water concentrations in these reactors.

Recently, Holstein and Machiels [11] studied the kinetics of the methanol oxidation to formaldehyde over an iron molybdenum oxide catalyst in a continuous flow reactor with external recycling at temperatures of 200–300 °C. The kinetics of the reaction could be well described by a power law rate expression, with the power of the methanol, oxygen and water partial pressures equal to  $0.94 \pm 0.06$ ,  $0.1 \pm 0.05$  and  $0.45 \pm 0.07$ , respectively. The measured activation energy was  $98 \pm 6$  kJ/mol.

More recently, Diakov et al. [12] experimentally investigated the kinetics of the methanol partial oxidation to formaldehyde and the formaldehyde partial oxidation to carbon monoxide. With a plug flow reactor model they demonstrated that the methanol reaction order for the formaldehyde formation reaction is one half and the oxygen reaction order is zero.

Thus, the lack of detailed kinetic data capable of describing all the products observed in the ODH of methanol, over supported vanadium based catalysts, led us to investigate this reaction also from a kinetic point of view. In this work, we wish to propose a complete kinetic analysis on a supported vanadium based catalyst ( $4.69V_{\text{graf}}/\text{TSm}$ ), resulted from the catalytic screening as the best one in terms of both activity and selectivity. The effect of several operative variables such as: temperature, contact time, methanol/oxygen feed molar ratio and water feed concentration was investigated.

## 7.2 Catalyst and support preparation

Details about the preparation of the support indicated with the acronym TSm are reported in Chapter II.

The vanadium-based catalyst investigated, indicated with the acronym  $4.69V_{\text{graf}}/\text{TSm}$ , was prepared by putting the described support in contact with a solution of vanadyl tri-isopropoxide ( $\text{VO}[\text{O-iPr}]_3$ , Aldrich 99.999%,  $d=0.963\text{g/ml}$ ), dissolved in anhydrous dioxane. The grafting reaction was performed for 5h in a well stirred jacketed glass reactor, under inert helium atmosphere. The solid obtained was filtered, washed with dioxane, oven-dried at  $120\text{ }^\circ\text{C}$  overnight, heated at  $200^\circ\text{C}$  and then calcined at  $500\text{ }^\circ\text{C}$ .

The operative conditions used for preparing the support TSm and the vanadium catalyst  $4.69V_{\text{graf}}/\text{TSm}$ , respectively, are reported in Table 7.1 together with the resulted physico-chemical properties of the solids obtained.

**Tab. 7.1:** Operative conditions used for the preparation of the catalysts and some related properties.

| Precursor /solvent /support   | Acronym                    | Ti(O- <sup>i</sup> Pr) <sub>4</sub><br>(g) | Supp.<br>(g) | Volume of<br>Solvent<br>(cm <sup>3</sup> ) | MO <sub>x</sub><br>% wt | S <sub>BET</sub><br>(m <sup>2</sup> /g) | Pore<br>volume<br>(cm <sup>3</sup> /g) |
|---|----------------------------|--|--------------|--|-------------------------|---|--|
| Ti(O-Pr <sup>i</sup> ) <sub>4</sub> /Dioxane/SiO <sub>2</sub>                   | TSm                        | 10.79                                      | 24           | 400  | 7.29 <sup>a</sup>       | 278                                     | 1.70                                   |
| VO(O-Pr <sup>i</sup> ) <sub>3</sub> /Dioxane/TiO <sub>2</sub> .SiO <sub>2</sub> | 4.69V <sub>grat</sub> /TSm | 0.65                                       | 3            | 50   | 4.69 <sup>b</sup>       | 200                                     | 1.02                                   |

<sup>a</sup>Percentage by weight of supported TiO<sub>2</sub>  
<sup>b</sup>Percentage by weight of supported V<sub>2</sub>O<sub>5</sub>

### 7.3 Methods, Techniques and Operating conditions used in the catalytic runs

Kinetic runs were performed in a stainless steel tubular reactor with an internal diameter of 1 cm, kept isothermal with a fluidized bed of sand. Liquid methanol was fed, by a syringe pump, into a vaporizer chamber kept at 250 °C and was then sent, after the addition of a stream of oxygen and helium, into a stainless steel coil kept at the same temperature of the reactor. The composition of the gases at the outlet of the reactor was gas-cromatographically analyzed by withdrawing a sample with an on-line sampling valve kept at 170°C. The GC used was an HP 5890 instrument, with a Restek RT-Q-Plot 30 m × 0.32 mm column. Helium was used as the carrier gas.

The conditions used for the analyses were as follows: temperature held at 50°C for 2 min, increased at a rate of 5°C/min to 100°C and then at a rate of 20°C/min to 180°C for 5 min, and finally kept at this temperature for 5 min. A TCD detector kept at 250°C was used. Samples of powdered catalyst, generally 0.3g, were placed inside the reactor on a bed of glass wool. Two thermocouples located immediately upon and under the catalytic bed allowed the validity of the isothermal conditions to be controlled within  $\pm 1^\circ\text{C}$ .

The operative conditions adopted are listed in Table 7.2. Three different sets of kinetics runs were conducted.

The first set of runs was performed in the temperature range 140-200°C by changing the methanol residence time from 10 to 65  $\text{g}_{\text{cat}}^*\text{h/mol}_{\text{MeOH}}$  but keeping the molar ratio between methanol and oxygen constant (1:1).

The second set of runs was carried out at  $T = 160\text{ }^{\circ}\text{C}$  by significantly varying both the methanol residence time (from 10 to 65  $\text{g}_{\text{cat}} \cdot \text{h} / \text{mol}_{\text{MeOH}}$ ) and the feed molar ratio between methanol and oxygen.

The third set of kinetics experiments was conducted with the aim to investigate the effect of the presence of water in the feed on the catalytic performances. These last runs were carried out by using the following reaction conditions: 0.3g of catalyst, methanol residence time ranging from 10 to 65  $\text{g}_{\text{cat}} \cdot \text{h} / \text{mol}_{\text{MeOH}}$  while keeping at  $180^{\circ}\text{C}$  the reaction temperature. Water was added in the feed with an apparatus similar to that of methanol (syringe pump).

Results are reported in terms of the methanol conversion and product yields. The methanol conversion is defined as

$$C = (\text{number of moles of methanol reacted}) / (\text{number of moles of methanol fed})$$

while the yields of the  $i$ -th product is defined as

$$Y_i = (\text{number of moles of product } i \text{ formed}) / (\text{number of moles of methanol fed})$$

In Tab. 7.3 the experimental data obtained are reported.

**Tab. 7.2** – List of runs and related operative conditions (W=0.32g; Helium flow rate=30 ml/min)

| Run ID  | W/F<br>(g <sub>cat</sub> *h/mol <sub>CH3OH</sub> ) | Methanol                    | O <sub>2</sub>             | Water                       | Temperature<br>(°C) |
|---------|--|-----------------------------|----------------------------|-----------------------------|---------------------|
|         |  | feed flow rate              | feed flow rate             | feed flow rate              |                     |
|         |  | ( <i>liquid</i> )<br>(ml/h) | ( <i>gas</i> )<br>(ml/min) | ( <i>liquid</i> )<br>(ml/h) |                     |
| R1-R5   | 12.91  | 1.00                        | 10.07                      | -                           | 140-200             |
| R6-R10  | 16.13  | 0.8                         | 8.06                       | -                           | 140-200             |
| R11-R15 | 32.37  | 0.4                         | 4.06                       | -                           | 140-200             |
| R16-R20 | 61.46  | 0.21                        | 2.09                       | -                           | 140-200             |
| R21     | 12.91  | 1.00                        | 5.03                       | -                           | 160                 |
| R22     | 16.13  | 0.8                         | 4.04                       | -                           | 160                 |
| R23     | 32.37  | 0.4                         | 2.03                       | -                           | 160                 |
| R24     | 61.46  | 0.21                        | 1.05                       | -                           | 160                 |
| R25     | 12.91  | 1.00                        | 15.1                       | -                           | 160                 |
| R26     | 16.13  | 0.8                         | 12.11                      | -                           | 160                 |
| R27     | 32.37  | 0.4                         | 6.09                       | -                           | 160                 |
| R28     | 61.46  | 0.21                        | 3.14                       | -                           | 160                 |
| R29     | 12.91  | 1.00                        | 10.07                      | 0.08                        | 180                 |
| R30     | 16.13  | 0.8                         | 8.06                       | 0.065                       | 180                 |
| R31     | 32.37  | 0.4                         | 4.06                       | 0.04                        | 180                 |
| R32     | 61.46  | 0.21                        | 2.09                       | 0.02                        | 180                 |



| Tab. 7.3 – Experimental data |                    |           |  |                        |                                |         |         |                 |
|------------------------------|--------------------|-----------|--|------------------------|--------------------------------|---------|---------|-----------------|
| Run ID                       | W/F <sup>(1)</sup> | T<br>(°C) | Feed molar<br>ratio<br>CH <sub>3</sub> OH / O <sub>2</sub> | Methanol<br>Conversion | Products Yields <sup>(2)</sup> |         |         |                 |
|                              |                    |           |  |                        | F                              | MF      | DMM     | CO <sub>2</sub> |
| R1                           | 12.91              | 140       | 1  | 0.19034                | 0.01006                        | 0.00750 | 0.15517 | 0.01760         |
| R6                           | 16.13              | 140       | 1  | 0.20076                | 0.01193                        | 0.01071 | 0.15932 | 0.01879         |
| R11                          | 32.27              | 140       | 1  | 0.23034                | 0.04762                        | 0.01428 | 0.13506 | 0.03339         |
| R16                          | 61.46              | 140       | 1  | 0.25428                | 0.14727                        | 0.01535 | 0.03495 | 0.05671         |
| R2                           | 12.91              | 160       | 1  | 0.22961                | 0.01674                        | 0.01506 | 0.18860 | 0.00921         |
| R7                           | 16.13              | 160       | 1  | 0.27392                | 0.03294                        | 0.02120 | 0.20586 | 0.01391         |
| R12                          | 32.27              | 160       | 1  | 0.31864                | 0.09665                        | 0.02294 | 0.16824 | 0.03079         |
| R17                          | 61.46              | 160       | 1  | 0.38799                | 0.22947                        | 0.11163 | —       | 0.04688         |
| R3                           | 12.91              | 180       | 1  | 0.26222                | 0.10816                        | 0.02604 | 0.11275 | 0.01742         |
| R8                           | 16.13              | 180       | 1  | 0.33117                | 0.16248                        | 0.03415 | 0.11728 | 0.01726         |
| R13                          | 32.27              | 180       | 1  | 0.35806                | 0.22538                        | 0.07302 | 0.02467 | 0.03499         |
| R18                          | 61.46              | 180       | 1  | 0.57301                | 0.43106                        | 0.08626 | —       | 0.05569         |
| R4                           | 12.91              | 190       | 1  | 0.38276                | 0.21186                        | 0.04694 | 0.11200 | 0.01196         |
| R9                           | 16.13              | 190       | 1  | 0.41255                | 0.22471                        | 0.04972 | 0.12469 | 0.01343         |
| R14                          | 32.27              | 190       | 1  | 0.49893                | 0.38390                        | 0.07377 | 0.01696 | 0.02429         |
| R19                          | 61.46              | 190       | 1  | 0.82799                | 0.62684                        | 0.09231 | 0.00990 | 0.09894         |
| R5                           | 12.91              | 200       | 1  | 0.37585                | 0.24133                        | 0.04420 | 0.07531 | 0.01501         |
| R10                          | 16.13              | 200       | 1  | 0.48011                | 0.34829                        | 0.06027 | 0.04140 | 0.03016         |

|     |       |     |      |         |         |         |         |         |
|-----|-------|-----|------|---------|---------|---------|---------|---------|
| R15 | 32.27 | 200 | 1    | 0.68976 | 0.56172 | 0.07448 | 0.00821 | 0.04535 |
| R20 | 61.46 | 200 | 1    | 0.91946 | 0.72141 | 0.09027 | —       | 0.10778 |
| R21 | 12.91 | 160 | 0.66 | 0.28527 | 0.05027 | 0.01221 | 0.19741 | 0.02538 |
| R22 | 16.13 | 160 | 0.66 | 0.30141 | 0.06976 | 0.01529 | 0.18603 | 0.03603 |
| R23 | 32.27 | 160 | 0.66 | 0.32651 | 0.09424 | 0.01896 | 0.17373 | 0.03958 |
| R24 | 61.46 | 160 | 0.66 | 0.45710 | 0.29185 | 0.03756 | 0.03135 | 0.09634 |
| R25 | 12.91 | 160 | 2    | 0.19429 | 0.01721 | 0.00619 | 0.15924 | 0.01165 |
| R26 | 16.13 | 160 | 2    | 0.26533 | 0.03288 | 0.01179 | 0.20050 | 0.02015 |
| R27 | 32.27 | 160 | 2    | 0.30027 | 0.07750 | 0.01578 | 0.15293 | 0.05405 |
| R28 | 61.46 | 160 | 2    | 0.31312 | 0.13749 | 0.00689 | 0.02220 | 0.14651 |
| R29 | 12.91 | 180 | 1    | 0.31477 | 0.12573 | 0.02543 | 0.13139 | 0.03222 |
| R30 | 16.13 | 180 | 1    | 0.31684 | 0.12695 | 0.02514 | 0.13566 | 0.02909 |
| R31 | 32.27 | 180 | 1    | 0.40715 | 0.25941 | 0.04082 | 0.06218 | 0.04474 |
| R32 | 61.46 | 180 | 1    | 0.67661 | 0.50895 | 0.06176 | 0.00828 | 0.09761 |

(1) (g<sub>cat</sub>·\*h/mol<sub>CH<sub>3</sub>OH</sub>)  
(2) F: formaldehyde, MF: methyl formate, DMM: dimethoxymethane

7.4 Results and discussion

7.4.1 Experimental approach

As reported before, in order to investigate the kinetics of the ODH of methanol to formaldehyde, different sets of kinetic runs were conducted. Hereunder, we reported the kinetic data collected in the range of temperature (140-200 °C) by keeping unchanged the feed molar ratio between methanol and oxygen.

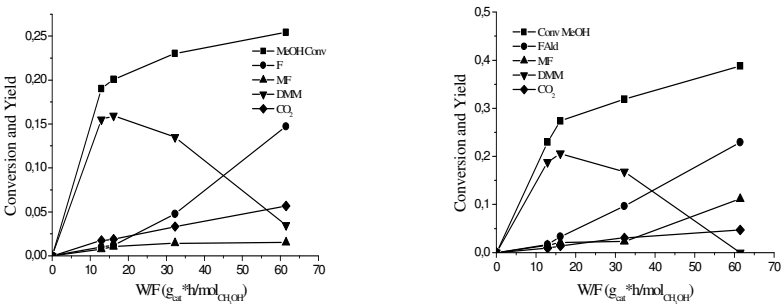


**Figure 7.1:** Methanol conversion/Products yields as function of contact time (W/F ) at two different temperatures: T= 140 °C (left) and T= 160 °C (right). (MeOH/O<sub>2</sub>=1:1)

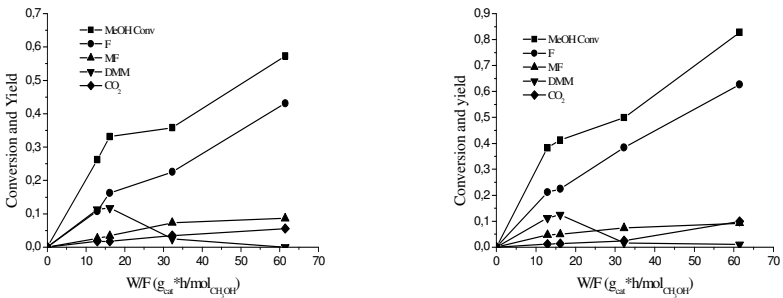


**Figure 7.2:** Methanol conversion/Products yields as function of contact time (W/F ) at two different temperatures: T = 180 °C (left) and T = 190 °C (right). (MeOH/O<sub>2</sub>=1:1)

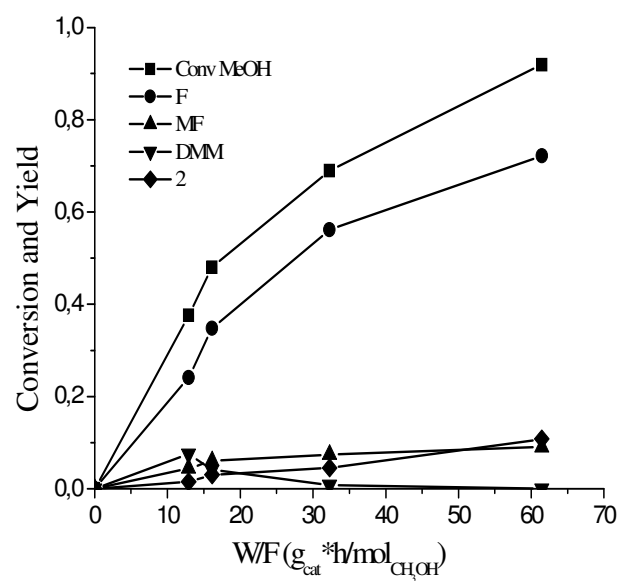


**Figure 7.3:** Methanol conversion/Products yields as function of contact time (W/F ) at T= 200 °C. (MeOH/O<sub>2</sub>=1:1)

As resulted from the plots reported in Figs 7.1, 7.2 and 7.3, we observed an increase of methanol conversion by increasing both temperature and contact time in all the range investigated. In particular, the catalyst tested seems to be highly selective towards dimethoxymethane at low temperature and towards formaldehyde at high temperature. A similar trend about the distribution of products was also detected as function of the temperature, as showed from the Figure 7.4.

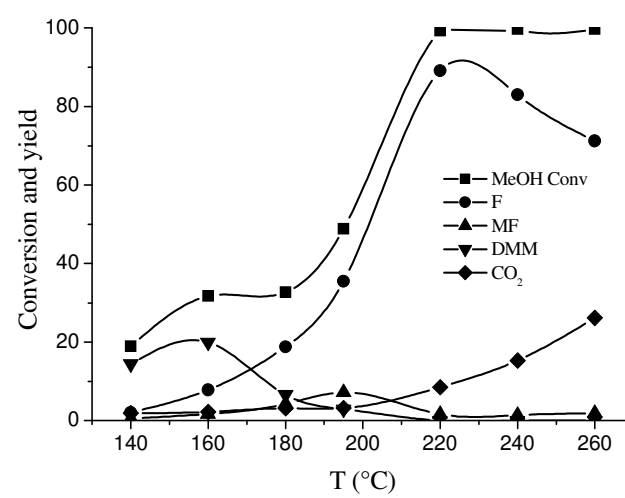


**Figure 7.4:** Methanol conversion/Products yields as function of temperature (Catalyst: 4.69Vgraf/TSm, W/F = 25 (g<sub>CAT</sub>\*h)/mol<sub>MeOH</sub>)

As can be seen, the main products observed were formaldehyde and dimethoxymethane, along with lower amounts of methyl formate and CO<sub>2</sub>. It is interesting to observe the positive effect of temperature on the methanol conversion, up to achieve a near complete conversion in this temperature range. On the contrary, an unusual trend consisting in an increase of formaldehyde selectivity, followed by a slight decreasing by further increasing the temperature reaction, was detected as a function of methanol conversion.

This trend may be explained by considering that the first reaction product, at low residence times when the methanol conversion is low, is dimethoxymethane which is then converted to formaldehyde by the reverse equilibrium reaction with water. In fact, at low temperature, the main product is dimethoxymethane, while, by increasing the

temperature and, consequently, with increasing the methanol conversion, an increase in formaldehyde formation was observed. The slight decrease of formaldehyde selectivity is due to the total oxidation to carbon dioxide, as confirmed by the slight increasing of the selectivity to CO<sub>2</sub>.

These results suggest this type of reaction sequence:



7.4.1.1 Effect of feed composition

As stated above, the second set of kinetic runs was carried out at T=160 °C by varying both the methanol residence time (from 10 to 65 g<sub>cat</sub>\*h/mol<sub>MeOH</sub>) and the feed molar ratio between methanol and oxygen (see R21-28 reported in Table 4.3). The data collected are reported in the following figures, Fig. 7.5 and Fig. 7.6.

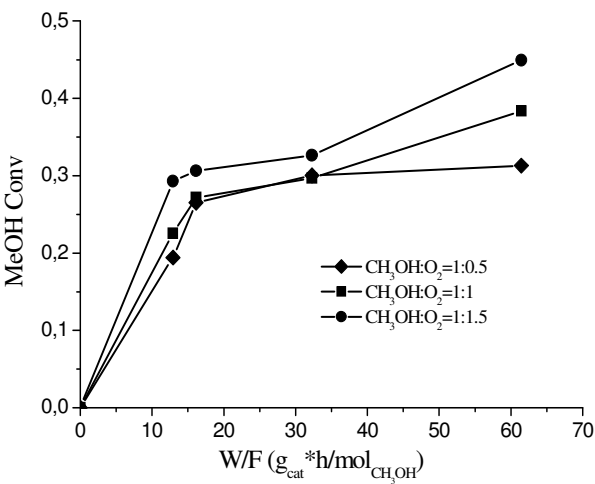


**Figure 7.5:** Methanol conversion as function of contact time at different methanol/oxygen ratios.

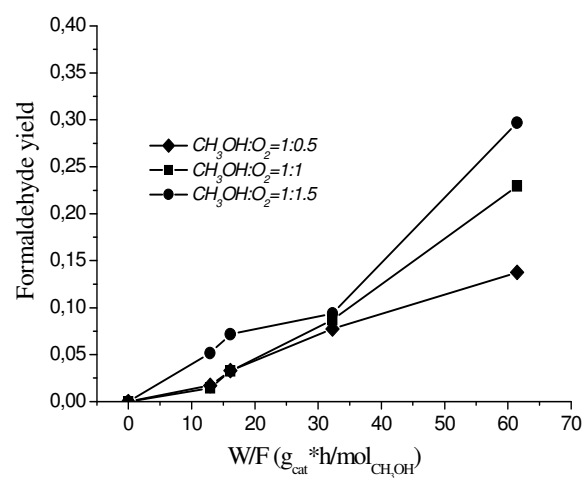


**Figure 7.6:** Formaldehyde yield as function of contact time at different methanol/oxygen ratios.

As can be seen, both methanol conversion and formaldehyde yield increase by increasing the contact time (W/F), in each case of feed composition reported. In particular, we observed a slight increase of both methanol conversion and formaldehyde yield in the case of feed composition characterized by a methanol/oxygen ratio of 1:1.5, notable specially at high contact times.

**7.4.1.2 Effect of presence of water in the feed**

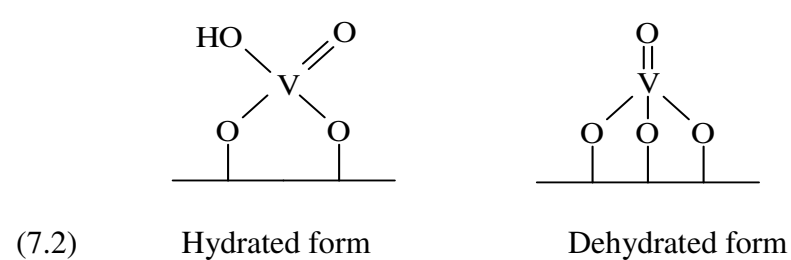
Some kinetic runs were conducted with the aim to investigate the effect of the presence of water in the feed on the catalytic performances. We used water concentrations very close to those used in the industrial field (see Table 7-3, R29-32 runs).

By analysing the data collected and reported in Table 7.3, we observed, especially at high contact time values, an increase of both methanol conversion and formaldehyde yields.

### 7.4.2 Theoretical approach

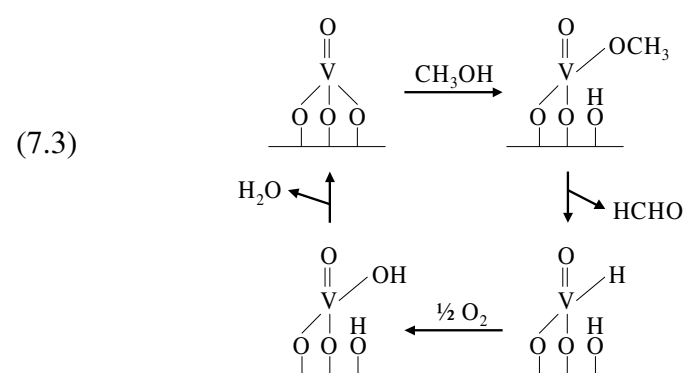
The detailed mechanism of alcohols partial oxidation to aldehydes is still under investigation. It is well known that the oxygen responsible of the oxidation is present in the lattice structure. This is supported by the experimental evidence that oxygenated compounds are formed onto catalyst surface also in the absence of gaseous oxygen, as in the case of acrolein synthesis from propylene on mixed Mo/Bi oxides [13]; in other reactions, as the n-butane oxidation to maleic anhydride, the gaseous oxygen seems to be responsible for the oxidation process [14]. However, all these reactions occur at a relatively higher temperature if compared with the one used in the present study. Very probably dehydrogenation is, in our case, the first reaction step which involves hydride formation while the gaseous oxygen is responsible for catalytic site re-oxidation.

Another uncertainty regards the structure of the active site that, in the case of vanadium-based catalysts, depends also on the vanadium load [14] and on the hydration condition of the environment. Despite the relatively high reaction temperature, the water produced could give place to the presence of a vanadium catalytic site in an hydrated form, characterized by a structure that is intermediate between the following ones:





Weckhuysen et al. [15] have proposed a reaction mechanism for the partial oxidation of methanol to formaldehyde, on vanadium-based catalysts, that involves a single vanadium surface site for which the vanadium oxidation state is nearly constant (V) and a limited reduction was observed. According to this mechanism, the conversion of methanol to formaldehyde occurs in four steps that can be schematically represented as follows:

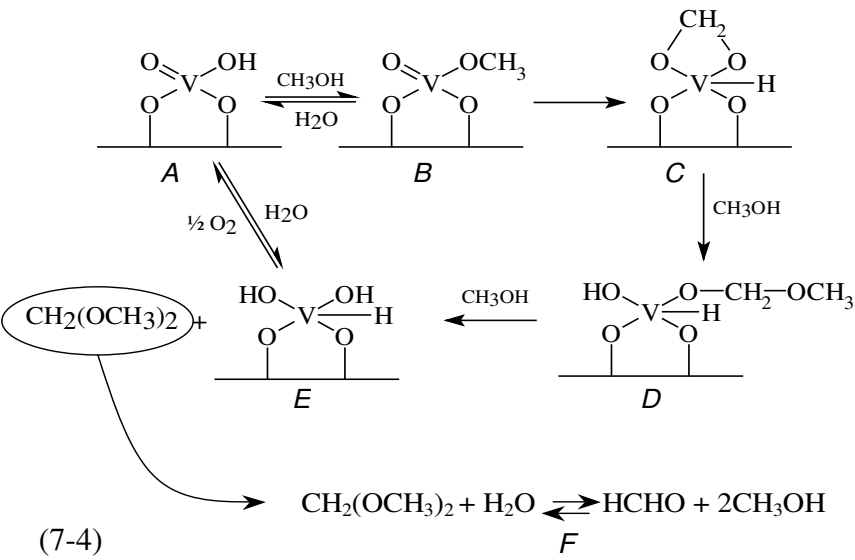


As can be seen from (7.3), the methoxydic intermediate  $\text{V}-\text{O}-\text{CH}_3$ , observed in literature through spectroscopy experiments [16], is the precursor to which the formaldehyde formation (assumed as the rate determining step) can be attributed while the molecular oxygen is the responsible for the catalytic site re-oxidation which is then restored by water elimination.

It is interesting to observe that the proposed mechanism (7.3) accounts only for the main reaction to formaldehyde, while in our investigation significant amounts of other products have been

observed, depending on the operative conditions adopted. In particular, at low contact time, the main reaction product was dimethoxymethane while, increasing the contact time, an increased concentration of formaldehyde was observed. This behavior suggests that the formation of dimethoxymethane and formaldehyde occurs in series and that dimethoxymethane is converted in formaldehyde by the reverse equilibrium reaction with water. As a further confirmation of this observation, an increase in selectivity to formaldehyde was generally observed in correspondence to an increase of methanol conversion (see Table 7.3).

On the basis of the observations reported, we hypothesized a mechanism for the catalytic cycle of the ODH of methanol that starts from a vanadium site in hydrated form, (A), and that can be schematized as follows:



The first elementary step in this mechanism, in agreement with different authors [17-19], is the formation of the methoxydic intermediate (B) by methanol dissociative adsorption. In the subsequent step this intermediate is rearranged into a dioxymethylenic surface species, spectroscopically observed [20] with the vanadium atom which presents a vanadium-hydride bond. The dioxymethylenic group can further react with methanol adsorbed from gaseous phase and lead to the formation of dimethoxymethane, at low conversion, and of formaldehyde by reverse equilibrium (F) when the conversion is high and water is present at a sufficiently high concentration in the system. The catalytic site in the initial form (A) is finally restored from the reduced site (E) by the intervention of gaseous oxygen and by water elimination, closing the cycle.

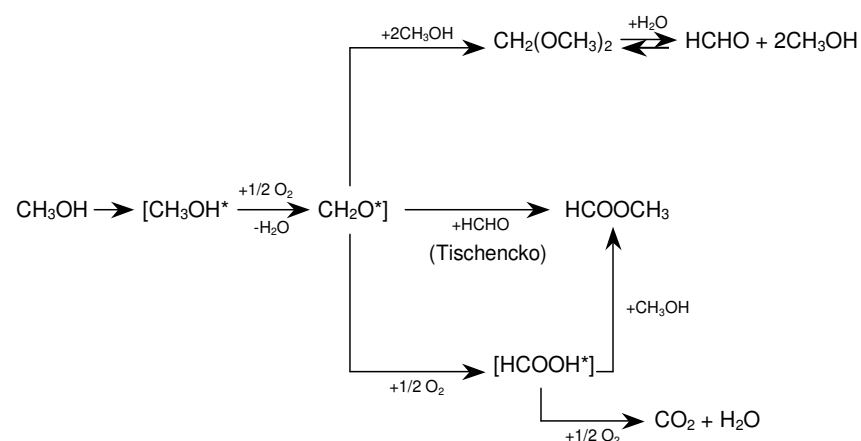
A mechanism substantially similar to (7-4) could be proposed also if we consider that where the initial vanadium site is in the dehydrated form.

According to the proposed mechanism, the presence of water is not detrimental for the formaldehyde production because it favorably promote the equilibrium reaction (F), as it has been confirmed by introducing small amounts of water (see Table 7.2) in the reactor feed obtaining a slight increase in formaldehyde yield (compare runs R3-8-13-18 with R29-30-31-32 of Table 7.3).

A further experimental observation is that  $\text{CO}_2$  formation appears significant only at high methanol conversion and this suggests that methanol is not directly involved in the total oxidation.

On the basis of the experimentally observed compounds and of their evolution with contact time, the following *rake-type* [20] reaction scheme can be proposed:

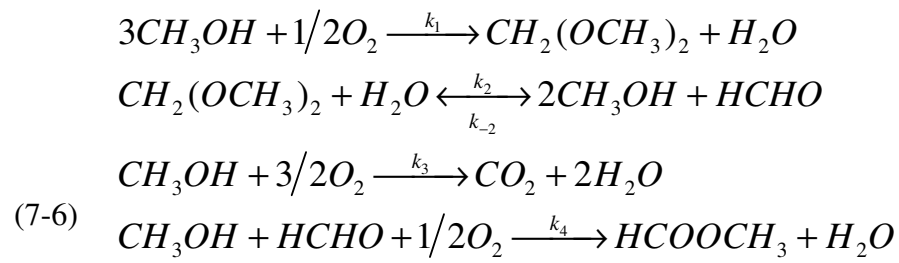
(7-5)



According to the scheme (7-5), the adsorbed forms of methanol, formaldehyde and formic acid give place, through desorptive reactions, to all the observed products. In particular, methyl formate and dimetoxymethane are formed by reaction between an adsorbed oxidized species and unreacted methanol from gas-phase. In this way, the formation of both the products mentioned is predominant at low conversion when methanol partial pressure is still relatively high. On the contrary, when methanol is almost completely converted, the expected predominant products are formaldehyde, methyl formate

(from Tischencko pathway between surface adsorbed methanol and gaseous formaldehyde) and carbon dioxide.

A comprehensive interpretation of the reaction scheme (4) in terms of elementary steps would involve too many parameters of difficult experimental evaluation. Thus, we adopted a simplified overall reaction scheme that takes in account all the products observed, represented as follows:



On the basis of this approximation, only five kinetic parameters are necessary to completely describe an isothermal run. By adopting the standard form of material balance equation, related to a tubular packed bed reactor (plug flow, absence of diffusion resistances), for each component  $j$  present in the gas phase:

$$(7-7) \quad -\frac{dF_j}{dW} = \sum_{i=1}^{N_r} \nu_{j,i} (-r_i)$$

Where  $F_j$  is the molar flow rate of the component  $j$ ,  $W$  is the total amount of catalyst loaded in the reactor,  $\nu_{j,i}$  is the stoichiometric coefficient of the component  $j$  in the reaction  $i$  and  $r_i$  is the  $i$ -th reaction rate. In order to integrate the ordinary differential equations

system (7-6) we have to introduce the expression for the reaction rates  $r_i$ . According to our model, the adopted expressions present the following form:

$$(7-8) \quad r_1 = \frac{k_1 P_M}{1 + \frac{k_1 P_M}{k_{ox} P_{O_2}^{0.5}}} * \frac{1}{1 + b_M P_M + b_W P_W}$$

$$(7-9) \quad r_2 = k_2 P_A P_W - \frac{k_2}{K_{eq}} P_M^2 P_F$$

$$(7-10) \quad r_3 = \frac{k_3 P_M}{1 + \frac{k_3 P_M}{k_{ox} P_{O_2}^{0.5}}} * \frac{1}{1 + b_M P_M + b_W P_W}$$

$$(7-11) \quad r_4 = \frac{k_4 P_M P_F}{1 + \frac{k_4 P_M}{k_{ox} P_{O_2}^{0.5}}} * \frac{1}{1 + b_M P_M + b_W P_W}$$

In the equations reported above,  $P$  are the partial pressures,  $k_i$  are the kinetic parameters and  $b_i$  are the adsorption parameters. As can be seen,  $r_1$ ,  $r_3$  and  $r_4$  are a combination of the Mars-Van Krevelen and Langmuir-Hinshelwood models (MVK-LH), by assuming that the re-oxidation of the catalytic site occurs, in the three cases, with the same rate and that only methanol and water compete for the adsorption onto the catalyst surface. The reaction 7-6 (2) is described with a standard second order reversible reaction rate (7-9). The kinetic parameters in the equations have been determined by nonlinear regression for the

fitting of all the experimental data and have been correlated with temperature by means of the Arrhenius equation.

In the Figure 7.6, the results of conversion and yield-values to formaldehyde are reported as a function of contact time for all the temperature-range investigated, in comparison with model prediction.

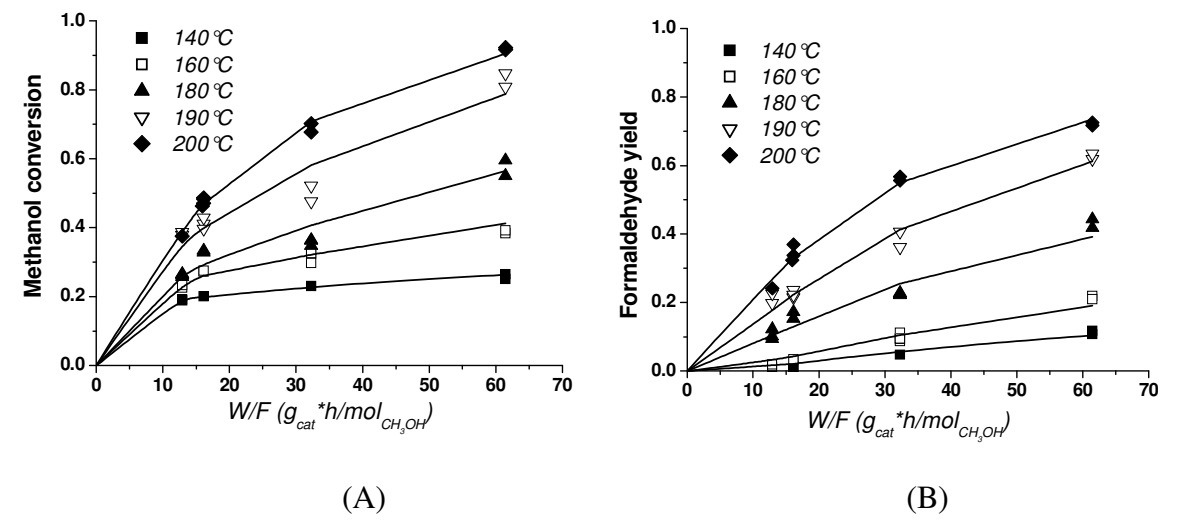


**Fig. 7.6:** Kinetic results at various reaction temperatures: comparison between kinetic model (continuous lines) and experimental data for (A) Methanol conversion as a function of methanol contact time  $W/F$  and (B) Formaldehyde yield as a function of methanol contact time ( $W/F$ ).



In Fig. 7.7 the agreement between the experimental products distribution, obtained for the set of runs R2-7-12-17, and the kinetic model is reported

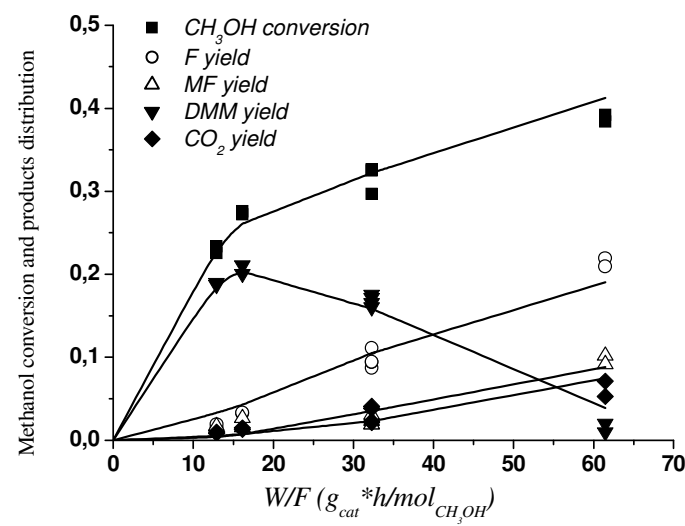


**Fig. 7.7:** Agreement between model behavior and experimental data of methanol conversion and products distribution as a function of methanol contact time W/F. Run R2-R7-R12-R17 at 160°C. Legend: F – formaldehyde, MF – methyl formate, DMM - dimethoxymethane

As an overall model agreement with respect to the experimental data, in Fig. 7.8 the parity plots are reported for both methanol conversion and formaldehyde yield.

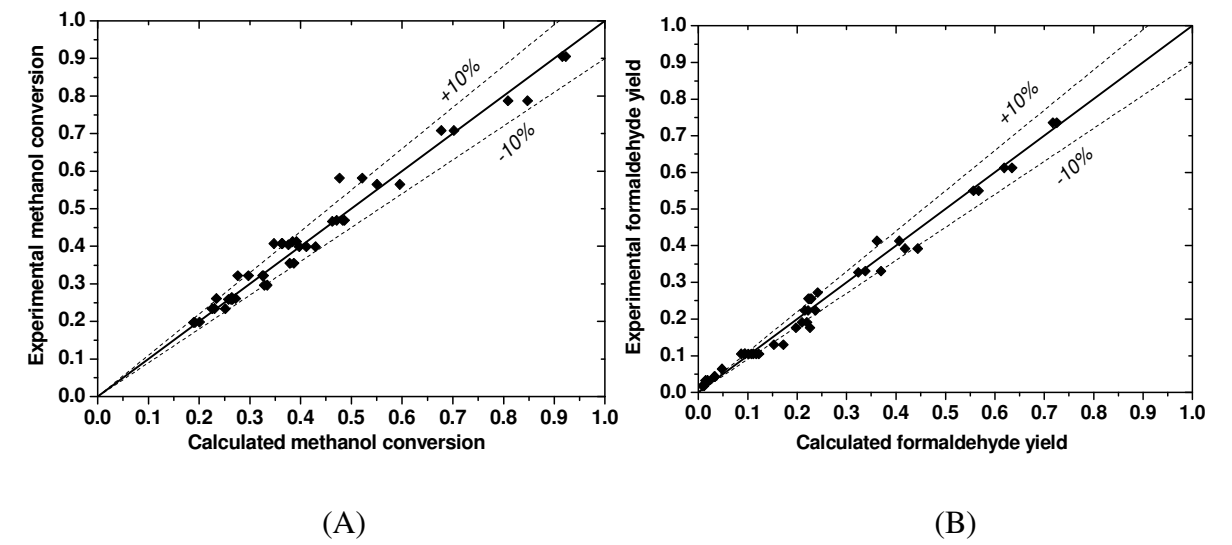


**Fig. 7.8:** Parity plots for (A) methanol conversion and (B) formaldehyde yield related to all the data collected. The absolute deviations of  $\pm 10\%$  between model and experimental data (dotted lines), are also reported.

As can be seen, the adopted model resulted in a satisfactory performance in the description of the experimental observations collected. The values of the kinetic and adsorption parameters, employed in the model, are reported in Tab. 7.4 while in Fig. 7-9 the main kinetic parameters are plotted against the reciprocal of the absolute temperature in the Arrhenius plot. From this plot, an evaluation of activation energies for formaldehyde and dimethoxymethane formation was possible and values of 20.4 and 11.1 kcal/mole, respectively, were obtained. These values are in agreement with those reported in the literature [20] in the range 10-20 kcal/mole for methanol ODH on supported and unsupported oxide catalysts. The equilibrium constant in equation (7-9), whose value is reported in Table 7.4, is in rather good agreement with the value obtained from thermodynamic calculations.

The values of the adsorption parameters for both methanol and water seem to indicate that adsorption effect is rather strong, although no discrimination between methanol and water was possible because both these components showed a similar behavior and no one can be neglected with respect to the other.

As mentioned above, the effect of the presence of water in the feed has no negative influence on catalytic activity, despite it seems to adsorb on the catalyst surface in competition with methanol. This behavior supports the proposed mechanism and reactions scheme in which water, at least in the explored concentration range, promotes the equilibrium reaction 7-6(2).

Table 7.4: Kinetic parameters

| Constant        | ln(A) or ln(b <sub>0</sub> ) | E <sub>A</sub> or ΔH<br>(kcal/mol) |
|-----------------|------------------------------|------------------------------------|
| k <sub>1</sub>  | 23.9 ± 2.6                   | 20.4 ± 2.3                         |
| k <sub>2</sub>  | 20.6 ± 1.1                   | 11.1 ± 1.0                         |
| k <sub>3</sub>  | 15.6 ± 4.8                   | 14.8 ± 4.2                         |
| k <sub>4</sub>  | 39.0 ± 3.2                   | 27.8 ± 2.8                         |
| k <sub>OX</sub> | 24.3 ± 3.8                   | 19.0 ± 3.4                         |
| b <sub>M</sub>  | -28.8 ± 4.9                  | -28.9 ± 4.3                        |
| b <sub>W</sub>  | -23.2 ± 8.9                  | -25.3 ± 7.9                        |

$k_i = A \cdot \exp(-E_A/RT) \quad i=1,2,3,4,OX$   
 $b_j = b_0 \cdot \exp(-\Delta H /RT) \quad j=M,W$   
 $K_{eq} = \exp(17.5-7548/T)$  experimental  
 $K_{eq} = \exp(13.7-6090/T)$  from thermodynamic calculations

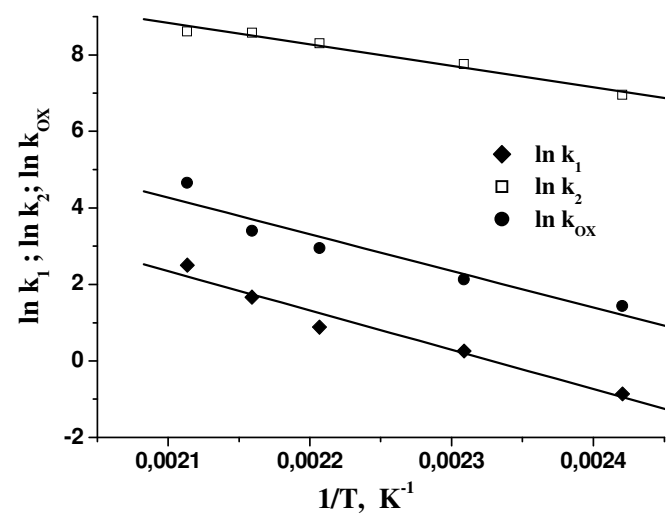


**Figure 7.4:** Arrhenius plot for the kinetic constants  $k_1$  (dimethoxymethane formation),  $k_2$  (formaldehyde formation) and  $k_{ox}$  (catalytic site re-oxidation).

The effect of methanol/oxygen feed molar ratio was also investigated and a general increase of conversion and yields were observed by decreasing this ratio, in particular at high contact time. In other words, the oxygen partial pressure seems to have a positive effect on methanol conversion, probably due to the increased efficiency in the catalytic site re-oxidation. This phenomenon has also been observed by other authors [21], according to which iron-molybdate catalysts seem to become less active in the presence of an excess of methanol.

7.5 Conclusions

The kinetics of the ODH of methanol to formaldehyde on vanadium-based grafting catalysts has been extensively investigated.

The effect of various operative conditions (temperature, contact time, feed composition) has been studied and a detailed kinetic model has been developed to interpret the collected integral data of a tubular packed-bed reactor.

The kinetic model was formulated on the basis of a reaction mechanism that led us to a rake-type reaction scheme in which all the observed products away from adsorbed species of methanol, formaldehyde and formic acid.

The agreement between the model and the experimental data can be considered satisfactory and the latter ones could be used, in perspective, to simulate pilot-plant data with a sufficient reliability.

## 7.6 References

- [1] J.M. Tatibouët, *Applied Catalysis A: General*, **1997**, 148, 213.
- [2] P. Mars,; D.W. van Krevelen, *Chem. Eng. Sci.*, **1954**, 3, 41.
- [3] B. M. Weckhuysen, D. E. Keller, *Catalysis Today*, **2003**, 78, 25.
- [4] S.A.R.K. Deshmukh et al., *Applied Catalysis A: General*, **2005**, 289, 240.
- [5] P. Jiru, B. Wichterlova, J. Tichy, in: Proceedings of the 3rd Congress, *Catalysis*, **1964**, 199.
- [6] P. Mars, D.W. Van Krevelen, *Chem. Eng. Sci.*, 1954, 3, 41.
- [7] J. Edwards, J. Nicolaidis, M.B. Cutlip, C.O. Bennet, *J. Catal.*, **1977**, 50, 24.
- [8] P. Jiru, J. Tichy, B. Wichterlova, *Coll. Czech. Chem. Commun.*, **1966**, 31, 674.

- [9] N. Pernicone, F. Lazzerin, G. Liberti, G. Lanzavecchia, *J. Catal.*, **1968**, 10, 83.
- [10] E. Santacesaria, N. Morbidelli, S. Carra, *Chem. Eng. Sci.*, **1981**, 36, 909.
- [11] W.L. Holstein, C.J. Machiels, *J. Catal.*, **1996**, 162, 118.
- [12] V. Diakov, B. Blackwell, A. Varma, *Chem. Eng. Sci.*, **2002**, 57, 1563.
- [13] B. Schiøtt and K.A.Jørgensen, *J.Phys. Chem.*, **1991**, 95, 2297.
- [14] G.C.Bond and S.F. Tahir , *Applied Catalysis*, **1991**, 71, 1.
- [15] G.C. Bond , *J. Catal.*, **1989**, 53, 116.
- [16] B.M.Weckhuysen, D.E.Keller, *Catalysis Today*, **2003**, 78, 25.
- [17] B.M. Weckhuysen, I.E. Wachs, in: H.S. Nalwa (Ed.), *Handbook of Surfaces and Interfaces of Materials*, Academic Press, San Diego, **2001**, 1, 613.
- [18] P. Forzatti, E. Tronconi, A.S. Elmi, G. Busca, *Appl. Catal. A: General*, **1997**, 157, 387.
- [19] N. Pernicone, F. Lazzerin, G. Liberti, G. Lanzavecchia, *J. Catal.*, **1968**, 10, 83.
- [20] G. Busca, *J. Mol. Catal.*, **1989**, 50, 241.
- [21] J.M. Tatibouët and J.E. Germain, *C. R. Acad. Sci., Paris*, **1979**, 289 (II), 305.

**List of symbols**

|           |   |
|-----------|---|
| $F_j$     | molar feed flow rate of component j-th - <b>mol/min</b>                                   |
| $W$       | catalyst weight loaded in the reactor - <b>g</b>  |
| $v_{j,i}$ | stoichiometric coefficient of the component j-th in the reaction i-th                     |
| $r_i$     | reaction rate of the reaction i-th - <b>mol/(min g<sub>cat</sub>)</b>                     |
| $k_i$     | reaction rate constant of the reaction i-th - <b>mol/(min g<sub>cat</sub> atm)</b>        |
| $b_j$     | adsorption parameter of the component j-th - <b>atm<sup>-1</sup></b>                      |
| $P_j$     | partial pressure of the component j-th - <b>atm</b>                                       |
| $k_{ox}$  | catalytic site re-oxidation constant - <b>mol/(min g<sub>cat</sub> atm<sup>0.5</sup>)</b> |
| $K_{eq}$  | equilibrium constant for reaction 7-6.2   |
| $C$       | methanol fractional conversion  |
| $Y_i$     | fractional yield to product i-th  |
| $N_r$     | number of reactions. -  |



# VIII

## EXPERIMENTAL SECTION

### **Kinetics of the oxidative dehydrogenation (ODH) of ethanol to acetaldehyde on $V_2O_5/TiO_2/SiO_2$ catalyst**

#### **Abstract**

In the present chapter, the kinetics of the Oxidative dehydrogenation of ethanol to acetaldehyde has been thoroughly investigated. Catalysts prepared by grafting vanadyl tri-isopropoxide on the surface of silica coated with  $TiO_2$  were found to be very active and selective.

Together with acetaldehyde, small amounts of by-products were obtained, including acetic acid, acetals, and  $CO_2$ . The kinetic behaviour of the catalysts was studied in the temperature range 100-

180 °C, by changing the ethanol residence time, the molar ratio between the reagents, and the vanadium loading.

A four-step mechanism was adopted, consisting of the following steps: (i) dissociative adsorption of ethanol onto vanadium, (ii)  $\alpha$ -hydrogen withdrawal by the metal to form acetaldehyde and a hydride group, (iii) oxidation of the formed hydride, and (iv) dehydration of the vanadium site to restore the original active site. This mechanism can be simplified and the resulting kinetic expression is similar to a Mars and van Krevelen kinetic expression. The reaction rates resulted to depend linearly on the vanadium loading.

## 8.1 Introduction

Interest in ethanol production from renewable natural sources as a possible alternative energy vector is increasing strongly throughout the world. For example, ethanol can usefully be used as a feedstock for producing acetaldehyde, ethyl acetate, acetic acid, ETBE, etc. Acetaldehyde can be obtained from ethanol by dehydrogenation, oxidation, and oxidative dehydrogenation, and different industrial techniques have been developed for these processes in the past [1,2] Acetaldehyde production via the oxidative dehydrogenation (ODH) of ethanol could be a promising alternative to the Wacker process, occurring more simply in a single step and in tubular reactors, provided that high activities and selectivities can be achieved under mild conditions.

The partial oxidation of ethanol over different catalytic systems has been studied by several authors [3-10]. In particular, supported  $V_2O_5$

based catalysts have been found to be active and selective in promoting the oxidative dehydrogenation of ethanol to acetaldehyde [8-11]. The reaction occurs under very mild conditions of temperature (150-250 °C) and pressure (1 atm) [9-11]. Moreover, in contrast to other ODH reactions, such as the ODH of light hydrocarbons that occurs at higher temperature, the surface oxygen of  $V_2O_5$  lattice is not directly involved in the ODH process, because the oxygen exchange reaction is too slow at the low temperatures used. Therefore, classical Mars and van Krevelen redox mechanism [12] is not operative in this reaction, and other redox mechanisms must be considered. Acetaldehyde, the main reaction product, is obtained with very high selectivities, even though this compound is more oxidable than ethanol. According to Oyama and Somorjai [8], unlike to the oxidative dehydrogenation of methanol to formaldehyde, the ODH of ethanol to acetaldehyde performed on  $V_2O_5$  based catalysts supported on  $SiO_2$  is not structure-sensitive. The same conclusion was reached by Lakshmi et al. [13] using  $V_2O_5$  catalysts prepared by impregnation on mixed oxides. Inamaru et al. [14] studied ethanol dehydrogenation on  $V_2O_5$  catalysts prepared by both impregnation and by chemical vapor deposition (CVD). They found that, in the latter case, the catalysts were more dispersed and more selective in the reaction. As well as the preparation method, also the support plays an important role.

According to the literature, vanadia catalysts constitute a relevant example of the influence of the interaction between catalytically active metal oxide particles and oxide carriers.

Several authors [15-17] have compared the properties of vanadia supported on different carriers ( $\text{SiO}_2$ ,  $\text{Al}_2\text{O}_3$ ,  $\text{TiO}_2$ ,  $\text{MgO}$ ,  $\text{ZrO}_2$ ) and have concluded that the nature of the dispersed surface metal oxide phase enables the vanadia, depending on which support is used, to become an effective catalyst for selective oxidation of aromatics, olefins and alcohols, as well as for selective catalytic reduction (SCR) of  $\text{NO}_x$  by  $\text{NH}_3$ . Titania (anatase) interacts strongly with an immobilized vanadia layer, generating a molecular dispersion of  $\text{V}_2\text{O}_5$ , but the system suffers from limited specific surface area and low resistance to sintering [9].

A way to obtain a titania surface with high, thermostable surface area and good mechanical properties is to apply  $\text{TiO}_2$  onto silica. Vanadia supported on the mixed oxide  $\text{TiO}_2/\text{SiO}_2$ , either co-precipitated or having the  $\text{TiO}_2$  directly applied to the silica, has been developed because of its selectivity as a catalyst for SCR of nitrogen oxides. Moreover, vanadia based systems such as  $\text{V}_2\text{O}_5/\text{TiO}_2$  and  $\text{V}_2\text{O}_5/\text{SiO}_2$  catalysts have been studied for selective oxidation of alcohols. In particular,  $\text{V}_2\text{O}_5$  and  $\text{V}_2\text{O}_5/\text{SiO}_2$  are very active and selective for oxidation of ethanol to acetaldehyde. By a proper selection of the catalytic oxide system and to acetaldehyde, acetic acid, or ethyl acetate, all of which can be used either as final products or as intermediates in synthetic routes.

Quaranta et al. [9] studied the ODH of ethanol to acetaldehyde on  $\text{V}_2\text{O}_5/\text{TiO}_2/\text{SiO}_2$  catalyst by comparing the catalytic performances with those of  $\text{V}_2\text{O}_5/\text{TiO}_2$  and  $\text{V}_2\text{O}_5/\text{SiO}_2$  catalysts. It was found that the coating of the silica carrier with a monolayer of  $\text{TiO}_2$  increased

substantially the activity of the catalyst, approaching that of the one supported on pure  $\text{TiO}_2$ , while it increased the selectivity to acetaldehyde as compared with the latter.

Despite the significant attention paid by various authors to the ODH of ethanol and to the action of vanadium-based catalysts, only one kinetic study has been published on this reaction, namely, the work by Gomez et al. using a  $\text{VMgO}$  as catalyst [11]. Other kinetic studies are available, but they are related to the use of other less active catalysts [4,5].

In the present work, therefore, we have studied the kinetics of the ODH of ethanol on a  $\text{V}_2\text{O}_5/\text{TiO}_2/\text{SiO}_2$  catalyst, prepared by grafting vanadyl tri-isopropoxide onto a support of silica coated with  $\text{TiO}_2$ . The  $\text{TiO}_2/\text{SiO}_2$  support has been prepared according to the multi-step grafting procedure, described in Chapter 2. The kinetic behaviour of the catalyst was tested by varying the reagent concentrations; the residence time; the temperature; the vanadium load; the acid and basic characteristics of the catalyst and the presence in the feed of reaction products such as water or acetaldehyde. A reaction scheme consisting of five reactions was developed for considering the evolution with time of all the reaction products, namely, acetaldehyde, acetic acid, carbon dioxide, acetals, and diethyl ether. A kinetic law for interpreting both the main reaction from ethanol to acetaldehyde and all other oxidations occurring in the reaction scheme was derived by assuming a redox mechanism occurring in the following four steps: (i) dissociative adsorption of ethanol on vanadium giving place to an ethoxy group, (ii)  $\alpha$ -hydrogen withdrawal by the metal to form

acetaldehyde and a hydride group, (iii) oxidation of the formed hydride, and (iv) dehydration of the vanadium site to restore the original active site. The kinetic law derived was found to be identical, in mathematical form, to the one that can be obtained from the classical Mars and van Krevelen mechanism [12]. A discussion of the kinetic behaviour of the reaction, the possible alternatives to the postulated reaction mechanism and the values obtained for the kinetic parameters conclude the chapter.

## 8.2 Catalyst and support preparation

The support of silica coated with  $\text{TiO}_2$  was prepared in a three-step grafting procedure, using titanium isopropoxide dissolved in toluene and a commercial silica (Grace S432), calcined at 500 °C for 8 h. The quantity of titanium isopropoxide dissolved in toluene and used in each grafting step was about 50% more than the amount corresponding to a monolayer, assuming a conventional stoichiometry of one hydroxyl per alkoxide molecule. After calcination, the silica was put into contact with the titanium alkoxide solution by refluxing at the boiling point of the solvent for 6 h under constant stirring. The solid obtained was then filtered, washed with toluene, dried at 100 °C, steamed at 190 °C to eliminate the residual alkoxide groups from the surface by hydrolysis, and finally calcined at 500° for 2 h. The procedure described above was then repeated two additional times to obtain the  $\text{TiO}_2/\text{SiO}_2$  support, that is, a silica support coated with more than a monolayer of  $\text{TiO}_2$ .

The catalysts were prepared by putting the described support into contact with a solution of vanadyl tri-isopropoxide, dissolved in *n*-hexane at room temperature for 24 h under helium atmosphere.

Some catalyst samples were also been prepared by dissolving the vanadyl triisopropoxide in other solvents, such as dioxane and tetrahydrofuran. In the latter case, titanium and vanadyl alkoxides were mixed with each other in a molar ratio of 12:1 and then treated with an equimolecular amount of water containing traces of HCl to promote partial hydrolysis and alkoxide condensation. The obtained precursor was, then, anchored directly onto the silica surface in the usual way. This procedure largely simplifies the preparation of well-dispersed vanadium catalyst. After the reaction, the samples were filtered, washed with the used solvent, dried at 105 °C, steamed at 190 °C for 2 h, and finally calcined at 500 °C for 2 h. Different catalyst samples were prepared with different vanadium loadings, as reported in Table 8.1, where the used supports and prepared catalysts are listed together with some of their relevant properties and the operating conditions employed. All of the reagents used were furnished by Fluka with the highest level of purity available.

**Table 8.1:** Operating conditions and reagents used in catalyst preparation and some related catalyst properties

| Silica Support  |                               |   |   |   |               |  |  |                                 |
|---|-------------------------------|---|---|---|---------------|--|--|---------------------------------|
| silica type   | thermal treatment temperature | specific surface area (m <sup>2</sup> /g)     |   | porosity (cm <sup>3</sup> /g)             |               | hydroxyl density (mmol/g)                    |  |                                 |
| GraceS432   | 500 °C                        | 282   |   | 1.02                                      |               | 0.92   |  |                                 |
| TiO <sub>2</sub> / SiO <sub>2</sub> Support, TiO <sub>2</sub> Load after Each Grafting Step                 |                               |   |   |   |               |  |  |                                 |
| sample  | step                          | TiO <sub>2</sub> anchored (mmol/g)            | TiO <sub>2</sub> (wt %)                       | specific surface area (m <sup>2</sup> /g) |               | porosity (cm <sup>3</sup> /g)                |  |                                 |
| TiO <sub>2</sub> –SiO <sub>2</sub>  | I                             | 0.88  | 7.0   | –   |               | –  |  |                                 |
| TiO <sub>2</sub> –SiO <sub>2</sub>  | II                            | 1.70  | 13.7  | –   |               | –  |  |                                 |
| TiO <sub>2</sub> –SiO <sub>2</sub>  | III                           | 2.23  | 17.8  | 274                                       |               | 0.96   |  |                                 |
| Catalyst Preparation and Properties   |                               |   |   |   |               |  |  |                                 |
| precursor/solvent/support   | acronym                       | VO( <i>i</i> –Pr) <sub>3</sub> used (mmol/g)  | TiO <sub>2</sub> –SiO <sub>2</sub> (g)        | hexane (mL)                               | <i>T</i> (°C) | V <sub>2</sub> O <sub>5</sub> content (wt %) | specific surface area (m <sup>2</sup> /g)    | porosity (cm <sup>3</sup> /g)   |
| VO( <i>Oi</i> -Pr) <sub>3</sub> / <i>n</i> -hexane/TiO <sub>2</sub> –SiO <sub>2</sub>                       | V/Ti–Si(1)                    | 0.07  | 6   | 75  | 25            | 0.65   | 243  | 0.30                            |
| VO( <i>Oi</i> -Pr) <sub>3</sub> / <i>n</i> -hexane/TiO <sub>2</sub> –SiO <sub>2</sub>                       | V/Ti–Si(4)                    | 0.40  | 6   | 75  | 25            | 3.56   | 258  | 0.28                            |
| Catalyst Preparation and Properties   |                               |   |   |   |               |  |  |                                 |
| precursor/solvent/support   | acronym                       | VO( <i>Oi</i> –Pr) <sub>3</sub> used (mmol/g) | Ti( <i>Oi</i> –Pr) <sub>4</sub> used (mmol/g) | SiO <sub>2</sub> (g)                      | solvent (ml)  | <i>T</i> (°C)                                | V <sub>2</sub> O <sub>5</sub> content (wt %) | TiO <sub>2</sub> content (wt %) |
| [VO( <i>Oi</i> -Pr) <sub>3</sub> + Ti( <i>Oi</i> -Pr) <sub>4</sub> ] <sub>h</sub> /THF/SiO <sub>2</sub>     | (V–Ti) <sub>h</sub> /Si(T)    | 0.55  | 6.91  | 6   | 100           | 25   | 2.23   | 7.17                            |
| [VO( <i>Oi</i> -Pr) <sub>3</sub> + Ti( <i>Oi</i> -Pr) <sub>4</sub> ] <sub>h</sub> /dioxane/SiO <sub>2</sub> | (V–Ti) <sub>h</sub> /Si(D)    | 0.58  | 6.74  | 6   | 100           | 25   | 1.91   | 6.75                            |



### **8.3 Catalyst and Support Characterization Techniques**

The titanium loadings were determined by using a colorimetric method [18]. The vanadium loading supported on the surface of the catalysts was determined by atomic adsorption spectroscopy, after dissolution in concentrated sulphuric acid.

The support and prepared catalysts were subjected to XRD analysis on an X3000 Seifert diffractometer equipped with a lithium fluoride monochromator on the diffracted beam. The scans were collected within the range of 4-44° (2 $\theta$ ) using Mo KR radiation.

Diffuse reflectance spectra were obtained on a Shimatzu AV2101 spectrophotometer. FTIR and DRIFT spectra were collected using a Nicolet AVATAR 360 instrument.

Textural analyses were carried out on a Thermoquest Sorptomatic 1990 instrument (Fisons Instruments) by determining the nitrogen adsorption/desorption isotherms at 77 K. The samples were thermally pretreated under vacuum overnight to 473 K (heating rate ) 1 K/min). Specific surface areas and pore size distributions were determined using the BET [19] and Dollimore- Heal [20] methods, respectively.

#### 8.4 Methods, Techniques and Operating Conditions used in the catalytic runs

Kinetic runs were performed in a stainless steel tubular reactor with an internal diameter of 1 cm. The reactor was externally jacketed and kept isothermal with a fluidized bed of sand. Liquid ethanol was fed, by a syringe pump, into a vaporizer chamber kept at 170 °C and was then sent, after the addition of a stream of oxygen and helium, into a stainless steel coil kept at the same temperature as the reactor. The composition of the vapors at the outlet of the reactor was analyzed gas-chromatographically by withdrawing small samples through an on-line sampling valve kept at 150 °C. The gas chromatograph used was an HP 5890 instrument, with a Restek Rt-Q-Plot 30 m × 0.32 mm column. Helium was used as the carrier gas. The conditions used for the analyses were as follows: temperature held at 40 °C for 2 min, increased at a rate of 20 °C/min to 160 °C, and then maintained at this temperature for 20 min. A thermal conductivity detector (TCD) kept at 210 °C was used for detection. All TCD response factors were determined independently by analysis of different binary systems consisting of ethanol in a mixture with each individual reaction product. Samples of powdered catalyst, generally 0.3 g, were placed inside the reactor on a bed of glass wool. Two thermocouples located immediately upon and under the catalytic bed allowed the validity of the isothermal conditions to be controlled.

Three different sets of kinetics runs were performed. Kinetic runs were mainly performed on a single catalyst containing 3.56 wt % of V<sub>2</sub>O<sub>5</sub>. A feed rate of inert diluent (helium) of 22 cm<sup>3</sup>/min was kept

constant during all runs. The first set of runs was performed in the temperature range 100-180 °C by changing the ethanol residence time from 9 to 70 g<sub>cat</sub>·h/mol but keeping the molar ratio between ethanol and oxygen constant. The second set was carried out in the temperature range 140-160 °C by significantly varying both the ethanol residence time (from 10 to 200 g<sub>cat</sub>·h/mol) and the molar ratio between ethanol and oxygen. The third set of runs is related to the effect of the vanadium loading on the activity and was conducted on all available catalysts containing different amounts of V<sub>2</sub>O<sub>5</sub>, as can be seen in Table 8.1. In these latter experiments, 0.5 g of catalyst was used in each run performed in a temperature range of 100-190 °C with a constant ethanol residence time of 26.6 g<sub>cat</sub>·h/mol.

Results are reported in terms of the ethanol conversion and product yields.

The ethanol conversion is defined as

$$C = (\text{number of moles of ethanol reacted}) / (\text{number of moles of ethanol fed})$$

while the yields of the *i*th product is defined as

$$Y_i = (\text{number of moles of product } i \text{ formed}) / (\text{number of moles of ethanol fed})$$

## 8.5 Results and Discussion

### *Catalyst and Support Characterization*

The operating conditions used in the preparation of the supports and catalysts, together with some properties of the resulting materials,

are reported in Table 8.1. In the same table, the particular amount of  $\text{TiO}_2$  loaded on  $\text{SiO}_2$  after each grafting step is also reported. As can be seen from the data reported, the  $\text{TiO}_2$  loading progressively increases with each grafting step, but to a lower and lower extent.

Examination of the X-ray diffraction pattern of the support obtained after three grafting steps reveals very small crystallites of anatase and a predominant amorphous deposit of  $\text{TiO}_2$ . XPS analyses of similar  $\text{TiO}_2/\text{SiO}_2$  samples [21] showed that an atomically homogeneous dispersion is achieved for lower  $\text{TiO}_2$  coverages corresponding to less than a monolayer (from 0.6 to 1.0), after which small aggregates and crystallites can be formed. The original  $\text{SiO}_2$  support shows an intense FTIR absorption band at  $3747\text{ cm}^{-1}$ , corresponding to isolated silanol groups ( $\text{Si-OH}$ ) [22,23]. These silanol groups are strongly reduced as a consequence of titanium isopropoxide grafting, as can be seen in Figure 8.1.

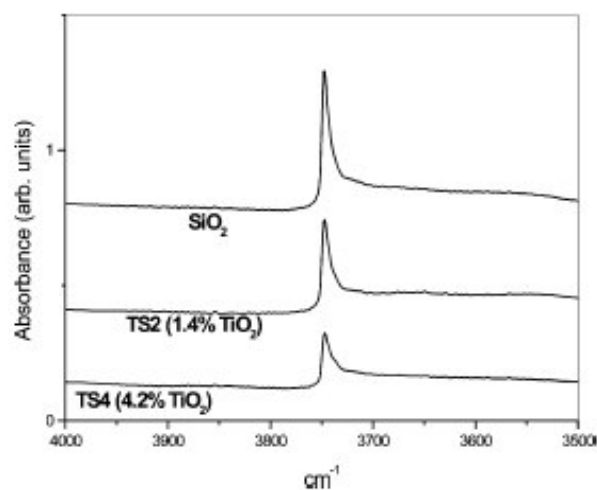


**Figure 8.1:** FTIR spectra of silica at different titanium loadings in comparison with the spectrum of pure silica.

This demonstrates the efficacy of the alkoxide grafting reaction in dispersing titanium on the silica surface.

Table 8.1 reports also a list of the prepared catalysts and their main related properties. As can be seen, the specific surface area is negatively affected by the increase of vanadium loading in the range considered. XRD analysis indicates the absence of crystalline V<sub>2</sub>O<sub>5</sub>. This observation was also confirmed by examining the DRIFT spectra, which showed a moderate increase of the signal corresponding to V-O-V bonds with increasing vanadium loading, that is, the occurrence of vanadium aggregation, probably giving rise to polymeric linear species anchored on TiO<sub>2</sub> surface.

**Catalyst Results**

The kinetic results obtained in three different sets of catalytic runs, together with the operating conditions employed in each case, are gathered in Tables 8.2, 8.3, 8.4.

In particular, Table 8.2 reports the results of the runs performed by changing temperature (100- 180°C) and ethanol residence time (10-65 g<sub>cat</sub>·h/mol) but keeping the molar ratio between ethanol and oxygen constant.

In contrast, in Table 8.3 the results obtained in the runs performed by changing the temperature (140-160 °C), the ethanol residence time (10-200 g<sub>cat</sub>·h/mol) and the molar ratio between the reagents are reported.

Finally, Table 8.4 reports the results of the kinetic runs performed at different temperatures (130-190 °C) on different catalysts characterized by a different vanadium contents. In these latter runs, the other operating conditions, such as the ethanol residence time and reagent molar ratio, were kept constant.

In correspondence with each experimental flow rate and temperature combination, different samples of the gaseous outlet mixture were withdrawn and sent to the GC for analysis, to evaluate the ethanol conversion and product yields. All the data reported in the tables mentioned above are averaged values for both the conversion and yields, evaluated under steady-state conditions, although all available data were used for the mathematical regression analysis.

**Table 8.2:** Operating Conditions and Experimental Results for Runs Performed with a Constant Ethanol/Oxygen Molar Ratio.

| <i>WF</i><br>(g <sub>cat</sub> /h·mol <sub>EtOH</sub> ) | catalyst<br>(g) | feed composition              |                             |                             | temperature<br>(°C) | ethanol<br>conversion <sup>a</sup><br>(%) | product yield <sup>a</sup> (%) |             |         |                 |               |
|---|-----------------|-------------------------------|-----------------------------|-----------------------------|---------------------|---|--------------------------------|-------------|---------|-----------------|---------------|
|   |                 | ethanol<br>(liquid)<br>(mL/h) | oxygen<br>(gas)<br>(mL/min) | helium<br>(gas)<br>(mL/min) |                     |   | acetaldehyde                   | acetic acid | acetals | CO <sub>2</sub> | ethylic ether |
| 17.7  | 0.33            | 1.10                          | 7.70                        | 22                          | 100                 | 3.24                                      | 3.07                           | –           | 0.11    | –               | 0.06          |
| 26.6  | 0.33            | 0.73                          | 5.13                        | 22                          | 100                 | 3.67                                      | 3.39                           | –           | 0.18    | –               | 0.10          |
| 64.8  | 0.33            | 0.30                          | 2.10                        | 22                          | 100                 | 10.19                                     | 9.29                           | –           | 0.69    | –               | 0.21          |
| 9.7   | 0.33            | 2.00                          | 13.96                       | 22                          | 120                 | 3.62                                      | 3.31                           | –           | 0.03    | –               | 0.29          |
| 17.7  | 0.33            | 1.10                          | 7.70                        | 22                          | 120                 | 6.54                                      | 6.14                           | –           | 0.22    | –               | 0.17          |
| 26.6  | 0.33            | 0.73                          | 5.13                        | 22                          | 120                 | 7.01                                      | 6.55                           | –           | 0.25    | –               | 0.20          |
| 64.8  | 0.33            | 0.30                          | 2.10                        | 22                          | 120                 | 13.91                                     | 12.95                          | –           | 0.57    | –               | 0.39          |
| 9.7   | 0.33            | 2.00                          | 13.96                       | 22                          | 140                 | 9.74                                      | 9.03                           | –           | 0.39    | –               | 0.32          |
| 17.7  | 0.33            | 1.10                          | 7.70                        | 22                          | 140                 | 11.35                                     | 10.28                          | 0.02        | 0.69    | –               | 0.37          |
| 26.6  | 0.33            | 0.73                          | 5.13                        | 22                          | 140                 | 23.23                                     | 21.22                          | –           | 1.31    | –               | 0.72          |
| 64.8  | 0.33            | 0.30                          | 2.10                        | 22                          | 140                 | 28.54                                     | 25.92                          | –           | 1.56    | –               | 1.05          |
| 9.7   | 0.33            | 2.00                          | 13.96                       | 22                          | 160                 | 23.67                                     | 20.16                          | 0.09        | 1.65    | 0.88            | 0.89          |
| 17.7  | 0.33            | 1.10                          | 7.70                        | 22                          | 160                 | 30.96                                     | 26.78                          | 0.07        | 2.03    | 0.90            | 1.18          |
| 26.6  | 0.33            | 0.73                          | 5.13                        | 22                          | 160                 | 37.16                                     | 31.79                          | 0.15        | 2.67    | 1.12            | 1.43          |
| 64.8  | 0.33            | 0.30                          | 2.10                        | 22                          | 160                 | 58.79                                     | 48.46                          | –           | 5.59    | 2.46            | 2.26          |
| 9.7   | 0.33            | 2.00                          | 13.96                       | 22                          | 170                 | 31.12                                     | 28.13                          | 0.04        | 1.09    | 0.38            | 1.48          |
| 26.6  | 0.33            | 0.73                          | 5.13                        | 22                          | 170                 | 54.25                                     | 45.82                          | 0.09        | 4.90    | 1.41            | 2.03          |
| 64.8  | 0.33            | 0.30                          | 2.10                        | 22                          | 170                 | 68.88                                     | 57.93                          | –           | 6.77    | 0.84            | 1.56          |
| 9.7   | 0.33            | 2.00                          | 13.96                       | 22                          | 180                 | 48.28                                     | 40.51                          | 0.13        | 3.97    | 1.71            | 1.95          |
| 26.6  | 0.33            | 0.73                          | 5.13                        | 22                          | 180                 | 76.51                                     | 63.15                          | 0.10        | 7.78    | 2.48            | 2.99          |
| 64.8  | 0.33            | 0.30                          | 2.10                        | 22                          | 180                 | 86.43                                     | 69.21                          | –           | 11.08   | 2.83            | 3.30          |

<sup>a</sup> Conversion and yields are averaged values

**Table 8.3:** Operating Conditions and Experimental Results for Runs Performed with a Variable Ethanol/Oxygen Molar Ratio.

| <i>WF</i><br>(g <sub>cat</sub> /h·mol <sub>EtOH</sub> ) | catalyst<br>(g) | feed composition              |                             |                             | temperature<br>(°C) | ethanol<br>conversion <sup>a</sup><br>(%) | product yield <sup>a</sup> (%) |             |         |                 |               |
|---|-----------------|-------------------------------|-----------------------------|-----------------------------|---------------------|---|--------------------------------|-------------|---------|-----------------|---------------|
|   |                 | ethanol<br>(liquid)<br>(mL/h) | oxygen<br>(gas)<br>(mL/min) | helium<br>(gas)<br>(mL/min) |                     |   | acetaldehyde                   | acetic acid | acetals | CO <sub>2</sub> | ethylic ether |
| 9.7   | 0.33            | 2.00                          | 7.7                         | 22                          | 140                 | 11.96                                     | 11.06                          | –           | 0.52    | –               | 0.38          |
| 26.6  | 0.33            | 0.73                          | 7.7                         | 22                          | 140                 | 17.83                                     | 16.30                          | –           | 0.86    | –               | 0.67          |
| 48.6  | 0.33            | 0.40                          | 7.7                         | 22                          | 140                 | 28.35                                     | 25.84                          | –           | 1.41    | –               | 1.09          |
| 97.3  | 0.33            | 0.20                          | 7.7                         | 22                          | 140                 | 58.28                                     | 52.50                          | –           | 4.73    | –               | 1.05          |
| 194.6   | 0.33            | 0.10                          | 7.7                         | 22                          | 140                 | 81.43                                     | 70.04                          | –           | 5.04    | –               | 7.33          |
| 9.7   | 0.33            | 2.00                          | 7.7                         | 22                          | 160                 | 27.24                                     | 23.42                          | 0.07        | 1.70    | 0.85            | 1.20          |
| 11.4  | 0.33            | 1.70                          | 7.7                         | 22                          | 160                 | 28.20                                     | 24.16                          | 0.09        | 2.04    | 0.78            | 1.14          |
| 14.9  | 0.33            | 1.30                          | 7.7                         | 22                          | 160                 | 31.85                                     | 27.39                          | 0.04        | 2.31    | 0.82            | 1.29          |
| 19.5  | 0.33            | 1.00                          | 7.7                         | 22                          | 160                 | 41.25                                     | 35.40                          | –           | 3.06    | 1.10            | 1.63          |
| 26.6  | 0.33            | 0.73                          | 7.7                         | 22                          | 160                 | 58.64                                     | 47.97                          | –           | 6.22    | 2.15            | 2.30          |
| 48.6  | 0.33            | 0.40                          | 7.7                         | 22                          | 160                 | 88.97                                     | 69.39                          | –           | 9.39    | 6.94            | 3.24          |
| 97.3  | 0.33            | 0.20                          | 7.7                         | 22                          | 160                 | 87.26                                     | 70.00                          | –           | 7.82    | 6.40            | 3.03          |
| 149.7   | 0.33            | 0.13                          | 7.7                         | 22                          | 160                 | 100.0                                     | 78.14                          | –           | 10.09   | 9.19            | 2.57          |
| 194.6   | 0.33            | 0.10                          | 7.7                         | 22                          | 160                 | 99.59                                     | 87.93                          | –           | 10.37   | –               | 1.29          |

<sup>a</sup> Conversion and yields are averaged values





Additional kinetic runs were then performed to evaluate the effect on the reaction rate of the presence of water in the feed stream. To this end, a mixture of water and ethanol in a molar ratio 1:1 was used. The results obtained are collected in Table 8.5. As can be seen by comparing the conversions and yields gathered in this table with those reported in Table 8.3, obtained under the same conditions, the ethanol reaction rate is negatively affected by the presence of water in the feed stream.

Another interesting observation is that the selectivity is strongly increased, changing from 85 to 95%, because of the absence of some by-products such as acetals and CO<sub>2</sub>.

**Table 8.5:** Operating conditions and experimental results for runs performed with a 1:1 ethanol/water molar ratio in the feed.

| <i>WF</i><br>(g <sub>cat</sub> /h·mol <sub>EtOH</sub> ) | catalyst<br>(g) | feed composition              |                             |                             | temperature<br>(°C) | ethanol<br>conversion<br>(%) | product yield (%) |             |         |                 |               |
|---|-----------------|-------------------------------|-----------------------------|-----------------------------|---------------------|------------------------------|-------------------|-------------|---------|-----------------|---------------|
|   |                 | ethanol<br>(liquid)<br>(mL/h) | oxygen<br>(gas)<br>(mL/min) | helium<br>(gas)<br>(mL/min) |                     |                              | acetaldehyde      | acetic acid | acetals | CO <sub>2</sub> | ethylic ether |
|   |                 | (mL/h)                        | (mL/min)                    | (mL/min)                    |                     |                              |                   |             |         |                 |               |
| 9.7   | 0.33            | 2.00                          | 7.7                         | 22                          | 160                 | 20.30                        | 19.22             | –           | 0.07    | –               | 0.74          |
| 26.6  | 0.33            | 0.73                          | 7.7                         | 22                          | 160                 | 55.11                        | 53.19             | –           | –       | –               | 1.91          |
| 48.6  | 0.33            | 0.40                          | 7.7                         | 22                          | 160                 | 63.91                        | 61.67             | –           | –       | –               | 2.24          |
| 97.3  | 0.33            | 0.20                          | 7.7                         | 22                          | 160                 | 81.01                        | 78.54             | –           | –       | –               | 2.47          |

In addition, two other kinetic experiments were conducted to evaluate the influence of the acid-base properties of the catalysts. In one case, ethanol containing a small amount of pyridine was fed into the reactor, kept at 160 °C, which contained 0.31 g of a catalyst with a  $V_2O_5$  content of 3.56%, giving a residence time of 26.6  $g_{cat} \cdot h/mol$ .

In Figure 8.2, the ethanol conversions obtained after the addition of a stoichiometric amount of pyridine (123.6  $\mu mol/g$ ) and two and three times this quantity are reported.

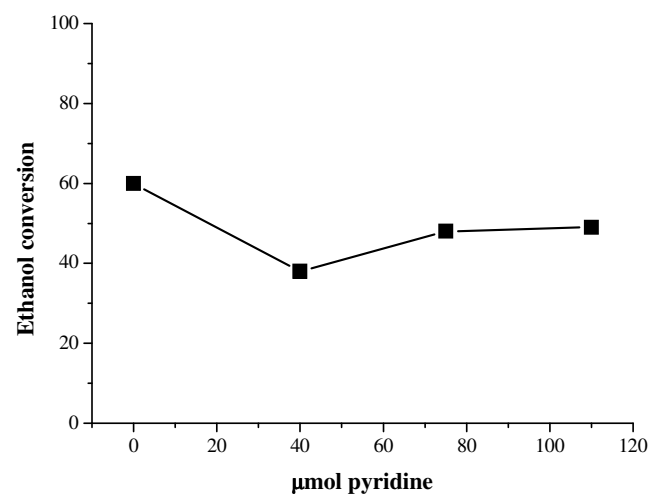


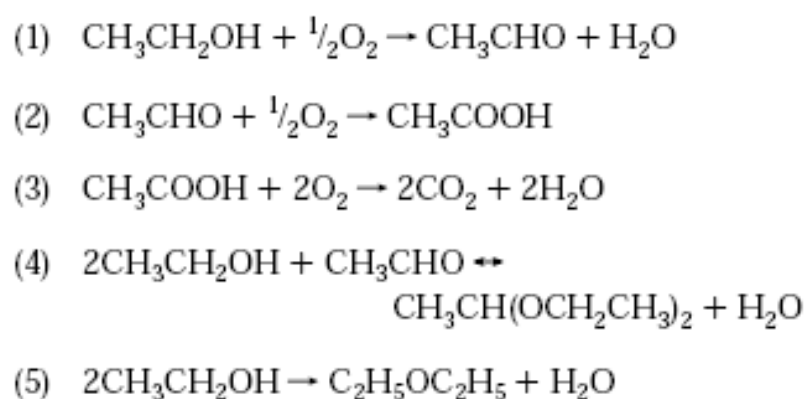
**Figure 8.2:** Ethanol conversion vs amount of pyridine fed to the reactor

As can be seen, the activity of the catalyst initially decreased slightly and then remained constant. The selectivities remained roughly unchanged. The conclusion is that the acid character of the catalyst does not influence this reaction and the slight decrease of activity observed initially can reasonably be attributed to the steric hindrance of the adsorbed pyridine.

The second experiment consisted of saturating the catalyst with CO<sub>2</sub>, to observe the eventual effect of basic sites on the reaction rate. The conversion remained unchanged, in agreement with the TPD observations [24], according to which no basic sites of reasonable strength are present on the surface of this catalyst.

### ***Reaction Kinetics and Mechanism***

On the basis of the observed products, we assumed the following reaction scheme:



To simplify the kinetic approach, we assigned a number to each of the components as follows: 1, ethanol; 2, acetaldehyde; 3, acetic acid; 4, acetal; 5, carbon dioxide; 6, oxygen; 7, water; and 8, ethyl ether.

Because the reactor is isothermal, it is possible to evaluate the concentration profiles of both the reagents and the products inside the reactor by integrating the differential equation

$$\frac{dF_i}{dW} = \sum_{j=1}^{N_r} \alpha_{ij}(r_j) \quad (1)$$

with  $i=1-8$  representing the involved components as numbered above and  $j=1-5$  representing the reactions in the assumed scheme;  $\alpha_{i,j}$  represents the corresponding stoichiometric coefficients for component  $i$  in reaction  $j$ . The integration is possible only after the definition of the kinetic laws for each of the five mentioned reactions.

In order to define the kinetic laws for the oxidation reactions (eqs 1-3), we first considered the four-step reaction mechanism depicted in **Chart 1**, which has been proposed by different authors for the ODH of ethanol on different oxide catalysts [3] and for the ODH of methanol on vanadium-based catalysts.

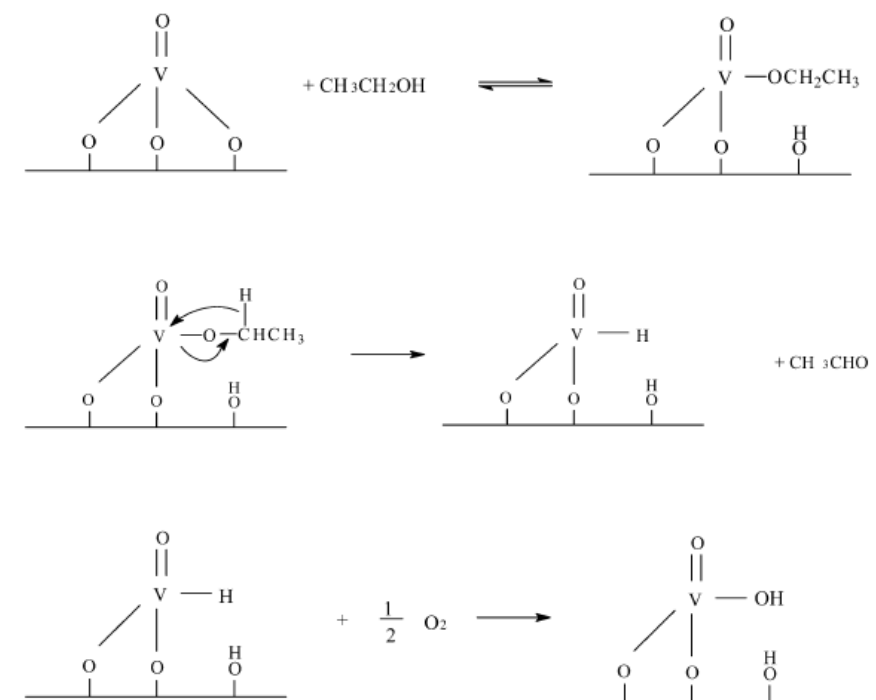


**Chart 1**

An alternative mechanism could be suggested in which the first step is the chemisorption of oxygen to form a vanadium peroxy radical that can withdraw the  $\alpha$ -hydrogen from ethanol, thereby favouring the formation of acetaldehyde. Reduction of the peroxide by decomposition would restore the original catalytic site. A similar mechanism was suggested to explain the oxidation of butane to maleic anhydride by Agaskar et al. [24] However, this mechanism can probably also be simplified to a Mars and van Krevelen-like mechanism for interpreting the kinetic data.

By considering the previously reported mechanism and assuming the second and third steps to be the slowest, it is possible to depict it in a compact way in which only two reactions appear, the first being reduction and the second oxidation (see *Chart 2*).



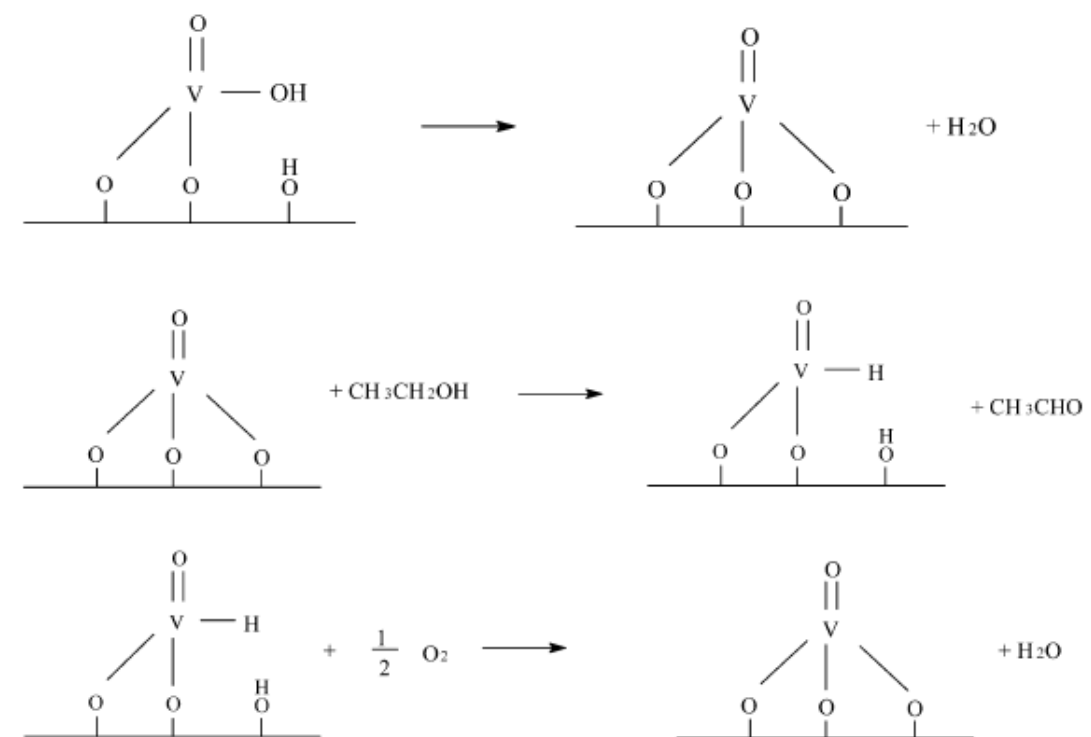
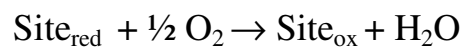
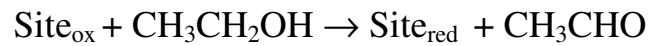


**Chart 2**

The two reactions can also be written as



This mechanism is formally identical to that of Mars and van Krevelen [12] and gives rise, therefore, to the following kinetic laws for the oxidation reactions

$$r_1 = \frac{k_1 P_1}{1 + \frac{k_1 P_1}{k_{\text{ox}} P_{\text{O}_2}^{1/2}}} \quad (2)$$

$$r_2 = \frac{k_2 P_2}{1 + \frac{k_2 P_2}{k_{\text{ox}} P_{\text{O}_2}^{1/2}}} \quad (3)$$

$$r_3 = \frac{k_3 P_3}{1 + \frac{k_3 P_3}{k_{\text{ox}} P_{\text{O}_2}^{1/2}}} \quad (4)$$

where  $k_{\text{ox}} P_{\text{O}_2}^{1/2}$  is the rate of the active site re-oxidation, which is the same in all cases.

Simpler kinetic laws were adopted for the reactions 4 and 5, considering that the contributions of these reactions are very low

$$r_4 = k_4 P_2 \quad (5)$$

$$r_5 = k_5 P_1^2 \quad (6)$$

For what concerns the temperature dependence, all of the kinetic parameters appearing in eqs 2-6 were expressed in terms of two parameters according to the Arrhenius law:

$$K_j=A_j \exp(-E_j/RT) \tag{7}$$

Then, the system of differential eqs 1 was numerically integrated using a fourth-order Runge-Kutta method. All kinetic data related to Tables 8-2 and 8-3 were subjected to mathematical regression analysis involving minimization of the objective function:

$$\Phi(\beta)=\sum_{j=1}^N [X_i^{\text{exp}}-X_i^{cal}(\beta)]^2 \tag{8}$$

where  $X$  represents the conversion or a yield,  $N$  is the number of experimental runs, and  $\hat{a}$  is the vector of the kinetic parameters. The best fitting parameters obtained are reported in Table 8.6.

**Table 8-6:** Arrhenius Parameters for the Considered Reactions

| reaction  | $\ln K=\ln A-E_a/RT$ |                  | correlation coefficient |
|---|----------------------|------------------|-------------------------|
|   | $\ln A$              | $E_a$ (kcal/mol) |                         |
| ethanol $\rightleftharpoons$ acetaldehyde           | $12.61 \pm 1.75$     | $10.9 \pm 1.4$   | 0.9347                  |
| catalytic site reoxidation                          | $10.47 \pm 1.46$     | $11.7 \pm 1.2$   | 0.9593                  |
| acetaldehyde $\rightleftharpoons$ acetic acid       | $27.04 \pm 25.95$    | $35.2 \pm 21.3$  | 0.6365                  |
| acetic acid $\rightleftharpoons$ CO <sub>2</sub>    | $44.56 \pm 33.32$    | $47.1 \pm 27.4$  | 0.6517                  |
| ethanol + acetaldehyde $\rightleftharpoons$ acetals | $5.46 \pm 5.08$      | $7.5 \pm 4.2$    | 0.6675                  |
| ethanol $\rightleftharpoons$ ethylic ether          | $48.64 \pm 22.01$    | $47.0 \pm 18.1$  | 0.7925                  |

In Figure 8.3 the conversions of ethanol obtained at different temperatures for the runs of Table 8.2 are reported as a function of the ethanol residence time. Symbols are experimental data whereas lines are calculated. The deviation observed for the run performed at the high temperature of 180 °C is probably due to the difficulty of controlling the bed temperature, considering the strong exothermicity of the reaction (-41.35 kcal/mol). The agreement obtained in the other cases is satisfactory.

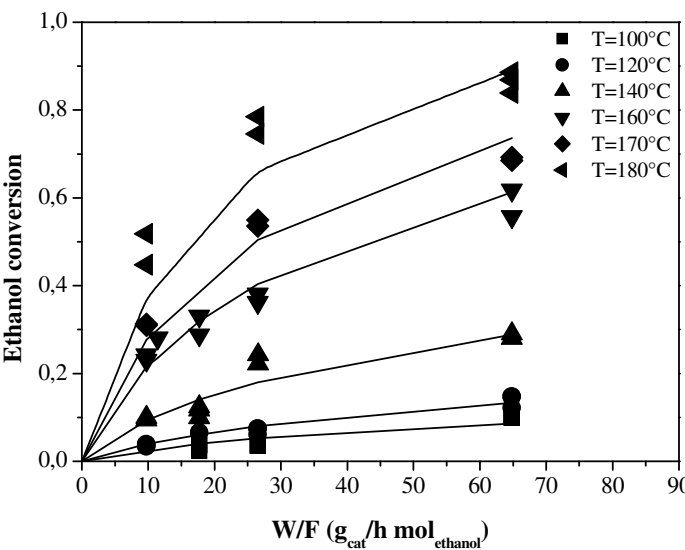


**Figure 8.3:** methanol conversion as fuction of residence time for a feed with constant ethanol/oxygen molar ratio at different temperatures.

In Figure 8.4, the simulation results obtained for the same runs but related to the yields of the main reaction product – acetaldehyde - are reported.

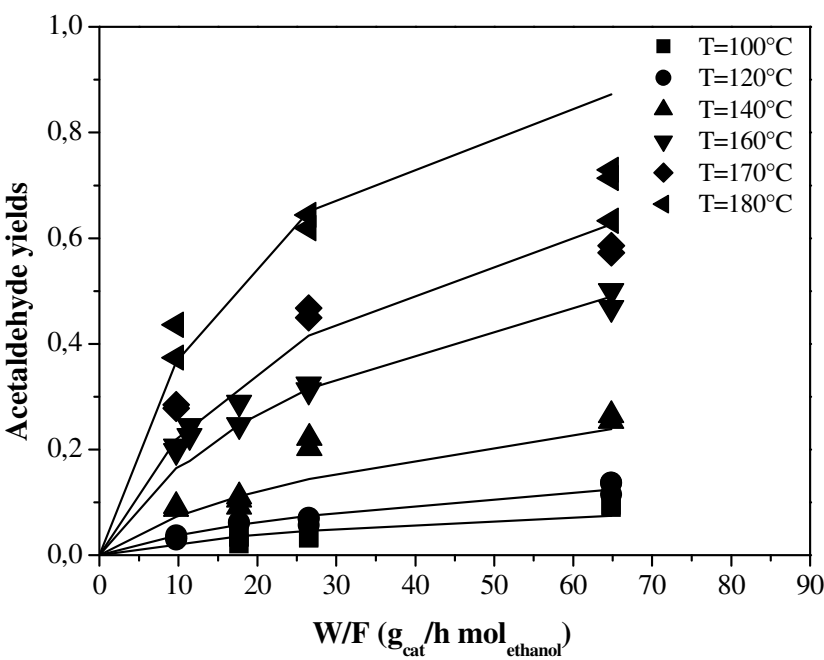


**Figure 8.4:** Acetaldehyde yield as a function of residence time for a feed with constant ethanol/oxygen molar ratio at different temperatures.

In Figure 8.5, the conversions of ethanol obtained at the two different temperatures of 140 and 160 °C are reported as a function of the ethanol residence time. These kinetic runs correspond to the second set of runs reported in Table 8-3 in which the ratio between the reagents was largely changed. Again, symbols represent experimental data, and lines are calculated. The obtained agreement is quite satisfactory.

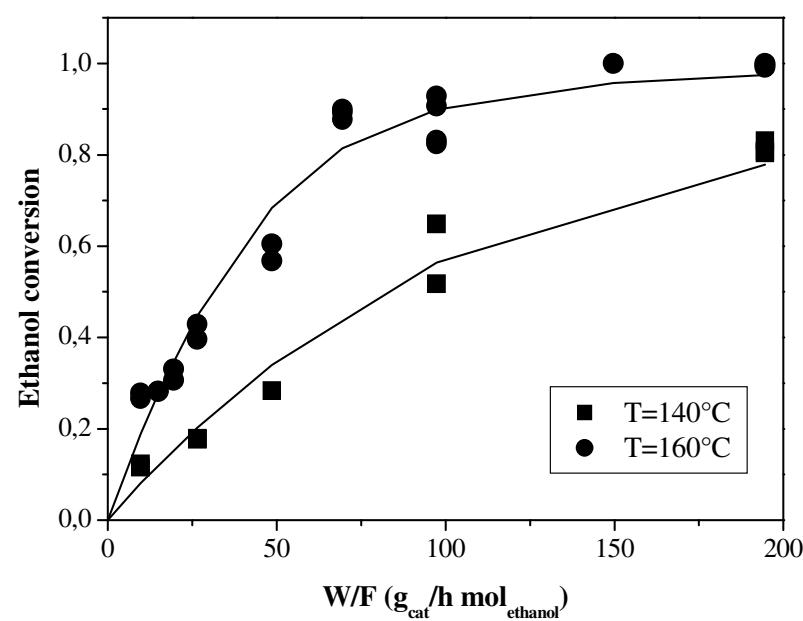


**Figure 8.5:** Ethanol conversion as a function of residence time for a feed with constant ethanol/oxygen molar ratio at different temperatures.

In Figure 8.6, the simulation results obtained for the same runs as Figure 8.5 but related to the yields of acetaldehyde are reported.

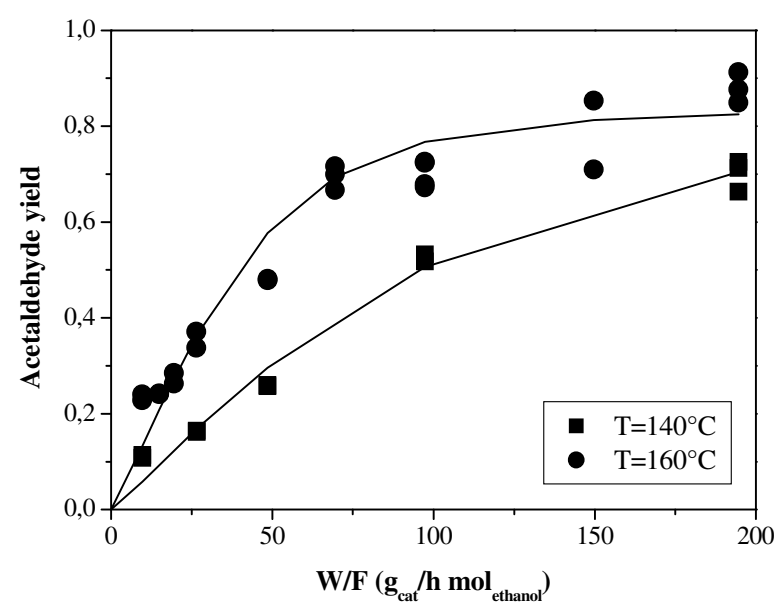


**Figure 8.6:** Acetaldehyde yield as a function of residence time for a feed with variable ethanol/oxygen molar ratio at different temperatures.

In Figure 8.7, an example of the simulation of the evolution with time of the product distribution is reported for a fixed temperature of 160 °C. As can be seen, in all cases, a satisfactory agreement was obtained, but the validity of the adopted kinetic model can be better appreciated in Figures 8.8 and 8.9, where all of the experimental data for the ethanol conversions and acetaldehyde yields, respectively, are compared with the corresponding calculated values.

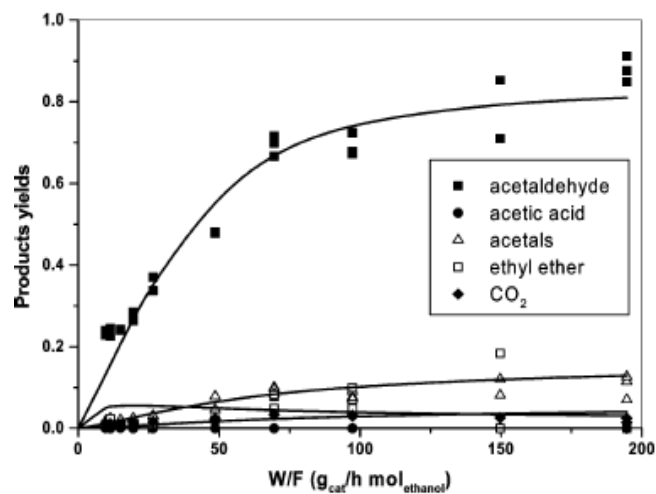


**Figure 8.7:** Acetaldehyde yields and by-product distribution as a function of residence time for a feed with variable ethanol/oxygen molar ratio at a temperature of 160 °C.

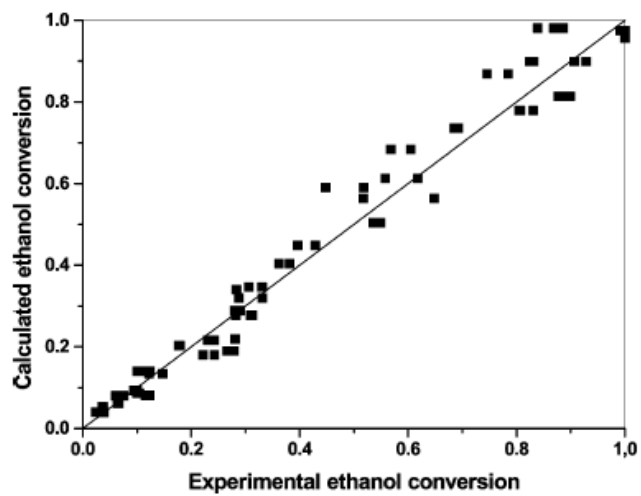


**Figure 8.8:** Calculated vs experimental ethanol conversions.



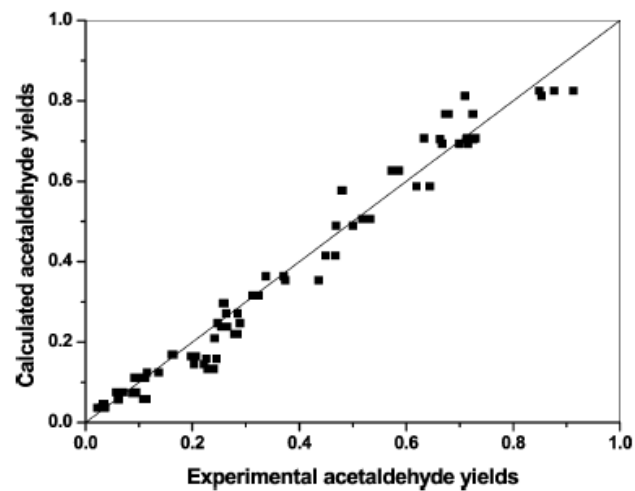


Figure 8.9: Calculated vs experimental acetaldehyde yields.

Finally, the Arrhenius plots for the kinetic constants  $k_1$  and  $k_{ox}$  are reported in Figure 8-10.

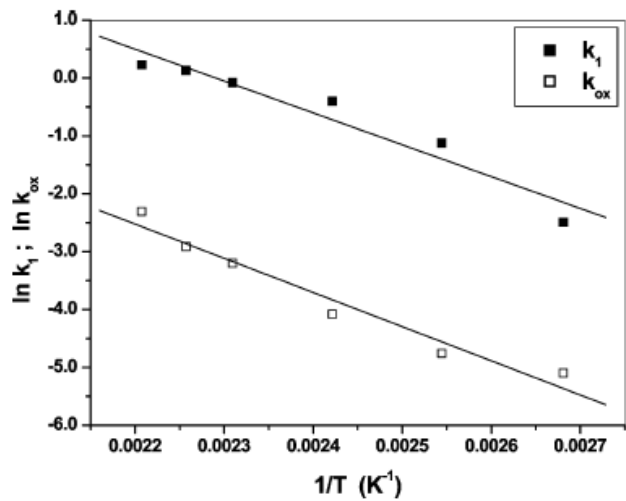


Figure 8.10: Arrhenius plots for the kinetic constants related to the ethanol oxidation and to reoxidation of the catalytic sites.

As can be seen, a linear trend was obtained in both cases. It is worth mentioning that the slopes in the two cases are similar, in agreement with the similar activation energies obtained in the regression analysis. This means that the ratio of  $k_1/k_{ox}$  can be considered roughly constant for different temperatures.

It is then clear that the catalyst re-oxidation is the lower step in the redox cycle; this is likely a peculiarity of the catalyst depending on both the type of vanadium sites prevalent on the surface and the chemical environment. In fact, we found that the activation energy for a  $V_2O_5/TiO_2/SiO_2$  catalyst is in agreement with the values found by Quaranta et al [9]. The activation energy found by Gomez et al. [11] was, on the contrary, higher (16.2 kcal/mol for the main oxidation reaction and 23.5 kcal/mol for the catalyst re-oxidation) on a VMgO catalyst. This clearly shows the advantage of the use of  $TiO_2$  as support oxide for the vanadium chemical environment.

It is worth mentioning, finally, that ethanol oxidation to acetaldehyde is probably structure-insensitive, as suggested by Oyama and Somorjai [8], when crystalline aggregates of  $V_2O_5$  are present in catalysts containing high vanadium amount. In this case, V–O–V bonds, which are largely prevalent, promote the reaction. When molecular dispersion is obtained, the V–O–support bonds become primarily responsible for the observed activities and selectivities. The selectivities, in the latter case, are higher than those observed for poorly dispersed and crystalline  $V_2O_5$  catalysts [9,10].

The runs performed on well-dispersed catalysts, with different vanadium loadings, can be roughly interpreted assuming a linear

dependence of the reaction rate with the vanadium catalyst concentration, as can be appreciated in Figure 8.11.

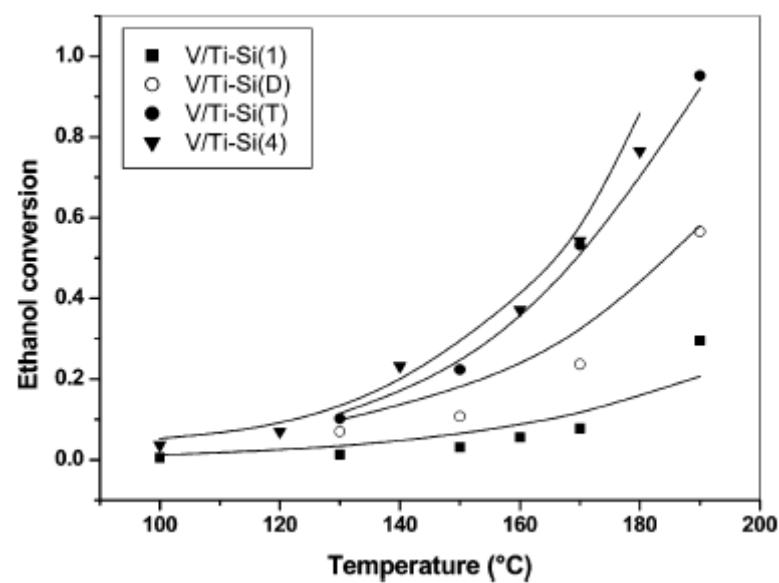


**Figure 8.11:** Ethanol conversion for catalysts at different vanadium loadings. The curves are simulations obtained by correlating kinetic constants with vanadium content.

8.6 Conclusions

Very active and selective catalysts have been prepared by grafting vanadyl alkoxide onto a silica support coated with TiO<sub>2</sub>. This type of catalyst (V<sub>2</sub>O<sub>5</sub>/TiO<sub>2</sub>/SiO<sub>2</sub>) gives rise to high conversion of ethanol to acetaldehyde at very low temperature (130-180 °C), which represents a useful perspective in view of industrial applications. The high dispersion of the catalyst strongly improves the selectivity and the activity is a linear function of supported vanadium amount.

Acetaldehyde is relatively stable on this catalyst and this is the reason for the high selectivities observed. The acid and basic

properties of the catalyst have a minimal influence on the catalyst performance in this reaction, and therefore, only the redox properties are responsible for the reaction. The mechanism of the reaction does not involve surface lattice oxygen, because, at the temperature used, the oxygen exchange reaction is too slow.

We have suggested two different possible mechanisms that, when simplified, correspond in the kinetic analysis to a classical Mars and van Krevelen kinetic law. The kinetic parameters for all of the occurring reactions were evaluated and the activation energy found for the main reaction to acetaldehyde is in agreement with the values reported in the literature on the same type of catalyst. The VMgO catalyst, in contrast, exhibited higher activation energies for both ethanol oxidation to acetaldehyde and catalyst re-oxidation. This means that the TiO<sub>2</sub> represent a favourable chemical environment for the vanadium catalytic reactions in the ODH of ethanol to acetaldehyde, in agreement with the suggestion made by other authors that V-O-support bonds are determinant for the activity and selectivity of different reactions, because the effect of the support is often dramatic.

## 8.7 References

- [1] Acetaldehyde. In *Ullmann's Encyclopedia of Industrial Chemistry*, 6th ed.; Wiley-VCH: Weinheim, Germany, 2002; Vol. A1, pp 31-44.
- [2] A. Chauvel; G. Lefebvre; L. Castex, Technip, Paris, 1986; Vol. 2, p 33.
- [3] H. Idriss; E.G. Seebauer, *J. Mol. Catal. A: Chem.*, **2000**, 152, 201.

- [4] S. Tsuruya; M. Tsukamoto; M. Watanabe; M. Masai, *J. Catal.*, **1985**, 93, 303.
- [5] B. Parlitz; W. Hanke; R. Fricke; M. Richter; U. Roost; G. Ohlmann, *J. Catal.*, **1985**, 94, 24.
- [6] T.R. Ling; Z.B. Chen; M.D. Lee, *Appl. Catal. A: Gen.*, **1996**, 136, 191.
- [7] V. Bagiev; G. Dadashev; K. Adzhamov; T. Alkhazov, *Kinet. Katal.*, **1992**, 33 (3), 460.
- [8] S. Oyama; G.A. Somorjai, *J. Phys. Chem.* **1990**, 94, 5022.
- [9] N.E. Quaranta; J. Soria; V. Cortes Corberan; J.L.G. Fierro, *J. Catal.* **1997**, 171, 1.
- [10] E. Santacesaria; A. Sorrentino; R. Tesser; M. Di Serio; A. Ruggiero, *J. Mol. Catal. A: Chem.*, **2003**, 204-205, 617.
- [11] M.F. Gomez; L.A. Arrua; M.C. Abello, *Ind. Eng. Chem. Res.*, **1997**, 36, 3468.
- [12] P. Mars; D.W. van Krevelen, *Chem. Eng. Sci.*, **1954**, 3, 41.
- [13] J.L. Lakshmi; N.J. Ihasz; J.M. Miller, *J. Mol. Catal. A: Chem.*, **2001**, 165, 199.
- [14] K. Inamaru; M. Misono; T. Okuhara, *Appl. Catal. A: Gen.*, **1997**, 149, 133.
- [15] Y. Murakami, M. Inomata, K. Mori, T. Ui, K. Suzuki, A. Miyamoto and T. Hattori, p. 531, Elsevier, Amsterdam, 1983.
- [16] J. Kijenski, A. Baiker, M. Glinski, P. Dollenmeier and A. Wokaun, *J. Catal.*, **1986**, 1, 101.
- [17] I.E. Wachs and F.D. Hardcastle, Chem. Inst. Canada, Ottawa, **1988**, 3, 1449.
- [18] F.R.D. Snell; L.S. Ettre, Interscience - New York, **1974**, 19, 107.

- [19] S. Brunauer; P.H. Emmet; E. Teller, *J. Am. Chem. Soc.*, **1938**, 60, 309.
- [20] D. Dollimore; G.R. Heal, *J. Appl. Chem.* **1964**, 14, 109.
- [21] E. Santacesaria, M. Cozzolino, M. Di Serio, A.M. Venezia, R. Tesser, *Applied Catalysis A: General*, **2004**, 270, 177.
- [22] E. Astorino; J.B., Peri, R. J. Wiley, *J. Catal.* **1995**, 157, 482.
- [23] C.U. I. Odenbrand; S. L. T. Andersson; L.A. Andersson, H. Brandin, J.G.M.; G. Busca, *J. Catal.*, **1990**, 125 (2), 541.
- [24] P.A. Agaskar, L. De Caul, R.K. A. Grasselli, *Catal. Lett.*, **1994**, 23, 339.

**List of Symbols**

$A_j$  = pre-exponential factor for kinetic constant  $k_j$

$E_j$  = activation energy for kinetic constant  $k_j$

$F_i$  = molar flow rate of component  $i$  in the feed

$k_j$  = kinetic constant for reaction  $j$

$k_{\text{ox}}$  = kinetic constant for catalytic site reoxidation

$P_1$  = partial pressure of ethanol in the gas mixture

$P_2$  = partial pressure of acetaldehyde in the gas mixture

$P_3$  = partial pressure of acetic acid in the gas mixture

$P_{\text{O}_2}$  = partial pressure of oxygen in the gas mixture

$r_j$  = rate of reaction  $j$

$W$  = weight of catalyst loaded in the reactor

$X_i^{\text{calc}}$  = calculated values of conversion or yields

$X_i^{\text{exp}}$  = experimental values of conversion or yields

$\alpha_i, j_j$  = stoichiometric coefficient of component  $i$  in reaction.





# Notes

## Methanol vs Ethanol oxidative dehydrogenation (ODH) on V/TiO<sub>2</sub>/SiO<sub>2</sub> catalysts

### General comments

The results obtained about the ODH of methanol to formaldehyde and ethanol to acetaldehyde, reported and discussed in Chapter VII and VIII, respectively, showed that vanadia supported by *grafting* on TiO<sub>2</sub>-coated silica (V<sub>2</sub>O<sub>5</sub>/TiO<sub>2</sub>/SiO<sub>2</sub>) are very active and selective catalysts because they are able to promote the mentioned reactions under mild conditions of both temperature and pressure. In particular, for the given support (TiO<sub>2</sub>/SiO<sub>2</sub>), the catalysts prepared by *grafting* resulted more active and selective than the impregnated ones. This is due to the higher surface molecular dispersion of vanadium sites that is possible to achieve by using the grafting preparation method.

By comparing the catalytic performances of supported vanadia catalysts in the ODH of methanol and ethanol to the corresponding aldehydes, we found some similarities but also some differences, especially about the reaction mechanisms, that it is worth to report.

First of all, for both the mentioned reactions, we found that:

- A high surface dispersion of supported vanadium sites is fundamental to improve both the activity and the selectivity to the desired products. It was found that the coating of the silica carrier with a monolayer of  $\text{TiO}_2$  increases substantially not only the activity, but also the selectivity, as compared to those of the one supported on pure  $\text{TiO}_2$ . This is in agreement with the literature, according to which the oxygen in the V–O–support bond is critical for these catalytic oxidation reactions.
- Only redox sites are responsible for the reactions. The acid and basic properties of the catalysts have a minimal influence on the catalyst performances.

The main differences between the two ODH reactions were found about the reaction mechanism.

Although in both cases oxidation occurs via hydride formation on the active site and successive oxidation of the hydride to water, justifying the use of a like Mars and van Krevelen kinetic model, in the case of the ODH of methanol we observed the formation as a first step of a methoxydic intermediate anchored on the catalytic site, while, for ethanol the intermediate formed is different.

# GENERAL CONCLUSIONS

Catalysis is undoubtedly and will remain for a long time the most prominent scientific and practical answer to the simultaneous challenges of technological development and environmental protection. Because of about 90 % of chemicals are nowadays produced *via* a catalytic process of from a precursor produced catalytically, catalysis constitutes more than other field, a milestone of human welfare. Within this context, catalysis is, on a side, crucial to promote innovations in the chemical industry, but, on the other side, it is also a particular exciting tool for which fundamental interdisciplinary research must be accentuated by close collaborations between chemists, physicists and engineers.

Heterogeneous catalysts are characterized by a very complex architecture, referred to chemicals, structural and textural levels, which all have a deep impact on the catalytic performances. Because of the multi-level complexity, the feeling is now that more attention has to be paid to the characteristics of the catalytic materials, in a “back to basics” approach focused on defined precursors and innovative preparation methods.

The aim of this thesis has been to provide understanding of the relationships between the surface chemical properties of supported

titania and vanadia based catalysts and the catalytic performances, by investigating mainly the effect of preparation method, nature of the support and metal loading on the catalytic behaviour. In order to achieve these objectives, the research has been performed on three different levels: preparation, characterization and study of the catalytic performances.

The first part (part A) of the thesis aims to investigate the preparation, the characterization and the reactivity properties of  $\text{TiO}_2/\text{SiO}_2$  catalysts in two different reactions: transesterification of refined oils with methanol (*biodiesel production*) and the epoxidation reaction of cyclooctene with cumene hydroperoxide. The second part (part B) is completely dedicated to the study of the catalytic performances of supported vanadia catalysts in the ODHs of both n-butane to butenes and methanol to formaldehyde. Finally, in Part C the kinetic study of vanadium based catalysts in the ODHs of both methanol to formaldehyde and ethanol to acetaldehyde is analysed in detail. This last part of the thesis aims at having a complete understanding of the catalytic mechanism of  $\text{V}/\text{TiO}_2/\text{SiO}_2$  catalysts in the mentioned reactions.

Part A demonstrated that several factors are critical in controlling the dispersion capacity or the maximum surface coverage of titanium oxide species on silica, such as the concentration of surface hydroxyls and the specific surface area of silica. Site isolation and the maximum number of Ti–O–Si bridging bonds per Ti atom for isolated  $\text{TiO}_4$  sites are, in general, responsible for the highest specific catalytic activity (TOF) of the silica-supported titania catalysts. The *grafting* of

$\text{Ti}(\text{O}-\text{Pr}^i)_4$  onto silica surface appeared very useful as preparation method to obtain a good surface dispersion of the supported Ti species and the most suitable acidity for type and strength. In particular, the catalytic tests in biodiesel production showed that isolated  $\text{Ti}^{4+}$  cations have an appropriate Lewis acid strength to catalyze efficiently the transesterification of refined oil with methanol. Finally, the catalytic data obtained in the epoxidation reaction of cyclooctene with cumene hydroperoxide showed that both the activity and selectivity are influenced by the coordination environment of the surface titanium. A homogeneous surface titanium is a fundamental requirement to obtain a high stability, in order to prevent leaching phenomena and, consequently, good catalytic performances.

In Part B the deep investigation of the catalytic performances of supported vanadium based catalysts in the ODH reactions demonstrated mainly the effect of vanadium loading and nature of support on the catalytic behaviour. In particular, the beneficial effect in the use of  $\text{TiO}_2/\text{SiO}_2$  support for preparing highly dispersed vanadium catalysts was well assessed. Moreover, catalysts prepared by *grafting* resulted more active and selective than the impregnated ones in the ODH of both butane to butenes and methanol to formaldehyde. In the latter case, the catalytic results obtained demonstrated that, as well as formaldehyde (the main product observed), a wide range of by-products (e.g. dimethyl ether, dimethoxymethane, methyl formate, carbon oxides, hydrocarbons) can be obtained depending on both the redox properties and the acidity of

the catalyst which, in turn, depend on the interaction between the active phase and the support. It is thus very important to tune both the catalysts properties and the operative conditions to obtain good catalytic results, especially in terms of formaldehyde selectivity. A positive trend of selectivity with conversion was observed for all the catalysts of the  $V_{\text{graf}}/\text{TSM}$  series and attributed to the reaction sequence: methanol  $\rightarrow$  dimethoxymethane  $\rightarrow$  formaldehyde. This was explained by considering that the first reaction product, at low residence times when the methanol conversion is low, is dimethoxymethane which is then converted to formaldehyde by the reverse equilibrium reaction with water. As a further confirmation of this observation, an increase in the selectivity to formaldehyde was generally observed in correspondence to an increase of methanol conversion

Part C allowed to draw a clear picture of the catalytic mechanism of the Oxidative Dehydrogenation of both methanol and ethanol to the corresponding aldehydes on  $V_2O_5/\text{TiO}_2/\text{SiO}_2$  catalyst. An exhaustive set of experimental runs was conducted in both cases by investigating several operative conditions. The investigation of the ODH of methanol to formaldehyde showed, on the basis of the catalytic results exposed in Chapter VII of part B, an hypothesis of mechanism for the catalytic cycle of the ODH of methanol according to which the first elementary step in this mechanism is the formation of the methoxydic intermediate by methanol dissociative adsorption. In the subsequent step, this intermediate is rearranged into a dioxymethylenic surface species with the vanadium atom which presents a vanadium-hydride

bond. The dioxymethylenic group reacts further with methanol adsorbed from gaseous phase leading to the formation of dimethoxymethane, at low conversion, and of formaldehyde by reverse equilibrium when the conversion is high and water is present at a sufficiently high concentration in the system. The catalytic site in the initial form is finally restored from the reduced site by the intervention of gaseous oxygen and by water elimination, closing the cycle. This reaction mechanism led us to develop a *rake-type* reaction scheme in which all the observed products away from adsorbed species of methanol, formaldehyde and formic acid. A kinetic model was developed as a combination of the Mars-Van Krevelen and Langmuir-Hinshelwood models (MVK-LH), by assuming that the re-oxidation of the catalytic site occurs with the same rate and that only methanol and water compete for the adsorption onto the catalyst surface. The agreement between the model and the experimental data was considered very satisfactory. The kinetic investigation of the ODH of ethanol to acetaldehyde, conducted on the same type of catalyst and exposed in Chapter VIII, demonstrated that a high surface catalyst dispersion strongly improves the selectivity to acetaldehyde and the activity is a linear function of vanadium loading. Two different possible mechanisms were suggested that correspond in the kinetic analysis to a classical Mars and van Krevelen kinetic law. The kinetic parameters for all of the occurring reactions were evaluated and the activation energy found for the main reaction to acetaldehyde is in agreement with the values reported in the literature on the same type of catalyst.

By concluding, the experimental work of this PhD thesis highlights that the *Grafting* of metal alkoxides onto the surface of oxides rich of hydroxyls is a very innovative method to prepare highly dispersed supported metal oxide catalysts. The main peculiarity of this technique is that it is possible to modify in a tailored way the surface chemical properties of an oxide by the introduction of surface-bound catalytic species, without altering the original mechanical and structural properties. This methodology provides heterogeneous and “single-site” supported catalysts which possess superior properties relative to catalysts with the same composition, but prepared by traditional aqueous methods, i.e. impregnation and coprecipitation. As consequence, a strong improvement of catalyst activity and selectivity and a high resistance to the deactivation are obtained.



*Thanks are due to MIUR (Italian Minister of Research and Education) –PRIN–2005038244 for the financial support*



*Curriculum Vitae* - Mariangela Cozzolino

May 14, **1979** - Born in Naples (Italy)

***Education***

July 17, **2003** - *Master's degree in **Industrial Chemistry** (cum laude)*  
University of Naples "Federico II" - Faculty of Science MM.FF.NN -  
Department of Chemistry - Naples **Industrial Chemistry Laboratory**  
(**NICL**)

1992-1997 Liceo Scientifico "C. Colombo", Marigliano (Naples) (I)  
**Diploma di Maturità Scientifica**

***Communications to conferences***

**1. EUROPACAT VI, 31 Aug.-04 Sept. 2003, Innsbruck**

M. Cozzolino, R. Tesser, M. Di Serio, E. Santacesaria

Poster: "Oxidative Dehydrogenation (ODH) of n-butane on vanadium-ased catalysts prepared by grafting

**2. DGMK Conference "C<sub>4</sub>-C<sub>5</sub>-Hydrocarbons: Routes to higher value-added products",13-15 Oct 2004, Munich (Germany)**

M. Cozzolino, R.Tesser, M. Di Serio, E. Santacesaria

Oral: "Oxidative Dehydrogenation of n-butane on V<sub>2</sub>O<sub>5</sub>-TiO<sub>2</sub>/SiO<sub>2</sub> catalysts prepared by grafting titanium and vanadium on silica

**3. Second PhD Chem-Meeting-CIRCC, 18-20 November 2004, San Servolo Island-Venice (Italy)**

M. Cozzolino, R.Tesser, M. Di Serio, E. Santacesaria

Oral: "Acid and redox catalysts preparation by grafting metal alkoxides on the surface of oxides".

**4. XVI Congresso Nazionale di Chimica Industriale, 14-17 Giugno 2005, Verbania (Italy)**

M. Cozzolino, R.Tesser, M. Di Serio, E. Santacesaria

Oral: " Vanadium oxide-based catalysts for the oxidative dehydrogenation (ODH) of methanol to formaldehyde".

**5. VIII Seminar on Catalysis 2005, 19-24 June 2005, Verbania (Italy)**

M. Cozzolino, R. Tesser, M. Di Serio, E. Santacesaria

Poster: Vanadium based catalysts: preparation, properties, and performances in the ODH of n-butane.

**6. EUROPACAT VII, 28 Aug.-01 Sept. 2005, Sofia (Bulgaria)**

M. Cozzolino, R. Tesser, M. Di Serio, E. Santacesaria

Oral: “ Chemical adsorption study of titanium and vanadyl alkoxide on silica by grafting”

M. Cozzolino, R. Tesser, M. Di Serio, E. Santacesaria

Poster: “ Oxidative dehydrogenation of methanol to formaldehyde”

**7. DGMK /SCI Conference ”Oxidation and functionalization: Classical and alternative Routes and Sources”, October 12-14, 2005, Milan, Italy.**

M. Cozzolino, R.Tesser, M. Di Serio, E. Santacesaria

Oral: “Methanol and Ethanol Oxidative Dehydrogenation (ODH) to the corresponding aldehydes on Vanadium-based Catalysts

**8. 4<sup>th</sup> Scientific Meeting of the Wallonia Network for Nanotechnologies (NanoWall) “Nanostructured Surfaces: Funtionalization and Reactivity”, Université Libre de Bruxelles, Decemebr 19, 2005, Bruxelles**

M. Cozzolino, R.Tesser, M. Di Serio, E. Santacesaria

Poster: “ Nanodispersed Titanium and Vanadium oxide Catalysts prepared by grafting”

**9. International Symposium “Catalysis on oxide-type materials. Theory and experiment :share needs and capabilities”, Krakow, Poland, November 17-19, 2005**

M. Cozzolino, R. Tesser, M. Di Serio, E. Santacesaria

Oral: “Supported vanadium oxide based catalysts: preparation, characterization and catalytic performances”

**10. Second Concorde Conference “Nucleation, Growth, Microstructure and Matrices for Creating Nano-Dispersed Redox Oxide Catalysts in Oxidation Catalysis”, Thessaloniki, January 26-28<sup>th</sup>, 2006**

M. Cozzolino, R. Tesser, M. Di Serio, E. Santacesaria

Oral: “Grafting of metal alkoxides on high-surface supports: an advanced technique for the preparation of Nanostructured catalysts”

**11. Third Concorde Conference “Catalytic Nano-Oxide Research and Development in Europe: Present and Future”, Seville, Spain, 17-19<sup>th</sup> May 2006**

M. Cozzolino, R. Tesser, M. Di Serio, E. Santacesaria

Oral: “Kinetics of the oxidative dehydrogenation (ODH) of methanol to formaldehyde by supported vanadium-based catalysts”

**12. 9<sup>th</sup> International Symposium “Scientific bases for the preparation of heterogeneous catalysts”, Louvain-la-Neuve, Belgium, September 10-14, 2006.**

M. Cozzolino, R. Tesser, M. Di Serio, E. Santacesaria

Oral: “Preparation, Characterization and catalytic performances of highly supported TiO<sub>2</sub>/SiO<sub>2</sub> catalysts in Biodiesel production”

**13. XXII Congresso Nazionale della Società Chimica Italiana, Florence, Italy, September 10-15, 2006**

M. Cozzolino, R. Tesser, M. Di Serio, E. Santacesaria

Poster1: “Supported vanadium oxide catalysts: a promising catalytic system for the ODH of n-butane to butenes”.

Poster2: “A comparative study of the catalytic performances of different supported V<sub>2</sub>O<sub>5</sub> catalysts in the ODH of methanol to formaldehyde”.

**14. 4<sup>th</sup> School on Catalysis - Catalyst design from molecular to industrial level, September 20-24, 2006, Tsars Village (suburb of St. Petersburg), Russia.**

M. Cozzolino, R. Tesser, M. Di Serio, P. D’Onofrio, E. Santacesaria,

Oral: “Kinetics of the oxidative dehydrogenation (ODH) of methanol to formaldehyde by supported vanadium-based catalysts”.

***Research-experience abroad***

**UCL** - Université catholique de Louvain - Unité de catalyse et chimie des matériaux divisés, Louvain La Neuve (Belgique) - Laboratory of Prof. P. Ruiz and Prof. E. Gaigneaux from 29 Oct 2005 to 22 Dec 2005.

**Project**: “Study of surface properties of supported vanadium oxide catalysts” by Raman and XPS spectroscopies.

**Publication list**

14. M. Cozzolino, R. Tesser, M. Di Serio, **“TiO<sub>2</sub>/SiO<sub>2</sub> based catalysts”**, La Chimica & L’Industria, Science&Technology, **October 2006**, 76.
  
13. M. Di Serio, M. Cozzolino, F. Cammarota, R. Tesser, P. Patrono, E. Santacesaria, **“From homogenous to heterogeneous catalysts in Biodiesel Production”**, submitted to Industrial & Engineering Chemistry Research, Proceedings of CAMURE-6 & ISMR-5, India, **2006**.
  
12. E. Santacesaria, M. Cozzolino, V. Balato, R. Tesser, M. Di Serio, F. Ruffo, **“Preparation and characterisation of dispersed palladium catalysts supported on carbon previously treated with different strong oxidants”**, "Chemistry for sustainable development", Proceedings of CARBOCAT II- International Symposium on Carbon for Catalysis, **2006**.
  
11. B. Bonelli, M. Cozzolino, R. Tesser, M. Di Serio, M. Piumetti, E. Garrone, E. Santacesaria, **“Study of the surface acidity of TiO<sub>2</sub>/SiO<sub>2</sub> catalysts by means of FT-IR measurements of CO and NH<sub>3</sub> adsorption”**, **2006**, submitted to Journal of Catalysis.
  
10. M. Di Serio, M. Cozzolino, R. Tesser, P. Patrono, F. Pinzaro, B. Bonelli, E. Santacesaria, **“Vanadyl Phosphate catalysts in Biodiesel Production”**, **2006**, submitted to Applied Catalysis A: General.
  
9. M. Cozzolino, R. Tesser, M. Di Serio, P. D’Onofrio, E. Santacesaria, **“Kinetics of the oxidative dehydrogenation (ODH) of methanol to formaldehyde by supported vanadium-based nanocatalysts”**, 3<sup>rd</sup> Concorde meeting (Seville), **2006**, submitted to Catalysis Today.
  
8. M. Cozzolino, R. Tesser, M. Di Serio, E. Santacesaria, **Grafting of titanium alkoxides on high surface SiO<sub>2</sub> support: an advances technique for the preparation of nanostructured TiO<sub>2</sub>/SiO<sub>2</sub> catalysts**, 2<sup>nd</sup> Concorde meeting proceedings, **2006**, submitted to Applied Catalysis A: General.
  
7. Di Serio, M.; Ledda, M.; Cozzolino, M.; Minutillo, G.; Tesser, R.; Santacesaria, E. **Transesterification of Soybean Oil to Biodiesel by Using Heterogeneous Basic Catalysts**. Industrial & Engineering Chemistry Research **45**(9), **2006**, 3009.
  
6. M. Cozzolino, R. Tesser, M. Di Serio, E. Gaigneaux, P. Eloy, E. Santacesaria, - **“Supported Vanadium oxide nanoparticles: effect of preparation method, support and type of precursor on the catalytic performances in the ODH of Methanol to Formaldehyde”**, Studies in Surface Science and Catalysis, E. Gaigneaux et al. (Editors), **2006**, *162*, 697.

5. M. Cozzolino, R. Tesser, M. Di Serio, M. Ledda, G. Minutillo, E. Santacesaria – **“Preparation, characterization and catalytic performances of highly dispersed supported TiO<sub>2</sub>/SiO<sub>2</sub> catalysts in Biodiesel production”**, Studies in Surface Science and Catalysis, E. Gaigneaux et al. (Editors), **2006**, 162, 299.
4. Cozzolino, M.; Tesser, R.; Di Serio, M.; Santacesaria, E. **“Methanol and ethanol oxidative dehydrogenation (ODH) to the corresponding aldehydes on vanadium-based catalysts”**. DGMK Tagungsbericht (**2005**), 2005-2 (Proceedings of the DGMK/SCI-Conference "Oxidation and Functionalization: Classical and Alternative Routes and Sources", **2005**).
3. Cozzolino, M.; Tesser, R.; Di Serio, M.; Santacesaria, E. **“Oxidative dehydrogenation of n-butane on vanadium-based catalysts prepared by grafting”**. DGMK Tagungsbericht (**2004**), 2004-3 (Proceedings of the DGMK-Conference "C4/C5-Hydrocarbons: Routes to Higher Value-Added Products", 2004), 117-124.
2. Santacesaria, E.; Cozzolino, M.; Tesser, R.; Di Serio, M. **Skeletal isomerization of 1-butene to isobutene over acid catalysts obtained by grafting silicon alkoxide on γ-alumina**. DGMK Tagungsbericht (2004), 2004-3(Proceedings of the DGMK-Conference "C4/C5-Hydrocarbons: Routes to Higher Value-Added Products", 2004), 77-85.
1. E. Santacesaria, M. Cozzolino, M. Di Serio, A.M. Venezia, R. Tesser, **Vanadium based-catalysts prepared by grafting: preparation, properties and performances in the ODH of n-butane**, Appl. Catal. A: General 270, **2004**, 177-192.